Faculty of Science

Department of Biology

The impact of cadmium in the maize leaf growth zone

Het effect van cadmium in de groeizone van het maïsblad

Thesis submitted for the degree of Doctor of Science: Biology at the University of Antwerp to be defended by Jonas BERTELS.

Promotor:

Prof. dr. ir. Gerrit T.S. Beemster

Antwerp, 2020

Most of the analyses described in this PhD thesis were conducted in, and by, the Integrated Molecular Plant Physiology Research (IMPRES) group at the University of Antwerp, Belgium.

Frequent collaboration and communication between IMPRES and the Centre for Environmental Sciences – Environmental Biology group (Hasselt University, Prof. Dr. Ann Cuypers) formed the basis for the success of the PhD study.

Cooperation with Systemic Physiological and Ecotoxicological Research group (SPHERE, UA, Prof. Dr. Lieven Bervoets) allowed for precise Cd and mineral measurements in the leaf tissue.

Cooperation with the Laboratory of Molecular Plant Biology (KU Leuven, Prof. Dr. Ir. Wim Van den Ende) allowed us to measure several carbohydrate levels in the leaf tissue.

The PhD study was financially supported by the FWO (Flemish Science Foundation), grant number: G0B6716N

Table of contents

CHAPTER 3: Cadmium inhibits cell cycle progression and specifically accumulates in the maize (*Zea mays* L.) leaf meristem

CHAPTER 4: A genome-wide, multilevel analysis of the effects of cadmium in the maize leaf growth zone

CHAPTER 6: Conclusions and future perspectives

SUPPLEMENTARY DATA

List of abbreviations

ABA	abscisic acid
ACC	1-aminocyclopropane 1-carboxylic acid
APX	ascorbate peroxidase
AsA	ascorbate
ATSDR	Agency for Toxic Substances and Disease Registry
B73	a maize inbred line, named B73
bm	*brown midrib*
CAD	cinnamyl-alcohol dehydrogenase
CAT	catalase
CAX1	CATION EXCHANGER 1
Cd	cadmium
CONTAM	Panel on Contaminants in the Food Chain
CWI	cell wall invertase
c-Z	cis-zeatin
c-Z-OG	cis-zeatin O-glucoside
c-ZR	cis-zeatin riboside
DAPI	4’,6-diamidino-2-phenylindole
DHZ	dihydrozeatin
DHZR	dihydrozeatin riboside
DH-ZR-OG	dihydrozeatin riboside-O-glucoside
DW	dry weight
FDR	false discovery rate
FLL	final leaf length
FRAP	ferric reducing antioxidant power
FW	fresh weight

GA	Gibberellin, typically followed by a number, specifying the gibberellin (e.g. GA1)
GMP	guanosine monophosphate
GO	gene ontology
GR	glutathione reductase
GWAS	genome-wide association
GSH	glutathione
HMA	heavy metal ATPase
HR-ICP-MS	High Resolution Inductively Coupled Plasma Mass Spectrometry
IAA	indole-3-acetic acid
incw	cell wall invertase gene symbol (maizeGDB)
iP	isopentenyladenine
Irt	iron-regulated transporter
JA	jasmonic acid
JA-ACC	jasmonyl-ACC
LER	leaf elongation rate
LFC or LogFC	$\log_2$ fold change
l_{mer}	length of the meristem
maizeGDB	maize genetics and genomics database (www.maizegdb.org)
mcm	minichromosome maintenance
MDA	Malondialdehyde
NADPH	nicotinamide adenine dinucleotide phosphate
NGS	Next Generation Sequencing
N_{mer}	number of cells in the meristem
NRAMP	natural resistance-associated macrophage protein
PAL	phenylalanine ammonia lyase

PC	principle component, typically followed by a number, specifying the principle component
PCA	principle component analysis
qPCR	quantitative Polymerase Chain Reaction
QTL	quantitative trait loci
RIL	recombinant inbred line
rlog	regularized log
ROS	reactive oxygen species
RRG	relative root growth
SA	salicylic acid
SNP	single nucleotide polymorphism
SOD	superoxide dismutase
t-Z	trans-zeatin
t-ZR	trans-zeatin riboside
W22	a maize inbred line, named W22
ZIP	Zrt- and Irt-like protein
Zrt	zinc-regulated transporter

Summary

Cadmium (Cd) is a heavy metal that is introduced into the environment naturally, e.g. through volcanic activity and weathering, and anthropogenically, e.g. through mining and phosphate fertilizers. Plant roots take up Cd and transport it to the shoot. Cadmium perturbs growth mainly through displacement of other essential minerals (e.g. zinc, iron and calcium) from their functional sites due to its chemical similarity. Some of the displaced ions, e.g. Zn and Fe, can in turn cause oxidative stress through Fenton reactions, where metal ions catalyse hydrogen peroxide to highly reactive oxygen species. The study of the effect of Cd on plant growth has already made tremendous progress (**chapter 1**), yet the inhibition of leaf growth through its effects on dividing and elongating cells in growing leaves received little attention. In my PhD study, I therefore set out to study the effects of Cd on the leaf growth zone.

We opted to use the maize leaf for these studies, since, in contrast to other model species, it provides ample and easy to sample material of dividing and elongating cells. To identify this meristematic and elongating tissue, and to gain insight on cellular parameters related to cell division and elongation, a kinematic analysis needs to be performed. I tackled experimental limitations by automating the data analysis involved in kinematic analysis of leaf growth. This lead to the creation of *leafkin*, an R package that contains four functions which allow the user to perform all calculations in a kinematic analysis (**chapter 2**). In addition, it allows cell length profiles and leaf elongation rates to be easily extracted, which in turn can be used in separate analyses. *leafkin* therefor lowers the barrier to kinematic analysis of leaf growth, speeds up the analysis considerably and eliminates the chance for human errors in an otherwise repetitive and time-consuming task.

After establishing a control, mild Cd (46.5 mg $Cd \cdot kg^{-1}$ dry potting soil) and severe Cd (372.1 mg $Cd \cdot kg^{-1}$ dry potting soil) treatment in a range finding experiment (B73 maize inbred line), I performed a kinematic analysis and flow cytometry analysis (**chapter 3**). My results showed that Cd inhibits leaf growth through a reduction of the

meristematic cell number and by impairing the cell cycle at the G1/S transition resulting in an increased cell cycle duration. Mature cell length, the end product of cell elongation, remained unaffected. In addition, I found lower expression of key cell cycle genes (*wee1*, *minichromosome maintenance 4* and *cylin-B2-4*) when plants were exposed to Cd. Dividing and elongating cells can directly get in contact with Cd, since I found that Cd predominantly accumulates in the meristem, after which its concentration declines in the elongation zone. Through the combination of Cd concentration, determined throughout the maize leaf growth zone, with the velocity profile of the tissue, I found that Cd deposition is highest in the meristem and gradually declines throughout the elongation zone. These findings prompted us to determine which biological processes are affected by Cd in these distinct developmental zones.

To reveal these Cd affected processes in the meristem, elongation zone and mature zone of the maize leaf (B73), I performed a genome wide transcriptome study across the maize leaf growth zone (**chapter 4**). This resulted in a broad range of Cd affected processes, which led me to perform biochemical analysis of several phytohormones, minerals and two oxidative stress related parameters. I showed that Cd caused an increase in stress hormone levels (i.e. salicylic acid, abscisic acid and 1-aminocyclopropane 1-carboxylic acid (ACC, an ethylene precursor)) and a decrease of growth promoting hormones (i.e. gibberellin 1 and trans-zeatin riboside). For gibberellin 1, I was able to directly link changes in the spatial distribution of this phytohormone to changes in transcript levels of key gibberellin synthesis and degradation genes. In addition, I revealed a potential new role for conjugated ACCs and specific cytokinins in the response to Cd. Regarding the measured minerals, I mainly found manganese to be the most strongly and consistently Cd affected nutrient. Lastly, lipid peroxidation and antioxidant potential was increased throughout the entire maize leaf growth zone, demonstrating that Cd resulted in oxidative stress in all developmental stages.

The transcriptome study also indicated that the maize leaf growth zone carbohydrate metabolism could be affected by Cd. This prompted us to screen maize carbohydrate

mutants, which revealed a Cd sensitive mutant with reduced cell wall invertase activity (**chapter 5**). Indeed, when the mutant and its genetic background (W22 maize inbred line) were expose to Cd, I found total soluble sugar, glucose, fructose and sucrose levels to be increased in the leaf growth zone of W22 under Cd stress, where the mutant had reduced fructose levels under each treatment. In addition, I also observed that cell wall invertase activity increased under Cd stress in the leaf meristem, where the mutant failed to increase this activity. A kinematic analysis showed that the extra reduction in growth of the mutant under Cd stress could be attributed to a severe reduction in meristematic cell number, in combination with a longer cell cycle duration. Finally, a transcriptome study of meristematic tissue of both mutant and W22 revealed raffinose production to be upregulated under Cd stress, especially when cell wall invertase activity is reduced.

In conclusion (**chapter 6**), by using the maize leaf as a model for growth, we were able to study the impact of Cd on leaf growth in distinct stages of growth (i.e. cell division and elongation). I showed that Cd mainly inhibited cell cycle progression, potentially due Cd directly interacting with this process since it is deposited in the meristem. Reduced meristem size might be related to the reduced gibberellin 1 levels, a key phytohormone for meristem size determination, where its levels might already be controlled at the transcriptome level. In addition, reduced cell cycle gene expression might be related to reduced trans-zeatin riboside levels in the meristem. Finally, I have shown that, in defence to Cd, the plants alters its carbohydrate metabolism and that perturbations therein can result in extra sensitivity to Cd.

Samenvatting

Cadmium (Cd) is een zwaar metaal dat op natuurlijke wijze (bv. door vulkanische activiteit en verwering van gesteentes) en door de mens (bv. door mijnbouw en fosfaathoudende meststoffen) vrijkomt in het milieu. Plantenwortels nemen Cd op en transporteren het naar het bovengrondse deel van de plant. Het verstoort de groei van planten doordat het andere, essentiële, mineralen (bv. zink, ijzer en calcium) vervangt van hun functionele bindingsplaats op proteïnen door zijn chemische gelijkenissen. Sommigen van de vrijgemaakte ionen, zoals Zn en Fe, veroorzaken op hun beurt oxidatieve stress door hun deelname aan Fenton reacties, waarbij deze metaalionen de omzetting van waterstofperoxide naar hoog reactieve zuurstofradicalen katalyseren. De studie van het effect van Cd op plantgroei heeft al grote vooruitgang geboekt (**hoofdstuk 1**), echter, hoe het groei inhibeert door zijn impact op delende en expanderende cellen in het blad heeft tot nu toe slechts weinig aandacht gekregen. Mijn doctoraatsstudie had daarom tot doel om het effect van Cd in de bladgroeizone te onderzoeken.

We hebben ervoor gekozen om onze analyse uit te voeren op het maïsblad omdat het, in tegenstelling tot bladeren van andere plantensoorten, veel en makkelijk te bekomen materiaal oplevert van delende en expanderende cellen. Om inzicht te krijgen in de cellulaire parameters die betrekking hebben op celdeling en expansie en om deze zones te identificeren, dient er een kinematische analyse te worden uitgevoerd. Bij het uitvoeren van deze techniek vormt de data analyse vaak een struikelblok. Dit heeft geleid tot het maken van *leafkin*, een R pakket waarmee de gebruiker alle stappen van de betreffende data analyse kan uitvoeren met slechts vier functies (**hoofdstuk 2**). Daarnaast staat het de gebruiker toe om eenvoudig cellengteprofielen en bladgroeisnelheden te bekomen, dewelke in andere analyses gebruikt kunnen worden. *Leafkin* verlaagt hierdoor aanzienlijk de drempel om een kinematische analyse van bladgroei uit te voeren, versnelt deze analyse en elimineert aanzienlijk de kans op menselijke fouten in een anders repetitieve en tijdrovende analyse.

Na het vaststellen van een relatief lage Cd (46.5 mg $Cd \cdot kg^{-1}$ droge potgrond) en een zware Cd (372.1 mg $Cd \cdot kg^{-1}$ droge potgrond) behandeling, naast de controle behandeling zonder Cd, in een doseringsstudie, heb ik een kinematische en flowcytometrische analyse uitgevoerd (**hoofdstuk 3**). Mijn bekomen resultaten tonen aan dat Cd bladgroei remt door een afgenomen aantal meristematische cellen, die er daarnaast ook nog eens langer over doen om te delen doordat ze minder vlot doorheen de G1/S transitie van de celcyclus lopen. Daarbovenop vond ik ook dat belangrijke celcyclus genen (*wee1*, *minichromosome maintenance 4* and *cylin-B2-4*) werden neergereguleerd onder Cd stress. Door middel van metaalbepalingen, toonde ik aan dat de delende en expanderende cellen rechtstreeks in contact komen met Cd aangezien Cd hoofdzakelijk accumuleert in het meristeem, waarna de concentraties afnemen doorheen de elongatiezone. Door deze metaalbepaling te combineren met de snelheid waarmee dit bladweefsel voortbeweegt (i.e. zich verwijdert vanaf de bladbasis), kon ik afleiden dat de Cd depositie het hoogste is in het meristeem en geleidelijk afneemt doorheen de groeizone. Deze bevindingen waren de aanzet om na te gaan welke biologische processen verstoord werden door Cd in deze specifieke ontwikkelingszones.

Om na te gaan welke processen een impact ondervinden van Cd in het meristeem, de elongatie zone en de mature zone van het maïsblad (B73), heb ik een genoomwijde transcriptoomstudie uitgevoerd in elk van deze zones (**hoofdstuk 4**). Dit leverde een breed scala aan beïnvloedde processen op, dewelke me aanzette tot een verdere analyse van verscheidene planthormonen, mineralen en twee oxidatieve stress parameters. Hierbij toonde ik aan dat Cd zorgde voor een toename van de stresshormonen (i.e. salicylzuur, abscisinezuur, 1-aminocyclopropaan 1-carbonzuur (ACC, een ethyleenprecursor)) en een afname van de groeihormonen (gibberelline 1 en trans-zeatine riboside). Wat betreft gibberelline 1, slaagde ik erin om een directe koppeling te maken met veranderingen in de genexpressie van belangrijke enzymen met functies in gibberelline synthese en afbraak. Daarnaast vond ik ook nog een nieuwe potentiële rol voor geconjugeerde ACCs en specifieke cytokinines in de

response op Cd. Met betrekking tot de gemeten mineralen, nam ik waar dat de afname in mangaanconcentratie doorheen de groeizone het sterkste en de meest consistente was van alle gemeten mineralen. Tenslotte vond ik een toegenomen oxidatie van vetten, tezamen met een toegenomen antioxidant capaciteit doorheen de gehele groeizone van het maïsblad. Dit toont aan dat Cd resulteert in oxidatieve stress in alle ontwikkelingsstadia van bladgroei.

De resultaten van de transcriptoomstudie gaven ook aan dat Cd het koolhydraatmetabolisme in de groeizone verstoorde. Deze vaststelling gaf aanleiding tot een screening van maïsmutanten, hetgeen een Cd-sensitieve mutant met gereduceerde celwandinvertase-activiteit onthulde (**hoofdstuk 5**). Wanneer de suikerniveaus van de mutant en zijn genetische achtergrond (W22 inteelt lijn) nader onderzocht werden, vonden we inderdaad dat het totaal aantal opgeloste suikers, glucose, fructose en sucrose allemaal toegenomen waren in de groeizone van W22 onder Cd stress, waarbij de mutant bij alle behandelingen lagere fructose niveaus vertoonde. Daarenboven nam ik ook waar dat de celwandinvertase-activiteit toenam in het meristeem van W22 onder Cd stress, waarbij de mutant deze stijging in activiteit niet vertoonde. Een kinematische analyse van beide lijnen toonde aan dat de extra reductie in groei bij de mutant onder Cd stress te herleiden was tot een sterk afgenomen aantal meristematische cellen, in combinatie met een langere celcyclusduur. Tenslotte wees een transcriptoomstudie van meristematisch weefsel van beide lijnen uit dat zowel in de mutant, als in W22, raffinoseproductie mogelijks opgereguleerd is onder Cd stress, zeker wanneer celwandinvertase-activiteit is gereduceerd.

We kunnen dus besluiten (**hoofdstuk 6**) dat, door gebruik te maken van het maïsblad als model voor groei, het mogelijk was om de impact van Cd op bladgroei in de verschillende stadia van groei (i.e. celdeling en celexpansie) te onderzoeken. Ik toonde aan dat Cd hoofdzakelijk groei remt door celdeling te remmen, mogelijks doordat Cd direct interageert met dit proces aangezien het lokaal wordt afgezet. De gereduceerde meristeemgrootte zou mogelijk te verklaren zijn door de afgenomen hoeveelheden

gibberelline 1, aangezien het een belangrijke functie heeft in het bepalen van de meristeemgrootte. De transcriptoomdata gaf ons inzicht in de wijze waarop deze gibberelline 1 hoeveelheden afnamen. Daarenboven kon de afname in genexpressie van celcyclus genen mogelijks in verband worden gebracht met de afgenomen trans-zeatine riboside hoeveelheden in het meristeem. Tenslotte heb ik ook nog aangetoond dat, als reactie op Cd stress, de plant zijn koolhydraatmetabolisme aanpast en dat verstoringen in dit metabolisme resulteren in extra gevoeligheid voor Cd stress.

Thesis aim, scope and outline

Much is known about the impact of cadmium (Cd) stress on plants and the plant's response to this form of abiotic stress. However, it is remarkable that the impact of Cd in the growth zone of monocotyledonous leaves remained largely unstudied. This growth zone hosts the two cellular processes driving growth, i.e. cell division and cell elongation. Due to the clear separation of these two cellular processes in distinct zones, studying the impact of cadmium in both of these zones could make a significant contribution to our understanding of the impact of metals on plant growth.

The aim of my PhD study, presented in this thesis, was to assess the impact of Cd in the maize leaf growth zone. The scope of my thesis is therefore the growing fifth leaf of maize seedlings, in which I studied the effect of Cd in a series of integrated experiments. Through these experiments, I provide insight on the impact of Cd at the organ, cellular, biochemical and molecular level throughout the maize leaf growth zone. In addition, I developed a particular interest in data analysis using R, a statistical programming language. Pursuing this interest, I developed *leafkin*, an R package for automated kinematic data analysis. Together with an introductory chapter, I will present the results collected during my PhD study in the following chapters:

In **chapter 1**, I provide an introduction to Cd stress in plants and the maize leaf growth zone. I first highlight how Cd is introduced into the environment and taken up by the plant, after which I discuss the impact of Cd and the plant response at several biological levels (i.e. plant, organ, cellular, biochemical and molecular level). Hereafter, I briefly introduce the maize leaf growth zone, which should allow the reader to better understand the tissue on which all of the analyses were performed.

Research questions:

- What is already known about Cd stress in plants?
- Why is the maize leaf growth zone an ideal model to study the impact of abiotic stress on growth?

In **chapter 2**, I introduce and discuss *leafkin*, an R package I developed to perform all the calculations required during the kinematic analysis of monocot leaves, using only four functions. The aim of *leafkin* is to make kinematic data analysis faster, more accessible and less prone to human errors.

Research question:

- Can automation improve the data analysis involved in kinematic analysis of monocot leaves?

In **chapter 3**, I focus mainly on the cellular aspects of cadmium inhibited leaf growth (quantification of several cell cycle and elongation parameters through kinematics), combined with a more in-depth study of the cell cycle (qPCR of cell cycle genes and flow cytometry). In addition, through the combination of kinematics and Cd measurements, we were able to reveal that Cd is deposited in the meristem and elongation zone of the leaf, rather than the mature blade.

Research questions:

- What is the cellular basis of Cd inhibited leaf growth?
- Could the effect of Cd on growth be related to its accumulation in the maize leaf growth zone?

In **chapter 4**, I present the results of a genome wide transcriptome study to reveal the Cd-impacted processes in dividing, elongating and mature cells. In addition, several phytohormones were measured, where the transcriptome data is linked to changes in these phytohormone levels. Also, pointers to differentially expressed metal transporters prompted me to analyse several other minerals throughout the growth zone, data which is also presented in this chapter. Finally, to provide a context with regards to oxidative stress, I also present biochemical data on lipid peroxidation and antioxidative power.

Research questions:

- Which biological processes does Cd impact in the maize leaf growth zone?

- How does Cd affect phytohormone levels in the maize leaf growth zone?
- How does Cd affect mineral levels in the maize leaf growth zone?
- Does the meristem and elongation zone experience oxidative stress under Cd growth conditions?

In the final results chapter, **chapter 5**, I focussed my research on Cd affected carbohydrate metabolism. Pointers toward cell wall invertase (CWI), revealed in chapter 4, were used to select a Cd sensitive CWI mutant. Both in the mutant and its genetic background (W22), we obtained several carbohydrate levels, performed a kinematic analysis, analysed the transcriptome in the meristem, determined CWI activity and analysed photosynthetic parameters under control and Cd-stress conditions.

Research questions:

- Does Cd affect carbohydrate levels in the maize leaf growth zone?
- Do maize mutants in sucrose metabolism differ in their Cd stress response?

At the end of the thesis, in **chapter 6**, I conclude the presented work by addressing the main findings in an overall conclusion. As is the case in most studies, new insights result in new questions raised. These opportunities for future studies and experiments conclude the thesis.

Chapter 1

An overview of the current knowledge on the impact of cadmium on plant growth and functioning

Cadmium in the environment

Cadmium (Cd) is a heavy metal. In this case, we are not referring the music genre, but its chemical meaning, i.e. it is part of metals in groups 3 to 16 in periods 4 and higher (the transition and post-transition metals; Hawkes, 1997). The reason for metals to be referred to as *heavy* is due to their density, being above 5 g/cm^3 (Tchounwou *et al.*, 2012). Frequently, poisonous characteristics are attributed to this group of elements, which, in the case of Cd, are kidney and skeletal damage, cardiovascular disease and cancer (Järup, 2003).

In our daily lives, we encounter Cd on a daily basis, luckily most of the time in trace amounts. One of the most prominent causes for human Cd exposure, is tobacco. A cigarette contains about 0.5-1.5 µg Cd, of which smokers take up an estimated 1 µg Cd per 20 cigarettes smoked (Scherer and Barkemeyer, 1983). Besides cigarettes, trace amounts of Cd can be found in food, e.g. oysters, mussels, vegetables and cereals (World Health Organization, 2011), which can lead to human Cd exposure levels exceeding the recommendations of the Agency for Toxic Substances and Disease Registry (ATSDR) and the Panel on Contaminants in the Food Chain (CONTAM, European Food Safety Authority; Clemens *et al.*, 2013). To reduce dietary intake of Cd, considerable effort is undertaken to limit dietary Cd by breeding for crop traits related to low Cd uptake. For instance the accumulation of Cd in grain of rice cultivars is frequently investigated (e.g. Yu *et al.*, 2006; SHI *et al.*, 2009; Chen *et al.*, 2016). In addition, as recently reviewed by Clemens (2019), genome editing techniques (e.g. CRISPR-Cas) could significantly improve food safety by for instance expressing tailored transporter proteins in specific cell types and membranes, mainly to lower Cd levels in the edible organs. Also, the possibilities to decrease Cd uptake in plants are extensively studied, for example by enhanced suberization of roots through application of silicon in the soil (Kuliková and Lux, 2010; Wu *et al.*, 2019) or Cd immobilization in the soil through biochar amendments (Bashir *et al.*, 2018; Rafique *et al.*, 2019) .

Before plants and animals can take up Cd, it must be released into the environment, either through natural or human activities. Natural activities include volcanic activity, weathering and erosion. Among the human activities releasing Cd are mining, smelting and refining of non-ferrous metals, fossil fuel combustion, incineration of municipal waste and phosphate fertilizers (World Health Organization, 2010). Therefore, Cd is omni-present, making Cd pollution a global problem. For instance, in China, approximately 20 million hectares, around one-fifth of its total cultivatable soil, are contaminated with Cd (Cai *et al.*, 2019). In Belgium, the Campine region is known for historical Cd pollution through zinc refineries. Here, 280 km^2 is enriched with Cd, meaning that more than 1 mg Cd per kg dry soil is present, where normally only 0.1 to 0.5 mg Cd/kg dry soil is present (Vlaams Parlement, 1998). In the Netherlands, 420 km^2 is contaminated with several metals, including Cd, lead and zinc (Van Slycken *et al.*, 2013).

Cadmium uptake and transport throughout the plant

Being sessile organisms, plants cannot flee from unfavourable conditions that result in biotic or abiotic stress. Biotic stress is stress caused by other organisms, either being pathogens or biota wounding the plant (e.g. mechanical, insect, herbivory). Abiotic stress is caused by physical or chemical changes in the plant's environment, where drought, high salinity, cold, heat, high light and toxic compounds are among the most common causes (Fujita *et al.*, 2006). Being already toxic at low doses, Cd can impose high levels of abiotic stress on plants.

The first plant organ to come into contact with Cd is the root, of which its uptake depends on the soil properties and plant structure and physiology. An important soil property for Cd mobility is soil pH, in conjunction with soil type and presence of organic matter (Eriksson, 1989). Cadmium can be bound to Fe-oxides, to negatively charged clay surfaces and to hydroxyl groups along clay particle edges. Organic matter contains negatively charged sites through its phenol and carboxyl groups which can bind Cd. Since the degree of protonation of these negatively charged groups varies with pH, Cd-

adsorption onto these group will vary with pH, where a decrease in soil pH has shown to increase Cd-bioavailability in the soil (Eriksson, 1989). In addition, plant physiology and structure can affect Cd uptake. For instance, in maize, Redjala *et al.* (2011) demonstrated a relation between root structure and Cd uptake, depending on Cd exposure conditions. When plants were Cd exposed in hydroponics, both symplastic (intracellular, the cytoplasm and vacuolar compartments) and apoplastic (extracellular, cell wall) adsorption of Cd was increased compared to aeroponics. Reason for this are changes in apoplastic barrier formation (Casparian bands and suberin lamellae), which develop closer to the root tip in aeroponics (even closer in soil), hindering Cd entry into the apoplast. In rice, also a relation between Cd and root tip number per root surface area was revealed, where a lower number of root tips per root surface area led to lower Cd uptake and translocation (Huang *et al.*, 2019*b*). Plants alter the direct environment surrounding the root by secreting root exudates (e.g. phenolics, amino acids, organic acids, proteins) in the rhizosphere. This can augment the plants tolerance to Cd by impeding the entry of Cd ions into the root (Bali *et al.*, 2020). However, it should be noted that phytosiderophore (low molecular weight metal-chelants) exudation can also elevate Cd uptake by increasing the mobility of Cd in the soil (Awad and Römheld, 2000). Finally, microorganisms, residing in the rhizosphere in a symbiotic relation with the plant, can impact Cd uptake by the plant. For instance, *Serratia* sp. K3 significantly enhanced Cd accumulation in the roots and shoots of *Vetiveria zizanioides* (Liu *et al.*, 2020).

Eventually, when Cd reaches the plant root surface, it is taken up by the cells through natural resistance-associated macrophage protein 5 (NRAMP5). Here, it was shown that *Nramp5* knockout rice (Oryza sative) largely lost the ability to take up Cd and Mn (Sasaki *et al.*, 2012). In addition, Zrt- and Irt-like protein family transporters (Zrt: zinc-regulated transporter, Irt: iron-regulated transporter, ZIP family), which normally transport zinc, iron and manganese across cellular membranes have been linked to Cd-uptake as well (Dubey *et al.*, 2018; Spielmann *et al.*, 2020). Once Cd has entered the rhizodermis, it reaches the xylem sap stream through the apoplastic and the cell-to-

cell (symplastic and transcellular) pathway (Kreszies *et al.*, 2018). Along the apoplastic pathway, Cd reaches the xylem sap through free spaces and cell walls of the rhizodermis and cortex. Along the symplastic pathway cell-to-cell transport of Cd occurs through plasmodesmata and the transmembrane pathway transports Cd through the cell wall and aquaporins in the membrane. Once it reaches the vascular tissue, heavy metal ATPases (e.g. AtHMA2 and AtHMA4 in *Arabidopsis thaliana*) are responsible for xylem loading of Cd in the root vascular tissue, after which it reaches the shoot through the xylem sap stream (reviewed by Takahashi *et al.*, 2012). The radial transport of Cd from the rhizodermis to vascular tissue and thereafter to the shoot is quite swift. In rice, Cd already appeared in the shoot base region at 1 h after feeding (Fujimaki *et al.*, 2010). Once Cd reaches the base of the stem, it is loaded into the phloem at the nodes and directed to young growing leaves (Kobayashi *et al.*, 2013). In rice, the accumulated Cd in the leaves can be remobilized and transported to the rice panicles during the booting and maturing stages (Zhou *et al.*, 2018). Low-affinity cation transporter (*OsLCT1*) was shown to be an important transporter at the nodes for phloem loading of Cd, where it was shown that knockdown plants of *OsLCT1* accumulated approximately half as much Cd in the grains as compared to the control plants (Uraguchi *et al.*, 2011). Taken together, these results indicate that Cd can readily be taken up and (re)distributed to the across the plant.

Cadmium impact and the plant response at different biological levels

Once inside the plant, abiotic stress caused by Cd perturbs the plant at different biological levels. In the following paragraphs, our knowledge about the impact of Cd at the plant, organ, cellular, biochemical level and molecular level, is reviewed. A key aspect in this context is the distinction between the active response of the plant to Cd or perturbation caused by Cd itself. Active plant responses will be mainly addressed in the biochemical level section below.

Cd impact at plant and organ level

At plant and organ level, common parameters for measuring the impact of Cd are plant height, fresh and dry weight, leaf elongation rate and seed production. At very low Cd levels (in lower µM range or less), studies report a positive or neglectable impact on plant growth (Sobkowiak and Deckert, 2003; Arduini *et al.*, 2004; Cui *et al.*, 2017), yet, in most studies where 5 µM or more is used, decreasing growth and biomass is the common response (note that 5 µM is already environmentally realistic (Keunen *et al.*, 2011); *). Besides changes in fresh or dry weight, it has also been shown that Cd treatment can cause shifts in the dry weight to fresh weight ratio (i.e. increase; Moya *et al.*, 1993). In addition, Cd affects the visual appearance of the plant can change due to chlorosis and necrosis (Baryla *et al.*, 2001; Vatehová *et al.*, 2016).

Reduced growth at organ level in response to Cd is frequently reported. For rice roots, lateral root primordia and lateral root density are significantly reduced by Cd stress (Ronzan *et al.*, 2018). Other examples for negatively impacted root growth can be found for Arabidopsis (Cui *et al.*, 2017), pea (Fusconi *et al.*, 2007), barley (Demecsová *et al.*, 2020), *Kandelia obovate* (a mangrove species; Pan *et al.*, 2020), *Brassica rapa* (canola; Lv *et al.*, 2017), *Brassica napus* (Benáková *et al.*, 2017), soybean (Finger-Teixeira *et al.*, 2010).

The impact of Cd at shoot level can for instance be monitored by height measurements and tiller number. In wheat, both parameters significantly declined already at the lowest Cd treatment used (30 ppm, soil), which could be linked to a significant drop in fresh and dry weight (Saleh *et al.*, 2020). At leaf level, several parameters can be measured to assess Cd impact, such as leaf area (Nada *et al.*, 2007), leaf mass (Nada *et al.*, 2007), leaf number (Elobeid *et al.*, 2012) and rosette diameter (Hendrix *et al.*, 2018), all of which are significantly reduced under Cd growth conditions.

(*) *It should be noted that comparing Cd concentrations between experiments is not straightforward, since toxicity and plant response can vary widely depending on solution/soil composition.*

Being part of the shoot, reproductive organs and seed production are also negatively impacted by Cd. For instance, in Arabidopsis, chronic exposure to 5 and 10 µM Cd resulted in a drastic reduction of silique number (i.e. seed capsule; Keunen *et al.*, 2011). In *Pistia stratiotes L.* (an aquatic plant), Cd reduced the number of daughter rosettes (vegetative reproduction) and inflorescences on the mother rosettes (Silva *et al.*, 2013). Cadmium stored in the vegetative tissue can be remobilized to the seeds (Rodda *et al.*, 2011), yet also absence of net remobilization of Cd from leaves to seed was described, supporting a direct pathway of Cd transport from roots to seed through a xylem-to-phloem transfer in the stem (Harris and Taylor, 2013). Finally, seeds, exposed to Cd, can have reduced germination (Liu *et al.*, 2012). However, during the experiments performed in the studies presented in this thesis, no aberrant germination rates were noted for maize seeds germinating in Cd enriched potting soil, perhaps due to the short time required (coleoptile emerges around 3 to 4 days after sowing) for the seeds to germinate.

Cd impact and response at the cellular level

At the cellular level, organ growth and final size is strictly regulated by cell division and cell elongation. Therefore, the growth inhibition by Cd needs to be related to one or both of these processes. Based on a meta-analysis, Gázquez and Beemster (2017) revealed that meristem cell number, rather than mature cell size determines the final size of plant organs.

A reduced number of cells contributing to cell division is frequently proportional to meristem size reduction. Studies, which have quantified meristem size changes under Cd stress, reported Cd negatively affected meristem size in roots of wheat, pea and Arabidopsis (Fusconi *et al.*, 2007; Pena *et al.*, 2012; Yuan and Huang, 2016; Bruno *et al.*, 2017). In addition, cells take longer to progress through the cell cycle since they are halted at both the G1/S and G2/M transition (Cui *et al.*, 2017; Cao *et al.*, 2018). This delayed cell cycle progression can also be associated with the expression of key cell cycle genes, encoding for example cyclins and cyclin dependent kinases (CDKs). Under

Cd stress, expression of these genes seems to be downregulated, as reported in Zhao *et al.* (2013) who found that 12 out of 17 cell cycle-related genes had severely reduced transcript levels in Cd exposed rice roots.

Cadmium can also impact cell elongation and size, however, the negative effect on cell production seems to be the main cause for Cd growth inhibition. For instance, in *Scenedesmus quadricauda* (a green algae species), 60 µM Cd completely inhibited DNA replication, whereas only a decrease in cell growth rate and similar or larger final cell sizes were observed (Bišová *et al.*, 2003). In growing rice leaves, mature cell length was significantly reduced under Cd stress, which was related to the observed leaf elongation rate reduction under lower Cd concentrations (10 µM; Huybrechts *et al.*, 2020). Changes in cell expansion could be related to the effect of Cd on cell wall composition (addressed below) or endoreduplication. In leaves of Arabidopsis (Hendrix *et al.*, 2018), lower endoreduplication levels were observed in conjunction with respectively reduced cell surface area. However, it could well be that the impact of Cd on endoreduplication could be organ specific, since in roots of *Pisum sativum* and *Arabidopsis thaliana*, Cd exposure resulted in increased ploidy levels (Fusconi *et al.*, 2006; Repetto *et al.*, 2007; Cui *et al.*, 2017; Cao *et al.*, 2018). Therefore, in a recent review by Huybrechts *et al.* (2019), it was suggested that Cd exposure stimulates the endocycle in roots and inhibits it in leaves.

Cd impact and response at the biochemical level

At the biochemical level, Cd has a wide and diverse impact and sets active plant responses in motion. Well established effects and responses are related to reactive oxygen species (ROS) metabolism, cell wall composition, carbohydrate levels and phytohormone levels and these will be discussed in more detail below.

Reactive oxygen species and Cd scavenging (ROS)

It is commonly accepted that cadmium stress results in an oxidative challenge for the plant (Cuypers *et al.*, 2010, 2012; Loix *et al.*, 2017; Huybrechts *et al.*, 2019). Since Cd is unable to generate ROS directly, it belongs to the non-redox-active metals (which for

example also include arsenic and scandium, as opposed to redox-active metals like Fe and Cu). Redox-active metals can produce ROS directly through the Fenton reaction, where Cu^{1+} (copper) and Fe^{2+} (iron) ions catalyse the decomposition of hydrogen peroxide (*Cu^{1+} can be formed though reduction of Cu^{2+} by superoxide*), resulting in the production of highly reactive hydroxyl radical (Jomova *et al.*, 2012). Iron ions can also reduce molecular oxygen (O_2), leading to superoxide radical production. Cadmium can displace redox-active metal ions from their functional sites in proteins (e.g. Fe-ions; Huybrechts *et al.*, 2019), which can increase ROS-levels as described above. In addition, Cd can increase ROS production by interfering with ROS-producing nicotinamide adenine dinucleotide phosphate (NADPH) oxidase and functioning of organelles known for high ROS generation such as chloroplasts and mitochondria (Cuypers *et al.*, 2010). Reactive oxygen species can in turn damage lipids, proteins and nucleic acids. A key indicator for ROS induced membrane damage are increased malondialdehyde levels, which is frequently reported in plants exposed to Cd stress (Ortega-Villasante *et al.*, 2011; Zhao *et al.*, 2012; Zhou *et al.*, 2019*b*; AbdElgawad *et al.*, 2020).

Cadmium, as a non-redox-active metal, perturbs ROS-metabolism through depletion of the non-enzymatic antioxidant glutathione (GSH), metallothioneins (MTs; gene-encoded cysteine-rich polypeptides) and phytochelatins (PCs; GSH oligomers synthesized non-ribosomally by phytochelatin synthases; Joshi *et al.*, 2015; Huybrechts *et al.*, 2019). In response to these direct effects of Cd, the plant actively responds to limit the resulting damage.

Tobacco seedlings actively produce GSH, which allows PC production, resulting in increased PC content (Vögeli-Lange and Wagner, 1996). Glutathione, MTs and PCs can bind Cd-ions, effectively reducing the free Cd^{2+}-ions (Leverrier *et al.*, 2007; Joshi *et al.*, 2015). Phytochelatin-Cd complexes are transported into the vacuole by vacuolar membrane ABC-type transporters for sequestration of harmful Cd^{2+}-ions in the vacuole (Cobbett, 2000). In addition, HMA3, a tonoplast pump, could also play a role in vacuolar Cd sequestration. Here, high expression levels of *HMA3* in *Noccaea*

caerulescens (a Cd hyperaccumulator, formerly known as *Thlaspi caerulescens*) were linked to its Cd tolerance (Ueno *et al.*, 2011). However, Cd-binding by PCs seems to be the primary protective mechanism against Cd-stress (Sylwia *et al.*, 2010).

In response to Cd stress, plants also upregulate antioxidative enzyme pathways involving superoxide dismutase (SOD) and catalase (CAT) and increase metabolite antioxidant ascorbate (AsA) levels (Jozefczak *et al.*, 2014). In addition, activities of ascorbate peroxidase (APX) and glutathione reductase (GR), key enzymes in the glutathione-ascorbate cycle, are also upregulated, mediating hydrogen peroxide detoxification (Liu *et al.*, 2007).

Cell wall

To protect the cells from the harmful effects of Cd, the plant actively modifies its cell wall to provide a physical barrier to Cd. The plant cell wall consists out of a primary (cellulose, hemicellulose and pectin) and secondary cell wall (cellulose, hemicellulose and phenolic components, i.e. lignin) and its modifications in response to Cd stress have been extensively reviewed (Parrotta *et al.*, 2015; Loix *et al.*, 2017). Lignification of the cell wall in response to Cd is commonly reported (Wang *et al.*, 2018; Chiao *et al.*, 2019), where mainly physical barrier characteristics are attributed to this cell wall component. Lignification of the cell wall can make these cell walls more rigid, therefor, while limiting Cd passage thought the cell wall, Cd-induced lignification can also slow down growth when occurring in the elongation zone (Schutzendubel *et al.*, 2001; Dos Santos *et al.*, 2004).

Besides providing a physical barrier for Cd passage, the cell wall is also an important binding site for Cd, where it binds to lignin and negatively charged carboxyl, hydroxyl and thiol groups (Basso *et al.*, 2005; Krzesłowska, 2011). Especially low-methylesterified pectins are frequently put forward as an important Cd-retaining cell wall component, since the normally bound Ca^{2+}-ions can be replaced by divalent Cd^{2+} cations (Dronnet *et al.*, 1996). Finally and interestingly, when comparing metallicolous to non-metallicolous populations of *Arabidopsis halleri*, it was found that both

populations altered their cell walls in response to Cd, but increased tolerance was mainly attributed to other mechanisms, like vacuolar sequestration (Meyer *et al.*, 2015).

Carbohydrates and photosynthesis

Cadmium stress can also result in altered carbohydrate levels, where both increased (Moya *et al.*, 1993; Devi *et al.*, 2007; Shahid *et al.*, 2019) and decreased (Costa and Spitz, 1997; Kim *et al.*, 2004) levels have been reported. One of the reasons why plants might actively increase soluble sugars levels could be related to the antioxidant properties of sucrose (Stoyanova *et al.*, 2011; Peshev and Van Den Ende, 2013). In addition, the close relationship of carbohydrates with mitochondrial respiration and fatty acid beta-oxidation makes carbohydrates inherently occupy a central role in the cellular redox balance (Couée *et al.*, 2006; Keunen *et al.*, 2013).

Decreased carbohydrate levels could be related to an increased energy demand for the augmented defensive response and/or to an altered source-sink partitioning in response to the imposed stress (Rosa *et al.*, 2009). Another viable explanation for altered carbohydrate levels could be the negative impact of Cd on photosynthesis. Cadmium stress can result in decreased chlorophyll a, chlorophyll b, carotenoids, net photosynthetic rate, stomatal conductance, transpiration rate and water use efficiency (as reviewed by Hasan *et al.*, 2009; Rizwan *et al.*, 2016, 2017 and references therein). The reduced photosynthesis can be explained by Cd-induced damage to light harvesting complex II and photosystems I and II (Krupa, 1988, 1999; Küpper *et al.*, 2007), where Cd-induced iron-deficiency negatively impacts electron flow around photosystem I (Siedlecka and Baszynski, 1993). In addition, Cd interferes with the functioning of stomatal guard cells, which it enters through the Ca^{2+} channels, mimicking intracellular Ca^{2+} and resulting in stomatal closure (Perfus-Barbeoch *et al.*, 2002).

Phytohormones

Plant hormones are a large and diverse group of compounds, amongst which are the brassinosteroids, auxins, strigolactones, salicylic acid (SA), abscisic acid (ABA), gibberellins, jasmonic acid, ethylene and cytokinins (Sytar *et al.*, 2019). During the past five years, several extensive reviews on the phytohormone response to Cd stress and heavy metal stress in general have been published, providing an excellent overview on this topic (Asgher *et al.*, 2015; Rajewska *et al.*, 2016; Bücker-Neto *et al.*, 2017; Jalmi *et al.*, 2018; Guo *et al.*, 2019*a*; Sharma *et al.*, 2020).

One of the more prominent stress hormones in the plant response to abiotic stress, is the phenolic compound SA, which is frequently associated with, for example, stress affected redox homeostasis in plants (Liu *et al.*, 2016). In wheat, plants responded to cadmium by increasing their endogenous SA levels in both roots and leaves (Tajti *et al.*, 2019). Next to SA, increased ABA levels were also described in two wheat varieties, in conjunction with decreased stomatal conductance and photosynthetic rates (Guo *et al.*, 2019*b*). As described above, Cd stress can result in stomatal closure, which could also be linked to the reported increased ABA levels (Mittelheuser and Van Steveninck, 1969). Finally, in an excellent review on ethylene signalling under metal stress (Keunen *et al.*, 2016), a supporting role for ethylene signalling in response to Cd stress across various plant species was observed. Overall, plants increased expression and activity of ACC synthase and ACC oxidase (ACC: 1-aminocyclopropane-1-carboxylic acid) in response to Cd, where both enzymes are crucial for ethylene production. Using an *acs2-1acs6-1* double knock-out *Arabidopsis thaliana* plants, Schellingen *et al.* (2015) revealed that ethylene synthesis in response to Cd stress is required to respond to the early oxidative challenge, where the mutant exhibited lower transcript levels of genes involved in glutathione production.

For the growth regulating hormones, the levels of auxin, specifically indole-3-acetic acid (IAA), were found to be reduced after growing in Cd contaminated soil up until jointing stage of wheat (i.e. internodal tissue elongation to form a stem; Guo *et al.*, 2019*b*). Also, in the primary roots of *Sorghum bicolor* seedlings, IAA levels were

reduced which was linked to an increase in IAA oxidase activity (Zhan *et al.*, 2017). Gibberellins could also have an important role in the plant response to Cd, since gibberellin 3 (GA3) application as a foliar spray on Cd exposed *Parthenium hysterophorus* countered the negative impact of Cd by promoting cell division, with increased growth and biomass as a result (Hadi *et al.*, 2014). Improved mitotic activity in Cd-stressed root meristems of *Vicia faba* by foliar application of GA3 was also reported by Mansour and Kamel (2005). Finally, plants could also actively slow down growth under Cd stress by reducing zeatin riboside levels in the leaves, which was shown in two wheat cultivars and oilseed rape (Yan *et al.*, 2016; Guo *et al.*, 2019*b*). Since cytokinins perform roles in proliferation and differentiation of plant cells (Corbesier *et al.*, 2003; Sakakibara, 2006), its reduced levels can be linked to observed growth reductions under Cd stress.

Since phytohormones orchestrate a wide range plant processes and are able to regulate the stress responses, priming plants and even seeds with phytohormones can improve plant performance under heavy metal stress (Sneideris *et al.*, 2015; Sytar *et al.*, 2019; Gul *et al.*, 2020). One of the plant hormones that is receiving a lot of attention with regards to plant priming for Cd stress, is salicylic acid. Pretreatment of plants with SA was shown to be beneficial for the mitigation of Cd damage through the modification of reactive oxygen species levels (Guo *et al.*, 2019*a*). Interestingly, SA pretreatment stimulated ROS production in cells, which acts as a signal to activate the antioxidant system to increase the plants resistance to subsequent Cd stress. These findings prove that knowledge, collected in fundamental research, can be put to use to make plants able to cope with adverse growth conditions imposed by Cd.

Cd response at the molecular level

In line with the central dogma of molecular biology, first introduced by Francis Crick in 1957, sequential “information” in the genome is copied to mRNA, which is then used to create proteins (Crick, 1970). It is through these proteins that plants and all other living organisms orchestrate every biological process and their active response to

biotic and abiotic stress. Inherently, this means that the transcriptome and the proteome can provide valuable insight in which processes the plant adjusts, initiates and halts in response to Cd. The following paragraph presents a small sample of findings related to Cd stress in plants, obtained through molecular analyses.

A powerful genome-wide approach to study the effect of Cd is comparative transcriptomics. Microarray analyses of the roots of *Arabidopsis thaliana* and the more tolerant *Arabidopsis halleri* revealed several heat-shock proteins and heat-shock transcription factors in the rapid response to Cd (Weber *et al.*, 2006). In addition, the upregulation of a ZIP metal transporter, which is a marker for Zn-deficiency in the same transcriptome study also confirmed Cd-caused Zn-deficiency (Weber *et al.*, 2006). Also a role for CATION EXCHANGER 1 (a vacuolar Ca^{2+}/H^{+} exchanger) in the response of *Arabidopsis thaliana* to Cd was highly correlated with the expression of genes involved in the oxidative stress response, supporting the role of CAX1 in the regulation of cytosolic ROS accumulation (Baliardini *et al.*, 2016). In *A. thaliana*, Opdenakker *et al.* (2012) analysed transcript levels of several ROS- and signalling-related enzymes, revealing Cd induced hydrogen peroxide production through an induction of NADPH oxidases. This was followed by an induction of gene regulation through the MAPK signalling cascade (e.g. MPK3/6) and transcription factors (e.g. WRKY's).

Genome based studies, using differences in genomes across large panels of accessions can reveal quantitative trait loci (QTL) to single nucleotide polymorphisms (SNPs, revealed through genome-wide association: GWAS). For instance, using 270 *Indica* rice strains, Liang *et al.* (2018) revealed close to 80 000 genome SNPs, of which 32 SNPs were associated with Cd accumulation. These genetic markers can be valuable for the development of low Cd-accumulating rice, since this set of SNPs was related to 61.25% of the variation in Cd concentration in grains. Another GWAS study, performed on maize, revealed polymorphisms in *ZmHMA2* and *ZmHMA3* genes which were correlated with leaf Cd concentration in leaves under respectively low and various Cd levels (Cao *et al.*, 2019). In addition, a foundation was laid for marker-assisted selection of low Cd accumulating maize. In *Arabidopsis thaliana*, a QTL mapping study was

performed on a recombinant inbred line (RIL) population using the relative root growth (RRG) rate response to Cd as quantitative trait, revealing three QTLs, together explaining in total nearly 50% of the variation in the RRG rate response (Fischer *et al.*, 2017). As a final example, a QTL analysis was performed on a F2 population of *Arabidopsis halleri* × *Arabidopsis lyrata*, where the accumulation of several minerals and Cd was monitored when grown under Cd excess. Their study revealed one major QTL for shoot Cd accumulation, where the heavy metal ATPase HMA4 was put forward as the gene underlying the QTL (Willems *et al.*, 2010).

A comparative proteomics study of rice seedlings, a molecular regulatory network was revealed, related to carbohydrate metabolism, redox reactions and signal transduction (Liu *et al.*, 2019). In *Microsorum pteropus*, an aquatic cadmium hyperaccumulator, proteins related to energy metabolism and antioxidant activity were revealed (Lan *et al.*, 2018). Here, a comparison between root and leaf tissue resulted in a limited overlap, containing only proteins involved in basal metabolism, suggesting a difference in the mechanisms to deal with Cd in roots and leaves. Next to levels of proteins, also post-translational modifications can play an important role in plant responses. For Cd stress in rice, Fang *et al.* (2019) compared a Cd-sensitive and tolerant line, revealing differentially phosphorylated proteins. Enzymes involved in carbon metabolism, proteolysis, RNA helicases, and DNA replication/transcription/repair were upregulated in the tolerant line and were suggested to contribute to Cd tolerance, where oxidoreductases, pathogenesis related proteins and genes related to ethylene biosynthesis and substances transportation were shared by both lines and therefore part of a more general response to Cd.

In conclusion, genome wide transcriptome and proteome analyses can increase our understanding of Cd stress and tolerance in plants. As emphasised in a review by Verbruggen *et al.* (2013), transcriptome and genome analyses can be used to better understand metal hyperaccumulation and the evolution of such traits in plants. In addition, it provides entry points for targeted analyses of specific pathways,

metabolites and genotypes, which can further improve our mechanistic understanding of Cd stress in plants and their response.

The maize leaf - introducing the model for studying growth

As introduced above, much is known about the negative impact of Cd on plant functioning. However, how Cd specifically inhibits (monocot) leaf growth is largely unknown. The maize leaf growth zone provides an ideal organ to study the impact of biotic and abiotic (e.g. Cd) stress on growth and to study growth itself through the use of e.g. mutants (Avramova *et al.*, 2015*a*; Sprangers *et al.*, 2020). The growing maize leaf maintains a steady state growth zone for at least three days, starting from the time of its emergence from the sheet of older leaves. This means that, within this period, the growth zone contains a meristem and elongation zone of roughly stable size, where respectively cell division and cell elongation take place (Figure 1). These two key processes drive growth at the cellular level. By kinematic analysis, the position of these developmental zones can be determined, allowing directed sampling of dividing and elongating cells for further studies (Sprangers *et al.*, 2016).

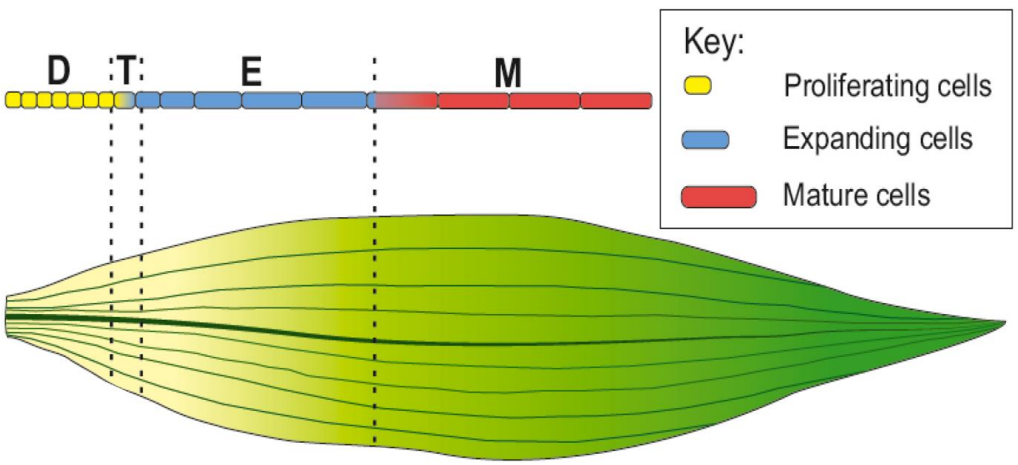

Figure 1. The maize leaf growth zone (Avramova *et al.*, 2015*c*)**.** D, division zone (i.e. the meristem); E, elongation zone; M, maturation zone; T, transition zone (sometimes added to indicate cells transitioning from cell proliferation to expansion).

The meristem is positioned at the base of the leaf (length: approx.. 15 mm in B73), which is followed by the elongation zone (length: approx. 55 mm in B73; Bertels *et al.*, 2020). These zones therefor provide ample material for both molecular, metabolite and biochemical analyses, where frequently, tissue amounts can become a limiting factor (Avramova *et al.*, 2015*a*). For example, in drought stressed maize, it was shown that drought tolerant lines had higher antioxidant levels and higher activities of redox-regulating enzymes (catalase, peroxidase, ascorbate peroxidase and glutathione reductase) throughout the growth zone and especially in the meristem (Avramova *et al.*, 2017). In addition, a microarray study revealed the downregulation of 32 cell cycle genes under drought stress in the sampled meristematic tissue, which provided a basis in understanding the drought inhibited cell cycle (Avramova *et al.*, 2015*b*). For advanced molecular analyses (i.e. next-generation sequencing) it is important that the maize genome has been fully sequenced and annotated, allowing for easy transcriptome analyses (Schnable *et al.*, 2009).

Taken together, since to date no large-scale studies have been performed to investigate cadmium inhibited leaf growth in the monocot growth zone, the PhD study presented in this thesis employed the maize leaf growth zone as a model to study Cd inhibited leaf growth at the organ, cellular, biochemical and molecular level.

Chapter 2

leafkin – An R package for automated kinematic data analysis of monocot leaves

Jonas Bertels & Gerrit T.S. Beemster

Published in Quantitative Plant Biology:

Bertels J, Beemster GTS. 2020. leafkin — An R package for automated kinematic data analysis of monocot leaves. Quantitative Plant Biology **1**.
https://doi.org/10.1017/qpb.2020.3

Integrated Molecular Plant Physiology Research Group (IMPRES), Department of Biology, University of Antwerp, 2020 Antwerp, Belgium.

An R package for automated kinematic data analysis of monocot leaves.

Abstract

Growth is one of the most studied plant responses. At the cellular level, plant growth is driven by cell division and cell expansion. A means to quantify these two cellular processes is through kinematic analysis, a methodology that has been developed and perfected over the past decades, with in-depth descriptions of the methodology available. Unfortunately, after performing the lab work, researchers are required to perform time-consuming, repetitive and error-prone calculations. To lower the barrier towards this final step in the analysis and to aid researchers currently applying this technique, we have created *leafkin*, an R-package to perform all the calculations involved in the kinematic analysis of monocot leaves using only four functions. These functions support leaf elongation rate calculations, fitting of cell length profiles, extraction of fitted cell lengths and execution of kinematic equations. With the *leafkin* package, kinematic analysis of monocot leaves becomes more accessible than before.

Introduction

The effect of genetic modification and the impact of biotic or abiotic stress on plants is frequently evaluated by measuring growth. Growth is often quantified on whole plant (e.g. dry mass) or organ (e.g. root or leaf length) level (Erickson, 1976; Poorter and Garnier, 1996). However, it represents the combined result of two processes at the cellular level, i.e. cell division and cell expansion (Beemster *et al.*, 2003). Therefore, various studies have quantified these cellular processes, often linking them to data from biochemical and molecular assays for a more mechanistic understanding of different growth responses (Sprangers *et al.*, 2016). The importance of growth analysis at the cellular level is clearly demonstrated by a meta-study by Gázquez and Beemster (2017), who identified the regulation of the transition from cell division to cell expansion as the key cellular mechanism for organ size regulation.

Monocotyledonous leaves are ideally suited for the quantification of cell division and expansion, because they are linear, steady-state growing organs. This means that, for a certain period during their development, a growth zone with a stable meristem and elongation (expansion in longitudinal direction) zone size is present at the base of the leaf, resulting in an approximately constant leaf elongation rate (Schnyder *et al.*, 1990; Muller *et al.*, 2001). We consider the maize leaf an ideal model organ to study leaf growth regulation because it hosts a large growth zone, providing ample material for biochemical and molecular analyses in relation to cellular growth responses (Avramova *et al.*, 2015*c*).

The methods of plant growth analysis have made considerable progress over the past century. In the classical approach, which started to evolve in the 1920's (Blackman, 1919; West *et al.*, 1920), the relative growth rate is calculated by dividing the difference in ln-transformed plant weight over time (Poorter and Garnier, 1996). Two decades later, Sinnot (1939) pointed out that transparent root meristems could be studied under water immersion lenses, where drawings made at intervals from one to several hours allowed researchers to track cell division by the formation of new cell

walls and cell elongation by changes in cell sizes. Sinnott's publication was followed by the work of Goodwin & Stepka (1945) and Erickson & Sax (1956), who developed a more mathematical foundation for the determination of cell division and cell elongation rates by combining velocity fields and cell length profiles in roots. Later, in the late 1970's, early 1980's, the foundation for kinematic growth analysis was laid by applying equations from fluid dynamics to describe plant organs as linear structures with a flux of cells (or substances such as minerals) passing at each position determined by local velocity and density (Gandar, 1980; Silk, 1984; Silk & Erickson, 1979). Growth zones are composed of the meristem, a region of small dividing cells, and the elongation zone, where cells rapidly increase in cell size due to cell expansion. Cells are displaced by cell division and cell elongation until they stop growing and enter the mature part of the leaf.

The kinematic analysis for the study of organ growth has been adopted by a limited number of laboratories (summarised by Gázquez & Beemster (2017) and Sprangers *et al.* (2016)). In the past decade, a considerable effort was undertaken to make the methodology more accessible for non-specialised labs by detailed method descriptions for the kinematic analysis of roots and leaves (Rymen *et al.*, 2010; Nelissen *et al.*, 2013). Most recently, a video tutorial was published, demonstrating step by step how to perform a kinematic analysis on maize and other monocot leaves (Sprangers *et al.*, 2016). A significant difficulty that remains when performing this kinematic analysis on monocot leaves, is the processing of raw data and a correct application of mathematical equations involved. In our experience, the analysis of the acquired data can be daunting and the repetitive manual processing of a large number of measurements is error-prone.

To help novices with the application of a kinematic analysis on monocotyledonous leaves and to simplify and accelerate the work of researchers already employing this technique, we developed *leafkin*, a simple to use R-package, which performs all required calculations using only four functions. Once familiar with these four functions, time required for kinematic data analysis is reduced to a couple of minutes and human

errors in the analysis are avoided (e.g. selecting wrong cells in Excel), while errors in the input data are more easily identified (e.g. by inspecting cell length plots). Also, a user manual is provided as supplementary material (Supplementary File 2.1), which is accompanied by a full example dataset and tutorial script (available on https://github.com/impres-lab). These can be used to familiarize new users with the required datasets and *leafkin* functions, prior to analysing their own datasets.

In the methods section of this article, we describe the required datasets and the used methodology for each of the functions. In the results section, we illustrate the use and outcome of the functions, with special attention to parameter settings for more control on the generated output. In the discussion, we highlight the advantages and limitations of the package.

Methods

User manual

In the user manual (Supplementary File 2.1, presented at the end of the chapter), the practical steps of the kinematic analysis are introduced in more detail. It also provides a flowchart that illustrates the links between the collected data and *leafkin* functions. Hereafter, it provides more details on the requirements for, and installation of *leafkin*, followed by a step-by-step description of its use in the kinematic data analysis. Next, the manual discusses potential errors and provides additional information on tidy and wide data (data formats which are referred to in this article). Finally, all formulas used by the *leafkin* library are presented in the manual.

Practical steps of kinematic analysis

In short, in order to study the growth of a specific leaf at the cellular level by kinematic analysis, around 15 plants are required for each treatment/genotype to be studied. First, the length of the leaf is measured, starting after it emerges from the whorl of older leaves, usually on a daily basis. After tracking leaf growth for a couple of days (in maize: at least 3 days), 5 to 7 plants are dissected during the period of steady-state growth for microscopy, allowing the remainder of the plants to reach their final leaf length. During the dissection, the growth zone of the leaf of interest is isolated (e.g. the basal 10 cm of a maize leaf, i.e. starting where the leaves are attached to the stem). In this growth zone, meristem size (through DAPI staining of the nuclei) and cell length profiles are determined (Sprangers *et al*., 2016; Supplementary File 2.1).

Required datasets

The practical work results in three datasets, i.e. leaf lengths, cell lengths and meristem sizes, all of which are required by *leafkin*. The raw data can be entered in a spread sheet program (e.g. Microsoft Excel), but needs to be saved as tab-delimited text files. We advise to use this format because importing Excel files directly into R may transform date-times into numbers, rendering them unusable by the *leafkin* functions.

The leaf length data file requires a column with unique plant ID's, followed by multiple columns containing leaf length measurements, expressed in millimetres (Table 1A). The first row contains the headers, which should be *plant_id* for the first column, while the following column headers are in the date-time format *yyyy/mm/dd hh:mm* (or *yyyy/mm/dd hh:mm:ss*), indicating when measurements were made.

The cell length measurements should be organised in three columns (Table 1B). The first column (header = *plant_id*), holds the plant ID for each measurement. The second column (header = *position*) contains the position of the cell length measurements relative to the leaf base (in centimetres) and is followed by the cell lengths themselves (in micrometres) in the third column (header = *cell_length*). Cell length measurements of all plants are combined in these three columns.

The third file should contain the meristem size measurements (Table 1C). The first column (header = *plant_id*), contains the unique plant ID's, whereas the second column (header = *mer_length_um*), contains meristem sizes (in micrometres).

It is important to note that units and column names should be strictly respected. Also, plant ID's should be identical across all three files, since these are used to combine the data originating from the different measurements.

Table 1. Example data and column description for the datasets required for kinematic analysis using *leafkin.* A: Example of leaf length measurements data and column descriptions. B: Example of cell length measurements data and column descriptions. C: Example of meristem length measurements data and column descriptions. The types char, int and double refer to respectively characters (i.e. everything which includes letters, or numbers specified to be handled as letters), integers (i.e. numbers without decimals) and double (i.e. numbers which can contain decimals).

A. Leaf length measurements data and column descriptions

Example data

plant_id	2016/12/13 10:00	2016/12/14 10:00	2016/12/15 10:00	2016/12/16 10:16	2016/12/17 10:00
C.1	142	216	293		
C.2		142	212	296	
C.3		196	277	360	436
C.4		194	268	352	
…					

Column description

COL	HEADER	TYPE	BRIEF DESCRIPTION
1	plant_ID	char or int	Contains the plant ID for which leaf lengths were measured.
2-LAST	data time format yyyy/mm/dd hh:mm(:ss)	int or double	Contains leaf length measurements in millimetre on a certain day-time. Time can be in hh:mm or hh:mm:ss.

B. Cell length measurements data and column descriptions.

Example data

plant_id	position	cell_length
C.1	0.01	27.18
C.1	0.01	23.71
C.1	0.01	23.68
C.1	0.01	22.23
…	…	…

Column description

COL	HEADER	TYPE	BRIEF DESCRIPTION
1	plant_ID	char or int	Contains the plant ID for which cell lengths were measured.
2	position	int or double	Contains the position at which cell lengths were measured in centimetre.
3	cell_length	int or double	Contains cell length measurement in micrometre.

C. Meristem length measurements data and column descriptions.

Example data

plant_id	mer_length_um
C.1	12423
C.2	14792
C.4	12350
C.7	14568
…	…

Column description

COL	HEADER	TYPE	BRIEF DESCRIPTION
1	plant_ID	char or int	Contains the plant ID for which meristem lengths were measured.
2	mer_length_um	int or double	Contains the length of the meristem in micrometre.

Software requirements

The *leafkin* package works with R version 4.0.0 or higher (R Core Team, 2014). Windows users are advised to install Rtools40 (a toolchain bundle which aids building R packages locally) in order to install *leafkin* without warnings related to Rtools (https://cran.r-project.org/bin/windows/Rtools/). Installing RStudio, an integrated development environment for R, is recommended to increase the ease of use of R code (a free open source edition is available on https://rstudio.com/ (RStudio Team, 2015)).

Sample data, tutorial script and leafkin installation

A sample dataset and tutorial R-script are available on the IMPRES-lab GitHub page (https://github.com/impres-lab). Sample data originated from a kinematic analysis, performed in (Bertels *et al.*, 2020). We highly recommend first time users to download the sample data and tutorial script and use these in conjunction with the user manual (Supplementary File 2.1).

The *leafkin* package is maintained on the IMPRES-lab GitHub page. Prior to *leafkin* installation, the *install_github()* function from the *devtools* package is used to install *leafkin* directly from the GitHub repository (i.e. *devtools::install_github("impres-lab/leafkin")*, more details in the user manual, Supplementary File 2.1).

leafkin user functions

The user functions of the package are *calculate_LER()*, *get_pdf_with_cell_length_fit_plots()*, *get_all_fitted_cell_lengths()* and *kinematic_analysis()*. These four functions allow the user to perform all calculations needed to perform a kinematic analysis of monocotyledonous leaves.

calculate_LER()

calculate_LER() calculates the leaf elongation rate (LER, i.e. the length increase of a leaf per unit time in $mm \cdot h^{-1}$) for each plant using the leaf length measurements (formula 1) and will, by default, output the mean values for each plant using the first two time-intervals. The user can specify three parameters, i.e. *leaf_length_data*, *n_LER_for_mean* and *output*. *leaf_length_data* is the parameter to which the imported leaf length data have to be assigned. These leaf length data must be imported into R beforehand as a data.frame or tibble (a modern format of a data.frame). Next, *n_LER_for_mean* indicates how many intervals with corresponding LERs are to be used to calculate the mean LER (default = 2), starting from the first measurement. In case a number larger than the number of LERs available is specified, only the available intervals will be used (Table 2A and B). Finally, *output* determines the format of the output of the function. By default, *output* is set to *"means"*, causing the *calculate_LER()* function to return mean LER for each plant. However, the user can also choose to set the *output* parameter to *"tidy_LER"* and *"wide_LER"*, which will result in returning a tibble containing all calculated LERs, either in a tidy (Table 2C) or wide format, respectively (see user manual, Supplementary File 2.1, for more information on tidy and wide data formats). These can be used to visualise the LER over time (useful to check the steady-state assumption during the period used to calculate the average LER).

$$LER = \frac{LL_2 - LL_1}{t_2 - t_1} \qquad (1)$$

Leaf elongation rate formula (*LER*), with LL_x being the leaf length measurement x (in mm) and t_x being the time at which LL_x was taken (in data time format yyyy/mm/dd hh:mm(:ss)).

Typically, leaf lengths are measured once a day, however, using multiple measurements per day is also possible (note: in this case, consider increasing *n_LER_for_mean* to cover a sufficiently large time-interval). During LER calculation, the function skips time-points with missing measurements and adjusts the corresponding time-intervals accordingly, ensuring that the function can handle missing data (Table 2D). The calculated LERs and mean LERs are stored within the function and depending on how the user specified the *output* parameter, mean LERs or all LERs are returned.

Table 2. The output of the *calculate_LER()* function. **A.** The output of the *calculate_LER()* function with the number of LERs (*n_LER_for_mean*) set to 2, i.e. all plants have enough measurements to support the calculation of the LER mean. **B.** The output of the *calculate_LER()* function with the number of LERs (*n_LER_for_mean*) set to 4, i.e. plants harvested for microscopy analysis only have two LERs, though the function still correctly calculates the mean LER, while for plants with more measurements, the LER changes (small arrows) because more calculated LERs are incorporated in the mean value. **C.** The output of *calculate_LER()* with the *output* parameter set to *tidy_LER*, allowing access to the individually calculated LERs. **D.** Illustration of how the *calculate_LER()* function handles variable time intervals (i.e. not all 24h time intervals) and missing data. Notice how time intervals, growth intervals and LERs are corrected accordingly (full red arrows).

A

plant_id	mean_plant_LER [mm/h]
C.1	3.145833
C.10	3.1875
C.11	3.145833
C.2	3.208333
C.3	3.416667
C.4	3.291667
C.5	3.125
C.6	3.208333

B

plant_id	mean_plant_LER [mm/h]
C.1	3.145833
C.10	3.1875
C.11	3.239583
C.2	3.208333
C.3	3.364583
C.4	3.291667
C.5	3.09375
C.6	3.28125

C

plant_id	date_and_hour	leaf_length [mm]	time_hours [h]	growth_mm [mm]	LER [mm/h]
C.1	2016/12/13 10:00	142			
C.1	2016/12/14 10:00	216	24	74	3.083333333
C.1	2016/12/15 10:00	293	24	77	3.208333333
C.10	2016/12/14 10:00	157			
C.10	2016/12/15 10:00	229	24	72	3
C.10	2016/12/16 10:00	310	24	81	3.375
C.11	2016/12/14 10:00	151			
C.11	2016/12/15 10:00	221	24	70	2.916666667
C.11	2016/12/16 10:00	302	24	81	3.375
C.11	2016/12/17 10:00	382	24	80	3.333333333
C.11	2016/12/18 10:00	462	24	80	3.333333333

D

plant_id	date_and_hour	leaf_length [mm]	time_hours [h]	growth_mm [mm]	LER [mm/h]
C.1	2016/12/13 10:00	142			
C.1	2016/12/14 09:23	216	23.38333333	74	3.164647185
C.1	2016/12/15 08:16	293	22.88333333	77	3.364894392
C.10	2016/12/14 09:23	157			
C.10	2016/12/15 08:16		22.88333333		
C.10	2016/12/16 10:00	310	25.73333333	153	3.147068906
C.11	2016/12/14 09:23	151			
C.11	2016/12/15 08:16	221	22.88333333	70	3.058994902
C.11	2016/12/16 10:00		25.73333333		
C.11	2016/12/17 10:00		24		
C.11	2016/12/18 10:00	462	24	241	3.268535262

get_pdf_with_cell_length_fit_plots()

get_pdf_with_cell_length_fit_plots() is a function to smooth and interpolate cell length data (Rymen *et al.*, 2010) and evaluate the resulting fits. The function creates a pdf containing plots of fits (and first derivatives) in the working directory, together with the input cell length data (*fit_plots_using_bandwidth_multiplier_X.pdf*).

The *get_pdf_with_cell_length_fit_plots()* function requires the cell length data (*cell_length_data* parameter), which are to be imported beforehand in R as a data.frame or tibble. Next, the user can specify the *interval_in_cm*, *bw_multiplier* and *output_bw_tibble* parameters of the function. In absence of user specified values, defaults will be used. In short, *interval_in_cm* is the interval used to calculate fitted cell lengths (in centimetres, default = 0.1), *bw_multiplier* allows the user to manipulate the calculated bandwidth of the data (default = 1; a number between 0 and 1 will result in a stricter fit that more closely follows the raw data, whereas a number larger than 1 will increase the smoothing) and *output_bw_tibble* will return the calculated bandwidths in a tibble when set to TRUE (default = FALSE). The bandwidth, manipulatable by the bw_multiplier parameter, is calculated within the function using the dpill function of the KernSmooth package and determines the strictness of the fit based on the distribution of the input data (Ruppert *et al*. (1995)).

The created pdf-file with the plotted cell lengths and fit curves can be used to evaluate the cell length fits for each plant and to check the impact of a range of bandwidth multipliers on these fits. A good fit does not overly follow minor local variations in cell length, but closely fits the global profile (Figure 1B). When the *bw_multiplier* value is too low, e.g. 0.3, too much local variation is introduced in the fit, especially in the mature region, where cell length can be considered approximately constant (Figure 1A). Inversely, when the *bw_multiplier* value is too high, e.g. 3, oversmoothing occurs, particularly affecting fitted cell sizes in the meristem (Figure 1C).

In the created pdf file, also the calculated bandwidths for each individual plant are plotted in the final graph. If, for some plants, the function was unable to calculate the optimal bandwidth (for example when an insufficient number of cell length measurements was provided), there will be missing data in the bandwidth plot, the concerned cell length fit plots will yield no fit and a warning message will be printed in the console of RStudio. In this case, when extracting all the fitted cell lengths in the next step, an alternative bandwidth should be provided in the *get_all_fitted_cell_lengths()* function (see next section).

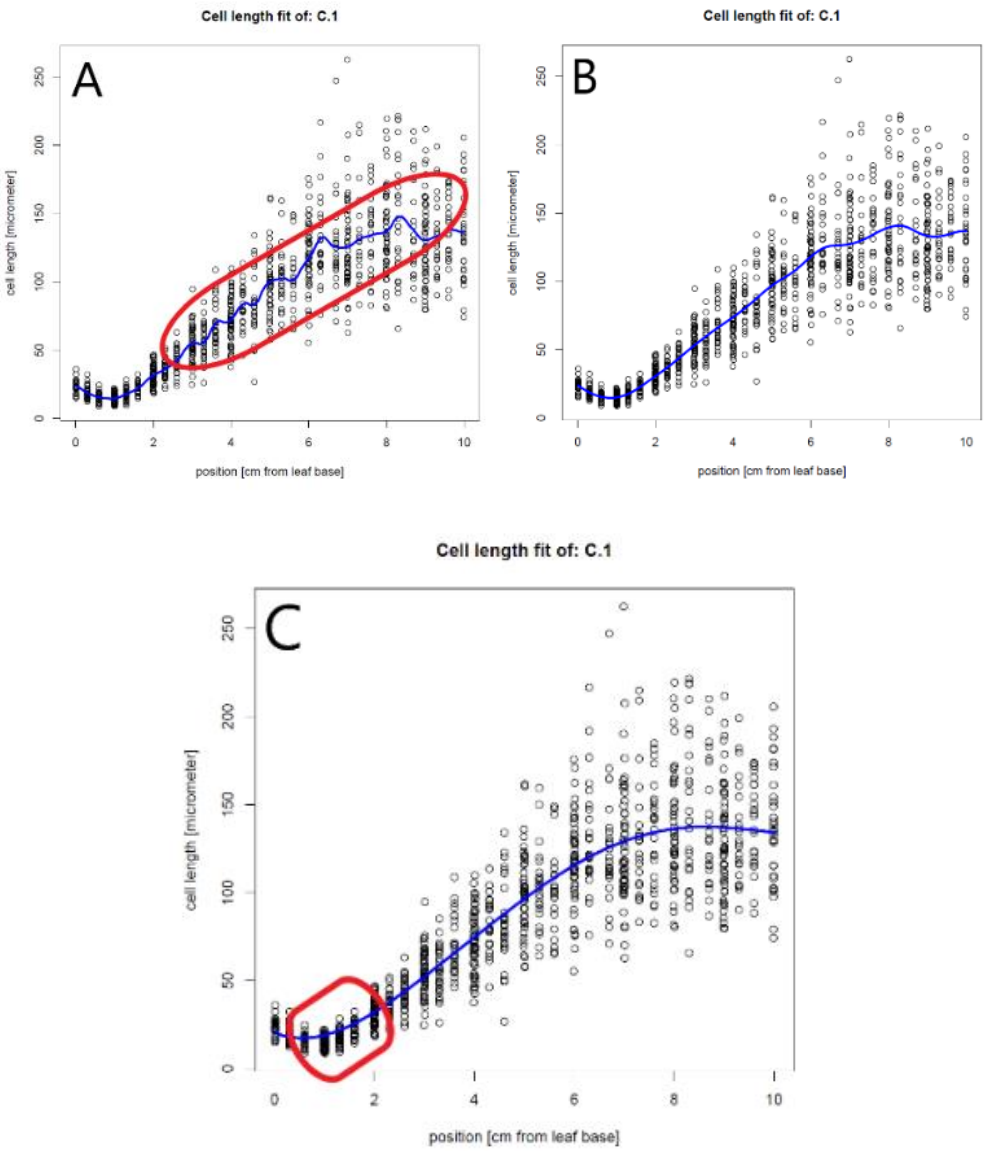

Figure 1. The effect of the bandwidth multiplier parameter on cell length fits. A. A very strict fit of the cell lengths by setting the *bw_multiplyer* to 0.3. A strict fit can result in too much variation in the fit (encircled in red). **B.** Fitted cell length data, using the calculated bandwidth (bandwidth multiplier = 1). **C.** A more loose fit of the cell lengths by setting the *bw_multiplyer* to 3. A loose fit can result in oversmoothing and thereby poor fitting of the cell sizes, especially at the end of the meristem (encircled in red) and/or the end of the growth zone.

get_all_fitted_cell_lengths()

The function *get_all_fitted_cell_lengths()* returns the fitted cell lengths throughout the growth zone, using the same method as the *get_pdf_with_cell_length_fit_plots()* function. It has some of the parameters with the same default and meaning as in the *get_pdf_with_cell_length_fit_plots()* function, i.e. *cell_length_data*, *interval_in_cm* and *bw_multiplier.* Additionally, it has the *alternative_bw* and *tidy_cell_lengths* parameter.

alternative_bw allows the user to set an alternative bandwidth which is used for plants for which no bandwidth could be calculated (default = 0.5). Users can determine this alternative bandwidth by using the output of the *get_pdf_with_cell_length_fit_plots()* (*output_bw_tibble* as TRUE), which will cause the function to return all calculated bandwidths. The mean of the returned bandwidths usually is a suitable alternative bandwidth.

Next, the *tidy_cell_lengths* parameter controls the output of the *get_all_fitted_cell_lengths()* function and is TRUE by default. This setting causes the function to return the fitted cell lengths in a tidy format, which is the format that is required as input for the *kinematic_analysis()* function. Setting *tidy_cell_lengths* to FALSE will return the cell lengths in a wide, more human readable, format.

kinematic_analysis

When mean LERs and fitted cell lengths for each plant are obtained, the kinematic analysis can be performed using the *kinematic_analysis()* function. The function requires the LER means output of the *calculate_LER()* function and tidy cell lengths output of the *get_all_fitted_cell_lengths()* function as input (as tidy tibbles), together with meristem sizes (*meristem_size_micrometre* parameter) as a data.frame or tibble. The meristem sizes should be imported into R beforehand. Hereafter, the function performs all the kinematic calculations for each plant present in the tidy cell lengths tibble. It is therefore necessary that these plants are also represented in the LER and meristem size data, where they need to have exactly the same plant ID's. For each

plant ID, the function collects the LER, cell lengths and meristem size. Hereafter, it performs all calculations involved in a kinematic analysis, previously described in detail (Rymen *et al.*, 2010; Nelissen *et al.*, 2013; Sprangers *et al.*, 2016). These calculations were implemented as functions (formulae 2-15) defined in the *functions_needed_by_kinematic_analysis.R* script inside the package.

$$L_{gz} = \min\left(position_{(cell\ size > P95_{cell\ size})}\right) \qquad (2)$$

The growth zone size (L_{gz}) is the first position where cell size exceeds the 95-percent value of the cell sizes (calculated using formula 14).

$$l_{mat} = \frac{\sum_{i=p}^{n} cell\ length_i}{n-p} \qquad (3)$$

The mature cell length (l_{mat}) is the average cell length between the first position after the growth zone (p) and the final measurement (n).

$$P = \frac{LER}{l_{mat}} \qquad (4)$$

The cell production rate (*P*) is calculated by dividing the leaf elongation rate (*LER*) by the mature cell length l_{mat}.

$$N_{mer} = CCN_i + \left((CCN_{i+1} - CCN_i) \times (L_{mer} \bmod interval\ size)\right) \qquad (5)$$

The number of cells in the meristem (N_{mer}) is determined by the cumulative cell number (CCN) at position *i*, where *i* is the last position which is still located within the meristem size, plus the difference in CNN between position *i* and *i+1*, multiplied by the meristem length (L_{mer}) modulo interval size (CNN is calculated using formula 15).

$$l_{mer} = cell\ length_i + \left((cell\ length_{i+1} - cell\ length_i) \times (L_{mer} \bmod interval\ size)\right) \qquad (6)$$

The length of the cells leaving the meristem (l_{mer}) is determined by the cell length at position *i*, where *i* is the last position which is still located within the meristem size, plus the difference in cell length between position *i* and *i+1*, multiplied by the meristem length (L_{mer}) modulo interval size.

$$N_{gz} = CCN_i \qquad (7)$$

The number of cells in the growth zone (N_{gz}) is equal to the cumulative cell number at position *i*, where *i* is the position at which the length of the growth zone L_{gz} was determined.

$$N_{el} = N_{gz} - N_{mer} \qquad (8)$$

The number of cells in the meristem (N_{mer}) is determined by subtracting the number of cells in the growth zone (N_{gz}) by the number of cells in the meristem (N_{mer}).

$$D = \frac{P}{N_{mer}} \qquad (9)$$

The average cell division rate (D) is determined by dividing the cell production rate (P) by the number of cells in the meristem (N_{mer}).

$$T_c = \frac{\ln 2}{D} \qquad (10)$$

The cell cycle duration (T_c) is determined by dividing the natural logarithm of 2 by the average cell division rate (D).

$$T_{el} = \frac{N_{el}}{P} \qquad (11)$$

The time in the elongation zone (T_{el}) is determined by dividing the number of cells in the elongation zone (N_{el}) by the cell production rate (P).

$$T_{div} = \log_2 N_{mer} \times T_c \qquad (12)$$

The time cells spend in the meristem (division zone, T_{div}) is determined by the log2 of the number of cell in the meristem (N_{mer}) multiplied by the cell cycle duration (T_c).

$$R_{el} = \frac{\ln l_{mat} - \ln l_{div}}{T_{el}} \qquad (13)$$

The relative cell elongation rate (R_{el}) is determined by the difference in the natural logarithm of mature cell length (l_{mat}) and the natural logarithm of the lengths of the cells leaving the meristem (l_{div}), divided by the time cells spend in the elongation zone (R_{el}).

$$P95_p = 0.95 \times \frac{\sum_{i=p}^{n} cell\ length_i}{n-p} \qquad (14)$$

The 95-percent value (P95) formula is used internally by the kinematic analysis function at every position (p) and multiplies 0.95 by the mean cell length for cell sizes starting at the current position up until the last determined cell length (n).

$$CCN_p = CCN_{p-1} + \frac{position_p - position_{p-1}}{\left(\frac{cell\ length_{p-1} + cell\ length_p}{2}\right)} \qquad (15)$$

Cumulative cell number (*CCN*) is a formula used internally by the kinematic analysis function to determine the cumulative number of cells at every position (*p*) by adding the cumulative cell number in the previous interval to the estimated number of cells in the current interval. The number of cells in the current interval uses the current and previous position to determine the size of the interval, which is divided by the average cell length in this interval (calculated by using the current and previous cell size).

Situational errors

In order to address errors or difficulties users are experiencing, inherent to the use of R and data files, we maintain an overview of user specific errors/difficulties and how to cope with them in the README.md file of the *leafkin* repository on the IMPRES-lab GitHub page.

Results

With the aim of making kinematics data analysis more accessible, we illustrate the use of the *leafkin* package on a recently published data set that was obtained in an experiment where maize seedlings were exposed to a control, a mild (46.5 mg Cd · kg^{-1} dry soil) and a severe (372.1 mg Cd · kg^{-1} dry soil) cadmium treatment, resulting in an inhibition of leaf elongation rate by 24 and 46%, respectively (Bertels *et al.*, 2020). The data are provided as a set of tab-delimited text files on the IMPRES-lab GitHub page (https://github.com/impres-lab). Plant IDs include reference to the treatments: control (C), mild (M) and severe (S), respectively. The treatment identifier is followed by the plant number. Together with these data, a tutorial script is provided on the IMPRES-lab GitHub, which, in conjunction with the user manual (Supplementary File 2.1), will quickly familiarize the user with the dataset structure and the possibilities of the *leafkin* package.

The analysis of kinematics data first involves the processing of leaf length measurements to obtain leaf elongation rates. Then, cell length data, obtained from the microscopy study, are analysed and processed in order to obtain the smoothed and interpolated cell length profile for each plant. Finally, the leaf elongation rates, estimated cell length profiles and meristem sizes are used to perform the kinematic analysis for individual plants.

Calculating average LERs

Leaf elongation rates are calculated using *calculate_LER()*. In maize, we typically dissect leaves three days after they have emerged from the whorl of older leaves, yielding three daily leaf length measurements. The remaining plants were tracked until they reached their final leaf length and have more measurements. For the dissected plants, the first three leaf length measurements can be used to calculate 2 LERs. For this reason we set *n_LER_for_mean* equal to 2 (default value) and *output* to “means” (default value), which causes the *calculate_LER()* function to use only the first two LERs to calculate the mean LER of each plant and return it (Table 2A).

Evaluating the fitting of cell length profiles

Individual cell length measurements and their position (see file description in methods) are used to determine the fitted cell length at every interval location along the leaf axis. Before extracting the fitted cell lengths (in the next step), the quality of the fit should be evaluated using the *get_pdf_with_cell_length_fit_plots()* function. This function creates a pdf file containing plots of all fitted cell lengths and their first derivatives in the working directory. Inspecting these plots allows assessment of the quality of the fit. For the interval parameter, we have set *interval_in_cm* to 0.1 cm, which resulted in cell lengths estimated at every millimetre. The default bandwidth multiplier of 1 (*bw_multiplier* parameter) resulted in a good fit (Figure 1B). Using the default bandwidth is advised to rule out subjectivity. However, some profiles, especially those with very short meristems, might require a tighter fit, hence the possibility to manipulate the fit. Lastly, the absence of a warning message and presence of a fitted cell length profile in all plots indicates that all bandwidths were successfully calculated.

Fitting cell length profiles

After checking the fitted cell lengths profiles, we retrieve the fitted cell lengths using the *get_all_fitted_cell_lengths()* function. For this, we use the same cell length measurements and parameter settings as in the *get_pdf_with_cell_length_fit_plots() function*. If needed, the mean of the calculated bandwidths can be used in the *alternative_bw* parameter if some bandwidth calculations failed. After running the function, the resulting fitted cell lengths are stored (as a tidy tibble) for use in the *kinematic_analysis()* function. Besides the use of these cell lengths in the *kinematic_analysis()* function, this data can also be used to calculate and plot average cell length profiles with error bars (Figure 2).

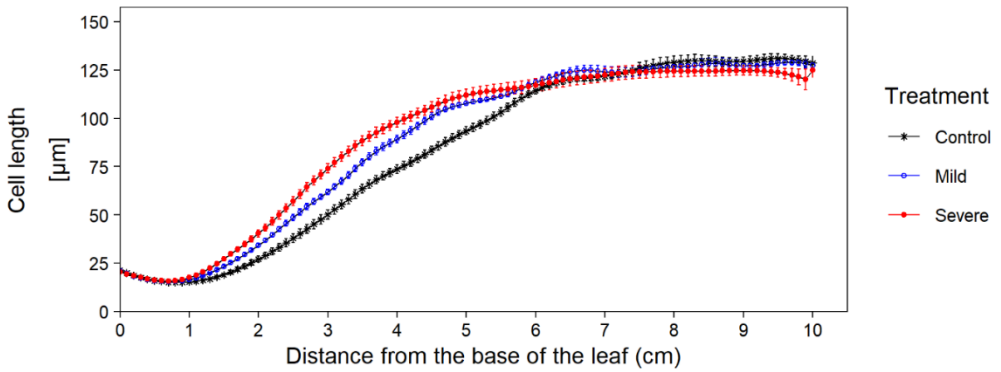

Figure 2. Averages of fitted cell length profiles for three cadmium treatments. Data originates from the sample dataset in which we analysed leaf growth of B73 plants, grown in control and cadmium spiked potting soil (mild and severe treatment), (Bertels *et al.*, 2020). This graph illustrates the added advantage of being able to plot cell length curves, since this plot illustrates that mature cell length is not affected by our treatment, however the growth zone size is affected (i.e. under cadmium conditions, cells reach their mature cell length closer to the base of the leaf). The code to recreate this plot is available in the tutorial R-script (https://github.com/impres-lab).

Kinematic analysis

Using the mean LERs and fitted cell length profiles for each plant obtained in the previous steps, combined with the measured meristem sizes, we next perform the actual kinematic analysis using the *kinematic_analysis()* function. Using this function, we perform all kinematic calculations simultaneously and obtain the results for the following parameters in a tibble: leaf elongation rate (LER, $mm \cdot h^{-1}$), length of the meristem (mm), length of the elongation zone (mm), length of the growth zone (mm), length cells leaving meristem (µm), mature cell length (µm), number of cells in meristem, number of cells in elongation zone, number of cells in total growth zone, cell production rate ($cells \cdot h^{-1}$), cell division rate ($cells \cdot cell^{-1} \cdot h^{-1}$), relative cell elongation rate ($\mu m \cdot \mu m^{-1} \cdot h^{-1}$), cell cycle duration (h), time cells spend in the meristem (h), time cells spend in the elongation zone (h) (Table 3A). Note that the LERs presented in this tibble are only the LERs of the plants involved in the microscopy study (i.e. the plants on which the kinematic analysis was performed). With the kinematic analysis completed, the results can be presented in a table, summarising the values as means plus standard error, whilst comparing treatments, genotypes, etc. as percentages compared to the reference treatment (Table 3B).

Table 3. Kinematic analysis output. A. Kinematic analysis data in R from individual plants after running the *kinematic_analysis()* function. **B.** Statistically processed kinematics data, as an illustration on how the final data set after analysis in R can be presented (Bertels *et al.*, 2020). Data shown are mean values plus standard error, where the percentage in the right column indicates differences relative to the control treatment, where an * indicates a significant difference ($p < 0.05$).

A.

plant_id	LER	meristem_size	length_of_growth_zone	…	length_of_cells_leaving_meristem	relative_cell_elongation_rate
C.1	3.145833	12423	72	…	17.00895	0.045889
C.10	3.1875	15500	82	…	19.02419	0.044031
C.2	3.208333	14792	66	…	17.56982	0.050553
C.4	3.291667	12350	62	…	18.24741	0.054594
C.7	3.125	14568	71	…	18.79564	0.049643
…	…	…	…	…	…	…

B.

Parameter	Control	Mild	Severe	Percentage change in Mild/Severe stress
Final leaf length (mm)	761 ± 16	634 ± 26	576 ± 47	-17* / -24*
Leaf elongation rate (mm·h^{-1})	3.23 ± 0.03	2.47 ± 0.05	1.74 ± 0.07	-24* / -46*
Length of the meristem (mm)	14.3 ± 0.7	12.2 ± 0.5	10.6 ± 0.5	-15* / -26*
Length of the elongation zone (mm)	56 ± 3	51 ± 3	48 ± 4	-8 / -14
Length of the growth zone (mm)	70 ± 3	64 ± 3	59 ± 4	-10 / -16
Length cells leaving meristem (µm)	18.0 ± 0.4	18.7 ± 0.4	18.5 ± 0.6	+4 / +3
Mature cell length (µm)	129 ± 3	127 ± 2	123 ± 3	-2 / -4
Number of cells in meristem	873 ± 43	720 ± 36	618 ± 32	-17* / -29*
Number of cells in elongation zone	999 ± 22	881 ± 31	829 ± 47	-12 / -17*
Number of cells in total growth zone	1872 ± 52	1602 ± 24	1448 ± 46	-14* / -23*
Cell production rate (cells·h^{-1})	25.0 ± 0.7	19.6 ± 0.4	14.2 ± 0.2	-21* / -43*
Cell division rate (cells·cell^{-1}·h^{-1})	0.029 ± 0.002	0.028 ± 0.001	0.023 ± 0.002	-5 / -19
Relative cell expansion rate (µm·µm^{-1}·h^{-1})	0.049 ± 0.002	0.043 ± 0.002	0.033 ± 0.002	-13 / -33*
Cell cycle duration (h)	24 ± 1	26 ± 1	30 ± 2	+5 / +25*
Time cells spend in the meristem (h)	238 ± 15	242 ± 13	282 ± 20	+2 / +19
Time cells spend in the elongation zone (h)	40 ± 2	45 ± 2	58 ± 3	+12 / +45*

Discussion

Kinematic analysis allows to relate spatial-temporal variations in rates of cell division and/or expansion to growth of different types of plant organs. These analyses have been adapted to the growth pattern of specific organs, but generally their application involves laborious, manual image analysis and data processing. This has presumably hampered their wider use. A number of tools have been developed to automate the image analysis of time-lapse images of growing root tips, allowing the analysis of cell expansion profiles (Walter *et al.*, 2002; van der Weele *et al.*, 2003) and the extraction of cell size distributions along an axis (Pound *et al.*, 2012) or in 3D structures (Pound *et al.*, 2012; Barbier de Reuille *et al.*, 2015), based on which dynamics of cell division and expansion can be determined. Although kinematic analyses of cell division and expansion along the axis of root tips (Goodwin and Stepka, 1945; Erickson and Sax, 1956) and monocotyledonous leaves (Volenec and Nelson, 1981; Schnyder and Nelson, 1987) have been performed for decades, to our knowledge, no tools have been developed to automate the kinematic analysis of this type of organ.

To address this, the *leafkin* package provides a user-friendly automation of the workflow of the kinematic analysis of monocotyledonous leaf growth and makes this analysis more accessible and reproducible than before. In combination with recent publications describing in detail the practical methodology (Rymen *et al.*, 2010; Nelissen *et al.*, 2013; Sprangers *et al.*, 2016), this package provides an additional tool to facilitate this analysis. It provides several benefits:

The analysis of LER not only provides the basis for the kinematic analysis of cell division and expansion, but can also be used independently to analyse longitudinal growth dynamics of monocotyledonous leaves (and other linear growing organs such as coleoptiles, hypocotyls, stem internodes, root tips) based on length data in function of time. The use of the *calculate_LER()* function omits the tedious task of calculating all time intervals and corresponding leaf elongation rates for each plant and allows for easy processing afterwards in R. The automated calculation of leaf elongation rates

and time intervals is particularly useful when, for some plants, data is missing, and growth and time intervals have to be adjusted accordingly (Table 2D).

Concerning cell length profiles, the user immediately obtains an overview of all cell length plots in one file for easy screening of the quality of the fit (using the *get_pdf_with_cell_length_fit_plots()* function), where in the past, these plots would have been created individually. Also, all the fitted cell lengths are created at once and can immediately be stored in one tibble after running the *get_all_fitted_cell_lengths()* function, which allows the user to easily create cell length plots and visualise differences in meristem size, growth zone size, cell elongation and mature cell length (Figure 2).

Once mean LERs and cell length fits are obtained, the next step is to combine the calculated LERs with the fitted cell length profiles and meristem sizes and perform the same set of calculations for each plant in the experiment. Using the *kinematic_analysis()* function, all these calculations are automatically performed for all plants at once, where a manual analysis would have taken significantly longer (e.g. for the example experiment, manual analysis would take an entire day, where calculation through the *leafkin* package would be finished under an hour (incl. data file preparation and quality control)). Next to time saving, manual data processing creates room for human error, where the use of the package prevents this.

Finally, and most importantly, using the package does not require in-depth knowledge of the underlying mathematics, making kinematics available for a broader audience of molecular and developmental biologists.

Critical remarks

The *calculate_LER()* automatically calculates mean LERs using a given number of calculated LERs, starting from the first LERs available for each plant. We have opted for this because, in our experience with rice and maize, the growing leaf is in its steady-state growth (i.e. when leaf elongation rates and cell length profiles are approximately stable for a significant period) when it emerges from the whorl of older leaves and it

maintains this quasi constant growth rate for several days. However, it is worthwhile to inspect the LER curve of the leaf over time to verify that its growth is approximately steady at the start of the leaf length measurements for other species and treatments. Setting the *output* parameter to *tidy_LER* and plotting the LERs over time will allow this. When, in the species of interest, steady-state growth occurs later, the individually calculated LERs can be used to calculate the appropriate steady-state mean LERs outside the package (set the *output* parameter of *calculate_LER()* function to *tidy_LER*). These means can then be provided as a tidy tibble by the user to the *kinematic_analysis()* function. If no steady-state is observed (e.g. the LER progressively decreases after emergence), then the LER calculated over the first time-interval is the best approximation. Incorporating non-steady-state behaviour requires additional time points for the cellular analysis to include time-dependent changes in the cell length profile in the kinematic equations (Silk, 1992; Beemster and Baskin, 1998). This is currently not supported by the *leafkin* package. For non-steady growing situations, including coleoptiles, hypocotyls and stem internodes, *calculate_LER()* and *get_all_fitted_cell_lengths()* are still useful for whole organ growth analysis and obtaining cell length profiles respectively. However, violation of the steady-state assumption and in case of coleoptiles and hypocotyls, the absence of a cell division zone, *kinematic_analysis()* is not suitable for the calculation of cellular parameters for these organs.

Automated data analysis cannot overcome mistakes in data collection and entry. The functions do check the input for structure and data format, but not whether the provided values make sense. It is therefore the responsibility of the user to monitor the quality of the data used. When, for instance, the cell length plots for a particular leaf do not look fluent, it is worth comparing the cell length profile and obtained kinematic results with other leaves in the same experiment, to evaluate their reliability. Also, the cause for outliers in the results of one or more parameters for a specific plant can potentially be revealed by evaluating the input data and cell length fits.

Finally, as a general note on the kinematic analysis of monocot leaves: the kinematic analysis described here is based on epidermal cell length measurements and meristem sizes determined by observing DAPI stained nuclei in the epidermis. The kinematic analysis therefore intrinsically represents the organ as a longitudinal file of cells of a well-defined cell type, in our case epidermal pavement cells located adjacent to stomatal files. Molecular, metabolite and other analyses of the corresponding zones can provide important insight into the underlying regulation of cell division and expansion (summarised by Sprangers *et al.*, 2016). However, when whole tissue analyses (e.g. flow cytometry and qPCR) are used and related to meristematic activity, small discrepancies can be observed when compared to the meristem size estimation in the kinematic analyses (based on DAPI stained nuclei of epidermal cells only). Specifically, epidermal cells in the monocot leaf growth zone are known to transition to cell elongation while underlying cell types are still undergoing cell division (Tardieu *et al.*, 2000; Huybrechts *et al.*, 2020; Bertels *et al.*, 2020). This should be taken into account when zone sizes, obtained through a kinematic analysis, are used to situate results of whole tissue analyses.

Conclusion

Kinematic analysis already exists for nearly a century (Goodwin and Stepka, 1945). The technique has been used extensively to investigate cell division and expansion in root tips (Gázquez and Beemster, 2017) and the technique has progressively been finetuned (Rymen *et al.*, 2010; Nelissen *et al.*, 2013; Sprangers *et al.*, 2016). With the *leafkin* package, we provide a tool for the automation of kinematic data analysis for monocotyledonous leaves. Raw data can be processed significantly faster and with less room for human error. Moreover, separate parts of the package can be of use. For example, the *calculate_LER()* function can be used to automatically calculate LERs for large sets of plants. Through providing a limited set of functions, in addition to the already extensively described methodology, we believe that *leafkin* makes kinematic analysis of monocotyledonous leaves more accessible than before, which can result in a more widespread and frequent application of this technique to rigorously quantify the cellular basis of leaf growth.

Acknowledgements

We would like to thank the members of the IMPRES research group and master students of the biology master program (Antwerp University) for testing the library and providing feedback.

Author contributions

J.B. wrote the manuscript, created the tables and figures and created the *leafkin* package and tutorial script. G.B. supervised the work and edited the manuscript.

Financial support

This work was supported by the Research Foundation Flanders (FWO) by project funding for J.B. [G0B6716N].

Conflicts of Interest

None.

Data and Coding Availability Statement

The *leafkin* package, sample data and tutorial script are available on the IMPRES lab GitHub page, https://github.com/impres-lab .

Chapter 3

Cadmium inhibits cell cycle progression and specifically accumulates in the maize (*Zea mays* L.) leaf meristem

Jonas Bertels[1], Michiel Huybrechts[2], Sophie Hendrix[2], Lieven Bervoets[3], Ann Cuypers[2], Gerrit T.S. Beemster[1]

Published in Journal of Experimental Botany:

Bertels J, Huybrechts M, Hendrix S, Bervoets L, Cuypers A, Beemster GTS. 2020. Cadmium inhibits cell cycle progression and specifically accumulates in the maize leaf meristem. Journal of Experimental Botany **71**, 6418–6428.
https://doi.org/10.1093/jxb/eraa385

[1] Laboratory for Integrated Molecular Plant Physiology Research (IMPRES), University of Antwerp, Groenenborgerlaan 171, 2020 Antwerpen, Belgium

[2] Centre for Environmental Sciences (CMK), Hasselt University, Agoralaan Building D, 3590 Diepenbeek, Belgium

[3] Systemic Physiological and Ecotoxicological Research (SPHERE), University of Antwerp, Groenenborgerlaan 171, 2020 Antwerpen, Belgium

Abstract

It is well known that cadmium (Cd) pollution inhibits plant growth, but how this metal impacts leaf growth processes at the cellular and molecular level is still largely unknown. In the current study, we show that Cd specifically accumulates in the meristematic tissue of the growing maize leaf, while Cd concentration in the elongation zone rapidly declines as the deposition rates diminish and cell volumes increase due to cell expansion. A kinematic analysis shows that, at the cellular level, a lower number of meristematic cells together with a significantly longer cell cycle duration explain the inhibition of leaf growth by Cd. Flow cytometry analysis suggests an inhibition of the G1/S transition, resulting in a lower proportion of cells in the S-phase and reduced endoreduplication in expanding cells under Cd stress. Lower cell cycle activity is also reflected by lower expression levels of key cell cycle genes (*putative wee1*, *cyclin-B2-4* and *minichromosome maintenance4*). Cell elongation rates are also inhibited by Cd, which is possibly linked to the inhibited endoreduplication. Taken together, our results complement studies on Cd-induced growth inhibition in roots and link inhibited cell cycle progression to Cd deposition in the leaf meristem.

Introduction

At the cellular level, plant growth is driven by cell proliferation and cell expansion. Cell proliferation, rather than cell expansion, determines the final size of organs, as shown by the meta-analysis performed by Gázquez and Beemster (2017). Abiotic stress often causes plants to grow at a slower rate by inhibiting cell division and expansion to varying degrees. For instance, under severe drought stress, maize leaf elongation rate was reduced by 63%, which could partially be explained by an increased cell cycle duration of 84% (Avramova *et al.*, 2015*b*). Also, Kavanová *et al.* (2006) showed that phosphorus deficiency reduced leaf elongation rate by 39% due to decreases in the cell production rate and final cell length. In Arabidopsis, West *et. al.* (2004) showed that salt stress resulted in reduced growth of roots due to a decrease in cell production and mature cell size.

After cells have stopped proliferating, they grow in size, further increasing organ size. In roots, monocotyledonous leaves and hypocotyls, this elongation mainly occurs along the longitudinal axis due to the transverse orientation of the cellulose microfibrils (Green, 1962; Crowell *et al.*, 2011). The increase in cell size is typically accompanied by endoreduplication (Sugimoto-Shirasu and Roberts, 2003). During endoreduplication, cells alternate between G1 and S-phases, skipping mitosis, doubling their genome with each completed S-phase (Sugimoto-Shirasu and Roberts, 2003). Endopolyploidy in plants can also be affected by abiotic stress, where plants typically increase endopolyploidy levels as an adaptive, plastic response to mitigate the effects of stress, as reviewed by Scholes and Paige (2015).

We use the maize leaf model system to study the impact of abiotic stress on organ growth because it allows to combine analyses at cellular, molecular and biochemical levels at high spatial resolution (Avramova *et al.*, 2015*c*). Maize leaf growth is driven by linearly organized growth processes: cell division in the meristem (i.e. a pool of continuously dividing cells, occurring at the base of the leaf typically in the first 1 to 2 centimetres) and cell elongation in the elongation zone (occurring directly apical of the

meristem and typically extending over 4 to 6 centimetres) (Avramova *et al.*, 2015*b*). When cells have reached their mature cell length, they enter the mature zone and form the emerged part of the blade. The longitudinal separation of these developmental stages allows sampling of dividing and elongating cells from a single leaf (Nelissen *et al.*, 2013). Moreover, the size of the maize leaf yields sufficient amounts of tissue for each of these developmental stages for biochemical and molecular analyses, making it an ideal plant system for these analyses (Avramova *et al.*, 2015*c*).

Industrial activities and the use of phosphate fertilizers have caused cadmium (Cd) disposition and accumulation on large surfaces across the world (Nagajyoti *et al.*, 2010). Though Cd is nonessential, plants take up this metal through transporters for essential bivalent cations such as calcium, iron and zinc (Verbruggen *et al.*, 2009). Being a non-redox active metal, Cd may cause oxidative stress indirectly by perturbing the plants' reactive oxygen species (ROS) metabolism (e.g. by inhibiting enzymes which function in antioxidative defence mechanisms (Cuypers *et al.*, 2010)). Despite the extensive antioxidant defence system of plants (Cuypers *et al.*, 2012), Cd stress may inhibit growth by causing ROS induced DNA damage (Hendrix *et al.*, 2018; Huybrechts *et al.*, 2019), impaired cell wall metabolism (Loix *et al.*, 2017), mitotic aberrations (Fusconi *et al.*, 2007; Silva *et al.*, 2013) and inhibited photosynthesis and respiration (Bi *et al.*, 2009).

The impact of Cd on growth and more specifically the cell cycle is mostly studied in synchronised cell cultures and roots that are directly exposed to Cd treatments, as recently reviewed by Huybrechts *et al.* (2019). These studies mainly report a halted cell cycle at G1/S and G2/M transitions. However, studies on how Cd impacts the growth of plant organs that are not directly exposed, especially leaves, are limited.

Therefore, the aim of our research is to determine the mechanism(s) by which Cd inhibits leaf growth, using the maize leaf as a model system. Our 2 key research questions are: 1. Does Cd reach the leaf growth zone and hence directly affect dividing

and elongating cells in the growing maize leaf and 2. What is the cellular basis of Cd inhibited leaf growth in maize (i.e. inhibition of cell division and/or cell elongation)? To tackle these research questions, we used a holistic approach, integrating data at the biochemical (i.e. mineral analysis), cellular (i.e. kinematic analysis and flow cytometry) and molecular level (i.e. gene expression analysis). Through this approach we show that Cd accumulates in the division zone of the leaf, where it inhibits cell cycle progression. Cd deposition continues in the elongation zone, where cell elongation rates are reduced, possibly due to an inhibition of the endocycle.

Material and Methods

Seeds, soil preparation and growth conditions

We grew maize plants (*Zea mays* L.*,* B73 inbred line, obtained from the North Central Regional Plant Introduction Station) in a growth chamber under controlled conditions (16-h day/8-h night, 25°C/18°C day/night, 200 $\mu mol \cdot m^{-2} \cdot s^{-1}$ photosynthetically active radiation, provided by high-pressure sodium lamps).

Peat potting medium (57% soil water content, Jiffy Products International B.V., The Netherlands) was spiked with 10 ml distilled water (control treatment) or 10 ml $CdSO_4$ solutions ($3CdSO_4 \cdot 8H_2O$, prepared in distilled water, Table 1). A fixed mass (650 grams) of potting medium was used for each individual pot (2.0L) to which the solutions were added dropwise under continuous mixing with a kitchen mixer (Kenwood kMix KMX50). Immediately after soil preparation, seeds were planted and the pots were placed in the growth room, covered with plastic wrap until germination. Pots were watered daily with tap water to maintain the original soil water content.

Table 1. Cd concentrations used in the experiments. Six different Cd doses were used for dose-response experiments, of which 3 treatments were selected for the detailed analyses in subsequent experiments.

Selected treatments (subsequent experiments)	Cadmium concentration in the 10 ml spiking solutions (mmol/l)	Cadmium concentration in wet soil (mg Cd / kg wet soil)	Cadmium concentration in dry soil (mg Cd / kg dry soil)
Control	**0**	**0**	**0**
Mild	**11.6**	**20**	**46.5**
	23.1	40	93.0
	46.3	80	186.0
Severe	**92.5**	**160**	**372.1**
	115.7	200	465.1
	138.8	240	558.1

Dose-Response and treatment selection

We determined leaf elongation rate and final leaf length of the fifth leaf of plants exposed to 6 Cd concentrations and a control treatment. To this end, leaf length was measured daily with a ruler from its emergence from the whorl of older leaves until it reached maturity and stopped growing. Leaf elongation rate was determined using the first 4 leaf length measurements of each plant, when growth was approximately steady-state.

Based on the dose-response, 3 treatments were selected for use in the subsequent experiments: a control, a mild (46.5 mg Cd · kg^{-1} dry soil) and a severe treatment (372.1 mg Cd · kg^{-1} dry soil). At 24 days after sowing, plants subjected to these treatments show a clear difference in size (Supplementary Figure 3.1).

Cadmium mineral analysis

We determined Cd concentrations in one-centimetre segments sampled along the maize leaf growth zone (i.e. 10 centimetres in total) and included a blade segment (middle of the remaining blade). Fresh weight of the sampled leaf segments was measured (AX124, Sartorius, Göttingen, Germany), after which they were oven-dried at 60 °C for 48 to 72 hours. Hereafter, segments from the same position and treatment were pooled (2-3 segments per pool). Sample digestion was performed by an overnight predigestion in aqua regia (1:3 nitric acid and hydrochloric acid), followed by 20 minutes high pressure high temperature digestion (Discover SP-D, CEM, Matthews, NC, USA), allowing the samples to boil at 200 °C. The samples were then diluted 40 times with trace metal grade ultrapure water, after which the Cd concentration was measured with high resolution inductively coupled plasma mass spectrometry (Element XR, Thermo Scientific, Bremen, Germany). We used blanks to correct for background trace metals and Rye grass European Reference Material CD281 samples as a reference.

Kinematic analysis

We performed a kinematic analysis on the fifth leaf as described by Sprangers *et al.* (2016). After the emergence of the fifth leaf from the whorl of older leaves, its length was measured daily with a ruler. Leaf elongation rate was determined using the first 3 leaf length measurements of each plant. Three days after emergence, 6 plants of each treatment (i.e. control, mild and severe, as determined in the dose-response experiment) were dissected for cell length and meristem size measurements, while the remaining plants (n = 4 to 5) were used to further measure growth until the final leaf length was reached. Cell length measurements (epidermal pavement cells directly adjacent to stomatal files) along the longitudinal axis of the leaf were performed on 1 centimetre sections that were fixed overnight in 70% ethanol and cleared, stored and mounted on slides in lactic acid. Cells were visualized using differential interference contrast microscopy (Zeiss Axio Scope.A1 microscope, Oberkochen, Germany) at 40x magnification and the length of abaxial epidermal cells adjacent to stomatal cell rows was determined using the online measurement module in the Axiovision software (Rel. 4.8, Zeiss). Leaf meristem size was determined using fluorescence microscopy of DAPI-stained (1 µg/ml 4',6-diamidino-2-phenylindole (DAPI) staining solution) leaf sections at 20x magnification by locating the most distal mitotic figure in epidermal pavement cells.

Cadmium flux and deposition

To determine the uptake of Cd along the growth zone we calculated Cd deposition rates using a kinematic approach combining velocity profiles with Cd concentrations in function of position along the growth zone (Meiri *et al.*, 1992). First, we determined cell flux, which is the number of cells passing by at a certain location per unit time. Cell flux outside the meristem was obtained by dividing leaf elongation rate by mature cell length. Inside the meristem, cell flux was set to zero at the base of the meristem, with a linear increase towards the end of the meristem, where cell flux equals the constant cell flux outside the meristem. Then, the velocity profile was obtained by multiplying local flux rates with local cell lengths and smoothed and interpolated using the locpoly

function of the KernSmooth package according to Rymen *et al.* (2010). This fit also yields the derivative of the velocity profile that corresponds to local relative cell expansion rates. Finally, the velocity in the middle of each segment was multiplied by the Cd concentration of the same segment and corrected for segment length and number of plants in the pooled sample, yielding the Cd flux. To retain the variance in the velocity and Cd values from separate experiments, velocities from every replicate were multiplied with all corresponding Cd concentrations, yielding a minimum of 24 (6x4) combinations per treatment. Hereafter, the local rate of Cd deposition was obtained as the derivative of this Cd flux using the locpoly function of the KernSmooth package.

Flow cytometry

For each treatment (Table 1), we sampled 10 one-centimetre segments along the maize leaf growth zone (n = 6). Samples were processed as described before (Hendrix *et al.*, 2018) using the CyStain PI Absolute P kit (Sysmex Partec). Using a CyFlow Cube 8 flow cytometer (Sysmex Partec), PI fluorescence intensity was determined using 488 nm excitation and 580 nm detection for a minimum of 7500 nuclei per sample. The number of 2C, 4C nuclei and S-phase nuclei were determined in R (v 3.6.1) using the flowCore package (v 1.50.0, Hahne *et al.* (2009) as described in Supplementary Figure 3.2).

Quantitative real-time PCR

We measured expression levels of 3 cell cycle genes: *putative wee1-like protein kinase (further referred to as wee1)*, which controls S-phase progression in plants by phosphorylation of CDKs and arrests S-phase progression under DNA stress (Cools *et al.*, 2011; Hu *et al.*, 2016); *mcm4*, part of the prereplication complex that mediates unwinding the DNA during S-phase (Masai *et al.*, 2010) and *cyclin-B2-4*, a member of the family of positive CDK regulators controlling G2-to-M transition (Scofield *et al.*, 2014). In addition, *wee1* and B-type cyclins are good indicators for cell cycle progression, since their expression levels have been shown to increase at the onset of

the S-phase and G2/M transition, respectively (Cools *et al.*, 2011). Samples were obtained from the first 5 centimetres of the fifth leaf's growth zone, 3 days after emergence. These 5 centimetres were dissected in 6 half centimetre segments, followed by 2 one-centimetre segments in 3 biological replicates per treatment, each consisting of a pool of 4 plants. Sections were frozen in liquid nitrogen and stored at -80°C. We ground the leaf material with a ball mill grinder (Retsch MM400, Verder NV, Aartselaar, Belgium), using ceramic balls. Total RNA was extracted using the RNeasy Plant mini kit (Qiagen, Hilden, Germany) and diluted to 0.4 $\mu g \cdot \mu L^{-1}$. First strand cDNA synthesis was performed using SuperScript™ II Reverse Transcriptase according to the manufacturer's protocol (Thermo Fisher Scientific, Waltham, Massachusetts, USA). The synthesised cDNA was used for quantitative real-time PCR using the SYBR™ Green Master Mix (Kaneka Eurogentec S.A., Seraing, Belgium). Expression values were normalised using *Zm00001d036201* (hypothetical protein) as reference gene (Supplementary Table 3.1 for housekeeping gene selection (Lin *et al.*, 2014)). Gene expressions values were calculated using the $2^{-\Delta\Delta C_T}$ method (Livak and Schmittgen, 2001), relative to the expression of the gene in the first segment of the control plants. Primers (Supplementary Table 3.2) were created using the NCBI primer designing tool available at https://www.ncbi.nlm.nih.gov/tools/primer-blast/ .

Statistics

Statistical analysis was performed in R (v. 3.6.1). For the kinematic analysis, we used a one-way ANOVA or a Kruskal-Wallis test depending whether assumptions for normal distribution (Shapiro-Wilk test) and homoscedasticity (Levene's test) were met. When there was a significant effect of treatment, we performed a Tukey's HSD test or pairwise Wilcoxon rank sum test. For the remaining analyses, a two-way ANOVA was performed (with segment in the growth zone and treatment as factors). When required, data was $\log_{10}$ transformed to improve the distribution or homoscedasticity. For cadmium concentration, flux and deposition statistics, only data for mild and severe treatments were used because cadmium concentrations in the control treatment were close to zero, resulting in a non-normal distribution of the residuals.

Results

Dose-Response

To determine the effect of Cd concentrations in the soil on the growth of maize leaves, we first performed a dose-response growth analysis. For studying the effect of abiotic stress on growth, we routinely study the 5th leaf of maize seedlings because its growth is independent on seed reserves, approximately steady state for about 5 days after emergence and affected by environmental conditions (Avramova *et al.*, 2017).

Leaf elongation rate (LER) was reduced by 25 to 57%, following a progressive, but non-linear decrease with increasing Cd concentrations (Fig. 1A). For all treatments the reduction in final leaf length was approximately half of that of the effect on LER (Fig. 1B), so that the highest dose only reduced final leaf length by 30%. The difference between the LER and final leaf length can be explained by a progressive increase of the duration of leaf elongation with increasing Cd levels, which partially compensates for the lower leaf elongation rate. Based on leaf elongation rate and final leaf length, we selected a mild (i.e. 46.5 mg Cd · kg dry soil^{-1}; inhibiting LER by 25%) and severe treatment (372.1 mg Cd · kg dry soil^{-1}; inhibiting LER by 52%) for further detailed analyses (Table 1).

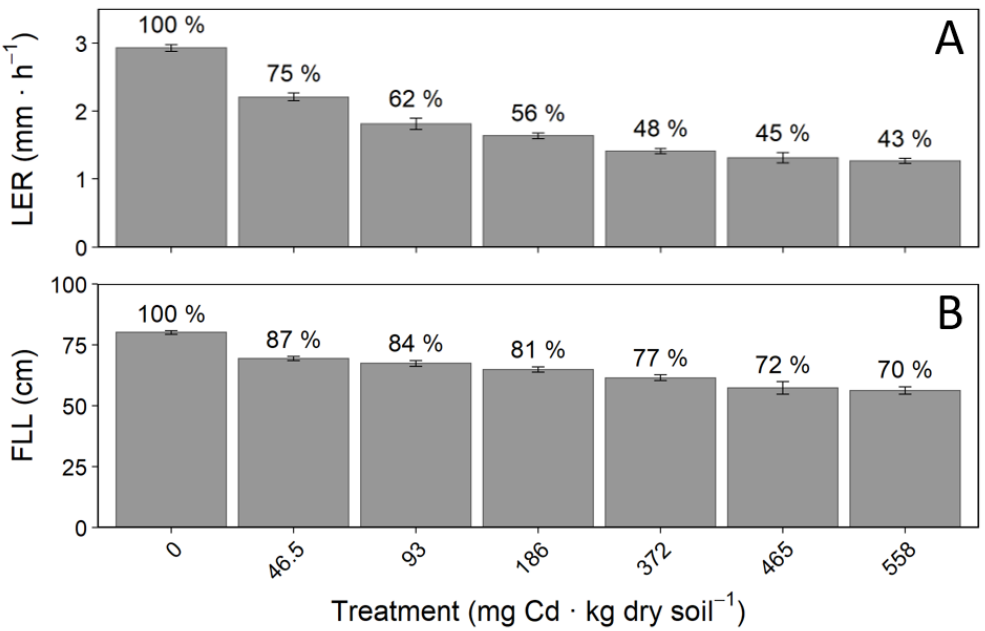

Figure 1. The effect of Cd dose on leaf elongation rate (LER, A) and final length (FLL, B) of the fifth leaf of maize seedlings. The percentages indicate the values for each treatment relative to the control treatment. The fifth leaf was measured daily after its emergence from the whorl of older leaves. LER for individual plants was determined over the first 4 days after leaf emergence. Data are mean values ± SE (n = 7).

Cadmium accumulation

Next, we set out to determine whether the growth inhibition could be due to Cd accumulation in the leaf growth zone. Severe Cd stress significantly increased the dry to fresh weight ratio of the leaf material (Supplementary Figure 3.3). On a fresh weight basis, Cd levels increased with increasing concentrations in the soil (treatment $p < 0.001$). On a dry weight basis, mild and severe Cd stress resulted in very similar values across the growth zone (Supplementary Figure 3.4). However, in both cases Cd levels were highest at the base of the leaf, followed by a steep decline towards the mature tissues (segment $p < 0.001$; Fig. 2A). These findings indicate that dividing cells at the base of the leaf are exposed to higher amounts of Cd compared to later developmental stages.

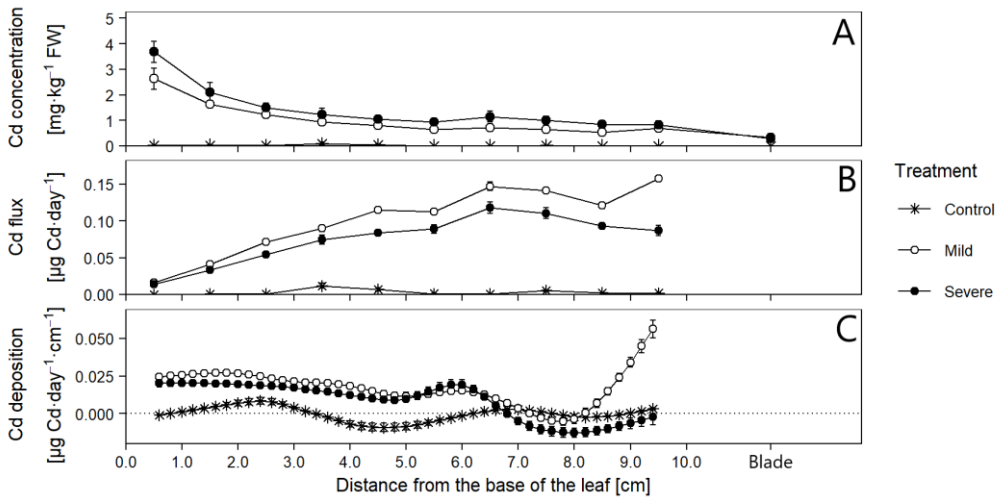

Figure 2. Cadmium concentration, flux and deposition along the growth zone of the maize leaf. The maize leaf growth zone was subdivided in 10 one-centimetre segments, starting from the base of the leaf. Blade segments were included in the Cd concentration measurements. **A.** Cadmium concentration based on fresh weight. Statistics for severe versus mild treatment (on $\log_{10}$ transformed data): $p_{treatment} < 0.001$, $p_{segment} < 0.001$, $p_{interaction\ treatment:segment} = 0.499$. **B.** Cadmium flux. This parameter illustrates the amount of Cd passing a position in the growth zone per day. Statistics for severe versus mild treatment (on $\log_{10}$ transformed data): $p_{treatment} < 0.001$, $p_{segment} < 0.001$, $p_{interaction\ treatment:segment} < 0.001$. **C.** Cadmium deposition rates. This parameter is the local derivative (i.e. slope) of Cd flux. Towards the end of the growth zone, high velocity (plot B) in combination with only minor changes in Cd concentration (plot A), causes relatively large fluctuations in flux and even more in deposition rates. We consider this artifacts. Statistics for severe versus mild treatment: $p_{treatment} < 0.001$, $p_{segment} < 0.001$, $p_{interaction\ treatment:segment} < 0.001$. Data shown are mean values ± SE (n = 5 (A), 24-30 (B), 24-30 (C)). SEs smaller than the symbol size are not plotted.

Kinematic analysis

Cadmium accumulation in the leaf meristem suggested that, if the effect of Cd on leaf growth is caused by local accumulation in the growing tissues, cell division would be primarily responsible for the growth inhibition by Cd. To address this possibility, we performed a kinematic analysis to quantify the effects on cell division and cell elongation. We first determined the cell length profile for the epidermal cells directly adjacent to the stomatal files. In the first centimetre from the base of the leaf, cells were small and cell size decreased slightly, while their size steeply increased in the 2-

4 centimetre region under severe Cd stress and in the 2-6 centimetre region under control conditions. Mature cell length was not affected by the treatments (Fig. 3A; Table 2).

The cell length data allowed us to calculate the velocity profile, which shows that the velocity at which cells move away from the base of the leaf gradually increases until it reaches a value equal to the leaf elongation rate at the end of the growth zone (Fig. 3B, Table 2). The derivative of the velocity curve yields relative cell expansion rates, which shows that increasing Cd levels progressively reduce the maximal expansion rates and the extent of the growth zone (Fig. 3C).

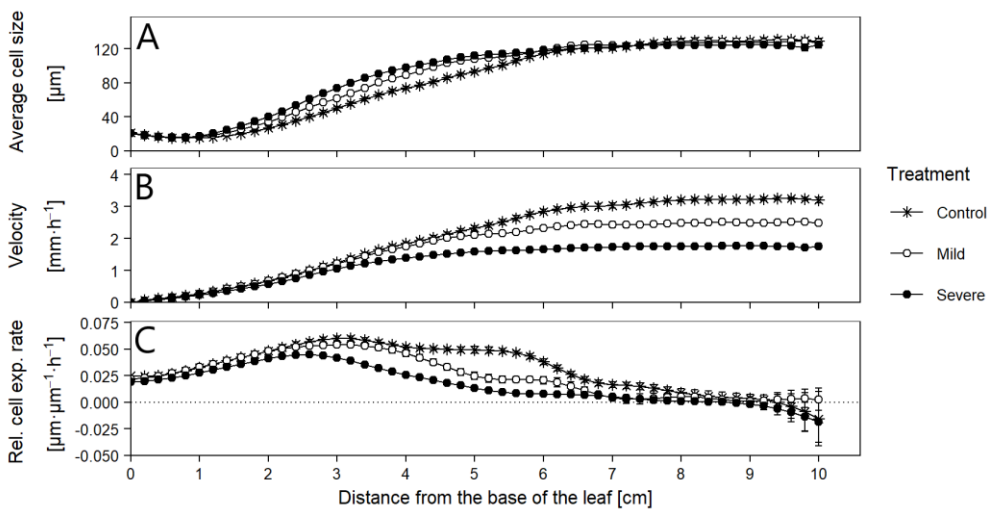

Figure 3. Kinematic analysis of the effect of Cd on cell growth in the maize leaf growth zone. A. Average cell size plotted every 2 mm along the growth zone. For related statistics, we refer to the kinematic analysis (Table 2) where the impact of Cd treatment on cell length (cells leaving the meristem and mature cell length) is presented. **B.** Tissue velocity plotted every 2 mm along the growth zone. For related statistics, we refer to the kinematic analysis (Table 2) where the impact of Cd treatment on velocity, i.e. leaf elongation rate, is presented. Leaf elongation rate corresponds to the maximum velocity reached in this graph. **C.** The relative cell expansion rates (rel. cell exp. rate). For related statistics, we refer to the kinematic analysis (Table 2) where the average relative cell expansion rates are presented. Data shown are mean values ± SE (n = 6). SEs smaller than the symbol size are not plotted.

Because mature cell size is not affected, the decrease in leaf elongation rate (by 24 and 46% for mild and severe stress respectively in this experiment; $p < 0.001$; Table 2) was almost entirely caused by a reduced cell production rate (-21% and -43% for mild and severe stress, respectively; $p < 0.001$; Table 2). Cell production in turn, is determined by the number of dividing cells in the meristem and their cell division rate. Cadmium stress significantly reduced the number of cells in the meristem (by 17% in mild and 29% in severe stress; $p < 0.001$; Table 2) and cell division rate (by 5 and 19%, in mildly and severely stressed plants; $p = 0.058$; Table 2), which relates to an increased cell cycle duration (from 24 hours in control conditions to 26 and 30 hours in mild and severe stress, respectively; $p = 0.0317$; Table 2). Although mature cell length was not affected, the relative cell elongation rate was inhibited by Cd (by -13 and -33% for mild and severe stress, respectively; $p < 0.001$; Table 2). This reduction in cell elongation rate, however, was compensated for by an increased time cells spend in the elongation zone (12% and 45% for mildly and severely stressed plants, respectively, $p < 0.001$; Table 2). The reduced number of dividing cells was reflected by a significant decrease in the size of the meristem ($p = 0.001$; Table 2). As a consequence, the size of the growth zone as a whole decreased from 70 mm down to 64 and 59 mm for plants under mild and severe treatment, respectively ($p = 0.054$; Table 2).

In summary, Cd inhibits leaf growth primarily by reducing the meristem size and inhibiting cell division and expansion rates.

Table 2. Kinematic analysis of the effect of Cd on cell division and cell expansion in the growing maize leaf.

Mild and severe treatment are compared to the control treatment and the difference is expressed as a percentage of the control values. Data are based on cells in a representative file of epidermal pavement cells directly adjacent to a stomatal file. * indicates significantly different ($p < 0.05$). Data are mean values ± SE (n = 10-11 for LER, n = 4-5 for FLL, n = 6 for the other parameters).

Parameter	Control	Mild	Severe	Percentage change in Mild/Severe stress
Final leaf length (mm)	761 ± 16	634 ± 26	576 ± 47	-17* / -24*
Leaf elongation rate ($mm \cdot h^{-1}$)	3.23 ± 0.03	2.47 ± 0.05	1.74 ± 0.07	-24* / -46*
Length of the meristem (mm)	14.3 ± 0.7	12.2 ± 0.5	10.6 ± 0.5	-15* / -26*
Length of the elongation zone (mm)	56 ± 3	51 ± 3	48 ± 4	-8 / -14
Length of the growth zone (mm)	70 ± 3	64 ± 3	59 ± 4	-10 / -16
Length cells leaving meristem (µm)	18.0 ± 0.4	18.7 ± 0.4	18.5 ± 0.6	+4 / +3
Mature cell length (µm)	129 ± 3	127 ± 2	123 ± 3	-2 / -4
Number of cells in meristem	873 ± 43	720 ± 36	618 ± 32	-17* / -29*
Number of cells in elongation zone	999 ± 22	881 ± 31	829 ± 47	-12 / -17*
Number of cells in total growth zone	1872 ± 52	1602 ± 24	1448 ± 46	-14* / -23*
Cell production rate ($cells \cdot h^{-1}$)	25.0 ± 0.7	19.6 ± 0.4	14.2 ± 0.2	-21* / -43*
Cell division rate ($cells \cdot cell^{-1} \cdot h^{-1}$)	0.029 ± 0.002	0.028 ± 0.001	0.023 ± 0.002	-5 / -19
Relative cell expansion rate ($\mu m \cdot \mu m^{-1} \cdot h^{-1}$)	0.049 ± 0.002	0.043 ± 0.002	0.033 ± 0.002	-13 / -33*
Cell cycle duration (h)	24 ± 1	26 ± 1	30 ± 2	+5 / +25*
Time cells spend in the meristem (h)	238 ± 15	242 ± 13	282 ± 20	+2 / +19
Time cells spend in the elongation zone (h)	40 ± 2	45 ± 2	58 ± 3	+12 / +45*

Cadmium flux and deposition

The decreasing Cd concentration with increasing distance from the leaf base (Fig. 2A) could be a consequence of dilution by cell growth, raising the possibility that all Cd is taken up by the dividing cells at the base of the leaf (Supplementary Figure 3.5 illustrates Cd dilution by growth). To verify this possibility, we used kinematics to calculate Cd deposition rates along the leaf growth zone.

Based on Cd concentration and tissue velocity, we calculated Cd flux and deposition rates. Cadmium flux, the bulk flow rate of Cd away from the leaf base, progressively increased in the first 6 to 7 centimetres, after which it became approximately constant (Fig. 2B) in both Cd treatments. Assuming steady state, the derivative of the flux curve yields the local rates of Cd deposition, which was highest at the base of the leaf where cells are actively dividing (Fig. 2C). Towards the end of the growth zone, high velocity (Fig. 3B) in combination with only minor changes in Cd concentration, caused relatively large fluctuations in flux and even more in deposition rates. We consider this artifacts. Nevertheless, our data show that although Cd concentrations rapidly drop once cells leave the division zone, deposition continues in elongating cells and stops around the end of the elongation zone.

Flow cytometry

To analyse which phase of the cell cycle was affected by Cd, explaining the increased cell cycle duration (Table 2), and to assess if there was an effect on endoreduplication in expanding cells, we performed flow cytometry on one-centimetre sections along the leaf base. The fraction of 4C cells relative to cells with a 2C DNA content was highest in the second centimetre of the leaf (Fig. 4A), where cells exit the meristem (Table 2). After an initial drop, DNA contents increased towards the end of the elongation zone, suggesting a limited amount of endoreduplication (Fig. 4A).

Furthermore, this analysis suggests active proliferation in the first 3 centimetres of the leaf for all treatments. This result appears in contrast with our kinematic analysis that shows a meristem size of 1 to 1.5 centimetres for the severely stressed and control leaves, respectively. This difference may be due to flow cytometry being performed on a mix of all cell types, while kinematics is based on epidermal pavement cells. Nevertheless, the reduced meristem size is clearly reflected in the more rapid drop of the 4C/2C ratio in the Cd-treated leaves. Consistent with active proliferation at the base and limited endoreduplication in the elongation zone, cells in S-phase could be

detected throughout the growth zone, with the highest levels in the second centimetre (Fig. 4B).

The 4C/2C ratio was reduced by severe Cd stress, whereas the mild treatment was very similar to the control treatment. Severe Cd stress reduced the fraction of S-phase cells throughout the growth zone, whereas at the leaf base mild stress was similar to the control treatment, but in the elongation zone resembled the severe stress.

In conclusion, the flow cytometry data support a reduced meristem size and a reduced 4C/2C ratio under Cd stress, suggesting an inhibition of the G1/S transition in both mitotic and endoreduplicating cells.

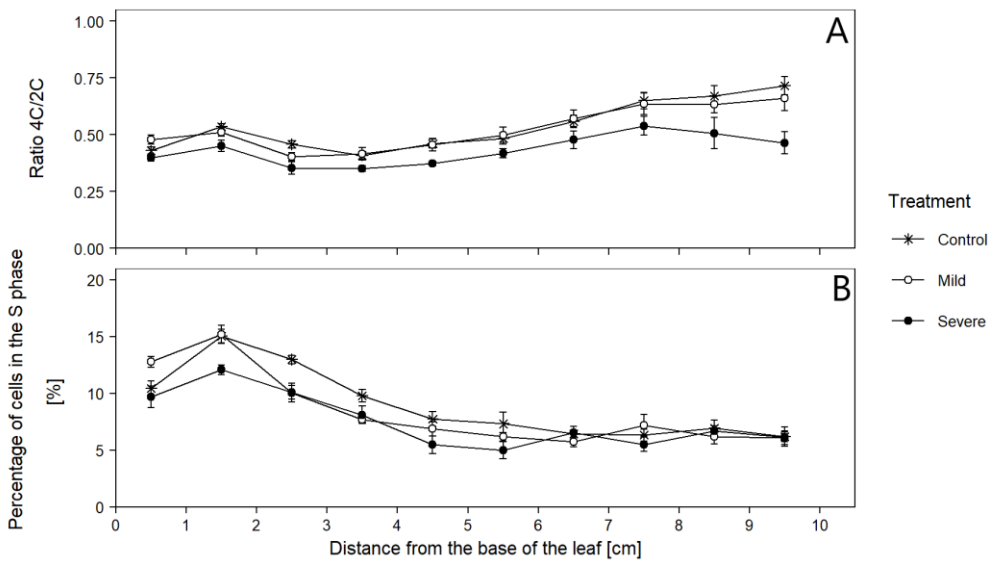

Figure 4. Flow cytometry analysis of the effect of Cd in the growth zone of maize leaves. The growth zone was subdivided in 10 one-centimetre segments, starting from the base of the leaf. **A.** Ratio 4C nuclei to 2C nuclei throughout the maize leaf growth zone. Statistics (data $\log_{10}$-transformed, two-way ANOVA): $p_{treatment} < 0.001$, $p_{segment} < 0.001$, $p_{interaction\ treatment:segment} = 0.611$. **B.** Percentage of nuclei in the S-phase throughout the maize leaf growth zone. Statistics (two-way ANOVA): $p_{treatment} < 0.001$, $p_{segment} < 0.001$, $p_{interaction\ treatment:segment} = 0.004$. Data shown are mean values ± SE (n = 6). SEs smaller than the symbol size are not plotted.

Quantitative real-time PCR

To better understand the molecular mechanism explaining the inhibition of cell division by Cd, we analysed the expression levels of 3 cell cycle regulatory genes: *wee1*, *mcm4* and *cyclin-B2-4.* The overall expression pattern of these genes reflected the distribution of cell division activity and the inhibition by Cd (Table 2), with the highest expression levels around 1 centimetre from the base (Fig. 5). Severe Cd stress reduced the expression of these cell cycle regulators throughout the growth zone and caused a more rapid drop between 1.5 and 3.5 centimetres from the base, reflecting the reduced cell division rate and shortening of the meristem (Table 2), respectively. The response to mild stress was similar to the severe stress in the basal centimetre, whereas in more distal positions it appeared similar to the control condition.

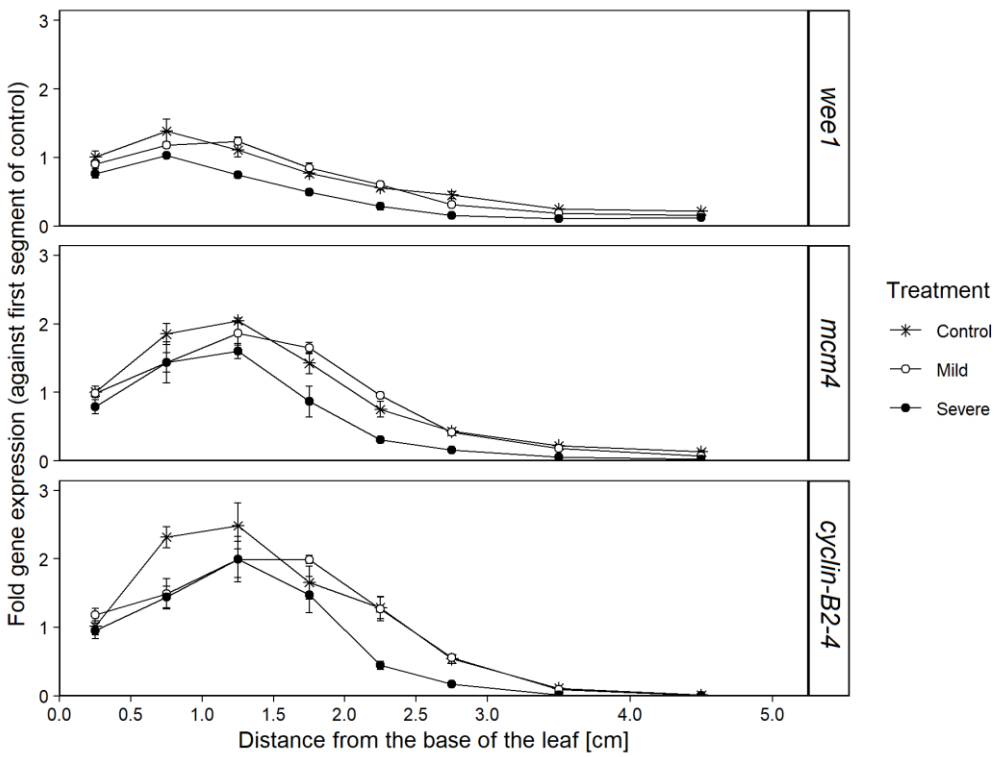

Figure 5. The effect of Cd on cell cycle gene expression in the growth zone of maize leaves. The first 3 centimetres were subdivided in half centimetre segments, while the remaining two centimetres were segmented in one centimetre pieces. Fold gene expression is calculated relatively to the expression level

of the control treatment's first segment. Statistics: data $\log_{10}$ transformed, two-way ANOVA $p_{treatment} < 0.001$, $p_{segment} < 0.001$ and $p_{interaction\ treatment:segment} < 0.001$. Data shown are mean values ± SE (n = 3). SEs smaller than the symbol size are not plotted.

Discussion

In order to answer our first research question, whether Cd could directly affect dividing and elongating cells in the growing maize leaf, we determined the Cd levels along the gradient of cell division and expansion at the base of the leaf into the mature blade tissue. Cd concentrations were highest at the base of the leaf, rapidly declined with increasing distance from the base and stabilised at around the 5th centimetre (Fig. 2A). This closely relates to our kinematics data, showing that the growth inhibition exerted by Cd is primarily caused by a reduced cell production in the meristem, located in the base of the leaf. Noteworthy, these observations demonstrate that whole leaf sampling, typically used to evaluate leaf Cd concentrations (e.g. Khaliq *et al.*, 2019; Masood *et al.*, 2016; Nada *et al.*, 2007; Shi *et al.*, 2019; Ye *et al*., 2018; Zhou *et al.*, 2018), underestimates the concentration in dividing and elongating cells .

Using kinematics, we were able to calculate Cd fluxes and Cd deposition rates. One possibility to account for the high levels of Cd in the meristem and their rapid decline in the elongation zone (Fig. 2A) could be that Cd is specifically deposited at the base of the leaf and diluted by cell expansion in the elongation zone. Under these circumstances, Cd flux in the elongation zone should remain constant, because the dilution of Cd and the increase in cellular velocity due to water uptake are directly proportional (Supplementary Figure 3.5). However, we observed a steady increase in Cd flux until at least the 4th centimetre (Fig. 2B), demonstrating that Cd deposition continues in the elongation zone. Cadmium deposition rates in the elongation zone are lower than those of water driving cell expansion, explaining the decreasing Cd concentrations from the leaf base towards the blade (Fig. 2A). Thus, while deposition rates are highest in the meristem of the growing maize leaf, Cd continues to be deposited while cells are expanding (Fig. 2C), suggesting that in elongating cells Cd is (passively) taken up with the influx of water required to drive cell growth. Interestingly, plants exposed to a mild Cd dose have a higher Cd flux compared to severely stressed plants (Fig. 2B), even though concentrations are higher in leaves exposed to the highest concentration (Fig. 2A). This is because both segment fresh weight and velocity

are higher under mild stress compared to severe stress, resulting in more tissue passing per unit time. When the flux is expressed on a fresh weight basis, compensating for the amount of tissue passing by (Supplementary Figure 3.6), severely stressed plants have a slightly higher Cd flux.

The past decade, Cd deposition in the meristem received attention in the shoot of eudicotyledonous and *Graminae* plants using a positron-emitting tracer imaging system together with positron-emitting Cd to trace the translocation and accumulation of Cd throughout the plant. This technique also showed that in rice Cd already accumulated at the base of the leaf after 1 hour of tracer exposure, whereafter the signal also increased in the rest of the sheet and in the blade (Fujimaki *et al.*, 2010; Kobayashi *et al.*, 2013). Radioactive Cd deposition was also studied in *Arabidopsis thaliana*, where Dauthieu *et. al.* (2009) showed that Cd was deposited throughout young leaves and that the zone of deposition retracted towards the base and petiole in older leaves. Young dicotyledonous leaves first consist entirely out of dividing cells, after which a cell cycle arrest front appears at the tip of the growing leaf which moves towards the petiole (Andriankaja *et al.*, 2012). Therefore, the pattern of Cd deposition in these leaves also broadly coincides with cell proliferation. In addition to leaves, predominant accumulation of Cd in the meristem also occurs in roots of rice (Zhao *et al.*, 2013*a*; Zhan *et al.*, 2017). Taken together, these results indicate that, during growth, Cd is mainly deposited and accumulated in dividing and elongating tissue.

Dividing and elongating tissue, acting as a Cd sink, is supported by the study performed by Kobayashi *et al.* (2013) on rice seedlings. They showed that the xylem transpiration stream facilitates Cd transport from the roots towards the shoot. However, once Cd reaches the base of the stem, it is loaded into the phloem at the nodes and mainly directed towards the young growing leaves. In the new leaves, Cd preferentially accumulated in the sheath (i.e. where the growth zone resides), whereas calcium was spread throughout the growing leaf.

To address our second research question, the cellular basis of Cd inhibited leaf growth in maize, we analysed the contribution of cell division and elongation to the growth inhibition by Cd. Our results indicate that Cd inhibited leaf growth by inhibiting cell production by up to 43 percent, while mature cell length remained largely unaffected. This is consistent with the meta-analysis performed by Gázquez and Beemster (2017), who showed that variations in meristematic cell number, rather than mature cell size, primarily determine organ size in plants. For *Graminae* leaves, they also showed that mature cell length is strictly controlled and does not contribute significantly to changes in leaf elongation rates, which matches the unaffected mature cell length in our analysis.

The main cause of a lower cell production rate in our study was a reduction in number of meristematic cells, resulting in shortening of the meristem size by up to 26 %. This reduced meristem size is consistent with Cd-induced meristem size reductions in roots of wheat, pea and Arabidopsis (Fusconi *et al.*, 2007; Pena *et al.*, 2012; Yuan and Huang, 2016; Bruno *et al.*, 2017). Although we confirmed the reduction in meristem in 3 independent experiments (i.e. kinematics study, quantitative real-time PCR of cell cycle genes and a flow cytometry study), there was discrepancy in the apparent meristem sizes. Based on our kinematics results data, meristem sizes ranged from 1 to 1.5 centimetres for severe to control condition respectively (Table 2), whereas cell cycle gene expression patterns suggested it to be considerably longer (up to 2.5 centimetres under control conditions when interpreting *cyclin-B2-4* expression data (Fig. 5)). In the flow cytometry results, the 4C/2C minimum at the meristem-elongation transition is reached 1 centimetre later by the control treatment (Fig. 4A), suggesting that cells are still dividing in the 2-to-3 centimetre segment under control conditions. This discrepancy between datasets can be related to the cell type studied by the different methodologies. In the kinematic analysis, epidermal pavement cells are studied, whereas in gene expression and flow cytometry study, whole leaf segments containing all cell types were used. Tardieu et al. (2000) showed that mesophyll cells can divide twice as long as epidermal cells, which could explain why the techniques

which incorporate all cell types (i.e. quantitative real-time PCR and flow cytometry) result in longer meristems compared to kinematic analysis, which is based only on epidermal pavement cells. Nevertheless, all data consistently showed that Cd reduces maize leaf meristem size.

Besides a significant reduction in meristem cell number, cell cycle duration also increased from 24 hours under control conditions to 30 hours under severe stress conditions. This means that cells divided at a lower rate because they were halted at some point(s) in the cell division cycle. Inhibited cell cycle progression under Cd stress has previously been reported mainly in roots and synchronised cell culture experiments. In roots of *Arabidopsis thaliana*, Cd inhibited the cell cycle mainly at the G2/M transition, resulting in a relative increase in 4C nucleic content at the cost of 2C nuclei (Cui *et al.*, 2017; Cao *et al.*, 2018). No significant effect of Cd on the proportion of cells in the S-phase was reported by Cao *et al.* (2018). However, detrimental effects of Cd on the S-phase were shown in synchronised plant cell cultures, where Cd administration during S-phase delayed the mitosis by 2 hours in tobacco cells (Kuthanova *et al.*, 2008) and Cd administration at the start of the cell cycle decreased the DNA-synthesis rate in soybean cells (Sobkowiak and Deckert, 2004). Also, in root apices of peas (*Pisum sativum L.*), Cd affected meristematic cells in the G1/S and G2/M transition, resulting in respectively less cells in the S- and M-phase. Inhibition of S-phase entry was also shown in a study on Cd stress in leaves of lettuce (Monteiro *et al.*, 2012). Though insignificant, Monteiro *et al.* (2012) showed an increase in percentage of G0/G1 cells, followed by a decrease in cells in the S-phase and G2-phase when grown under mild to severe Cd conditions (respectively 10 and 50 µM Cd). Cd-inhibited G1/S transition is consistent with our flow cytometry data in the meristem of the growing maize leaf, where we show a lower proportion of cells in the S-phase, together with an accumulation of cells with a 2C nucleic content (Fig. 4).

In order to better understand why cells were progressing slower through the cell cycle, we selected 3 key cell cycle genes, i.e. *wee1* and *mcm4* which have a function during the S-phase and *cyclin-B2-4*, a B-type cyclin controlling G2/M transition. *wee1*, a kinase of which transcript abundance peaks during S-phase progression (Cools *et al.*, 2011), controls cell cycle arrest upon DNA damage and is also important for meristem maintenance during replication stress (Hu *et al.*, 2016). Since Cd is linked to DNA damage in multiple studies (as reviewed by Huybrechts *et al.*, 2019), we expected *wee1* transcript levels to increase under Cd stress. Surprisingly, under severe Cd stress, expression levels of *wee1* were consistently lower compared to the control treatment over the entire meristem (Fig. 5). However, these results do reflect those of Cao *et al.* (2018) and Cui *et al.* (2017), who also found *wee1* downregulation under Cd stress in roots of Arabidopsis after 5 days of Cd exposure. Only low amounts of Cd caused a significant upregulation of *wee1* transcription (Cui *et al.*, 2017; Cao *et al.*, 2018).

We also found similar expression profiles for *mcm4* (helicase activity) and *cyclin-B2-4* (controlling G2/M transition), i.e. lower expression under severe Cd stress over the entire meristem compared to the control condition. Downregulation of B-type cyclins was also shown in the experiments of Cao *et al.* (2018) and Cui *et al.* (2017) and also in soybean suspension-culture cells, Cd reduced in *cyclin-B1* transcription (Sobkowiak and Deckert, 2003). Next, in Cd exposed shoots of wheat (*Triticum urartu*), 2 and 5 day Cd exposure reduced expression levels of multiple MCMs (Qiao *et al.*, 2019), whereas 48 hour exposure to the same Cd dose decreased *mcm2* transcript levels in roots of wheat seedlings (Pena *et al.*, 2012). Downregulation of cell cycle-related genes by Cd seems to be common, as this was also supported by findings of Zhao *et al.* (2013) who reported that 12 out of 17 cell cycle-related genes had severely reduced transcript levels in Cd exposed rice roots.

Taken together, exposure to of Cd appears to stops cells from entering the cell cycle (i.e. inhibited G1/S transition), which is supported by the lower proportion of cells in S-phase and with the 4C nuclei content found in our study. With less cells entering the cell cycle, transcript levels of cell cycle-related genes could be relatively less abundant.

We therefore hypothesize that under severe Cd stress, cells are hindered in entering the cell cycle in general, which could lead to an overall downregulation of most cell cycle genes.

Next, although mature cell length was unaffected, Cd significantly reduced relative cell elongation rate under severe stress. Nevertheless, cells did achieve the same mature cell length due to an increased time spent in the elongation zone. The inhibited cell elongation rate could be related to lower endopolyploidy levels in the elongation zone under severe stress, since DNA content is often linked to cell growth (Melaragno *et al.*, 1993; Sugimoto-Shirasu and Roberts, 2003) (Fig. 4). Based on our kinematics (Table 2) and cell cycle gene expression analysis (Fig. 5), we do not expect any cell division to occur further than 3 centimetres from the base of the leaf. Yet we do see a steady increase in 4C nuclei after this position, indicating a limited amount of endoreduplication to be present in the elongation zone. The endoreduplication process was negatively affected by our severe stress condition, where the 4C/2C ratio under severe stress stayed well below the one under control conditions over the entire elongation zone. However, the difference between control and severe Cd treatments on the 4C/2C ratio is quite constant from 1 to 7 centimetres, which could indicate that the process of endoreduplication itself is not really hampered, but the difference is there because a lower proportion of 4C nuclei was already present in the meristematic region under severe Cd stress. This difference in 4C/2C ratio is then retained throughout the elongation zone while the process of endoreduplication takes place at similar rates as in controls.

Because of the potential link between polyploidy level and cell growth, a reduced DNA content could negatively impact the process of cell elongation in the Cd exposed maize leaf growth zone. Similar to our results, Hendrix *et al.* (2018) related a decreased cell surface area to a lower extent of endoreduplication in leaves of Cd exposed Arabidopsis. However, in roots of *Pisum sativum* and *Arabidopsis thaliana*, Cd

exposure resulted in increased polyploidy levels (Fusconi *et al.*, 2006; Repetto *et al.*, 2007; Cui *et al.*, 2017; Cao *et al.*, 2018). Therefore, in a recent review by Huybrechts *et al.* (2019), it was suggested that Cd exposure stimulates the endocycle in roots and inhibits it in leaves.

Lastly, it is remarkable that an eight-fold difference in Cd dose between mild and severe treatments resulted in a limited difference in Cd accumulation throughout the growth zone while the effects on growth, cellular and molecular processes were quite apparent. The relatively small differences in accumulation could potentially be explained by a saturated uptake and/or transport, to which the mild stress conditions might already get close. Related to this saturated uptake, Huang *et al.* (2019) have shown that Cd uptake in rice increased steeply under incremental low Cd concentrations, yet, at higher concentrations, Cd uptake was levelling off when Cd concentrations further increased. It is not clear how a relatively small difference in Cd accumulation (a maximal difference of 40% in the meristem between mild and severe stress, t-test p-value: 0.11) could result in drastic differences in growth response. Perhaps, a very tight threshold level is exceeded under severe stress conditions, where the plant is still able to cope with the mild treatment and succumbs under severe stress. Passing the threshold level might result in a different subcellular distribution, affecting more and potentially important processes. Also, the impact of Cd on roots was not studied in the research presented here. It is very well possible that, in addition to the effects of locally accumulating Cd in the leaf, signals originating from the roots inhibit leaf growth. Therefore, further research should be undertaken to explore whether potential long-distance signals and potential threshold levels of metabolic and regulatory processes become affected. Comparing the mild and severe Cd treatments may provide an interesting entry into this issue.

Conclusion

Our primary objective was to understand how Cd uptake by the roots inhibits leaf growth in maize. We found that Cd inhibits leaf growth through a reduction of the meristematic cell number and by impairing the cell cycle at the G1/S transition resulting in an increased cell cycle duration. In addition, Cd inhibited cell elongation, which might be related to lower ploidy levels under severe Cd stress. We also showed that Cd predominantly accumulates in the meristem and that deposition of Cd continues at lower rates throughout the elongation zone, which implies direct impact of Cd on the cell cycle and cell expansion in the maize leaf growth zone.

This study opens perspectives to further investigate the impact of Cd on the physiology of the leaf growth zone of a monocotyledonous leaf. We have shown in this study and earlier (Avramova *et al.*, 2015*c*) that the maize leaf model allows sampling at subzonal resolution for a wide range of analyses. This will allow us to determine how and to what extent changes in micro- and macronutrient levels, phytohormone profiles, energy metabolism, cell wall metabolism, etc. in the leaf growth zone further explain the regulatory mechanisms by which Cd inhibits leaf growth.

Acknowledgements

This work was supported by the Research Foundation Flanders (FWO) by project funding for J.B. and M.H. [G0B6716N]. All authors participated in the conception of the topic. J.B. wrote the manuscript. G.B. edited the manuscript. J.B. made the figures and tables. J.B and L.B. performed the HR-ICP-MS measurements. M.H., S.H. and A.C. facilitated and helped with the flow cytometry measurements. We thank Geoffrey Hibbs and Leen Vandenberghe for their assistance with quantitative real-time PCR. All authors read and approved the final manuscript after critically revising it for important intellectual content. The authors declare that they have no conflicts of interest.

Chapter 4

A genome-wide, multilevel analysis of the effects of cadmium in the maize leaf growth zone

Jonas Bertels[1], Els Prinsen[1], Lieven Bervoets[2], Hamada AbdElgawad[1], Katrien Sprangers[1], Ann Cuypers[3], Gerrit Beemster[1]

[1] Laboratory for Integrated Molecular Plant Physiology Research (IMPRES), University of Antwerp, Groenenborgerlaan 171, 2020 Antwerpen, Belgium

[2] Systemic Physiological and Ecotoxicological Research (SPHERE), University of Antwerp, Groenenborgerlaan 171, 2020 Antwerpen, Belgium

[3] Centre for Environmental Sciences (CMK), Hasselt University, Agoralaan Building D, 3590 Diepenbeek, Belgium

Abstract

Although our knowledge of the impact of cadmium (Cd) on plants has already made tremendous progress (chapter 1), the impact on actively dividing and growing cells is still poorly understood. In chapter 3, we have shown that in the growth zone of maize leaves Cd levels were highest in the meristem and that Cd deposition continued until the end of cell elongation. To reveal which processes could be affected by this local Cd deposition, we analysed the transcriptome of the meristem, the elongation zone and the mature zone of growing fifth leaves under Cd stress and control conditions. Gene ontology and MapMan analysis revealed that photosynthesis, protein production, carbohydrate metabolism, cinnamic acid, phenylalanine, phytohormones, oxidative stress and metal ion homeostasis were affected by Cd. Based on these findings, we performed a detailed analysis of phytohormone levels in the maize leaf growth zone. This allowed us to link changes in gibberellin content to expression changes of a gibberellin 20-oxidase (downregulated under Cd stress) and a gibberellin 2-oxidase (upregulated under Cd stress). In addition, we found increased levels of two cytokinin O-glucosides (i.e. cis-zeatin O-glucoside and dihydrozeatin riboside-O-glucoside) under Cd stress, which could be linked to observed reduced levels of trans-zeatin riboside in the meristem. Regarding the stress hormones (of which several related genes were significantly affected in the MapMan regulation overview), we found 1-aminocyclo-propane 1-carboxylic acid (ACC, ethylene precursor), salicylic acid (SA) and abscisic acid (ABA) levels to be increased under Cd stress and we revealed a potential role for ACC conjugates in response to Cd stress. Next to the phytohormone analysis, we determined the profile of several minerals, malondialdehyde and ferric ion reducing antioxidant power (FRAP) across the maize leaf growth zone of control and Cd treated plants. Here we found that especially severe Cd stress reduced Ca, Cu, K, Mn and Zn levels across the maize leaf growth zone. Malondialdehyde and FRAP were increased, indicating that Cd induces oxidative stress in the maize leaf growth zone. Taken together, we identified effects of Cd on transcriptome and metabolome levels for hormones, mineral homeostasis and antioxidants in the maize leaf growth zone. For the gibberellin pathway we were able to directly relate gene expression changes to metabolite levels.

Introduction

Cadmium (Cd) is a non-essential metal, found in soils across the world. Historical industrial pollution (Cd-Zn smelters), municipal waste incineration, sludge application and enrichment of this metal in agricultural soil through phosphate fertilizers, exposes sessile plants to elevated Cd levels (Smolders and Mertens, 2013). In Flanders (Belgium), 280 km^2 is strongly enriched with Cd, so that more than 1 mg Cd per kg dry soil is present, compared to only 0.1 to 0.5 mg Cd/kg dry soil background levels (Vlaams Parlement, 1998). Though non-essential, Cd may be readily taken up by plant cells through transporters for essential nutrients like Fe^{2+}, Zn^{2+}, Mn^{2+} and Ca^{2+} (Clemens, 2006), after which it reaches the shoot through the xylem sap stream in just a few hours (Fujimaki *et al.*, 2010).

Once inside the plant cell, Cd induces oxidative stress indirectly by depleting the available GSH pool, replacing redox-active metal ions from their functional sites in proteins (e.g. Fe-ions), perturbation of mitochondrial functioning (major source of reactive oxygen species) and induction of NADPH oxidases as reviewed by Cuypers *et al.* (2010). The disruptive activity of Cd could therefor affect several biological processes. Genome wide (omics) approaches have been used to gain insight in this. In 2006, Weber *et al.* performed a micro-array study to compare the transcriptome of *Arabidopsis thaliana* to that of the hypertolerant *Arabidopsis helleri*, revealing that Cd-response genes (e.g. ZIP metal transporter) in *A. thaliana* showed a constitutive high expression in *A. halleri*. The past decade, studies started to implement Next Generation Sequencing (NGS) to investigate the effect of cadmium, mainly in roots of different plant species. For example, in the root and shoot of wheat, an NGS study revealed that genes related to DNA replication and phenylpropanoid biosynthesis were respectively downregulated and both up- and downregulated by Cd stress (Qiao *et al.*, 2019). Phenylpropanoid biosynthesis, next to glutathione metabolism, sulphur metabolism and nitrogen metabolism were significantly enriched among upregulated genes in roots of the low-Cd-accumulating winter wheat (Xiao *et al.*, 2019). Next generation sequencing also provided insight into how inoculation of maize with

arbuscular mycorrhizal fungi reduced Cd stress, identifying hundreds of genes related to hormone signalling, mitogen-activated protein kinase signalling and glutathione metabolism (Gu *et al.*, 2019). Also, comparative microRNA and transcriptome analyses revealed important roles of microRNAs in response to Cd stress through the regulation of specific target genes in rice and wheat (Zhong *et al.*, 2019; Zhou *et al.*, 2019*c*).

Knowledge collected using these high throughput analyses can direct further studies to investigate the roles of metabolites, minerals or phytohormones important in the plant's stress response. For instance, the exogenous application of phytohormones (e.g. auxin, gibberellins, salicylic acid) has already shown to reduce metal toxicity in plants by increasing antioxidant enzyme activity, increasing soluble phenolics, improving photosynthetic activity and reducing the inhibition of biomass accumulation by stimulating cell division (as reviewed by Sytar *et al.* (2019)). In addition, application of abscisic acid and salicylic acid significantly increased transport of Cd from root to shoot in tall fescue (*Festuca arundinacea*), providing the basis for novel strategies for phytoremediation of metal polluted soil (Zhu *et al.*, 2020).

Several genome-wide transcriptome studies have already provided insight on the Cd affected processes in plants. However, the impact of Cd on the transcriptome of actively proliferating and expanding cells, potentially explaining its effect on growth, has so far not been investigated. We showed that cadmium is specifically deposited in the meristem and elongation zone of the growing maize leaf, where it significantly reduced meristem cell number and inhibited cell cycle progression and cell elongation rate (chapter 3). Besides a direct effect on proliferation and cell elongation, local Cd deposition in the meristem and elongation zone might also impact growth indirectly by impinging on other biological processes. It is therefore that, in this current study, we performed a genome wide transcriptome analysis of the effect of Cd treatment on the maize leaf growth zone.

We hypothesise that a genome wide transcriptome study can reveal the effect of Cd, on processes specific for dividing, elongating or mature cells. The use of the maize leaf

growth zone as a model system will allow us to validate the relevance of transcriptional changes in key pathways by the analysis of related metabolite levels in the meristem, elongation zone and mature zone. In addition, due to the direct deposition of Cd in the growth zone (chapter 3), we also hypothesize that the content of other mineral ions is affected by the Cd treatments.

The following study will present the collected transcriptome data, where we revealed photosynthesis, protein production, carbohydrate metabolism, cinnamic acid, phenylalanine, phytohormones, oxidative stress and metal ion homeostasis to be affected. Based on this data, we analysed gibberellins, auxins, abscisic acid, cytokinins, 1-aminocyclo-propane 1-carboxylic acid (ACC, ethylene precursor) and its conjugates throughout the entire Cd exposed maize leaf growth zone and where possible, we related these levels to the transcriptome data. Through the analysis of mineral profiles across the maize leaf growth zone, we revealed shifts in mineral content, especially for Mn. Finally, we also obtained data on two key parameters related to oxidative stress (Malondialdehyde; MDA and ferric reducing antioxidant power; FRAP) to further expand the context of Cd impact in the maize leaf growth zone.

Material and Methods

Seeds, soil preparation, growth conditions and harvested plant material for biochemical and molecular analyses

We grew maize seedlings (*Zea mays L.,* B73 inbred line, obtained from the North Central Regional Plant Introduction Station) in a growth chamber under controlled conditions (16-h day/8-h night, 25°C/18°C day/night, 200 $\mu mol \cdot m^{-2} \cdot s^{-1}$ photosynthetically active radiation, provided by high-pressure sodium lamps).

Peat potting medium (57% soil water content, Jiffy Products International B.V., The Netherlands) was spiked with 10 ml distilled water (control treatment) or 10 ml $CdSO_4$ solutions ($3CdSO_4 \cdot 8H_2O$, mild (46.5 mg Cd / kg dry soil) and severe (372.1 mg Cd / kg dry soil) treatment, prepared in distilled water). Mild and severe treatment refers to the plant growth response, i.e. leaf elongation rate reduction, as described in chapter 3. It should be noted that mild stress is already relatively high compared to what is found in the environment. For instance, in the Campine region (Belgium), only high concentrations are found in the direct surroundings of sites of historical industrial activity (10-50 mg Cd / kg dry soil), where in the larger surrounding area, soil contamination is mainly diffuse and moderate (< 5 mg Cd / kg dry soil, Schreurs *et al.* (2011)). However, bioavailability may strongly depend on the soil-type and may be relatively low in our potting soil, containing a high fraction organic material. Therefore we selected concentrations that gave a clear growth response in the young maize seedling. A fixed mass (650 grams) of potting medium was used for each individual pot (2.0L) to which the solutions were added dropwise under continuous mixing with a kitchen mixer (Kenwood kMix KMX50). Thereafter, it was mixed for an extra two minutes to obtain a homogenous distribution of Cd. Pots were watered daily with tap water to maintain the original soil water content.

For all analyses, the fifth leaf was used and dissected 3 days after it emerged from the whorl of older leaves. The growth zone, present in the basal 10 cm of the maize leaf, was subdivided in one-centimetre segments. For mineral analysis, a blade segment

was also analysed, i.e. a one cm segment sampled in the middle of the left-over blade (after the growth zone was removed).

Next Generation Sequencing

Samples

Based on the kinematic analysis, the location of the meristem, elongation zone and mature tissue was determined. From each of these zones, one-centimetre segments were collected and tissue originating from 4 to 6 plants was pooled, resulting in three biological replicates for each treatment and zone combination. For the meristem, the first cm of the leaf was used. For the following zones, the sampling location depends on the treatment (Supplementary Figure 4.1). To ensure the centre of the elongation zone was used (i.e. where elongation rates peak), we used the third cm segment for leaves of the severe treatment and the fourth cm of leaves of the control and mild treatment. For mature tissue, we sampled the ninth cm segment of the severe treatment plants and the 10th cm for the control and mild treatments.

RNA extraction

The pooled leaf segments were magnalised using glass beads (MagNA Lyser, Roche Diagnostics GmbH, Mannheim, Germany) while regularly being cooled in liquid nitrogen. Approximately 50 mg of ground material of each sample was used for RNA extraction using the RNeasy Plant mini kit, after which concentration and purity was checked on the NanoDrop ND-1000 UV-VIS Spectrophotometer (Thermo Fisher Scientific, Wilmington, DE, USA) and RNA integrity was verified on a QIAxcel platform (Qiagen, Hilden, Germany).

Library preparation and Next-Generation Sequencing

The mRNA sequencing library was prepared using the TruSeq® Stranded mRNA sample preparation 96 rcx kit (Illumina™) following the low sample protocol according to Illumina™ guidelines. In short, mRNA was purified from 2 µg of total RNA by poly-T coated purification beads and subsequently enzymatically fragmented. The fragmented mRNA was transformed into cDNA and adapters in 12-plex formation were

ligated after the 3' end adenylation. After PCR enrichment, the library was quantified using PicoGreen® dye (Life Technologies™). An equal amount of DNA from twelve libraries was combined for pooling, generating eight pools. All pools were diluted to a concentration of 2 nM, determined with the Kapa SYBR® FAST universal qPCR kit (KAPA Biosystems™) and the average fragment size of all pools (needed for concentration calculations) was measured with the Bioanalyzer® (Agilent Technologies™). 2x 50 bp paired-end sequencing was performed using a HiSeq 1500 sequencer (Illumina™).

Raw data processing

We analysed the FASTQ-files containing the reads on the UseGalaxy.eu platform (Afgan *et al.*, 2018). Read quality was checked using FastQC (Afgan *et al.*, 2018). Based on this we used Trimmomatic (Bolger *et al.*, 2014) for an initial crop to 49 bases (49 bases kept starting from the start of the read), followed by a headcrop of 14 bases and sliding window trimming with an average base call quality of 20 across 4 bases. Applying these settings resulted in read lengths of mostly 35 bases. Paired-end reads were mapped to maize genome (release 46, available on https://plants.ensembl.org/Zea_mays/Info/Index) using HISAT2 (Galaxy default settings (Kim *et al.*, 2015)). Correct mapping to the genome at exons was checked using the Integrative Genome Viewer (Robinson *et al.*, 2011), after which the number of paired reads which mapped exons was counted using featureCounts (fragment size was filtered to be between 34 to 1000 bases and reads were not allowed to contribute to multiple features (Liao *et al.*, 2014)). Counts from all samples were combined in a single count table using Multi-Join (Gruening, 2014) and exported from the Galaxy server.

Statistics and count normalisation (DESeq2)

The raw counts were statistically analysed using DESeq2 (v 1.24.0) in R (version 3.6.1) for statistical analysis and to calculate log fold-changes (Love *et al.*, 2014). The effect of treatment, zone and their interaction was tested using the likelihood ratio to compare a full model against a reduced model, which allows to collect a p-value for

terms removed in the reduced model. To remove the dominant effect of zone in our study, we repeated the analysis for comparisons between treatments within each zone separately. To compensate for multiple testing, Benjamini & Hochberg corrected p-values, defined as false discovery rates (FDRs), were calculated. The adjusted p-value cut-off used was 0.05 (alpha) for the selection of significantly altered gene expression. Hereafter, statistics were performed for specific comparisons of interest, i.e. comparing the effect of specific treatments in a zone, and log fold changes were obtained. Counts were transformed using through regularized log (rlog) transformation, a functionality also provided by DESeq2. These normalised counts were used in the following steps where samples are clustered based on their expression profile.

Venn diagrams, cluster analysis and gene ontologies

Venn diagrams were created to obtain insight in the distribution of the genes that were significantly differentially expressed in the full model and in the zones for each treatment (Bardou *et al.*, 2014). For the full model, genes significant for treatment, zone and/or the interaction between treatment and zone (FDR < 0.05) were selected. For comparisons of treatments in each zone, genes significantly (FDR < 0.05) altered in each specific comparison of treatments (e.g. meristem severe vs meristem control, meristem mild vs meristem control and meristem severe vs meristem mild) were selected.

Cluster analysis was performed in MultiExperimentViewer (v 4.9.0). Prior to clustering, the normalize gene/rows function was used on the rlog transformed data to obtain expression values for each gene in the same range, resulting in overlapping expression patterns during clustering. Hierarchical clusters for sample tree construction of all samples were created using Pearson correlation as distance metric and the average linkage as linkage method. To obtain similar expression profiles within a zone, samples were clustered using quality threshold clustering for each zone separately (parameter settings: Pearson correlation as the distance metric, 0.5 as the maximum cluster diameter and a minimum cluster population of 50). Gene ontology

over-/underrepresentation for each cluster resulting from the quality threshold clustering were obtained through http://www.pantherdb.org/ (Thomas *et al.*, 2003), using the internal maize gene database as a background, a Fisher's exact test and false discovery rate p-value correction ($p < 0.05$).

Pathway visualisation through MapMap

Log-fold changes of significant genes (FDR < 0.05) for treatment contrasts in each zone were visualised using MapMan. For gene ID compatibility, the v4 gene IDs were replaced by IDs based on the v3 maize genome assembly using the v3_v4_xref.txt file from maizegdb.org. Due to some genes being split into multiple IDs when translating our original gene IDs (v4 assembly) to the MapMan gene IDs (v3 canonical transcript ID), a limited number of transcription results got duplicated. For instance, in the severe vs control contrast of the meristem, 1799 genes were entered in to MapMan (v3), which is slightly more than the 1768 genes originally obtained (v4).

Supplementary gene lists

Top 60 lists (based on highest absolute log fold-change values) were created of genes significant (FDR < 0.05) for treatment contrasts (i.e. mild versus control, severe versus control and severe versus mild), containing the respective log fold-changes (Supplementary Tables 4.1-4.9). Genes were functionally described using NCBI gene descriptions, available from the NCBI FTP-server: https://ftp.ncbi.nlm.nih.gov/. When no description was available, descriptions were obtained from http://www.gramene.org/. For selected overrepresented gene ontologies, a list of genes which resulted in this overrepresentation was obtained from http://pantherdb.org/ and FDR p-values and LFCs for the severe versus control contrast were added. Panther gene descriptions and gene families were retained (Supplementary Tables 4.10-4.15). For selected MapMan overviews, gene lists were extracted from within the selected MapMan overview. To this list, NCBI gene descriptions were added (Gramene descriptions were used when NCBI descriptions

were unavailable) and FDR p-values and LFCs for the severe versus control contrast were added (Supplementary Tables 4.16-4.18).

Phytohormone analysis

One-centimetre segments of the leaf growth zone were pooled in five biological replicates and snap frozen in liquid nitrogen (i.e. 4 plants per pool for control and mild treatment, 6 plants per pool for severe treatment). Tissue was then ground manually with pestles inside the Eppendorf tube, while frequently cooling the sample and all material used in liquid nitrogen. Hereafter, samples were split in three and tissue weight for each generated sample was obtained while remaining frozen in liquid nitrogen. Next, samples were magnalised using glass beads (MagNALyser, Roche, Vilvoorde, Belgium) at 6000 rpm for 10 seconds, alternating with sample cooling in liquid nitrogen. To facilitate the large number of phytohormones measured, different sets of three biological replicates were used from each treatment, implying that not always the same set of samples was used in each measurement.

Auxin, ABA, JA and SA analysis

Samples were extracted in 500 µL of 80% methanol. [C^{13}]-IAA [100 pmol, (phenyl-$^{13}C_6$)-indole-3-acetic acid, 99%, Cambridge Isotopes, Tewksbury, MA, USA], D6-ABA (150 pmol, [$^2H_6$](+)-*cis,trans*-abscisic acid, [(S)-5-[$^2H_6$](1-hydroxy-2,6,6-trimethyl-4-oxocyclohex-2-en-1-yl)-3-methyl-(2Z,4E)-pentadienoic acid], Olchemim, Olomouc, Czech Republic), D_4-SA (200 pmol, $C_7H_2{}^2H_4O_3$, Olchemim) and DHJA (200 pmol, Sigma) were added as internal tracers. After overnight extraction and subsequent centrifugation (20 min, 15,000g, 4 °C, Eppendorf 5810R, Eppendorf, Hamburg, Germany), the supernatants were aliquoted in two equal parts. One aliquot was acidified using 5.0 mL of 6.0% formic acid and concentrated on a reversed-phase (RP)-C18 cartridge (500 mg, BondElut Varian, Middelburg, The Netherlands). The compounds of interest [IAA, ABA, and the oxidation products IAA-OX, IAA-OH, indole-butyric acid (IBA)-OX, and IBA-OH, SA and JA] were eluted with 5.0 mL of diethyl ether and dried under nitrogen (TurboVap LV Evaporator, Zymark, New Boston, MA, USA).

The second aliquot was kept in 7.0 M NaOH for 3 h at 100°C under a water-saturated nitrogen atmosphere to hydrolyse all ether and ester conjugates. Afterward, the samples were acidified using 2.0 M HCl, concentrated on an RP-C18 cartridge (500 mg), and eluted with diethyl ether as described before. All samples were methylated using ethereal diazomethane to improve analysis sensitivity. Thus, all acid compounds were analysed as their corresponding methyl esters. Samples were dissolved in 10 µl hexane and analysed by GC-MS/MS for SA and JA (Waters Micromass Quattro micro GC (Waters; MA, USA) triple quadrupole with an integrated Agilent 6890N gas chromatography oven, and an electron impact (EI) ion source. The gas chromatography column used was a 15 m x 0.25 mm Agilent J&W "DB-5ms" with a film thickness of 0.25 µm (Agilent Technologies; CA, USA). Before each injection, the injector needle was prewashed 5x with 10 µl hexane. After each injection, the needle was washed 5x with 10 µl hexane and 5x with 10 µl DCM. The injection volume was 10 µl, and the injector operated in splitless mode. Carrier gas was helium, with a flow rate of 1 ml min^{-1}. The oven started isothermally at 50 °C for 2 minutes, then increased linearly to 300 °C at a rate of 25 °C min^{-1}. 300 °C was held for 3 minutes. Oven ramp took 15 minutes, and total run time was 21'40". Mass spectrometry operated in MRM mode. The EI ion source operated in positive ion mode, at 70 eV, inter-channel delay 10ms, inter-scan delay 10 ms. Afterwards, the remaining samples were dried, dissolved in 10%MeOH/H_2O and analysed using an Acquity UPLC system linked to a TQD triple quadrupole detector (Waters, Milford, MA, USA) equipped with an electrospray interface in positive mode. Samples (6.0 µL) were injected on an Acquity UPLC BEH C18 RP column (1.7 µm, 2.1 × 50 mm, Waters) using a column temperature of 30 °C and eluted at 0.3 mL/min with the following gradient of 0.01 M ammonium acetate (solvent A) and methanol (solvent B): 0−2 min isocratic 90/10 A/B; 2−4 min linear gradient to 10/90 A/B. Quantification was done by multiple reactant monitoring of selected transitions based on the MH+ ion (dwell time 0.02 s) and the most appropriate compound-specific product ions in combination with the compound-specific cone and

collision settings. All data were processed using Masslynx/Quanlynx software V4.1 (Waters). No JA was measured in the samples.

Gibberellin analysis

Samples were extracted overnight in 500µL acidified methanol pH 4.0 [80/20, methanol/5.0 mM formic acid-containing butylated hydroxytoluene (3−5 crystals)]. As internal tracers, D_2-GA1 ($C_{19}H_{22}{}^2H_2O_6$), D_2-GA4 ($C_{19}H_{22}{}^2H_2O_5$), D_2-GA8 ($C_{19}H_{22}{}^2H_2O_7$), D_2-GA9 ($C_{19}H_{22}{}^2H_2O_4$), D_2-GA15 ($C_{20}H_{24}{}^2H_2O_4$), D_2-GA19 ($C_{20}H_{24}{}^2H_2O_6$), D_2-GA20 ($C_{19}H_{22}{}^2H_2O_5$), and D_2-GA29 ($C_{19}H_{22}{}^2H_2O_6$; 20 pmol each, Olchemim) were added. After purification on an RP-C18 cartridge (500 mg), samples were derivatized with N-(3-Dimethylaminopropyl)-N'-ethylcarbodiimide hydrochloride (Sigma-Aldrich, 1.0 mg/sample, pH 4.0, 60 min, 37 °C under continuous shaking, Eppendorf thermomixer). Next, these derivatized samples were analysed using a UPLC-MS/MS equipped with an electrospray interface in positive mode (ACQUITY, TQD, Waters). Samples (6.0 µL, partial loop mode using a 10 µl sample loop) were injected on an ACQUITY BEH C18 column (2.1 × 50 mm; 1.7 mm, Waters) using a column temperature of 30 °C and eluted at 450 µL/min with the following gradient of 0.1% formic acid in water (solvent A) and 0.1% formic acid in acetonitrile (solvent B): 0−0.8 min isocratic 92/8 A/B; 0.8−5 min linear gradient to 60/40 A/B; 5−5.5 min linear gradient to 10/90 A/B. Quantification was done by multiple reactant monitoring of selected transitions based on the MH+ ion (dwell time 0.02 s) and the most appropriate compound-specific product ions in combination with the compound-specific cone and collision settings. Transitions are grouped in specific time windows according to the compounds specific retention time in order to keep the dwell time at 0.02s. All data were processed using Masslynx/Quanlynx software V4.1 (Waters).

Cytokinin analysis

Samples were extracted overnight in 500µL 80% MeOH, 500µl. As internal tracers, D_3-DHZR ([6-[$^2H_3$](4-hydroxy-3-methylbutylamino)-9-β-D-ribofuranosylpurine]), D_3-DHZ ([6-[$^2H_3$](4-hydroxy-3-methylbutylamino)purine]), D_5-ZN7G ([6-[$^2H_5$]((E)-4-hydroxy-3-methylbut-2-enylamino)-7-β-D-glucopyranosylpurine]), D_5-ZN9G ([6-[$^2H_5$]((E)-4-

hydroxy-3-methylbut-2-enylamino)-9-β-D-glucopyranosylpurine]), D_5-ZROG ([6-[$^2H_5$]((E)-4-hydroxy-3-methylbut-2-enylamino)-9-β-D-ribofuranosyl-O-β-D-glucopyranosylpurine]), D_5-9ZOG ([6-[$^2H_5$]((E)-4-hydroxy-3-methylbut-2-enylamino)-9-β-D-glucopyranosylpurine]), D_6-iP-7G ([6-[$^2H_6$] (3,3-dimethylallylamino)-7-β-D-glucopyranosylpurine]), D_6-iPR ([6-[$^2H_6$](3,3-dimethylallylamino)-9-β-D-ribofuranosylpurin) and D_6-iP ([6-[$^2H_6$](3,3-dimethylallylamino)purine]) were added (20pmol each, Olchemim). After centrifugation (15 min 14000 rpm, 4°C) samples were diluted to a final methanol concentration of max 10% and bound to a C18 cartridge (500 mg). All compounds of interest were eluted with 3 ml 80%MeOH. The samples were dried under nitrogen (Turbovap) and redissolved into 10% MeOH for analysis. Samples were analysed using a UPLC-MS/MS equipped with an electrospray interface in positive mode (ACQUITY, TQD, Waters). Samples (6.0 µL, partial loop mode using 10 µl sample loop) were injected on an ACQUITY UPLC BEH C18 1.7µm 2.1 x 50 mm in combination with an ACQUITY UPLC BEH C-18 VanGuard Pre-column, 1.7 µm, 2.1 mm X 5 mm, column temperature of 30 °C and eluted at 333 µL/min with the following gradient Solvent A: 1mM Ammonium Acetate, solvent B: Methanol,linear gradient: 0-1: 99.9/0.1 A/B; 1-7.5: linear gradient to 58.3/41.7 A/B; 7.5-9 gradient to 33.4/66.6 A/B; 9.1-10: 0.1/99.9 A/B. Quantification was done by multiple reactant monitoring of selected transitions based on the MH+ ion (dwell time 0.021 s) and the most appropriate compound-specific product ions in combination with the compound-specific cone and collision settings. Transitions are grouped in specific time windows according to the compounds specific retention time in order to keep the dwell time at 0.021s. All data were processed using Masslynx/Quanlynx software V4.1 (Waters).

Analysis ACC and conjugates

Samples were extracted in 500 µL ice-cold 80 % methanol. For quantification, D_4-ACC (250 pmol, $C_4H_3{}^2H_4NO_2$, Olchemim Ltd.) DHJA (200 pmol, (±)-3-oxo-2-pentyl-cyclopentane-1-acetic acid, Olchemim) and D_3-Methionine (1 nmol, L-Methionine-(methyl-d3), Sigma-Aldrich) were added. For the quantification of the ACC-conjugates M-ACC, JA-ACC en G-ACC, D_3-methionine is used as internal standard and the relative

response is determined using an unlabelled authentic standard for M-ACC (gift from prof. D. Van Der Straeten, UGhent). Half a milligram of OASIS HLB 0.3 µm solid phase bulk packing material (WATERS) was added to bind pigments. The packing material and cell debris were removed by centrifugation (14000 rpm, 4°C, 10 min) and the supernatant was filtered using a 0,2µm filter (chromafil syringe filter polyamide/nylon 0,2µm, Macherey-Nagel). The total amount of conjugates was determined as free ACC after acid hydrolysis in 2M HCl, under a nitrogen saturated atmosphere for 2h at 100°C.The ACC and its specific conjugates were analysed with ES+ UPLC-MS/MS with an ACQUITY UPLC BEH Amide, 1.7µm Column 2.1 x 100 mm and an ACQUITY UPLC BEH Amide VanGuard Pre-column, 1.7 µm, 2.1 mm X 5 mm. Solvent A: 0.1% FA in water, Solvent B: 0.1% FA in ACN, flow 0.4 mL/min, gradient 0-2 min:9/91, A/B, 2-3 gradient to 49/51, A/B, 3-4 gradient to 80/20 A/B using a column temperature of 30°C. Injection Mode: Partial Loop, Injection Volume 6 µL with partial loop injection using a 10 µl sample loop. Quantification was done by multiple reactant monitoring of selected transitions based on the MH+ ion (dwell time 0.041s) and the most appropriate compound-specific product ions in combination with the compound-specific cone and collision settings. All data were processed using Masslynx/Quanlynx software V4.1 (Waters).

Mineral analysis

Fresh weight of the sampled leaf segments (10 one-centimetre segments of the growth zone and a blade segment) was measured (AX124, Sartorius, Göttingen, Germany), after which they were oven-dried at 60 °C for 48 to 72 hours. Dry weight was determined with the accuracy of 1 µg (SE2 Ultra-micro balance, Sartorius, Goettingen, Germany). Hereafter, segments from the same position and treatment, but different plants, were pooled (2-3 segments per pool, n = 5). Sample digestion was performed by an overnight predigestion in aqua regia (1:3 nitric acid and hydrochloric acid), followed by high pressure high temperature digestion of 20 minutes (Discover SP-D, CEM, Matthews, NC, USA), allowing the samples to boil at 200 °C. The samples were then diluted 40 times with trace metal grade ultrapure water, after which the Cd

concentration was measured with HR-ICP-MS (High Resolution Inductively Coupled Plasma Mass Spectrometry, Element XR, Thermo Scientific, Bremen, Germany). Blanks were used throughout the analysis to correct for background trace metals. Rye grass European Reference Material CD281 samples were used as a reference. Recoveries of the certified material ranged from 58 to 116 %, where trace amount minerals (i.e. Cd and Mo) are responsible for the lower recovery value. Recovery of more abundant minerals ranged from 83 to 116%. Cadmium, Ca, Cu, Fe, K, Mg, Mn, Na and Zn concentrations were quantified. Co, Mo and Ni were below quantification limit (0.001 µg/L). S and B were affected by contamination and discarded.

Oxidative stress

Plant material was pooled in four biological replicates for each treatment to obtain at least 50 mg fresh weight (i.e. two, three and four plants per replicate for the control, mild and severe treatment respectively). Pooled material was then magnalised using glass beads (MagNALyser, Roche, Vilvoorde, Belgium) until the entire sample was reduced to fine powder at 6000 rpm for 10 seconds, alternating with sample cooling in liquid nitrogen. Hereafter, ground plant material was mixed in ice-cold 80% ethanol (MagNA Lyser, Roche Diagnostics GmbH, Mannheim, Germany) and supernatant was obtained after centrifugation at 14000 rpm for 30 minutes at 4°C. In the supernatant, MDA and FRAP levels were determined. MDA equivalents were determined using the thiobarbituric acid method, measuring absorbances at 440 nm, 532 nm, and 600 nm, as described in Hodges et al. (1999) and FRAP by using Trolox (Sigma-Aldrich, St. Louis, MO, USA) as a standard, as described in Benzie and Strain (1999).

Statistics of biochemical measurements

Assumptions for normality and homoscedasticity were tested using the Shapiro-Wilk test and Levene's test, respectively. When assumptions were not met, data was $\log_{10}$-transformed. Hereafter, the effect of treatment, segment and the interaction was tested using a two-way ANOVA. Statistics were performed in R (v. 3.6.1; R Core Team, 2014).

Results

Earlier we found that Cd inhibited leaf growth through a reduction of meristematic cell number, an increased cell cycle duration and an inhibited cell elongation rate (chapter 3). Using kinematics, we also showed that Cd is predominantly deposited in the meristem, with decreasing deposition rates in the elongation zone. These observations indicated that cadmium could exert its toxic effect locally in the leaf growth zone and have therefore opened the perspective for further investigations of the physiological impact of Cd in the meristem, elongation zone and mature zone.

To reveal the overall impact of the stress and specifically affected physiological processes in the leaf growth zone, we first used a genome wide transcriptome analysis.

Genome wide transcriptome analysis

Relations between the three developmental zones

The zone effect had the largest effect on transcription profiles. The expression of nearly half of all 46430 genes encoded in the maize genome (23086 genes; 49.7%) was significantly (FDR < 0.05) different between the three developmental zones, 12530 of which were solely affected by the effect of zone and not by Cd. Across all three zones, the expression of 7913 genes was significantly affected by cadmium stress. Among these, only 239 genes were uniquely affected by the cadmium treatment (i.e. expression levels were not significantly different between zones and did not show a significant interaction). For the interaction between zone and treatment, 6342 genes (13.7%) were significantly affected (FDR < 0.05), meaning that their transcription response to cadmium is different depending on the developmental stage (Figure 1). The dominant effect of zone on the transcriptome is also apparent when performing hierarchical clustering on the full set of samples (Figure 2). The primary grouping separates samples based on developmental zone. Within each zone cluster, samples are clustered based on treatment. In the meristem and elongation zone, control and mild samples are more closely related to each other, with severe stress samples

forming a separate group. In the mature zone, samples originating from the 2 cadmium treatments are clustered together, with control samples forming a separate group.

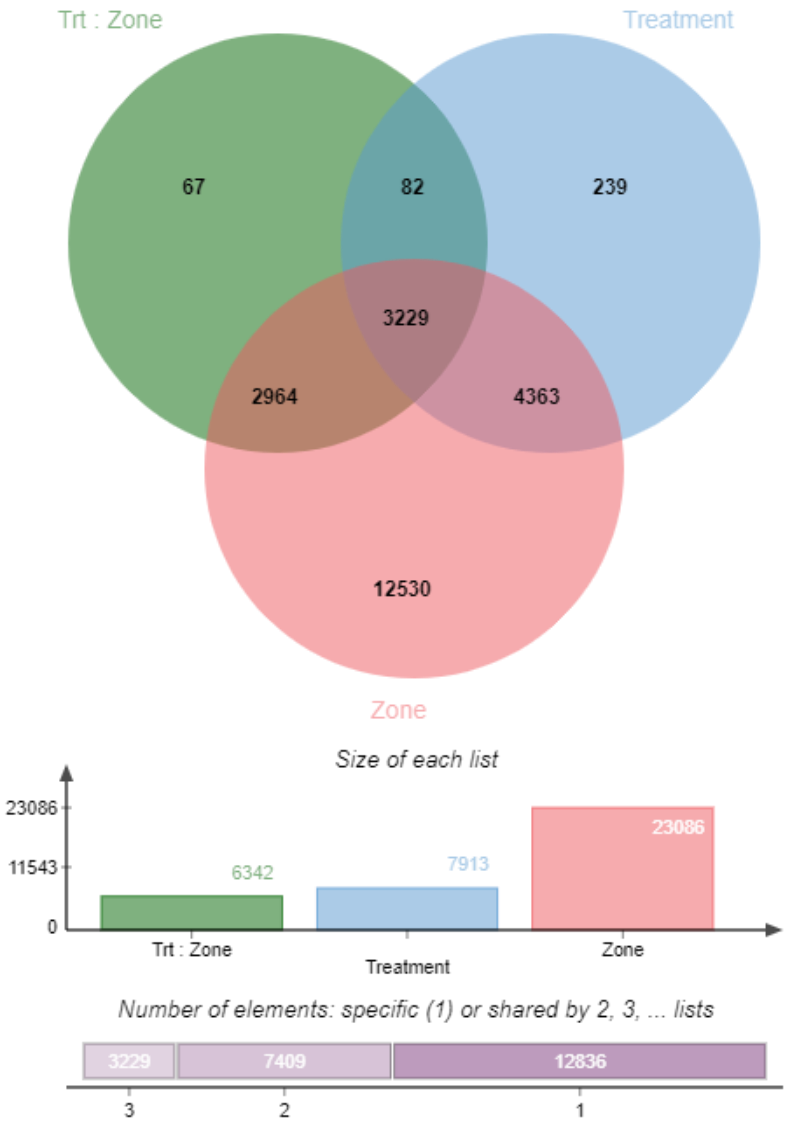

Figure 1. Venn diagram of the genes with a significant interaction between treatment and segment (Trt:Zone), treatment alone and zone alone. Below the Venn diagram, the total number of elements in each circle is given, followed by an overview of how many genes are shared by three, two or one circle(s). Venn diagram created with jVenn (Bardou *et al.*, 2014).

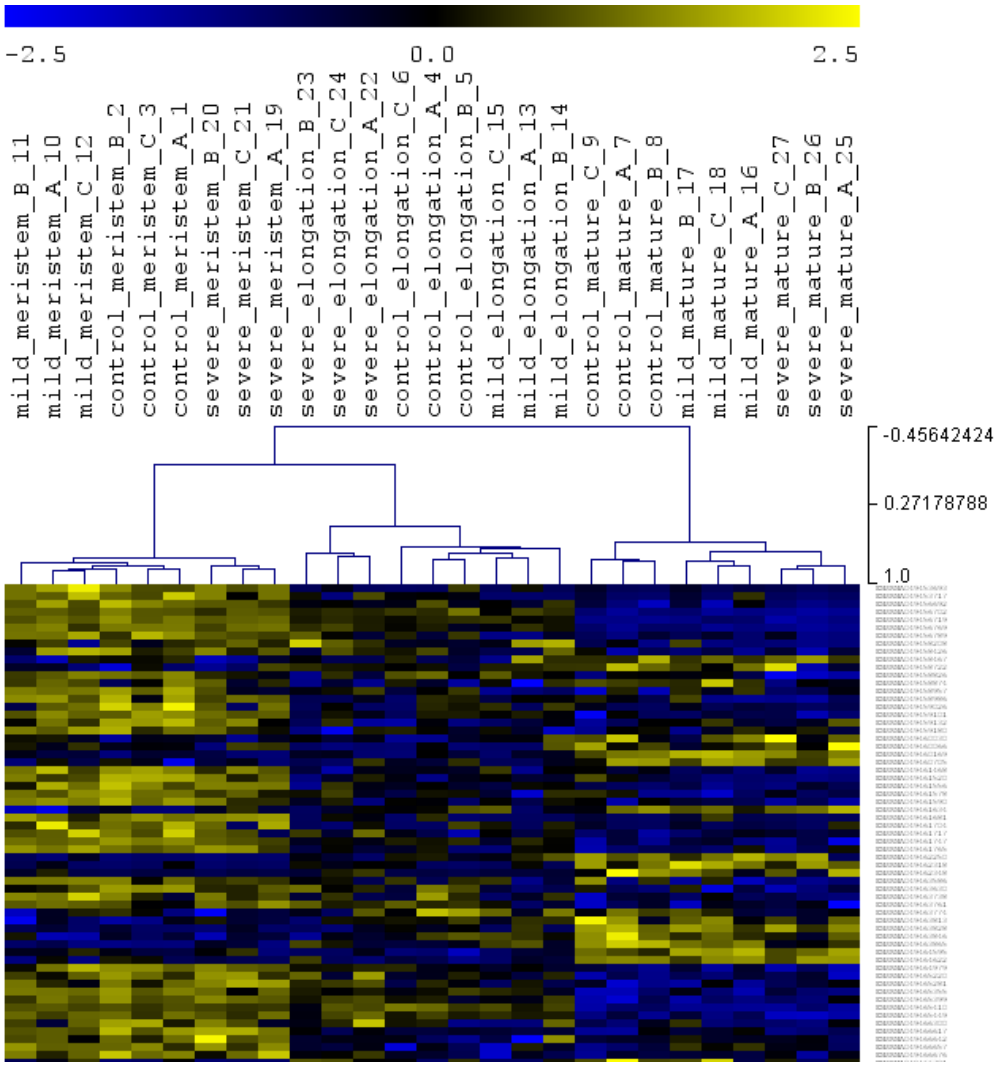

Figure 2. Hierarchical clustering using all sample counts for genes significant for the effect of treatment and/or zone and/or treatment:zone interaction. Counts were normalised using regularised log transformed data (DESeq2) and MeV gene/row normalisation (Multiple Experiment Viewer). Pearson correlation metrics were used for clustering. The sample name contains reference to the treatment (control, mild or severe), zone (meristem, elongation or mature zone), biological replicate label (A, B or C) and sample number.

We next examined the overlap and differences between each developmental zone for the significantly affected genes by severe Cd treatment. Here, 5113 out of 7911 differentially expressed genes (64.5%) were uniquely significant in one of the three zones, while the expression of only 601 genes (7.6 %) was affected by Cd in all three zones (Figure 3). Interestingly, the number of significantly altered genes in the

meristem is almost threefold lower compared to the elongation and mature zone (resp. 1768, 4512 and 5030 significantly (FDR < 0.05) altered genes), the opposite of what may have been expected based on Cd accumulation occurring primarily at the leaf base (chapter 3).

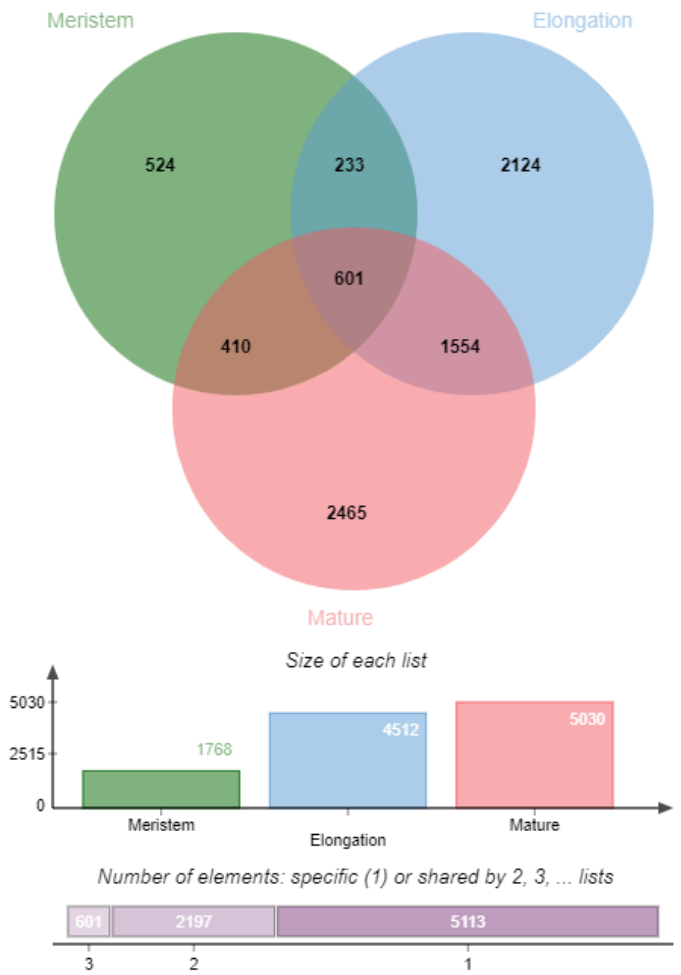

Figure 3. Venn diagram of the genes of which the expression was significantly altered for the severe versus control contrast in each of the three zones. Below the Venn diagram, the total number of elements in each circle is given, followed by an overview of how many genes are shared by three, two or one circle(s). Venn diagram created with jVenn (Bardou *et al.*, 2014).

The accurate reflection of the experimental setup in the transcriptome profile (Figure 2) is a good indication for the quality of the data. However, the dominant effect of the developmental zones masked the effect of the Cd treatment in subsequent analyses. Therefore, we further analysed the effect of treatment in each of the developmental zones individually, allowing us focus on the effect of cadmium in the meristem, elongation zone and mature zone.

Cadmium impact in each developmental zone

Meristem

At the transcriptome level, 1497 genes were significantly (FDR < 0.05) affected by Cd treatment when all meristem samples in the analysis (i.e. control, mild and severe treatments are combined (FDR < 0.05). Separate analysis of mild and severe stress yielded 58 (Supplementary Table 4.1) and 1768 (Supplementary Table 4.2 lists 60 genes with highest FC) significantly affected genes, respectively, showing the relatively small impact of the mild stress (Figure 4). When the transcriptome of severely stressed plants was tested against the ones of mild stress, we found 701 differentially expressed genes (Supplementary Table 4.3 lists 60 genes with highest FC), indicating that mild stress is intermediate to control and severe stress. Within the limited set of significantly affected genes under mild stress, metal ion transporters Zm00001d025623 (Vacuolar iron transporter 1) and Zm00001d016691 (Copper transport protein CCH) are significantly upregulated. In addition, we also found significant downregulation of a gibberellin 20-oxidase (Zm00001d013725), a key enzyme in the gibberellin synthesis pathway, under mild stress. Out of these 58 genes, 51 were also shared by the affected genes under severe stress, indicating that there is an overlap between the two stress levels. Genes, significantly affected by Cd treatment, were first analysed using QT-clustering, which clustered genes based on their transcription profile across the three treatments and resulted in three clusters (Figure 5).

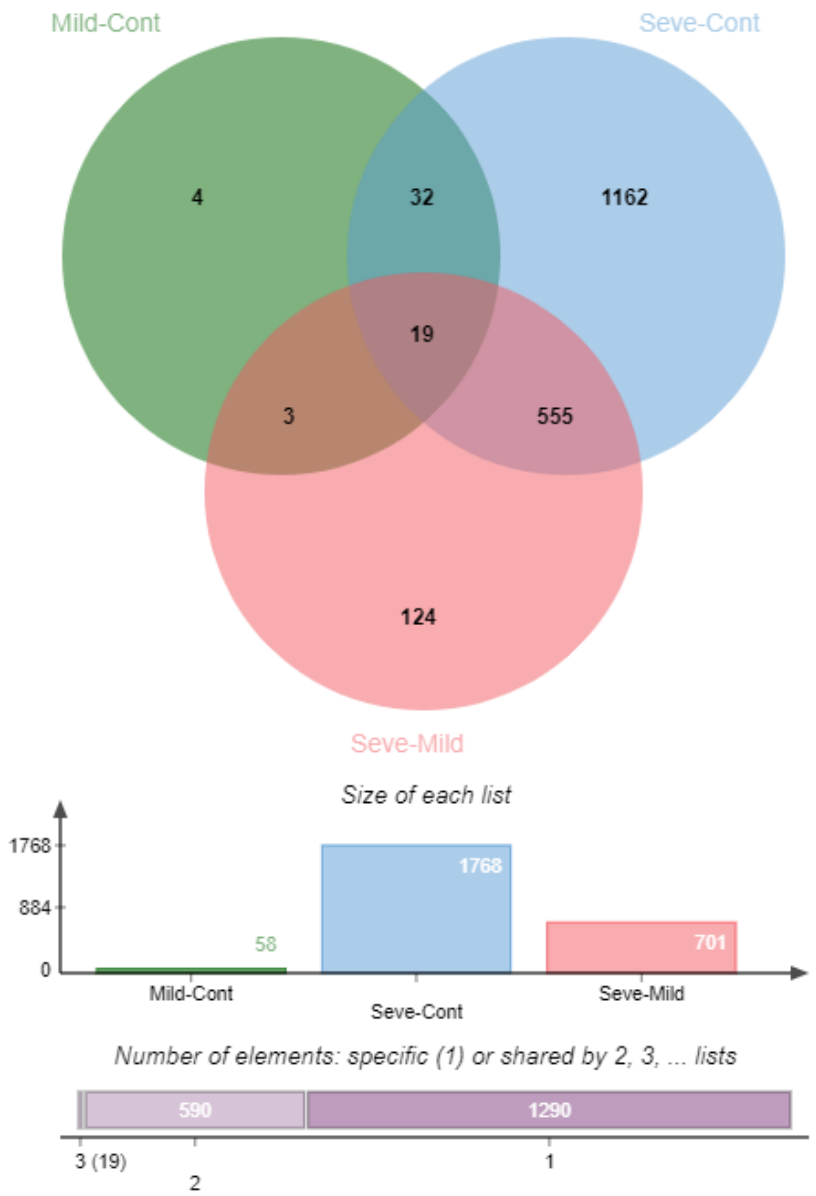

Figure 4. Venn diagram of the genes of which the expression was significantly altered in the meristem for three treatment specific contrasts. Below the Venn diagram, the total number of elements in each circle is given, followed by an overview of how many genes are shared by three, two or one circle(s). Treatments: Cont = control, Mild, Seve = severe. Venn diagram created with jVenn (Bardou *et al.*, 2014).

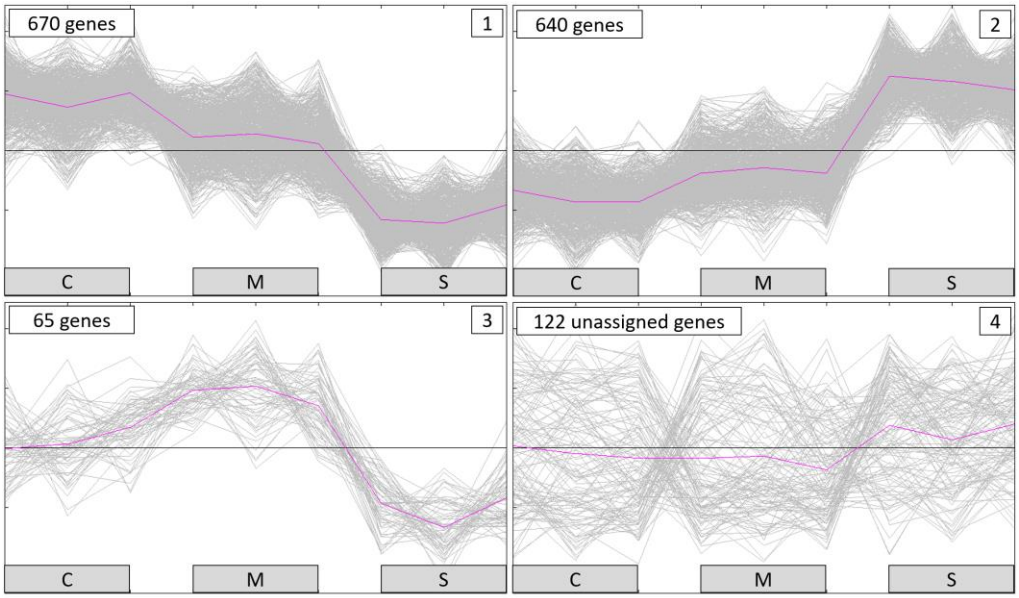

Figure 5. Expression profiles of genes significant (FDR < 0.05) for Cd treatment in the meristem, clustered by quality threshold clustering. Cluster diameter: 0.50, minimum cluster population: 50. C = control treatment samples, M = mild Cd treatment samples, S = severe Cd treatment samples.

Table 1. Top 15 overrepresented biological process gene ontologies in each of the QT-clusters (treatment significant, FDR < 0.05) for the meristem. Only FDR significant GOs (FDR < 0.05) were selected and summarised (based on semantic similarity) using REViGO. CL: cluster, FE: Fold enrichment. Note that the third cluster did only result in 8 GOs after processing in REViGO.

CL	GO ID	GO DESCRIPTION	FE
1	GO:0006422	aspartyl-tRNA aminoacylation	61.71
1	GO:0070407	oxidation-dependent protein catabolic process	41.14
1	GO:0006562	proline catabolic process	41.14
1	GO:0090116	C-5 methylation of cytosine	37.02
1	GO:1902626	assembly of large subunit precursor of preribosome	30.85
1	GO:0010216	maintenance of DNA methylation	24.68
1	GO:0002184	cytoplasmic translational termination	23.14
1	GO:0006323	DNA packaging	17.22
1	GO:0045903	positive regulation of translational fidelity	16.83
1	GO:0009749	response to glucose	16.1
1	GO:0006002	fructose 6-phosphate metabolic process	14.02
1	GO:0006101	citrate metabolic process	13.22
1	GO:0002181	cytoplasmic translation	13.09
1	GO:0006360	transcription from RNA polymerase I promoter	12.99
1	GO:0045910	negative regulation of DNA recombination	12.34
2	GO:0042549	photosystem II stabilization	49.75

CL	GO ID	GO DESCRIPTION	FE
2	GO:0009800	cinnamic acid biosynthetic process	22.62
2	GO:0018298	protein-chromophore linkage	19.04
2	GO:0006559	L-phenylalanine catabolic process	18.29
2	GO:0006021	inositol biosynthetic process	16.96
2	GO:0071577	zinc II ion transmembrane transport	14.35
2	GO:0009627	systemic acquired resistance	13.82
2	GO:0015994	chlorophyll metabolic process	11.96
2	GO:0006596	polyamine biosynthetic process	11.85
2	GO:0043467	regulation of generation of precursor metabolites and energy	11.85
2	GO:0015979	photosynthesis	10.88
2	GO:0009408	response to heat	9.79
2	GO:0042542	response to hydrogen peroxide	8.64
2	GO:0042908	xenobiotic transport	8.58
2	GO:0072350	tricarboxylic acid metabolic process	8.18
3	GO:0006272	leading strand elongation	> 100
3	GO:0009263	deoxyribonucleotide biosynthetic process	> 100
3	GO:1905268	negative regulation of chromatin organization	76.86
3	GO:0022616	DNA strand elongation	50.62
3	GO:0006323	DNA packaging	24.13
3	GO:0040029	regulation of gene expression, epigenetic	23.21
3	GO:0034654	nucleobase-containing compound biosynthetic process	6.36
3	GO:0033554	cellular response to stress	5.02

In cluster 1, the expression of 670 genes decreased with increasing Cd stress. This cluster was mainly enriched for GOs related to protein production, DNA methylation and carbohydrate metabolism (Table 1). The enrichment of GO terms *response to glucose* and *fructose 6-phosphate metabolic process* prompted us to closer inspect the sucrose-starch overview in MapMan (Figure 6). Here, we notice a down regulation of cell wall invertases (mainly Zm00001d003776, LFC: -3.1) and Zm00001d025354, LFC: -2.7) and upregulation of sucrose synthases Zm00001d029087, LFC: 2.7 and Zm00001d029091, LFC: 1.9). Sucrose synthase and invertases differ from each other by the fact that sucrose synthases can reversibly cleave sucrose, where invertases irreversibly hydrolase sucrose into glucose and fructose. Since sucrose synthases can synthesise sucrose and reversibly cleave it, we cannot deduce which end product is favourited. Yet, due to the downregulation of cell wall invertases, one could expect

sucrose or UDP-glucose/fructose to be the desired end product and not the free monosaccharide glucose. Finally, in the top altered genes under severe Cd stress, we also found 3 *SWEET* (sugars will eventually be exported transporter: Zm00001d016590, Zm00001d050577, Zm00001d015905) genes to be strongly upregulated under Cd stress, indicating an altered sugar transport under Cd stress (Supplementary Table 4.2).

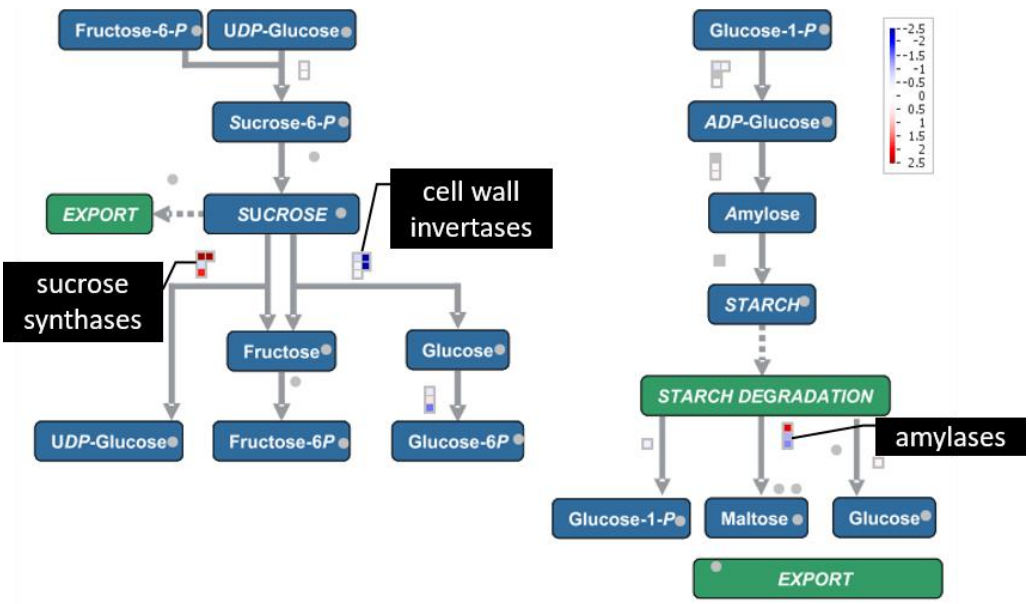

Figure 6. MapMan overview of the sucrose and starch metabolism for the severe versus control contrast in the meristem. Here, we notice a down regulation of cell wall invertases (blue boxes from sucrose to glucose and fructose) and upregulation of sucrose synthases (red boxes from sucrose to UDP-glucose and fructose) on the sucrose pathway (left). Colour gradient represents LFC. The coloured boxes besides arrows represent LFCs of genes, coding enzymes relevant for that reaction.

In cluster 2, 640 genes increased expression with increasing Cd stress. The gene set of cluster 2 was enriched for GOs related to photosynthesis, cinnamic acid, L-phenylalanine, inositol, metal ion transport and responses to abiotic stimuli (heat) and oxidative stress (hydrogen peroxide; Table 1). The GO category metal ion transport contained 24 genes related to different metals (i.e. sodium, calcium, zinc, potassium, iron, cadmium and copper, Supplementary Table 4.1), indicating that the homeostasis of other minerals could be affected by Cd accumulation. Of these 24 genes, zinc, iron

and copper transporters were most affected (Zm00001d036965, Zm00001d019228, Zm00001d025623, Zm00001d016691) and strongly upregulated (resp. LFCs of 3.9, 3, 2 and 1.5; Supplementary Table 4.10). Interestingly, two of these genes were also present in the small set of affected genes under mild Cd stress (i.e. Zm00001d025623 and Zm00001d016691; Supplementary Table 4.1), indicating that already under mild stress mineral levels could be affected by Cd.

Related to the photosynthesis GOs, the MapMan photosynthesis overview confirmed the upregulation of genes at the light reactions hub (Supplementary Figure 4.2). When consulting more specific MapMan mappings related to inositol, we notice a potentially upregulated production of myo-inositol, since two myo-inositol phosphate synthases are upregulated (Zm00001d048201 (LFC 1.6), Zm00001d028180 (LFC 1.4)) in the myo-inositol pathway overview (Supplementary Figure 4.3). Yet, myo-inositol serving as a cell wall precursor is less likely, since inositol oxygenase 2 (Zm00001d046234) is highly downregulated (LFC -7.5, cell wall precursors overview, Supplementary Figure 4.4). In fact, it is the most downregulated gene under severe Cd stress in the total set of 1768 significantly affected genes (Supplementary Table 4.2). Inositol oxygenase oxidises myo-inositol to glucuronic acid, which is then further processed to UDP-glucuronic acid, a principal precursor for several plant cell-wall polymer residues (e.g. xylose, arabinose and galacturonic acid; Kanter *et al.* (2005)). With myo-inositol being a central molecule in plant metabolism, these observations leads us to speculate that myo-inositol is likely used in other pathways, for instance in the esterification to auxin (IAA, indole-3-acetic acid) to form auxin conjugates, phytic acid biosynthesis for phosphate storage or the formation of O-methyl inositol for osmotic regulation (Loewus and Murthy, 2000).

In addition, related to cinnamic acid and phenylalanine GOs, several flavonoid and phenylpropanoid related genes were also significantly upregulated. Amongst the highest upregulated genes are phenylalanine ammonia lyases (PAL, 5 significantly upregulated, highest LFC: 1.84) and cinnamyl-alcohol dehydrogenases (CAD, 3 significantly upregulated, highest LFC: 2.24; Supplementary Figure 4.5). The PAL

enzymes catalyse the phenylalanine conversion to cinnamic acid, where CAD is an enzyme that functions in the last step of monolignol synthesis (Zhao *et al.*, 2013*b*). It were also mainly these PAL expressed genes that resulted in the overrepresented L-phenylalanine catabolic process GO (Supplementary Table 4.11). Cinnamic acid and phenylalanine might be considered as supporting GOs for salicylic acid production, since they are precursors in its production (Dempsey et al., 2011). Their upregulation could indicate increased SA levels.

The regulation overview in MapMan highlights a potential impact of cadmium in the meristem on IAA, ABA, jasmonate, SA and GA (Figure 7). Among the genes presented in this MapMan overview, we mainly find upregulated genes related to ABA, IAA and jasmonic acid (Supplementary Table 4.16). For ABA, several of these genes encode transcription factors and relate to ABA-regulated gene expression. For jasmonic acid, we find several lipoxygenases. Examining more closely the genes involved in the jasmonic acid (JA) synthesis pathway (Figure 8), there is a strong upregulation of these lipoxygenase genes involved in the transition from linolenic acid to 13(S)-hydroperoxylinolenic acid and transition of the latter to 13,13(S)-epoxylinolenic acid, which could indicate increased JA levels under severe Cd stress. In addition, in the late phases of gibberellin synthesis (Figure 8), we note a strong downregulation of a gibberellin 20-oxidase (Zm00001d013725, important for GA1 production, LFC of -3.1, also present in the 60 most strongly altered genes, Supplementary Table 4.2) and a high upregulation of a gibberellin 2-oxidase (Zm00001d037724, important for GA1 breakdown, LFC of 2.4), which suggests reduced GA1 levels (the most active GA in maize) in the severely stressed maize leaf.

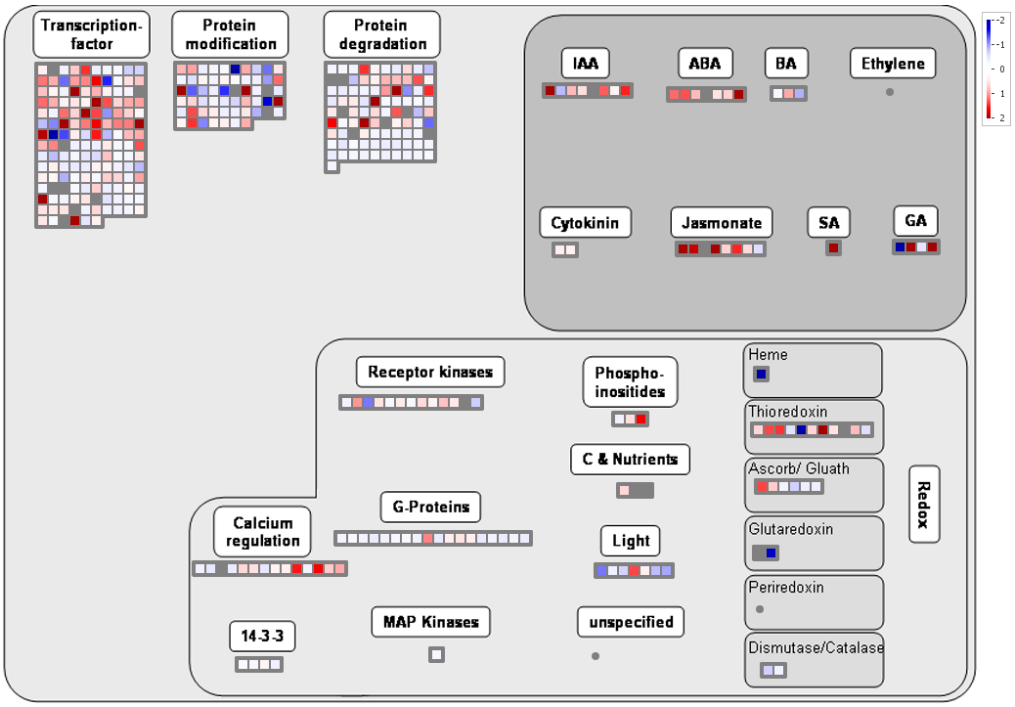

Figure 7. MapMan regulation overview of FDR significant genes (FDR < 0.05) for the severe vs control contrast in the meristem. Colour gradient represents LFC. The coloured boxes besides arrows represent LFCs of genes, coding enzymes relevant for that process.

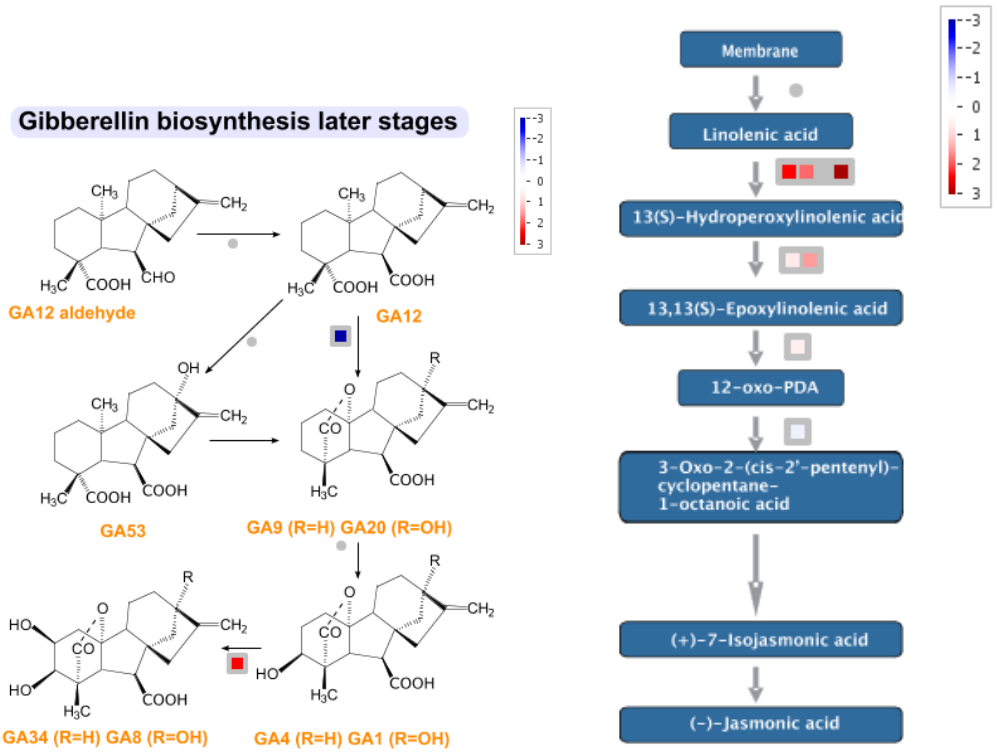

Figure 8. MapMan overview of the later stages of gibberellin biosynthesis (left) and JA synthesis (right) of FDR significant genes (FDR < 0.05) for the severe vs control contrast in the meristem. Here, we note a strong downregulation (blue square) of a gibberellin 20-oxidase (Zm00001d013725) and a high upregulation (red square) of a gibberellin 2-oxidase (Zm00001d037724) in the gibberellin pathway. On JA synthesis pathway, we note a high upregulation of genes involved in the transition from linolenic acid to 13(S)-hydroperoxylinolenic acid and transition of the latter to 13,13(S)-epoxylinolenic acid. Colour gradient represents LFC. The coloured boxes besides arrows represent LFCs of genes, coding enzymes relevant for that reaction.

Cluster 2 of the meristem samples also contained GOs related to cellular responses to abiotic stress (i.e. heat) (Table 1). This matches visualisations in the cellular response overview of MapMan, where a lot of genes are upregulated under severe Cd stress related to heat stress (Figure 9). Among these genes, there are several heat shock proteins (Supplementary Table 4.18), which could indicate that there is a need to stabilize proteins and membranes under Cd stress. In addition, cluster 2 also contained GOs related to oxidative stress and more specifically hydrogen peroxide. With regards to the genes in this response to hydrogen peroxide GO, there are 5 heat shock proteins are upregulated (Supplementary Table 4.12). Accumulation of hydrogen peroxide could induce heat shock proteins (Volkov *et al.*, 2006), hence the relation between this type of protein and the hydrogen peroxide related GO.

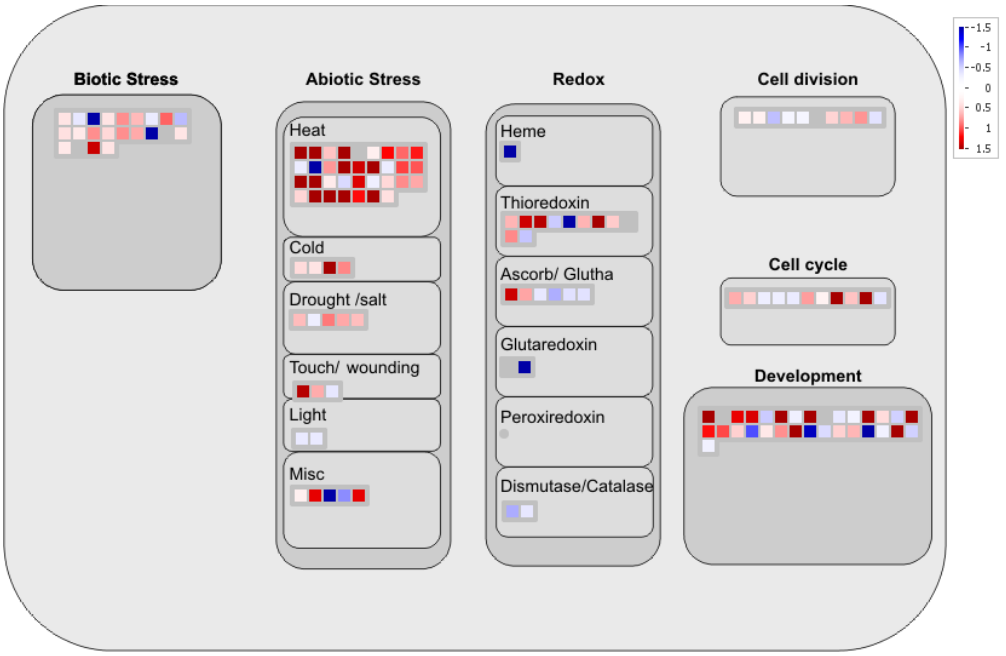

Figure 9. MapMan overview of the cellular response for the severe versus control contrast in the meristem. Colour gradient represents LFC. The coloured boxes besides arrows represent LFCs of genes, coding enzymes relevant for that process.

Cluster 3 contained 65 genes which showed an upregulation under mild stress and downregulation under severe stress and was enriched for GOs of cell cycle related processes, with gene ontologies like deoxyribonucleotide biosynthetic process, leading strand elongation, DNA strand elongation and DNA packaging (Table 1, Supplementary Table 4.13). When inspecting the most affected cell cycle genes in the cellular response overview in MapMan (Figure 9), we found two upregulated D-type cyclins (LFC 0.5 to 0.7) and a downregulated B-type cyclin (LFC -0.34)). The latter is the same B-type cyclin measured in chapter 3 using qPCR (chapter 3, Figure 5), where we also reported its significant downregulation. For the two other cell cycle genes measured by qPCR in chapter 3, the NGS data confer their downregulation, where the NGS data shows a significant (FDR < 0.05) downregulation of wee1 (Zm00001d053998, LFC = -0.5 ± 0.1) and minichromosome maintenance4 (Zm00001d044540, LFC = -0.3 ± 0.1).

Elongation zone

In the elongation zone 926 and 4512 genes were significantly affected by the mild and severe treatment, respectively (Figure 10, 60 most differentially expressed genes: resp. Supplementary Tables 4.4 and 4.5). The severe versus mild contrast resulted in the highest number of significantly altered genes, i.e. 6251 (Top 60 differentially expressed genes: Supplementary Table 4.6), which indicates that both Cd treatments differ more from each other than when they are compared against the control treatment. This observation is also supported by a PCA analysis of the individual samples, where the largest distance is observed between mild and severe treatment samples across PC1, which explains 90% of the variance in the datasets (Supplementary Figure 4.10). When testing the treatment effect over all three treatments together, 6153 genes were significantly affected, which grouped in 6 clusters based on their expression profile (Figure 11).

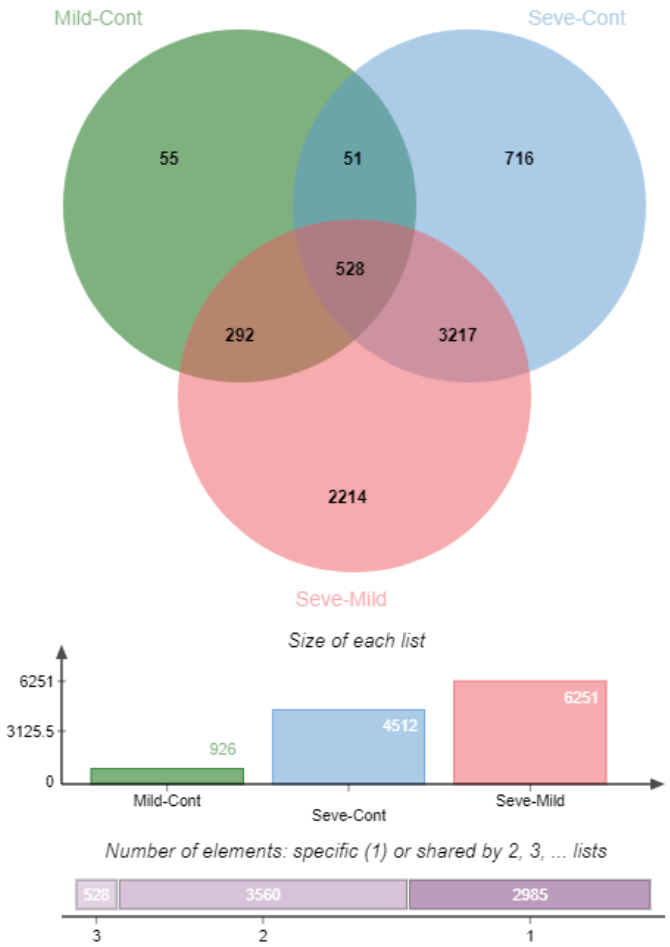

Figure 10. Venn diagram of the genes of which the expression was significantly altered in the elongation zone for a specific contrast of the treatments. Below the Venn diagram, the total number of elements in each circle is given, followed by an overview of how many genes are shared by three, two or one circle(s). Treatments: Cont = control, Mild, Seve = severe. Venn diagram created with jVenn (Bardou *et al.*, 2014).

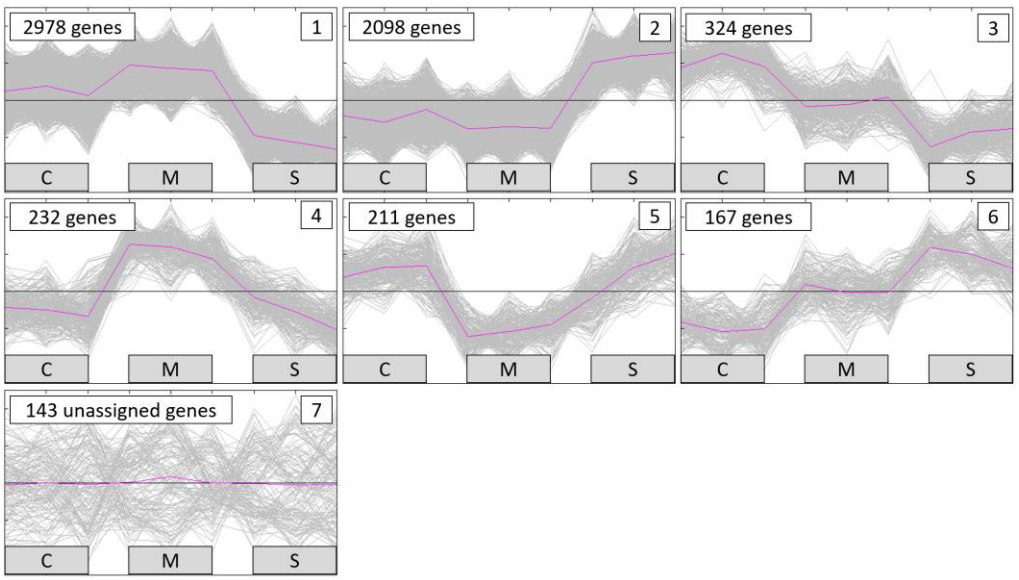

Figure 11. Expression profiles of genes significant (FDR < 0.05) for treatment in the elongation zone, clustered by quality threshold clustering. Cluster diameter: 0.50, minimum cluster population: 50. C = control treatment samples, M = mild treatment samples, S = severe treatment samples.

Gene ontology analysis of the first cluster, where 2978 genes were upregulated under mild stress and down regulated under severe stress, mainly related to photosynthesis (Table 2). In addition, the fourth cluster, containing 232 genes that were specifically upregulated only under mild stress, also contained GOs which mainly referenced photosynthesis. The MapMan photosynthesis overview confirmed the upregulation of photosynthesis related genes in the first and fourth QT cluster under mild Cd stress and their downregulation under severe stress compared to control (Supplementary Figure 4.6).

Table 2. Top 10 overrepresented biological process gene ontologies in each of the QT-clusters (treatment significant, FDR < 0.05) for the elongation zone. Only FDR significant GOs (FDR < 0.05) were selected and summarised (based on semantic similarity) using REViGO. CL: cluster, FE: Fold enrichment. Note that the fourth cluster did only result in 8 GOs after processing in REViGO.

CL	GO ID	GO DESCRIPTION	FE
1	GO:0042793	transcription from plastid promoter	12.04
1	GO:0032544	plastid translation	11.89
1	GO:0045038	protein import into chloroplast thylakoid membrane	10.7
1	GO:0010207	photosystem II assembly	10.7
1	GO:1903580	positive regulation of ATP metabolic process	10.7
1	GO:0042372	phylloquinone biosynthetic process	10.7
1	GO:1901259	chloroplast rRNA processing	10.7
1	GO:1901031	regulation of response to reactive oxygen species	9.55
1	GO:0010304	PSII associated light-harvesting complex II catabolic process	8.92
1	GO:0031221	arabinan metabolic process	8.92
2	GO:0051754	meiotic sister chromatid cohesion, centromeric	18.97
2	GO:0016572	histone phosphorylation	13.55
2	GO:0006561	proline biosynthetic process	10.84
2	GO:2000779	regulation of double-strand break repair	9.49
2	GO:0034063	stress granule assembly	9.49
2	GO:0032886	regulation of microtubule-based process	8.25
2	GO:0031145	anaphase-promoting complex-dependent catabolic process	7.99
2	GO:1903829	positive regulation of cellular protein localization	7.3
2	GO:0030261	chromosome condensation	7.03
2	GO:1904666	regulation of ubiquitin protein ligase activity	6.78
3	GO:0015671	oxygen transport	84.52
3	GO:0015669	gas transport	84.52
3	GO:0006435	threonyl-tRNA aminoacylation	63.39
3	GO:0001731	formation of translation preinitiation complex	29.26
3	GO:0002181	cytoplasmic translation	24.01
3	GO:0046940	nucleoside monophosphate phosphorylation	16.9
3	GO:0006450	regulation of translational fidelity	16.9
3	GO:0007007	inner mitochondrial membrane organization	15.85
3	GO:0010499	proteasomal ubiquitin-independent protein catabolic process	14.09
3	GO:0006637	acyl-CoA metabolic process	13
4	GO:0009768	photosynthesis, light harvesting in photosystem I	33.18
4	GO:0018298	protein-chromophore linkage	20.99
4	GO:0009833	plant-type primary cell wall biogenesis	16.81
4	GO:0015979	photosynthesis	13.07
4	GO:0030244	cellulose biosynthetic process	12.07
4	GO:0001101	response to acid chemical	5.25
4	GO:0009628	response to abiotic stimulus	4.53
4	GO:0008150	biological_process	1.28
5	GO:0043111	replication fork arrest	> 100
5	GO:0031120	snRNA pseudouridine synthesis	99.57
5	GO:0090116	C-5 methylation of cytosine	79.66
5	GO:0018279	protein N-linked glycosylation via asparagine	66.38
5	GO:1905269	positive regulation of chromatin organization	66.38
5	GO:0000727	double-strand break repair via break-induced replication	66.38
5	GO:0018196	peptidyl-asparagine modification	66.38

CL	GO ID	GO DESCRIPTION	FE
5	GO:0010216	maintenance of DNA methylation	59.74
5	GO:0070125	mitochondrial translational elongation	54.31
5	GO:0043570	maintenance of DNA repeat elements	49.79
6	No GOs		

In the second cluster, the expression of 2098 genes was specifically upregulated under severe Cd stress conditions. Here, GOs mainly related to the cell cycle and DNA maintenance. Also, the fifth cluster contained GOs related to DNA modification and maintenance. Here, 211 genes were specifically downregulated under mild stress conditions. The upregulation for cell cycle related genes under severe stress in cluster 2 is indeed present in the MapMan cellular response overview for the severe versus control contrast, but largely absent (and mainly down regulated) in de mild versus control contrast (Figure 12).

The third cluster contained 324 genes of which the expression levels decreased with increasing cadmium stress and to which GOs were mainly related to translational GOs. The last cluster (6) which contained 167 genes with a gradually increasing expression proportional to Cd levels. Presumably due to its relatively low number of genes, this cluster was not overrepresented for specific GO terms.

Mild versus Control:

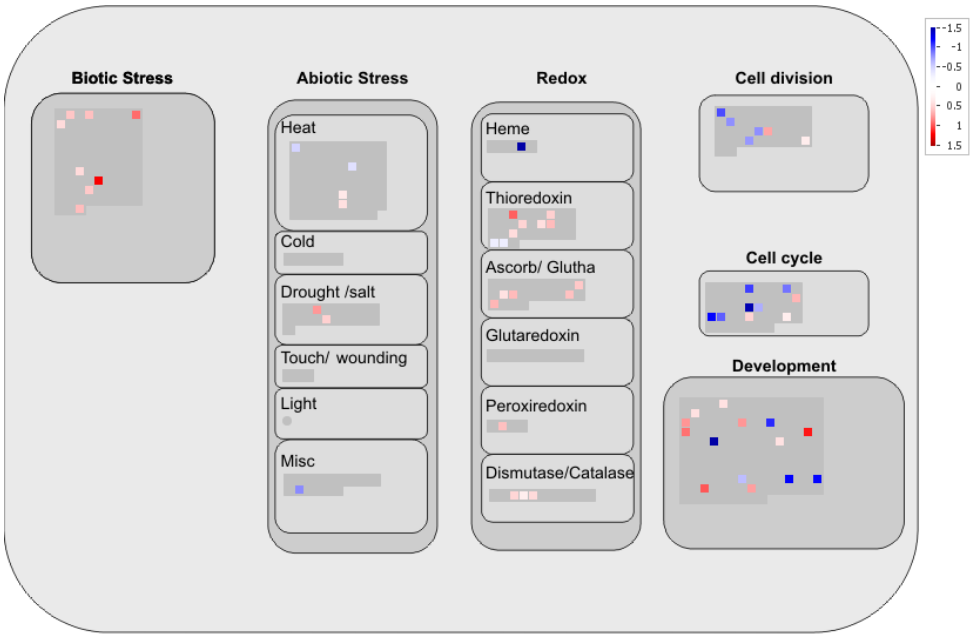

Severe versus Control:

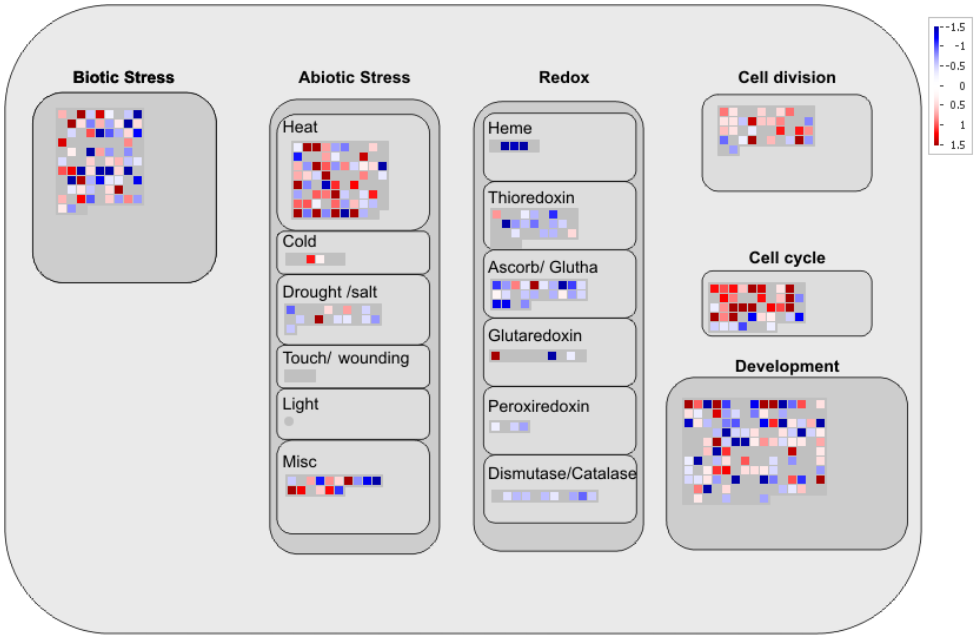

Figure 12. MapMan cellular response overview in the elongation zone for the mild (top) and severe (bottom) contrasts versus the control treatment. Colour gradient represents LFC. The coloured boxes besides arrows represent LFCs of genes, coding enzymes relevant for that process.

Mature zone

The impact of mild stress on the transcriptome profile increased further in the mature zone, resulting in 5506 significantly affected genes across all treatments. The expression of 2508 and 5030 genes was significantly affected by mild and sever stress respectively, where the difference between mild and severe treatment resulted in 2324 differentially expressed genes (Figure 13, see 60 most differentially expressed genes in Supplementary Tables 4.7, 4.8 and 4.9, respectively). A QT cluster analysis with the treatment affected genes created 6 clusters (Figure 14).

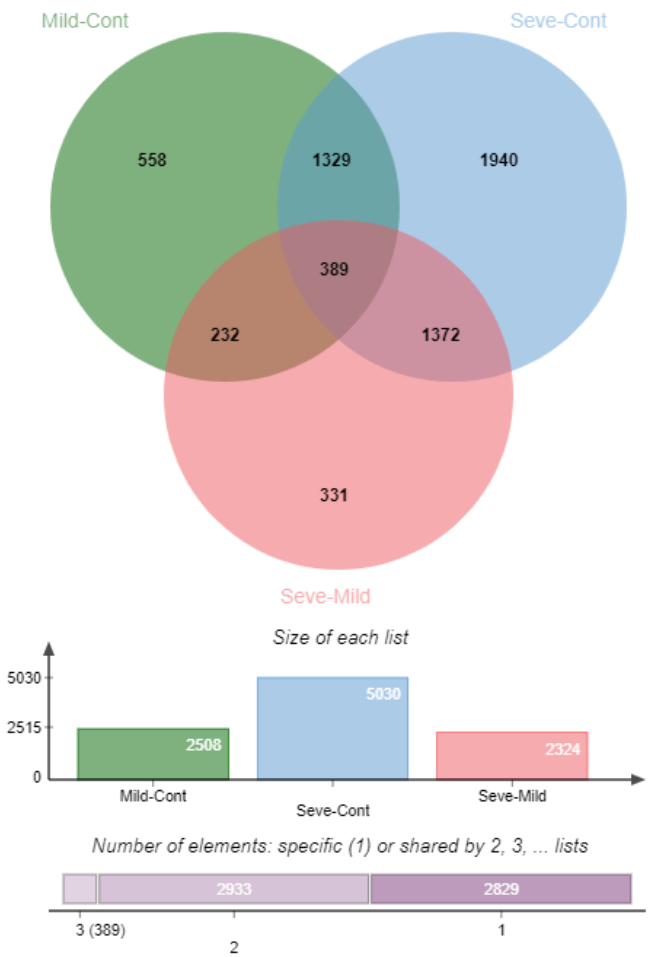

Figure 13. Venn diagram of the genes of which the expression was significantly altered in the mature zone for a specific contrast of the treatments. Below the Venn diagram, the total number of elements in each circle is given, followed by an overview of how many genes are shared by three, two or one circle(s). Treatments: Cont = control, Mild, Seve = severe. Venn diagram created with jVenn (Bardou *et al.*, 2014).

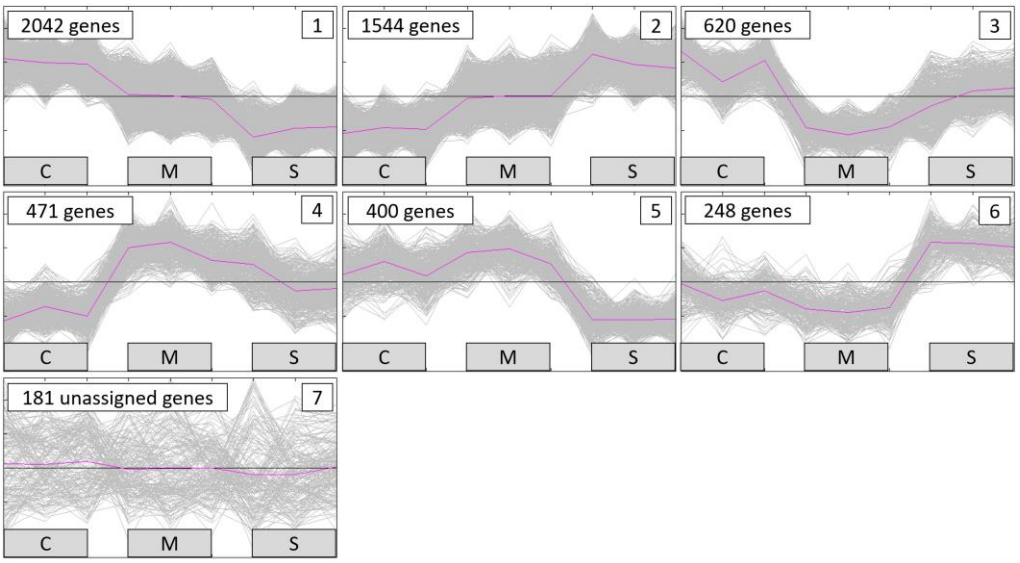

Figure 14. Expression profiles of genes significant (FDR < 0.05) for treatment in the mature zone, clustered by quality threshold clustering. Cluster diameter: 0.50, minimum cluster population: 50. C = control treatment samples, M = mild treatment samples, S = severe treatment samples.

The first and largest cluster (2042 genes), contained transcripts for which the expression decreased with increasing cadmium stress. This cluster was overrepresented for GO categories related to transcription and translation, oxidative stress and DNA replication (Table 3). When inspecting the more specific oxidative stress GOs, we find GOs related to positive regulation of superoxide dismutase activity, where two out of the three genes were chaperonins related to protein folding and stability (Supplementary Table 4.14).

Table 3. Top 10 overrepresented biological process gene ontologies in each of the QT-clusters (treatment significant, FDR < 0.05) for the mature zone. Only FDR significant (FDR < 0.05) GOs were selected and summarised (based on semantic similarity) using REViGO. CL: cluster, FE: Fold enrichment.

CL	GO ID	GO DESCRIPTION	FE
1	GO:1901671	positive regulation of superoxide dismutase activity	20.1
1	GO:0070681	glutaminyl-tRNAGln biosynthesis via transamidation	20.1
1	GO:0090143	nucleoid organization	20.1
1	GO:0006269	DNA replication, synthesis of RNA primer	16.08
1	GO:0042793	transcription from plastid promoter	16.08
1	GO:1902626	assembly of large subunit precursor of preribosome	13.4
1	GO:0070129	regulation of mitochondrial translation	11.48
1	GO:0031425	chloroplast RNA processing	11.16
1	GO:0006085	acetyl-CoA biosynthetic process	10.05
1	GO:0009098	leucine biosynthetic process	10.05

CL	GO ID	GO DESCRIPTION	FE
2	GO:0009627	systemic acquired resistance	8.57
2	GO:0009768	photosynthesis, light harvesting in photosystem I	8.3
2	GO:0018298	protein-chromophore linkage	5.77
2	GO:0030004	cellular monovalent inorganic cation homeostasis	4.68
2	GO:0002376	immune system process	4.17
2	GO:0009734	auxin-activated signaling pathway	3.47
2	GO:0015979	photosynthesis	2.88
2	GO:0009266	response to temperature stimulus	2.66
2	GO:0009607	response to biotic stimulus	2.4
2	GO:0009605	response to external stimulus	2.39
3	GO:0033356	UDP-L-arabinose metabolic process	36.76
3	GO:0006556	S-adenosylmethionine biosynthetic process	32.16
3	GO:0032012	regulation of ARF protein signal transduction	28.59
3	GO:0015790	UDP-xylose transport	26.8
3	GO:0042732	D-xylose metabolic process	19.3
3	GO:0009800	cinnamic acid biosynthetic process	17.54
3	GO:0031204	posttranslational protein targeting to membrane, translocation	17.54
3	GO:0007163	establishment or maintenance of cell polarity	13.54
3	GO:0006891	intra-Golgi vesicle-mediated transport	13.46
3	GO:0010417	glucuronoxylan biosynthetic process	12.51
4	GO:0009439	cyanate metabolic process	31.46
4	GO:0006000	fructose metabolic process	25.81
4	GO:0015995	chlorophyll biosynthetic process	22.37
4	GO:0009768	photosynthesis, light harvesting in photosystem I	21.65
4	GO:0030388	fructose 1,6-bisphosphate metabolic process	19.74
4	GO:0043467	regulation of generation of precursor metabolites and energy	15.98
4	GO:0006002	fructose 6-phosphate metabolic process	15.25
4	GO:0007623	circadian rhythm	14.8
4	GO:0048511	rhythmic process	14.8
4	GO:0018298	protein-chromophore linkage	13.7
5	GO:1900871	chloroplast mRNA modification	66.55
5	GO:0016122	xanthophyll metabolic process	66.55
5	GO:1903601	thermospermine metabolic process	66.55
5	GO:0051193	regulation of cofactor metabolic process	49.91
5	GO:0031221	arabinan metabolic process	33.27
5	GO:0000105	histidine biosynthetic process	30.71
5	GO:0052803	imidazole-containing compound metabolic process	30.71
5	GO:0006782	protoporphyrinogen IX biosynthetic process	29.95
5	GO:0006189	'de novo' IMP biosynthetic process	24.96
5	GO:0010027	thylakoid membrane organization	21.84
6	No GOs		

In the second largest cluster (1544 genes), gene expression levels increased with increasing cadmium stress. This cluster was overrepresented for GO terms related to responses to biotic and abiotic stress and photosynthesis. The MapMan photosynthesis overview indeed showed an upregulation of genes involved in the light reactions and Calvin cycle for the mild versus control contrast (Supplementary Figure 4.7; Table 3, Figure 14). Under severe stress, the majority of the genes involved in the photosynthesis processes are also upregulated, while some are now downregulated as well. When interpreting the results of cluster number 5, containing 400 genes specifically downregulated by severe Cd stress, we can understand this downregulation. For this fifth cluster, overrepresented GO categories were related to photosynthesis and more specifically to chloroplast mRNA modification, pigment biosynthesis, thylakoid membrane organization and protein localization to the chloroplast. Indeed, when consulting the photosynthesis MapMan overview (Supplementary Figure 4.7), we found downregulated genes in photosystem II for which the MapMan description made reference to the thylakoid of chloroplasts (in addition to calcium ion binding and oxygen-evolving complex; Supplementary Figure 4.7).

Cluster 3, containing 620 genes that were most strongly downregulated by mild stress and to a lesser extent by severe stress, revealed GOs related to cinnamic acid (next to GOs related to nucleotide sugars and intracellular transport (e.g. vesicle)). This cinnamic acid biosynthetic process GO enrichment was supported by three genes encoding phenylalanine ammonia-lyases (Supplementary Table 4.15), two of which overlapped with those found in the meristematic tissue (Supplementary Table 4.11). As mentioned in the meristem results section, cinnamic acid and phenylalanine might even be considered as supporting GOs for salicylic acid production, since they are precursors in its production (Dempsey *et al*., 2011). However, in the meristem, these GOs were coupled to genes which increased in expression level relative to Cd stress, where here, gene expression is lowered, which could indicate that SA levels might be lowered again in the mature tissue.

Interestingly, also the auxin-activated signalling pathway was in the top 10 of cluster 2. The MapMan regulation overview shows all represented hormones to be affected in the severe versus control contrast (Figure 15). Most of the auxin related genes involved in this overview are downregulated (Supplementary Table 4.17) and relate to auxin-induced/responsive proteins. Their downregulation could indicate reduced auxin levels. For ABA, jasmonate and SA, we mainly note significantly upregulated genes, where BA (6-benzyladenine), ethylene, cytokinins and gibberellins are both up- and downregulated (Supplementary Table 4.17). The upregulation of SA related genes contradicts the anticipated SA decline based on the downregulated genes related to cinnamic acid and phenylalanine, described at the results of cluster 1 and 3. When inspecting the overview of the late phases of gibberellin synthesis and jasmonic acid synthesis for the severe versus control contrast (Figure 16), similar conclusions to those in the meristem can again be made, where we noted a downregulated gibberellin 20-oxidase and an upregulated of gibberellin 2-oxidase, which, as in the meristem, suggests downregulation of GA1 levels. In the JA synthesis pathway the upregulation of lipoxygenase genes (Supplementary Table 4.17) involved in the transition of linolenic acid to 13(S)-hydroperoxylinolenic acid was observed (Figure 16), which might result in increased JA content.

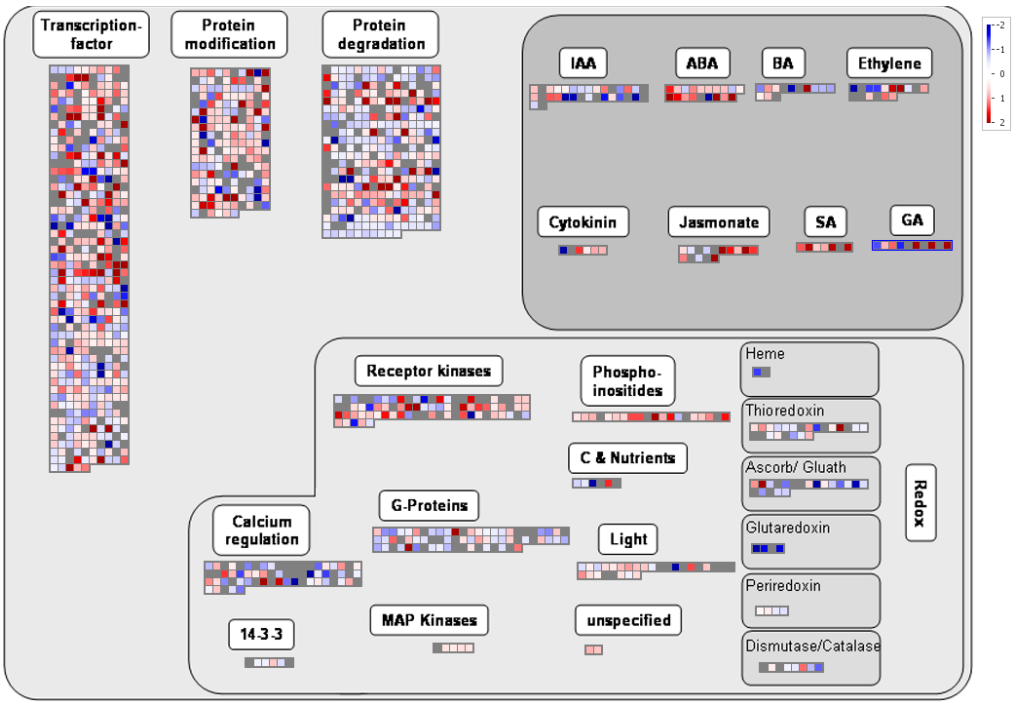

Figure 15. MapMan regulation overview of FDR significant genes (FDR < 0.05) for the severe vs control contrast in the mature zone. Colour gradient represents LFC. The coloured boxes besides arrows represent LFCs of genes, coding enzymes relevant for that process.

Cluster 4 contained 471 genes that were strongly upregulated by mild stress and to a lesser extent by severe stress. These genes overrepresented GOs related to photosynthesis, circadian rhythm and carbohydrate metabolism (intermediates of the glycolysis). When consulting the sucrose and starch pathway for the severe versus control contrast (Figure 17), the sucrose synthase and invertase genes are both up- and downregulated in the mature zone, making its interpretation inconclusive. In addition, starch degradation towards glucose is upregulated.

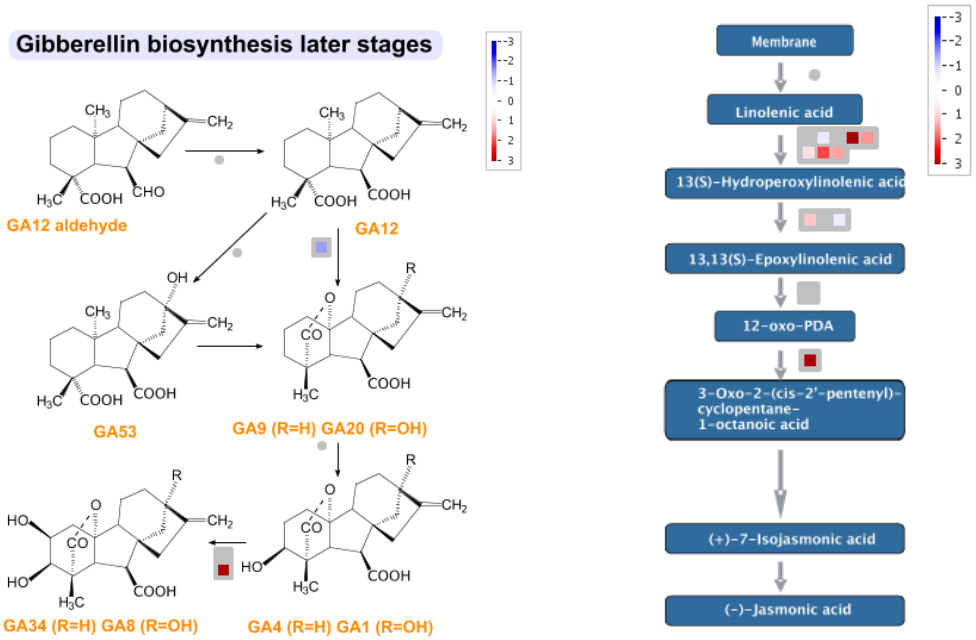

Figure 16. MapMan overview of the later stages of gibberellin biosynthesis (left) and JA synthesis (right) of FDR significant genes (FDR < 0.05) for the severe vs control contrast in the meristem. Here, we note a strong downregulation (blue square) of a gibberellin 20-oxidase (Zm00001d013725) and a high upregulation (red square) of a gibberellin 2-oxidase (Zm00001d037724) in the gibberellin pathway. On JA synthesis pathway, we note a high upregulation of genes involved in the transition from linolenic acid to 13(S)-hydroperoxylinolenic acid. Colour gradient represents LFC. The coloured boxes besides arrows represent LFCs of genes, coding enzymes relevant for that reaction.

Finally, cluster 6 contained 248 genes which were specifically upregulated under severe cadmium stress, but presumably due to its limited size did not result in significantly overrepresented GO terms.

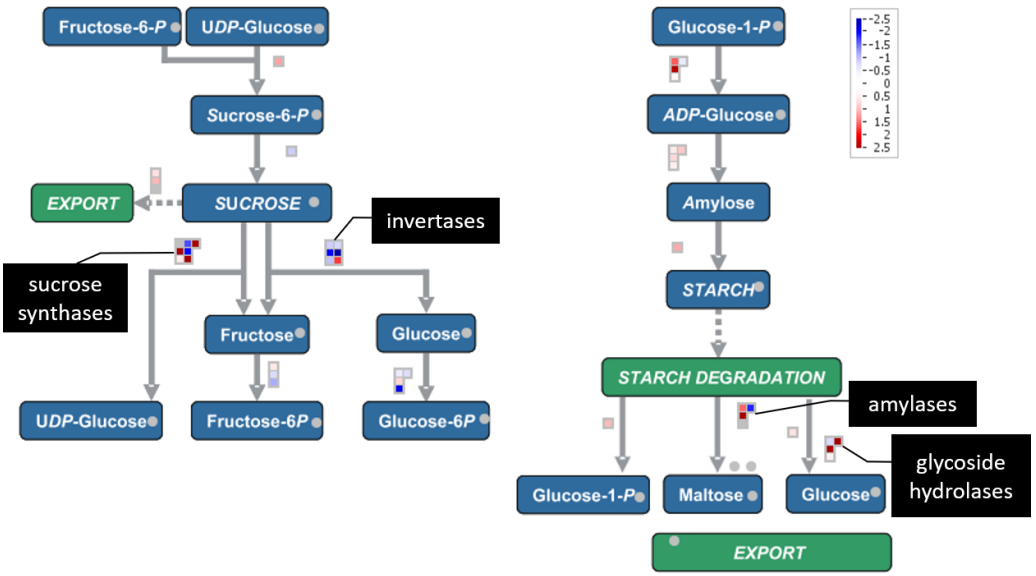

Figure 17. MapMan overview of the sucrose and starch metabolism for the severe versus control contrast in the mature zone. Colour gradient represents LFC. The coloured boxes besides arrows represent LFCs of genes, coding enzymes relevant for that reaction. Invertases: the highly downregulated genes (blue) are cell wall invertases, whereas the upregulated gene is a vacuolar invertase. Glycoside hydrolases: not much is known about these genes. For some, glycoside hydrolase activity and starch binding domains are attributed to them.

Transcriptome data supporting further metabolite analysis

Previously, we have shown that perturbed meristematic function largely explains the effect of Cd on leaf growth, coinciding with the Cd accumulation pattern. High Cd accumulation in the meristem could impact the transport of other minerals. Indeed, the transcriptome data revealed that the transcription of several mineral transporters (e.g. Zn, Fe and Cu transporters) was increased under Cd stress, which could affect mineral levels. In the same meristematic tissue, we found upregulated genes which resulted in the overrepresentation of the GO class “response to hydrogen peroxide”. Oxidative stress is known as a key factor in the global response of plants to Cadmium (Cuypers *et al.*, 2010). However, how the dividing and expanding cells are affected is much less known. In addition, the MapMan regulation overview of both the meristematic and mature tissue indicated that several phytohormone levels could be altered under Cd stress (e.g. gibberellins, which serve a key role in meristem size regulation (Nelissen *et al.*, 2012). Due to the central role of phytohormones in growth regulation and due to the important role of proper mineral homeostasis in plant growth (Singh *et al.*, 2013), changes in phytohormone and mineral levels could potentially provide an explanation for the observed growth inhibition. Therefore, to increase our understanding of how Cd inhibits leaf growth we decided to perform a detailed analysis of mineral and phytohormone levels across the maize leaf growth zone. In addition, we quantified malondialdehyde levels and ferric reducing antioxidant power to analyse Cd induced oxidative stress and antioxidant response.

Biochemical analyses

Phytohormones

In order to increase our understanding on how cadmium affects leaf growth, we performed an analysis of the effect of Cd on phytohormone levels (both stress and growth hormones) in the maize leaf growth zone.

Stress hormones

Severe Cd stress strongly increased ABA content over the entire growth zone under severe stress conditions, but not under mild stress conditions (Figure 18). This suggests that treatment intensity passes some sort of threshold for ABA synthesis when going towards high cadmium doses. A more dose dependent response was found for SA, which showed a progressive increase in SA content with increasing cadmium levels (Figure 18). Additionally, we note an increase in SA and ABA under severe stress conditions towards the mature tissue. Finally, JA was not detected in the tissue.

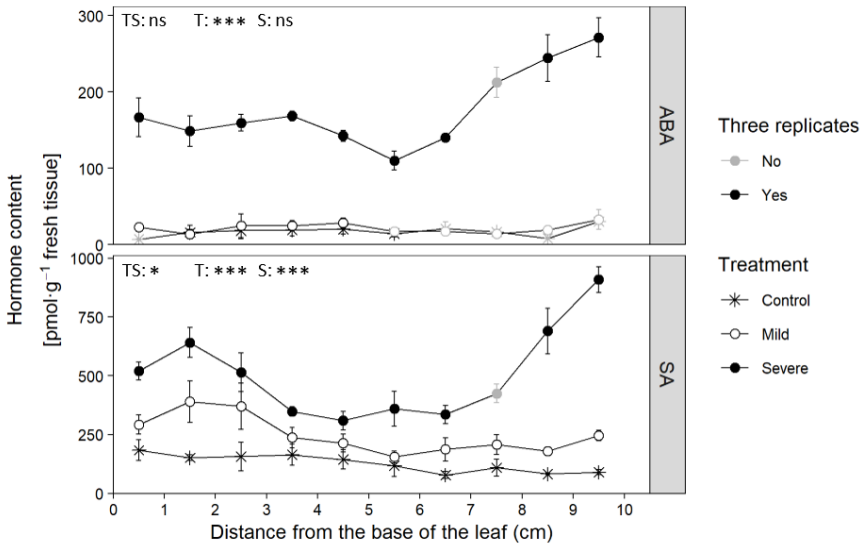

Figure 18. The effect of Cd on the levels of plant stress hormones ABA and SA in the maize leaf growth zone. Values are mean (n = 3), error bars are standard errors. When less than three measurements were available, the error bar and point is coloured grey. When no error bar is present, only one measurement was available. Note: ABA was not normally distributed after $\log_{10}$ transformation. TS: interaction treatment-segment p-value, T: treatment p-value, S: segment p-value. ns: not significant, * $p < 0.05$, ** $p < 0.01$, *** $p < 0.001$.

For ethylene, we measured its direct precursor ACC (1-aminocyclopropane-1-carboxylic acid) and three ACC conjugates (Figure 19). It should be taken into account that ACC can also induce ACC-specific responses by itself, since it has been recently shown that ACC can act as a negative regulator of growth itself (e.g. rosette development, hypocotyl elongation and root growth) (Vanderstraeten *et al.*, 2019). The ACC profile contained quite a lot of variation, yet it is clear that both cadmium treatments significantly increase ACC levels across the maize leaf growth zone. Striking is that the levels of conjugated ACC are about 10-fold higher under control conditions and 20 to 40-fold higher under severe and mild cadmium treatments compared to free ACC, respectively. The fact that mild stress conditions increased conjugated ACC levels is even more puzzling. More detailed analysis of the composition of the conjugated ACCs shows that these large amounts and the difference between mild and severe are mainly driven by high levels of malonyl-ACC (Figure 19). Jasmonyl-ACC on the other hand is present in lower amounts and shows a dose dependent response to cadmium levels used. Glutamyl-ACC is also different compared to the other two conjugates. Here, glutamyl-ACC is mainly present under control conditions and to a decreasing extent under severe and mild conditions, respectively. Next to treatment, also developmental stage (i.e. segment) seems to have a significant effect on certain ACC-conjugates, where glutamyl-ACC has higher levels in the meristematic region under control conditions and jasmonyl-ACC has higher levels towards the mature zone under mainly cadmium stressed conditions. These results demonstrate that, in the maize leaf growth zone, conjugated ACC dominates in absolute quantities and that the composition and gradient of these conjugates across the growth zone varies under cadmium stress. Nevertheless, overall ACC levels are clearly upregulated by Cd.

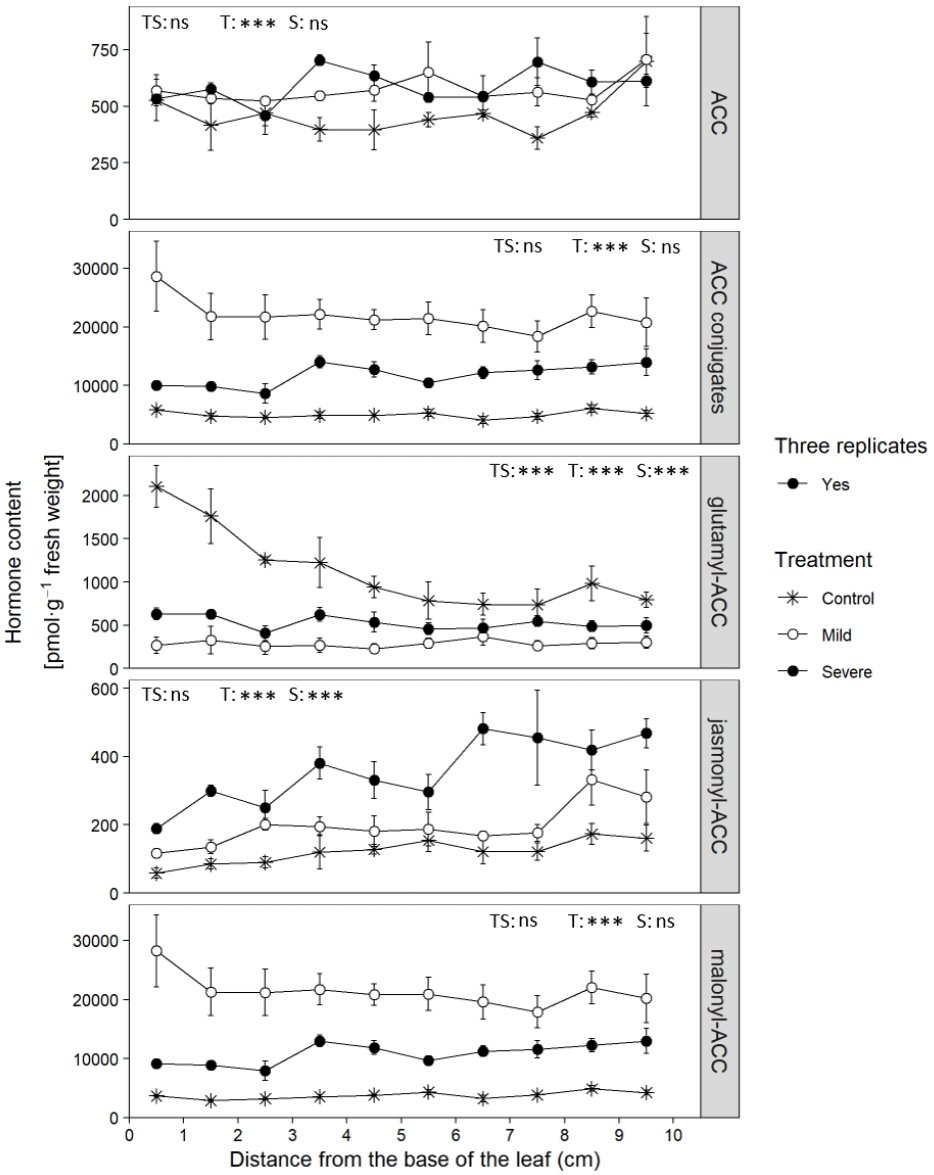

Figure 19. The effect of Cd on the ACC and ACC-conjugate levels in the maize leaf growth zone. Values are mean (n = 3), error bars are standard errors. For all segments/treatments, three replicates were available. Note: malonyl-ACC was not normally distributed after $\log_{10}$ transformation (p = 0.026 Shapiro-Wilk. test). TS: interaction treatment-segment p-value, T: treatment p-value, S: segment p-value. ns: not significant, * $p < 0.05$, ** $p < 0.01$, *** $p < 0.001$.

Growth promoting hormones

Gibberellins (GAs) are known to affect cell division and cell elongation. Increased endogenous GA levels result in larger plants and organs (Voorend *et al.*, 2016). In the maize leaf, GA1 is the most prominent bio-active gibberellin, with GA4 being present in lower quantities (Nelissen *et al.*, 2012). Consistent with Nelissen *et al.* (2012), GA1 levels peaked at the meristem/elongation zone transition in our results. GA1 levels were strongly reduced by severe stress and an early drop of GA1 levels was observed under both Cd stress conditions. In addition, GA19, an intermediate product for GA1, accumulated under severe cadmium stress in the meristematic region (Figure 20). GA20, the last intermediate of GA1 and being formed by GA19 oxidation, showed an impacted reduction, especially around the elongation zone.

The transcriptome data allow us to hypothesise the mechanism behind the altered GA-levels. Here, the lowered GA1 levels under severe cadmium stress conditions could be linked to increased expression of gibberellin 2-oxidase, which catalyses the GA1 oxidation to GA8, the main catabolic product of GA1 (Figure 20). In addition, a significant reduction of gibberellin 20-oxidase transcription, an enzyme which catalyses GA53, GA44, and GA19 oxidation to GA20, could limit precursor availability for GA1 production (Figure 20). This limited GA20-oxidase transcription could perhaps explain the increased accumulation of GA19.

GA7, another biologically active gibberellin, was detected in the maize leaf growth zone, but did not show a clear pattern related to segment or Cd treatment (Supplementary Figure 4.8). The remaining two bioactive gibberellins, GA3 and GA4 did not exceed detection levels. Yet, GA15 and GA9, two intermediates for GA4 and GA7, were detected and measured (Supplementary Figure 4.8). GA9 did not show a clear pattern across the growth zone, nor was it affect by the treatment, where GA15 was generally reduced under the severe Cd treatment across the maize leaf growth zone.

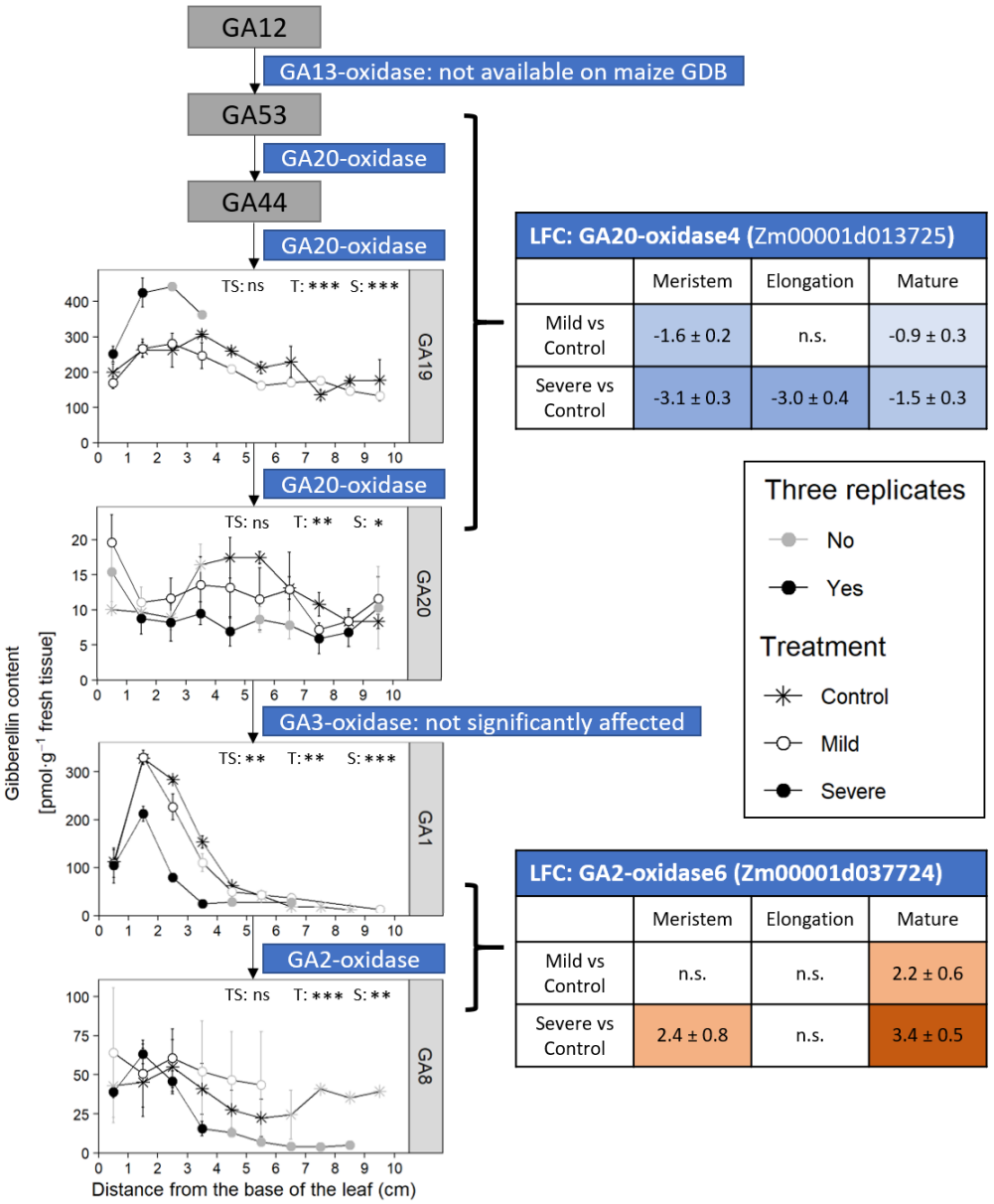

Figure 20. The effect of Cd on Gibberellin content and gibberellin oxidase gene expression in the maize leaf growth zone. Gibberellin content: Values are mean (n = 3), error bars are standard errors. When less than three measurements were available, the error bar and point is coloured grey. When grey and no error bar is present, only one measurement was available. TS: interaction treatment-segment p-value, T: treatment p-value, S: segment p-value. ns: not significant, * $p < 0.05$, ** $p < 0.01$, *** $p < 0.001$. Log Fold Changes (LFCs) for GA20-oxidase4 and GA2-oxidase6 are presented when significant (FDR < 0.05) for the mild vs control and severe vs control contrast for the meristem, elongation zone and mature zone, where red indicates an upregulation and blue indicates a downregulation. n.s. = not significant. The following gibberellins were not detected or had only a marginal number of measurements available: GA12, GA29, GA3, GA4, GA44 and GA5. Note: GA1 was not normally distributed, even after $\log_{10}$ transformation.

In the auxin biosynthetic pathway, the active auxin indole-3-acetic acid (IAA) and its precursor indole-3-butyric acid (IBA) were measured, together with their conjugated forms. Auxin has been shown to be important for placement of leaf primordia at the shoot apex, but also the positioning of the main vein and lateral veins in developing leaves (Scarpella *et al.*, 2010). In our maize leaves IAA levels are high in the meristem and decline across the growth zone, after which they stabilise around the fifth centimetre (Figure 21). However, they do not show big alterations in response to Cd, where only a small increase in IAA levels is noted in the first centimetres of the growth zone under mild stress, where severe stress is slightly higher compared to control in the mature tissue. The conjugates of auxin, typically referred to as the storage forms for the active plant hormone (Ludwig-Müller, 2011), show quite stable levels across the growth zone and are increased under both mild and severe Cd stress. A pattern, similar to IAA-conjugates, is found for IBA and IBA-conjugates, yet at levels around a 100-fold higher compared to IAA.

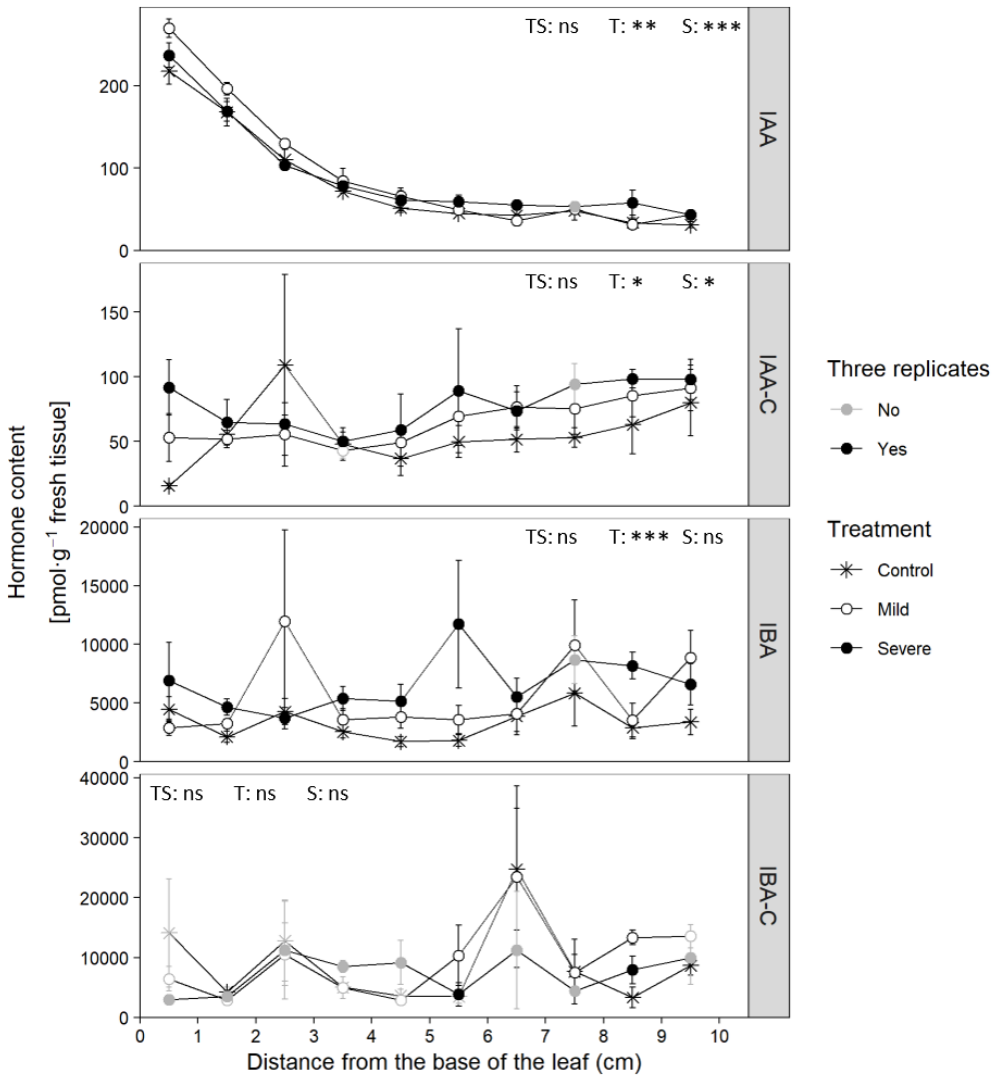

Figure 21. The effect of Cd on Auxin levels in the maize leaf growth zone. Values are mean (n = 3), error bars are standard errors. When less than three measurements were available, the error bar and point is coloured grey. When no error bar is present, only one measurement was available. Note: IAA was not normally distributed after $\log_{10}$ transformation. TS: interaction treatment-segment p-value, T: treatment p-value, S: segment p-value. ns: not significant, * $p < 0.05$, ** $p < 0.01$, *** $p < 0.001$.

The cytokinins are a large group of plant hormones, which are adenine derivates that carry a variable side chain at the N^6-position of the purine (Feng *et al.*, 2017). In the maize leaf growth zone we detected 9 cytokinins, two of which are O-glucosides, which are the inactive storage form of cytokinins. The others are active forms that have been related to stimulation of cell division, shoot initiation, biomass increase, transpiration rate increase and increase in antioxidant capacity (Suttle and Banowetz, 2000; Veach *et al.*, 2003; Sakakibara, 2006; Sytar *et al.*, 2019). Of the cytokinins measured across the maize leaf growth zone, four were significantly affected by the Cd treatment, i.e. cis-zeatin O-glucoside (c-Z-OG), dihydrozeatin riboside-O-glucoside (DH-ZR-OG), cis-zeatin riboside (c-ZR) and trans-zeatin riboside (t-ZR) (Figure 22). The inactive c-Z-OG and DH-ZR-OG dominated the absolute quantities across all cytokinins measured and showed a dose depend increase in response to cadmium. High quantities of the O-glucoside forms are to be expected, since O-glucosylation protects cytokinins from degradation by cytokinin oxidases and allows them to be stored (Veach *et al.*, 2003). This increase was most visible in the meristem, where both cytokinins also reached their maximum. Considering t-ZR, only low amounts were measured compared to c-Z-OG and DH-ZR-OG, with highest levels under control conditions in the meristem, followed by mild and even lower, severe. c-ZR was also on the low side in terms of absolute quantities, yet, unlike t-ZR, its levels increased in cadmium exposed plants towards the end of the growth zone. Cis-zeatin, trans-zeatin, dihydrozeatin, dihydrozeatinriboside and isopentenyladenine were measured but no clear effect of treatment was observed. Interrestingly, c-ZR increased in the mature tissue under severe Cd stress. In conclusion, the peak of the active t-ZR levels in the meristem was strongly decreased by Cd. Inversely, O-glucosilated (inactive) cytokinins strongly increased, perhaps explaining the downregulation of the levels of the active cytokinins.

In conclusion, three stress hormones, SA, ABA and ACC increased in the maize leaf growth zone in response Cd stress. Considering the growth promoting hormones in the growth zone, a clear decrease in gibberellic acid 1 and trans-zeatin riboside was found under Cd stress, while auxin levels only slightly increased or remained unaffected.

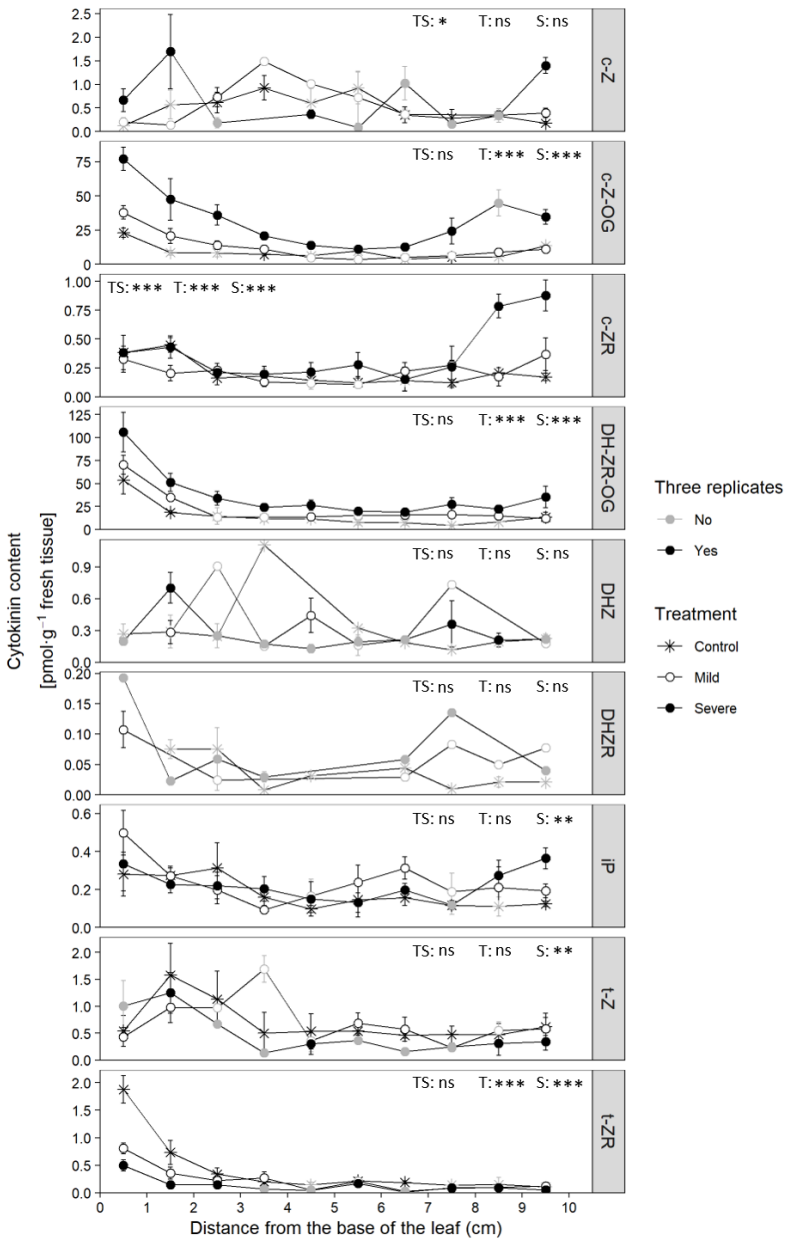

Figure 22. The effect of Cd treatments on Cytokinins in the maize leaf growth zone. Values are mean (n = 3), error bars are standard errors. When less than three measurements were available, the error bar and point is coloured grey. When no error bar is present, only one measurement was available. Note: DHZR not normally distributed after $\log_{10}$ transformation. TS: interaction treatment-segment p-value, T: treatment p-value, S: segment p-value. ns: not significant, * $p < 0.05$, ** $p < 0.01$, *** $p < 0.001$. c-Z: cis-zeatin, c-Z-OG: cis-zeatin O-glucoside, c-ZR: cis-zeatin riboside, DH-ZR-OG: dihydrozeatin riboside-O-glucoside, DHZ: dihydrozeatin, DHZR: dihydrozeatin riboside, iP: isopentenyladenine, t-Z: trans-zeatin, t-ZR: trans-zeatin riboside.

Mineral analysis

Earlier we showed that Cd is nearly absent in control leaves, but strongly accumulates at the base of leaves from Cd treated plants (chapter 3). Our genome wide transcriptome study showed a strong effect of Cd treatment on ion transporters of other minerals, suggesting an effect of Cd on the homeostasis of these other minerals (Supplementary Table 4.10). Therefore, we analysed mineral levels throughout the growth zone. Consistent with mineral study literature, we present our data on dry weight tissue basis (Figure 23). Mineral content expressed on fresh weight tissue basis (consistent with chapter 3) is presented supplementary (Supplementary Figure 4.9).

Under control conditions, calcium (Ca), copper (Cu), magnesium (Mg) and zinc (Zn) show a pattern similar to that of Cd across the growth zone, i.e. highest in the meristem and declining during cell elongation (Figure 23). Copper levels however increase slightly again in fully mature blade tissue. Iron (Fe), potassium (K), manganese (Mn) and sodium (Na) have more consistent levels across the growth zone, where Mn and Fe tend to be higher in fully matured blade tissue. Potassium shows slight, but significant increases around the end of cell elongation.

Severe Cd stress strongly reduced Ca, Cu, K, Mn and Zn content across the maize leaf growth zone. For K and Zn, this reduction is not present in fully matured blade tissue where it resembles control levels. Magnesium levels are also reduced by severe Cd stress, where this reduction is highest in the meristematic tissue. Sodium and iron levels are not much affected by Cd stress, though it should be noted that there is a reduction in Fe content in the mature blade tissue under severe Cd stress.

Under mild Cd stress, mineral contents are not so much affected, with the exception of Cu and Mn. For Cu, we observe a slight increase under mild Cd stress, whereas Mn, levels were reduced across the growth zone and in the blade tissue. Calcium, K and Zn, show a minor reduction under mild Cd stress.

When mineral content is expressed on fresh weight basis (Supplementary Figure 4.9), the profiles of the minerals remain essentially the same under control conditions. However, the reductions under severe Cd stress of Ca, K, Mg and Zn levels were not found on a fresh weight basis. This difference relates to a strongly increased DW to FW ratio (Supplementary Figure 3.2 of chapter 3), suggesting that an overall effect on water content rather than specific effects on the uptake of these minerals plays an important role. Nevertheless, a clear reduction in Mn content across the entire maize leaf growth zone, and reduced Ca and Zn content in the meristem are also observed on a FW basis.

In conclusion, we found that Cd treatments mainly reduced mineral contents across the maize leaf growth zone, where the effects on Mn contents were strongest. Notably, Ca, Cu, Mg, and Zn shared a similar distribution pattern across the growth zone as Cd (i.e. high in the meristem and reducing along the elongation zone).

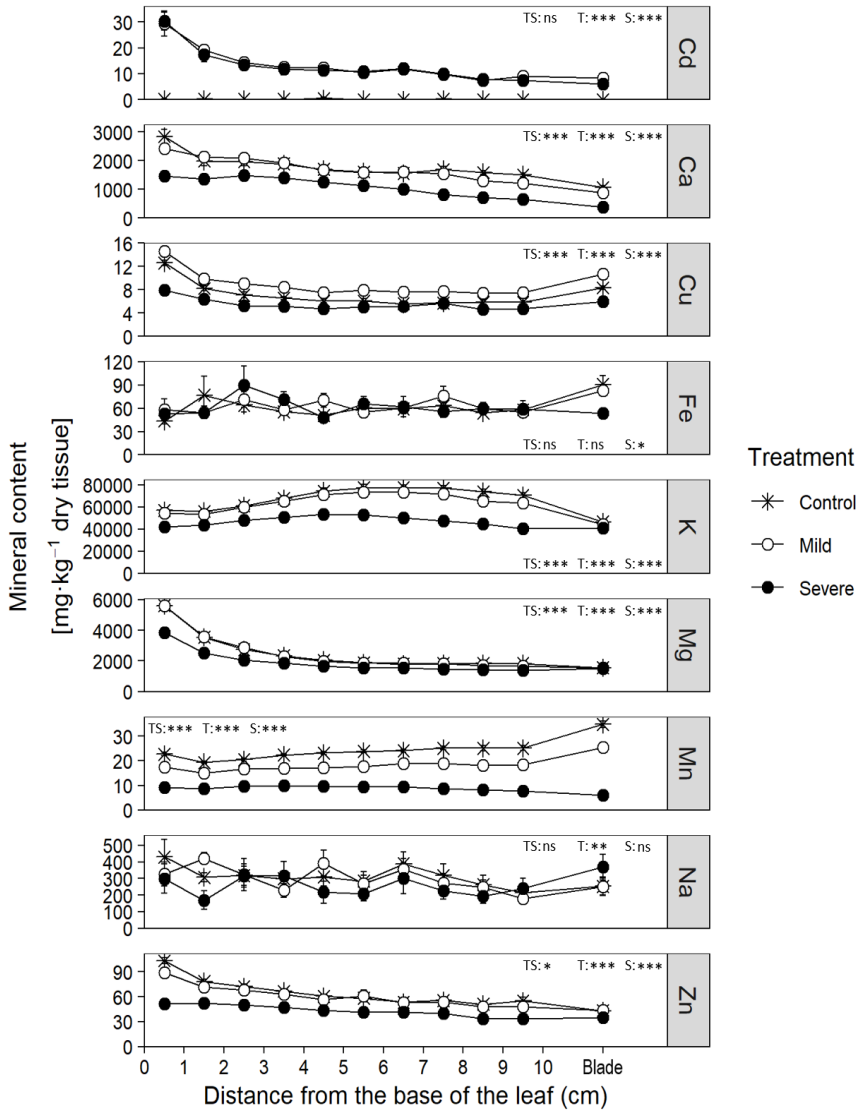

Figure 23 The effect of Cd on mineral levels in the maize leaf growth zone, expressed on a dry weight basis. Values are mean (n = 5), error bars are standard errors. When less than five measurements were available, the error bar and point is coloured grey. When no error bar is present, only one measurement was available. Do note that for most measurements, the error bars is too small to be visible beyond the point (i.e. the black points with seemingly no error bar). The following minerals were not detected or removed due to contamination: Co, Mo, Ni, Si and B. Note: Cd, Ca, Fe and K were not normally distributed after log10 transformation. TS: interaction treatment-segment p-value, T: treatment p-value, S: segment p-value. ns: not significant, * $p < 0.05$, ** $p < 0.01$, *** $p < 0.001$.

Oxidative stress

It is well known that cadmium exposure indirectly results in oxidative stress by depleting non-enzymatic antioxidant glutathione levels, the increase of free Fe (by replacement of Fe from its functional sites in proteins) and inhibition of antioxidant enzyme activity (Cuypers *et al.*, 2010; Huybrechts *et al.*, 2019). Yet, the impact of Cd on oxidative parameters is not yet described in the maize leaf growth zone. In addition, our gene expression data also indicated oxidative stress to occur particularly in the meristem, where Cd is accumulating (Figure 23) and which is primarily responsible for the observed growth inhibition (chapter 3, Table 2).

Therefore, to evaluate potential oxidative damage in the growth zone, we first determined MDA levels. Under control conditions MDA levels remained steady along the leaf growth zone. However, MDA levels increased towards mature leaf tissue when exposed to cadmium stress, with a strong increase in response to severe stress (Figure 24).

A typical response to oxidative stress is an increased antioxidative potential. A good overall measure for this trait is the determination of the ferric reducing antioxidant power (FRAP), which is based on the ability of phenols to reduce Fe^{3+} to Fe^{2+}, yet does not incorporate detection of radical quenching compounds, like thiols (e.g. glutathione; (Cerretani and Bendini, 2010). Severe Cd levels strongly induced FRAP and while mild stress conditions had a smaller, but still significant effect (Figure 24). Highest FRAP levels are found in the meristematic region under all conditions.

Taken together, through our observation of increased MDA levels under cadmium stress, we were able to confirm the oxidative stress GOs indicated by our transcriptome data. In response to the oxidative stress experienced in the maize leaf growth zone, the plant induces its defence mechanisms to cope with the generated ROS, as indicated by the increased FRAP under cadmium stress. However, the increased MDA levels suggest the plant is not able to completely nullify ROS related damage to membranes.

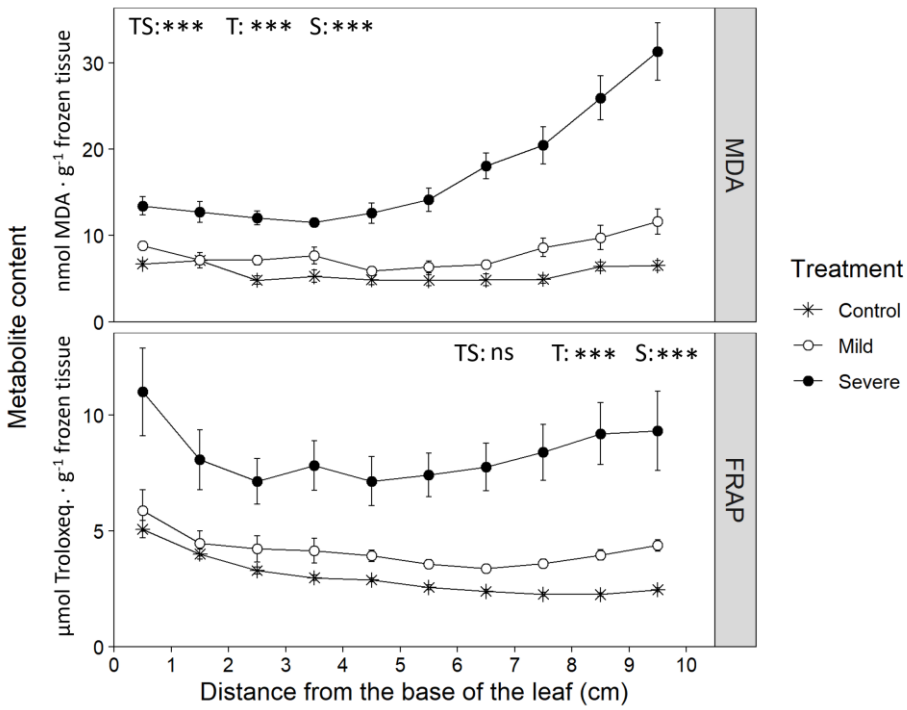

Figure 24. The effect of Cd on MDA levels and FRAP in the maize leaf growth zone. Values are mean (n = 4), error bars are standard errors. Note: MDA and FRAP were not normally distributed after $\log_{10}$ transformation, but their distribution did improve (W > 0.95 for both, $p < 0.05$, Shapiro Wilk test). TS: interaction treatment-segment p-value, T: treatment p-value, S: segment p-value. ns: not significant, * $p < 0.05$, ** $p < 0.01$, *** $p < 0.001$.

Discussion

The effect of Cd on plant growth and metabolism is often studied in roots. Here we present a first genome wide transcriptome study performed in the leaf growth zone of a monocotyledous species. This model system allows to directly study the effects of this stress directly on the growing tissues (Avramova *et al.*, 2015*c*). In chapter 3, we showed that Cd is specifically accumulating in the meristem at the base of the maize leaf growth zone. Kinematic analysis (chapter 3, Table 2) also showed that the inhibition of leaf growth by Cd is primarily related to cell proliferation in the meristem.

To reveal which processes might be affected by Cd that could explain the growth inhibition, we performed a genome wide transcriptome analysis on the leaf growth zone. This allowed us to compare its effects on dividing and elongating cells, the two key processes driving growth, but also mature tissues of the same leaf. The transcriptome data prompted us to further perform an extensive phytohormone study, next to a broad identification of mineral levels and two oxidative stress parameters in this tissue. The transcriptome data, in combination with the measured phytohormones, minerals and oxidative stress parameters, provides a basis to better understand effects of Cd on the cellular and whole leaf growth responses, studied in chapter 3.

Transcriptomic and biochemical responses to cadmium in the maize leaf growth zone

In the following paragraphs, we will first address the common ground of some of our reported GO categories with previously published transcriptome studies regarding Cd stress in plants. Hereafter, we will discuss our phytohormone, mineral and oxidative stress measurements in depth. Where possible and relevant, links between the measured biochemicals and transcriptome changes will be made. In addition, we will briefly discuss the effect of Cd on GOs related to cell cycle and translation which were also reported to be affected by Cd in our transcriptome study.

Similar transcriptome responses to Cd stress across different plants species

When comparing our results to published transcriptome analyses, we find similarities with the response to Cd observed in different plant species, indicating that the response to cadmium is, at least partially, conserved for some biological processes. In multiple clusters across the maize leaf growth zone, we report overrepresentation of cinnamic acid and L-phenylalanine GO categories (i.e. upregulated in the meristem and downregulated in the mature zone). Both GOs are strongly related to each other since these molecules are part of the phenylpropanoid biosynthesis pathway where phenylalanine is converted by phenylalanine ammonia lyase into cinnamic acid. Cinnamic acid is then further processed to produce cell wall components (lignins), pigments (e.g. flavonoids), and UV protectant and pest resistance compounds (e.g. coumarins) (Thomas and ElSohly, 2016). Enrichment for phenylpropanoid biosynthesis genes was also reported in Cd exposed roots of peanut (Chen *et al.*, 2019), rice (He *et al.*, 2015; Huang *et al.*, 2019*a*), wheat (Yue *et al.*, 2016*b*; Zhou *et al.*, 2019*c*; Qiao *et al.*, 2019), verbena (Wang *et al.*, 2019), field mustard (Sun *et al.*, 2019), switchgrass (Song *et al.*, 2018) and maize (Yue *et al.*, 2016*a*) and shoots of rice (Zhong *et al.*, 2019). Consistent with our findings, several of these studies also reported effects on sucrose and starch metabolism pathways (Peng *et al.*, 2015; Yue *et al.*, 2016*a*; Huang *et al.*, 2019*a*; Wang *et al.*, 2019; Xiao *et al.*, 2019; Zhong *et al.*, 2019; Zhou *et al.*, 2019*c*) and oxidative stress (He *et al.*, 2015; Peng *et al.*, 2015; Yue *et al.*, 2016*a*; Song *et al.*, 2018; Huang *et al.*, 2019*a*; Xiao *et al.*, 2019; Sun *et al.*, 2019). This leads us to conclude that different model systems share, at least partially, a common response to cadmium stress involving the phenylpropanoid, carbohydrate and antioxidant metabolism.

Several plant transcriptome studies also made reference to Cd affected phytohormone metabolism. GOs and KEGG pathways on gibberellins (diterpenoid biosynthesis (He *et al.*, 2015; Peng *et al.*, 2015; Chen *et al.*, 2019; Xian *et al.*, 2020)), salicylic acid (Zhong *et al.*, 2019), auxin (Yue *et al.*, 2016*a*; Zhao *et al.*, 2019), jasmonic acid (Yue *et al.*, 2016*b*; Zhao *et al.*, 2019) and plant hormone signal transduction in general (Peng *et al.*, 2015; Yue *et al.*, 2016*b*; Song *et al.*, 2018; Wang *et al.*, 2019; Zhou *et al.*, 2019*c*;

Xian *et al.*, 2020) were all reported in previous Cd studies. In our GO analysis, the *auxin-activated signalling pathway* was revealed in a gene expression cluster from mature samples where genes were upregulated under increasing Cd stress (Table 3, cluster 2 Figure 14). The MapMan regulation overview revealed several significantly up- and down-regulated genes for all represented hormones (IAA, ABA, BA, ethylene, cytokinin, jasmonate, SA and GA, with the exception for solely upregulated genes for SA), especially in the severe versus control contrast of the mature region (Figure 15). Xian *et al*. (2020) also used the MapMan regulation overview for the response of perennial grass leaves to Cd, where they showed an upregulation of 92.1% of the hormone-related genes, of which most were related to auxin, ethylene, ABA and jasmonate.

Phytohormones

The impact of metals on phytohormones has already seen a lot of progress and several reviews provide a good overview on how metals affect phytohormones (Maksymiec, 2007; Keunen *et al.*, 2016; Liu *et al.*, 2016; Bücker-Neto *et al.*, 2017; Shukla and Suprasanna, 2017; Vishwakarma *et al.*, 2017; Jalmi *et al.*, 2018; Guo *et al.*, 2019*a*; Sharma *et al.*, 2020), but also the inverse, how phytohormones affect the plants tolerance to metals (Asgher *et al.*, 2015; Sytar *et al.*, 2019; Emamverdian *et al.*, 2020). Yet, to our knowledge, never before were phytohormone profiles determined in the growth zone of growing monocot leaves exposed to metal stress where they potentially regulate the growth response. Based on indications for the involvement of several phytohormones by our own and published transcriptome studies, we performed a detailed phytohormone analysis of the Cd exposed maize leaf growth zone. In the following paragraphs, the stress hormones (SA, ABA and ACC (ethylene precursor)) are addressed first, followed by the growth promoting hormones (GAs, auxin and cytokinins). Where relevant and possible, links to the transcriptome study are made.

Stress hormones

Salicylic acid

Salicylic acid is a phenolic compound and has an important role in the plants response to abiotic stress, amongst which is metal stress (as reviewed by Liu *et al.*, 2016; Guo *et al.*, 2019*a*; Sharma *et al.*, 2020). In wheat, cadmium treatment increased endogenous SA levels in both roots and leaves (Tajti *et al.*, 2019). In the maize leaf growth zone, we also report increased SA levels across the entire growth zone, where SA levels increased relative to Cd dose (Figure 18). The importance of SA in the defence mechanisms of plants to cadmium stress is further emphasised by the increasing number of studies reporting on the protective effect of SA (pre-)treatment to counter Cd toxicity. For example, foliar SA application in menthol mint (*Mentha arvensis* L.) under Cd stress recovered chlorophyll content, shoot dry mass and rubisco activity, and reduced MDA levels, electron leakage and hydrogen peroxide levels. Its application also reduced leaf and root Cd concentrations, and increased N and K content in the leaves (Zaid *et al.*, 2019). Salicylic acid supplementation in maize hydroponics Hoagland's solution partially restored shoot and rood fresh weight, total chlorophyll and carotenoids content and protein content under Cd stress in maize seedlings, while also reducing Cd accumulation in root and shoot tissue (Singh *et al.*, 2019). Pre-treatment with SA primed tomato plants to better cope with Cd stress by decreasing Cd accumulation in roots, stems and leaves, but also increasing the biomass of all these organs. Depending on the genotype used, SA also decreased MDA levels (Wei *et al.*, 2018).

Related to our transcriptome data, the increased SA levels we report can be linked to the overrepresentation of cinnamic acid and phenylalanine GOs among Cd upregulated genes in the meristematic tissue (cluster 2, Table 1, Figure 5), though it should be mentioned that similar GOs were overrepresented in Cd downregulated genes of the mature tissue (cluster 3, Table 3, Figure 14). Salicylic acid is produced through mainly two pathways, being the isochorismate pathway and the phenylalanine ammonia-lyase (PAL) pathway (reviewed by Dempsey *et al.*, 2011). In

the PAL pathway, PAL converts phenylalanine to trans-cinnamic acid and ammonia, where trans-cinnamic acid is then further processed to SA (Dempsey *et al.*, 2011). Based on our transcriptome data, we hypothesised SA levels to be up in the meristem and decreasing in the mature tissue due to respectively up- and down-regulation of genes related to its synthesis. With the collected SA profiles, we can now revise this hypothesis, since we observed increased SA levels over the entire growth zone, with higher levels in both the meristem and mature tissue.

Abscisic acid

Where SA levels already increased at mild Cd stress levels, ABA levels were only markedly increased under severe stress (Figure 18). Increased ABA levels due to Cd stress was also described in leaves of two wheat varieties, in conjunction with decreased stomatal conductance and photosynthetic rates (Guo *et al.*, 2019*b*). Stomatal closure caused by ABA is well accepted phenomenon (Mittelheuser and Van Steveninck, 1969). Since cadmium is transported by xylem vessels from roots to shoots, reduced evaporation of water at the stomata can reduce xylem sap flow and thereby limit Cd transport to the shoot (Kobayashi *et al.*, 2013). Consistently, application of exogenous ABA effectively reduced transpiration rates and Cd concentration in rice, enhancing its tolerance (Hsu and Kao, 2003). Also in Arabidopsis, exogenous ABA application reduced Cd concentration in both shoots and roots and alleviated Cd-induced growth inhibition and photosynthetic damage (Pan *et al.*, 2020*b*). Since we only found strongly elevated ABA levels under severe Cd stress, we expect to have passed a certain threshold in stress levels exerted by the Cd treatment, where the maize seedlings try limit Cd uptake and transport to the leaf by reducing stomatal conductance in the mature tissues when under severe stress. In this context it is significant that ABA levels are particularly increased in the mature tissues (Figure 18). In chapter 5, Cd impacted stomatal conductance and photosynthetic rate is further studied on the fifth leaf of maize seedlings. Nevertheless, ABA levels are also strongly upregulated in the proliferating and expanding cells under Cd stress, suggesting they may also impact on the physiology and growth processes in these tissues.

Ethylene (ACC and ACC-conjugates) and jasmonic acid

Due to its gaseous nature the ethylene phytohormone is difficult to measure. Therefore, we instead measured its precursor 1-aminocyclo-propane carboxylic acid (ACC) and its conjugates (Figure 19). ACC by itself can act as a negative regulator of growth (e.g. rosette development, hypocotyl elongation and root growth) (Vanderstraeten *et al.*, 2019), but also strongly correlates (or is generally believed to be directly correlated) with the production of ethylene (Hoffman and Fa Yang, 1980; Grossmann and Retzlaff, 1997; Zia Ul Haq *et al.*, 2020). We found constant free ACC levels across the maize leaf growth zone that were significantly increased by Cd, yet, no clear difference between mild and severe Cd stress was noted. With ACC as a direct precursor to ethylene, our reported increased ACC levels are consistent with the increased ethylene levels reported in response to Cd across different organs and plant species (Keunen *et al.*, 2016). In a summary of 16 Cd studies, Keunen *et al.* (2016) revealed that in 14 studies, an increase in ethylene levels was observed in response to Cd stress.

ACC conjugates are normally referred to as the pool from which ACC can be made available, for it to be processed to ethylene. The importance of ACC conjugation under cadmium stress was highlighted by Schellingen *et al.* (2014), who reported increased levels of ACC conjugates in both roots and leaves of Cd-exposed Arabidopsis. Here, a large difference in content between free and conjugated ACC was reported, where, under control conditions, conjugated ACC was 10 times more present in roots and 50 to 100 times more present in leaves. Compared to our maize leaf growth zone, we reported a 10-fold difference in content when comparing conjugated ACC versus free ACC, indicating that also in the maize leaf growth zone, ACC conjugates dominate the total ACC pool.

Interestingly, the ACC conjugates showed clear differences in content related to Cd treatment, with highest levels under mild cadmium stress and intermediate levels under severe stress (Figure 19). Conjugated ACC levels being intermediate under severe Cd stress might be related to the high ABA levels recorded at this stress level,

since it was shown that ABA accumulation in maize primary roots restricted ethylene production (Spollen *et al.*, 2000).

To our knowledge, our study is the first one to determine the response of the three main ACC conjugates in response to Cd. Our data clearly demonstrate the importance of ACC conjugation, because each of the three conjugates responded differently to Cd. Malonyl-ACC is the major ACC conjugate and its profile strongly influences and closely matches the total ACC conjugates profile. When looking into glutamyl-ACC, we noted a strong decrease under Cd stress, with mildly stressed plants impacted the most. The last ACC conjugate, jasmonyl-ACC, was present in lowest levels, but did show a clear treatment effect, with increasing contents relative to Cd treatment. Due to this correlation between jasmonyl-ACC and Cd stress levels, this might indicate that jasmonyl-ACC could be the most important ACC-conjugate in controlling the response to Cd stress.

Interestingly, jasmonyl-ACC is a conjugation of jasmonic acid (JA) and ACC, where this conjugation was suggested to be a mechanism to control both hormones (Staswick and Tiryaki, 2004). In our study, JA levels were below detection limit. In previous reports, low JA levels after Cd exposure are frequently observed. In pea leaves, no free JA was measured under control and Cd conditions (14 days of Cd treatment) (Rodríguez-Serrano *et al.*, 2009). In soybean roots, 6 hours of Cd stress decreased JA to 10% of the levels under control conditions (Pérez Chaca *et al.*, 2014). In rice on the other hand, Cd exposure increased JA content in both roots and shoots the first 48h of Cd exposure, after which it strongly decreased again (Marilena *et al.*, 2019).

Based on our transcriptome study, we expected to find high JA levels due to the upregulation of enzyme transcripts in JA biosynthesis pathway in both the meristematic (Figure 8) and mature tissue (Figure 16). However, since we did not detect JA in the maize leaf growth zone under control and Cd conditions and since JA-ACC strongly increased under Cd stress, we suggest that the increased production of jasmonyl-ACC under Cd stress acted as a sink for any produced JA (Figure 19).

Growth promoting hormones

Gibberellins

In plants, GA1 and GA4 are the main bioactive GAs, where GA3 and GA7 are present at lower levels (Binenbaum *et al.*, 2018). In the maize leaf growth zone, GA1, and to a lesser extent GA4, serve an important function in determining meristem size (Nelissen *et al.*, 2012). Nelissen et al. (2012) showed that the maize leaf growth zone encompasses a distinctive GA1 peak, the location of which determines the transition of meristematic activity to cell expansion. In our gibberellin measurements, GA4 levels did not exceed detection levels, yet we did find distinctive GA1 peaks for all three treatments. Interestingly, the GA1 peak was considerably smaller under severe Cd stress and declined sooner under mild Cd stress (Figure 20). Based on our transcriptome data, we can now hypothesize that under Cd stress, the plant limits GA1 synthesis by downregulation of gibberellin 20-oxidase transcription. Since this enzyme catalyses the processing of GA1 intermediates, its reduction in transcript levels could explain the build-up of GA19 (Figure 20). In addition, increased transcript levels of GA2-oxidase indicated a tendency to increase GA1 breakdown to GA8.

Gibberellin application on plants exposed to cadmium stress seems to counter act the effect caused by Cd. For example, GA3 application as a foliar spray on Cd exposed *Parthenium hysterophorus* promoted cell division, with increased growth and biomass as a result (Hadi *et al.*, 2014). In Arabidopsis seedlings, grown on Cd containing agar, 5 µM GA supplementation to the agar (type of GA underspecified) improved root growth, reduced Cd content and reduced lipid peroxidation in the roots (Zhu *et al.*, 2012).

Taken together, the Cd reduced meristem size in the maize leaf growth zone, described in chapter 3, might be the result of lowered GA1 levels in the meristem-to-elongation zone transition tissue, which can partially explain why maize leaves grow slower under Cd stress. In addition, other studies have shown that growth inhibition under Cd stress might be reversed by GA application.

Auxins

The transcriptome also identified the *auxin-activated signaling pathway* GO to be overrepresented for genes which are upregulated in the mature tissue in response to Cd stress. Therefore, we measured two auxins, indole-3-acetic acid (IAA) and indole-3-butyric acid (IBA, auxin precursor), and their conjugates across the maize leaf growth zone (Figure 18). For the maize leaf growth zone, it is known that IAA levels are highest in the meristematic region and decline steeply in the first 3 to 4 centimetres of the leaf base (Nelissen *et al.*, 2012), a pattern which is perfectly matched by the IAA levels collected in our study. Cadmium stress increased IAA levels and its conjugates slightly. In other species and organs, Cd stress seems to decrease IAA levels, rather than increase. In wheat leaves, IAA levels were reduced after growing in Cd contaminated soil up until jointing stage (i.e. internodal tissue elongation to form a stem) (Guo *et al.*, 2019*b*). In the primary roots of *Sorghum bicolor* seedlings, Cd stress reduced IAA content, where the decrease in IAA levels was linked to an increase in IAA oxidase activity. In addition, naphthyl acetic acid (NAA, a synthetic auxin) supplementation alleviated Cd toxicity (Zhan *et al.*, 2017). Also in Arabidopsis seedlings, Cd stress reduced IAA content after 48h and 72h of Cd treatment. Here, IAA oxidase activity was also increased with increasing Cd concentrations, where 50 µM Cd significantly increased IAA oxidase activity after 24h of Cd exposure (Hu *et al.*, 2013). This discrepancy between species and organs might indicate that the IAA response to Cd could be species or organ specific, where reduced IAA levels are more common than the slightly increased levels reported in our study. However, most of these studies analyse whole plant/organ samples. This does not allow to discriminate between a sample containing a smaller fraction of proliferating cells with high IAA levels and lowered levels of IAA specifically in these cells or globally. Our study clearly shows that this spatial resolution is required to understand the role of IAA and other metabolites in controlling growth responses to specific treatments.

The IBA levels were also significantly affected by Cd, with increased levels of free IBA under Cd stress across the maize leaf growth zone (Figure 18). Conjugated IBA was

detected and measured, but a treatment or segment effect was not present. The observed increase in IBA levels might be related to defensive mechanisms to counter the toxic effect of Cd, as IBA supplementation to the growth medium restored antioxidative enzyme activities, antioxidants and MDA levels in the roots of mung bean seedlings (Li *et al.*, 2018). A relationship between IBA and Cd was further confirmed in *Stellaria media*, a Cd accumulator. Here, foliar IBA application promoted growth and Cd accumulation, suggesting foliar IBA application to enhance Cd extraction form soil (Lin *et al.*, 2018).

Cytokinins

Cytokinins are hormones which are only found in plants and they have been shown to perform roles in proliferation and differentiation of plant cells, shoot/root balance control and regulation of developmental transitions, senescence and floral induction (Corbesier *et al.*, 2003; Sakakibara, 2006). In the growing maize leaf, trans-zeatin (t-Z) has increased levels in the meristem, whereas isopentenyladenine (iP) levels are constant across the entire growth zone (Nelissen *et al.*, 2012). For iP, we also found relatively constant levels across the growth zone, without a treatment effect (Figure 22). The increased t-Z levels in the meristem were absent in our measurements, but we did find a marked increase of the trans-zeatin ribose (t-ZR) levels in the meristem under control conditions, where Cd caused a severe drop in these levels (Figure 22). Reduced zeatin riboside levels might be common response to Cd across plant species. In two wheat cultivars, Cd also reduced the levels of this cytokinin in the leaves (Guo *et al.*, 2019*b*). In oilseed rape a time dependent decrease of ZR in the leaves was reported in response to Cd (Yan *et al.*, 2016).

The levels of t-ZR were low compared to the O-glucoside compounds of cis-zeatin (c-Z-OG) and dehydrozeatin riboside (DH-ZR-OG), perhaps since O-glucosylation protected these cytokinins from degradation by cytokinin oxidases and allowed them to accumulate (Veach *et al.*, 2003). Higher levels of c-Z-OG reported in our study, were also reported by Hluska *et al.* (2016) in the 7 day old first leaf of maize under normal conditions. However, they did not find the relatively high DH-ZR-OG concentrations,

indicating that in relation to the Cd stress response, HD-ZR-OG might be more specific to the imposed Cd stress. Like t-ZR, these O-glucosylated cytokinins also showed marked increases in the meristematic region. Yet, unlike t-ZR, the levels of c-Z-OG and DH-ZR-OG increased drastically under Cd stress. Since free cytokinins are attributed to have a positive effect on cell proliferation, their increased O-glucosylation under Cd stress, resulting in reduced free cytokinin levels (t-ZR in our study) could be related to the reduced cell production under Cd stress, described in chapter 3.

Minerals

Our transcriptome analysis also revealed a potentially affected metal ion homeostasis, where the *zinc II ion transmembrane transport* GO and the *cellular monovalent inorganic cation homeostasis* GO were among the top overrepresented GOs in cluster 2 for the meristem and mature zone tissues, respectively (Table 1, Table 3). In both clusters, these genes are upregulated proportional to the cadmium dosage. The most strongly upregulated genes were transporters related to Zn, Cu and iron (Supplementary Table 4.10). Previously conducted transcriptome studies under Cd stress did not report these specific GOs, but multiple references were made to the *iron ion binding* GO in other studies (Peng *et al.*, 2015; Yue *et al.*, 2016*a*; Song *et al.*, 2018). These results, combined with the direct deposition of cadmium in the meristem and elongation zone (chapter 3), also prompted us to analyse the other metals across the maize leaf growth zone.

Most commonly, mineral content is expressed on dry weight basis (Supplementary Figure 4.9). Calcium is one of the most discussed mineral in Cd studies, since it competes with Cd for uptake, translocation and bindings sites (Lu *et al.*, 2010; Huang *et al.*, 2017; Loix *et al.*, 2017; Ye *et al.*, 2020). Studies on pea leaves (Rodríguez-Serrano *et al.*, 2009), almond seedling leaves (Nada *et al.*, 2007), tomato seedling shoots (Alyemeni *et al.*, 2018), wheat leaves (Gul *et al.*, 2020) and cowpea leaves (Santos *et al.*, 2018) have all shown a reduced Ca content under Cd stress, which is also confirmed by our Ca measurements relative to tissue dry weight. Since Ca participates in several aspects of cell division (e.g. nuclear envelope breakdown and reformation, cell plate

formation), its limited availability might be related to the reduced cell production, described in chapter 3 (Hepler, 1994). Lowered Cu, Fe, K, Mg, Mn, Na and Zn levels in different organs across several plant species have also been reported (Nada *et al.*, 2007; Rodríguez-Serrano *et al.*, 2009; Akhtar *et al.*, 2016; Li *et al.*, 2016; Alves *et al.*, 2017; Javed *et al.*, 2017; Santos *et al.*, 2018; Alyemeni *et al.*, 2018; Zaid *et al.*, 2019; Çatav *et al.*, 2019; Gul *et al.*, 2020; Carvalho *et al.*, 2020), illustrating that reduced mineral contents are the more general response to Cd stress when mineral levels are expressed relative to dry weight tissue. Related to these minerals, we are able to confirm reduced K, Mg, Mn, Zn and to a lesser extent, Na, across the maize leaf growth zone when expressed relative to dry weight. Reductions in these minerals can be related to growth inhibition. For instance, K is important for proper regulation of osmotic potential (important for cell elongation) and has a role in the activation of enzymes involved in respiration and photosynthesis (Singh *et al.*, 2013). Magnesium is required for ATP hydrolysis, the synthesis of DNA (important for cell division) and plays an important role in ribosomal subunit association and functioning (Williams, 2000; Guo *et al.*, 2011; Singh *et al.*, 2013). Zinc deficiency can stun growth since it negatively impacts photosynthesis and synthesis of auxin and starch (Singh *et al.*, 2013). For Fe, a clear response in the growth zone is absent, yet we also report reduced Fe levels in the blade tissue, especially under severe Cd stress. Reduced Fe levels can be expected, since Cd competes with Fe for uptake, which results in Fe deficiency and chlorosis, the latter because Fe is crucial for chlorophyll synthesis (Qin *et al.*, 2020). Copper levels, expressed on dry tissue weight basis, behave rather peculiar across the growth zone and blade, where we report increased Cu levels under mild stress, though reduced Cu levels under severe stress. Finally, we consistently observed Mn reductions across the entire growth zone under both mild stress. Manganese and cadmium share a major transporter (i.e. natural resistance-associated macrophage protein5) for their uptake (Sasaki *et al.*, 2012). Shared uptake mechanisms can result in competition for uptake. Such competition was shown in rice, where additional Mn supplementation to the

growth medium effectively reduced Cd uptake and translocation to the shoot (Rahman *et al.*, 2016).

In chapter 3, we decided to express Cd concentration based on fresh weight, rather than dry weight. This was due to the globally increased dry weight in proportion to the fresh weight under severe stress, that masked differences between mild and severe Cd levels in the leaf growth zone when Cd content was expressed on dry weight basis (Figure 23). The use of fresh weight to express Cd concentrations in the leaf does reveal a difference in Cd concentration between the mild and severe Cd treatment (Supplementary Figure 4.9), where Cd concentration increased with increasing Cd content in the soil. This could suggest that FW contents more closely relates to the observed response of the tissues. However, it should also be noted that the fresh weight of tissue can be quite subjective to changes (e.g. increased transpiration rates or water loss during dissection), where tissue dry weight is more stable. Therefore, it is common practice to express mineral content on dry weight tissue basis.

Regarding the other minerals, we believe that the observed increase of tissue dry weight relative to tissue fresh weight under severe Cd stress could contribute to the observed decrease of Ca, Cu, Fe (blade), K, Mg, Mn, Na and Zn content under severe Cd stress when mineral content is expressed on a dry weight basis (Figure 23). When expressing mineral content relative to fresh weight (Supplementary Figure 4.9), not all conclusions based on dried tissue weight basis are retained. For Cu, Fe and Na, we report mainly slight increases under Cd stress and the strong reduction of Ca, K, Mg and Zn under Cd stress is now largely absent. Manganese was the only mineral to retain clear reductions in content relative to Cd treatment when expressed relative to tissue fresh weight. Therefore, the reductions of several minerals expressed on dry weight basis might be related to the shifted dry-to-fresh weight ration when plants are exposed to Cd stress. Perhaps these findings might motivate future studies to also interpret mineral contents relative to fresh weight, or at least indicate any shifts in dry-to-fresh weight ratios, since dry weight is a factor which can also be altered by treatment and therefor affect the mineral content interpretation.

Oxidative stress

Oxidative stress is commonly reported in Cd transcriptome studies. For example, the *response to oxidative stress* GO was enriched in roots of Cd exposed rice (He *et al.*, 2015), winter wheat (Xiao *et al.*, 2019) and switchgrass (Song *et al.*, 2018). The effects of Cd on oxidative status of the plant are well known. Generally, Cd is known to create oxidative stress through depletion of the reduced GSH pool, the increase of free Fe (redox-active), affected antioxidant enzyme activity, amongst others (as reviewed by Cuypers *et al.*, 2010). Also, the link of redox state with growth regulation has been relatively well described (Kocsy *et al.*, 2013; Considine and Foyer, 2014). However, so far the effect of Cd in actively dividing and expanding cells has not received much attention, apart from the recently published work in rice leaves, where it was shown that Cd exposure significantly upregulated ascorbate peroxidase and catalase expression in the elongation zone and adjacent transition zones, highlighting a possible role for the Cd-induced oxidative challenge in leaf growth regulation (Huybrechts *et al.*, 2020).

Our gene expression of the meristematic tissue also indicated oxidative stress to occur. More specifically, the GO *response to hydrogen peroxide* was enriched for genes which were upregulated under Cd stress in the meristematic tissue (Table 1 , cluster 2). Hydrogen peroxide could serve as a potential signalling molecule in the plant response to metal phytotoxicity (Cuypers *et al.*, 2016; Nazir *et al.*, 2020). Most commonly, it is studied in the light of being a reactive oxygen species known to oxidise biological membranes, resulting in the generation of malondialdehyde (MDA). Many studies have already described marked MDA increases under Cd stress in several species: maize (Rizvi and Khan, 2019; Youssef *et al.*, 2020), pea (Sayed and Gadallah, 2019), tomato (Alves *et al.*, 2017), almond (Nada *et al.*, 2007), rice (Zhao *et al.*, 2012), wheat (Zhou *et al.*, 2019*b*) and mung bean (Li *et al.*, 2018). In the maize leaf growth zone, we can also confirm this increase in MDA levels over all developmental zones due to Cd. In addition, we report increased MDA levels towards tissue maturation under severe cadmium stress (Figure 24), which was rather unexpected given the higher Cd

deposition rates and concentration in the meristem and elongation zone (i.e. one would expect higher MDA levels in these zones). Despite the fact of MDA being rather unstable (Khoubnasabjafari *et al.*, 2015), increased MDA levels towards maturation might also be the result of its accumulation while cells are passing through the growth zone. At least, this MDA pattern throughout the maize growth zone under abiotic stress does not seem to be uncommon, since a similar gradient was also found in the severely drought stressed maize leaf growth zone (Avramova *et al.*, 2015*b*, 2017).

In relation to the plant's response and capacity to cope with the imposed oxidative stress, ferric reducing antioxidant power (FRAP) was increased in proportion to the Cd treatment over the entire growth zone. FRAP mainly measures the reducing power of phenols, like catechol, cinnamic acid and coumaric acid. Whilst being a good indicator of plants potential to cope with ROS, it should be kept in mind that it does not provide a complete picture, since FRAP does not incorporate detection of radical quenching compounds, like thiols (e.g. glutathione) (Cerretani and Bendini, 2010; Shalaby and Horwitz, 2015), which are also key antioxidants in coping with Cd stress (Sobrino-Plata *et al.*, 2014). Interestingly, FRAP also reached relatively high levels in the meristematic region under control conditions. This finding might be an indication of an activated antioxidative defence mechanisms in this crucial developmental region, even under control growth conditions.

Cell cycle

Cadmium affected cell cycle, revealed through KEGG pathway analysis of transcriptome data, was reported in the roots of wheat (Zhou *et al.*, 2019*c*) and maize (Yue *et al.*, 2016*a*), where genes were respectively down- and up-regulated. In the meristem transcriptome study presented here, one of the three clusters was almost solely dedicated to processes related to meristematic activities (Figure 5, Table 1, cluster 3). Here, genes were upregulated under mild stress and downregulated under severe stress when compared to the control treatment. Most of the genes in this cluster, are however insignificantly impacted by mild Cd stress since in total the transcription of only 58 genes significantly differed under mild stress. Yet, under severe

stress, downregulation of genes related to DNA strand elongation and DNA base synthesis can be related to inhibited cell cycle progression, which we described in chapter 3. This leaves us to speculate that perhaps under mild Cd stress, cadmium treatment hinders cell cycle related processes, for which cells try to compensate by slightly/insignificantly upregulating transcription of cell cycle related genes. Where under severe Cd stress, the response is to slow down the cell cycle to control for cadmium damage and to save energy for recovery and defence mechanisms.

A closer inspection of the significantly affected expression of cell cycle genes in response to Cd, we found slightly upregulated D-type cyclins and we confirmed the downregulated B-type cyclin of chapter 3. The upregulated D-type and downregulation of B-type cyclins suggests cells accumulating at the G1/S transition, which is consistent with the flow cytometry data in chapter 3. For the two other cell cycle genes measured by qPCR in chapter 3, we confirmed their downregulation in the current NGS study, where the NGS data reveals a significant (FDR < 0.05) downregulation of wee1 (Zm00001d053998, LFC = -0.5 ± 0.1) and minichromosome maintenance4 (Zm00001d044540, LFC = -0.3 ± 0.1).

Translation

Across the meristem, elongation zone and mature zone, GOs related to protein production (transcription, translation and ribosomal related GOs) also emerged from clusters where genes were downregulated with increasing Cd stress (i.e. cluster 1 meristem (Table 1, Figure 5), cluster 3 elongation zone (Table 2, Figure 11), cluster 1 mature zone (Table 3, Figure 14)). Interestingly, various types of stress, including water deficit, cold, hypoxia, reactive oxygen species and heavy metals, result in a significant decrease in global translation rates (as reviewed by Merchante *et al.*, 2017). Perhaps, the downregulation of the transcription of genes involved in translation also indicates decreased translation rates in the maize leaf growth zone in response to Cd stress. In addition, we also found reduced potassium levels. It is well-known that potassium ions serve an important role in subunit association of ribosomes and in the coordination of mRNA during protein synthesis (Rozov *et al.*, 2019). We also noted reduced Mg levels

under severe Cd stress. Magnesium is important for proper ribosomal subunit association and tRNA binding to the decoding site (Philipps, 1970; Guo *et al.*, 2011). Perhaps the overrepresented GOs addressed above, which were related to translation, could therefore be linked to the reduced Mg and K levels under Cd stress.

The dominant effect of developmental stage on the transcriptome profile

Throughout the growth zone, cells undergo very different developmental stages (i.e. cell division, elongation and maturation), which has a dominant impact on the transcriptome. This dominant impact is clearly present in the hierarchical clustering of all samples, collected over the three developmental zones, where we observed a strong separation of samples based on zone (Figure 2). In addition, we found that roughly half of all annotated genes in the maize genome were significantly (FDR < 0.05) affected by the effect of zone. This in stark contrast with around 17% of the genes that were significantly (FDR < 0.05) affected by Cd treatment (Figure 1).

By analysing each zone individually, we aimed to omit the strong effect of developmental stage and to bring forward Cd induced changes in the transcriptome for each zone. However, we believe that samples from the elongation zone from different treatments were still affected by developmental stage. In our mild stress samples, we found an upregulation of processes related to photosynthesis (cluster 1, Figure 11, Table 2). This upregulation is probably the result of a shorter growth zone under mild stress (cluster 2, Figure 11, Table 2), which results in mild stress tissue being relatively more mature tissue compared to control tissue since it is closer to the mature zone. For severe stress plants, we sampled one centimetre closer towards the meristem in an attempt to compensate for its reduced growth zone size. However, the transcriptome of the severe stress elongation zone samples now had upregulated genes related to cell cycle and DNA maintenance, which could indicate that dividing cells were still present in this tissue, even though the epidermis was already elongating. When inspecting the cell cycle gene expression in chapter 3 (Figure 5 in

chapter 3), we can indeed see that cell cycle genes (especially *cylcin-B2-4*) reach higher expression levels in the elongation zone segments for the severe treatment (2-3 cm) when compared to the expression levels of the control treatment segments (3-4 cm).

These observations imply that severe and mild treatment samples are developmentally furthest apart from each other. Indeed, when we consult the PCA analysis (Supplementary Figure 4.10), we observe that severe and mild treatment samples are furthest apart, with control treatment being in the middle. In addition, when statistically testing differential gene expression between treatments, we find most differentially expressed genes for the severe versus mild contrast, indicating that both Cd treatments differ more from each other compared to contrasts where Cd treatments are tested against control growth conditions.

We can therefore conclude that, even though the kinematic analysis of chapter 3 allowed us to locate the meristem, elongation zone and mature zone, it can hard to precisely sample tissue at exactly the same developmental stage, especially in the elongation zone. Moreover, we harvested 1 cm segments along the growth zone, so that selection of samples at approximately the same developmental stage was limited to whole cm steps (Supplementary Figure 4.1). A better approach in the future could be targeted sampling of tissue with millimetre resolution instead of centimetre resolution, after kinematic analysis is performed. In addition, the use of qPCR to first quantify a limited set of cycle genes and verify their absence in the targeted elongation zone segments might be a good guideline to start from and to confirm the absence of cell division in the elongating tissue (e.g. mitosis related B-type cyclins).

Conclusion

By performing a genome wide transcriptome analysis in the maize leaf growth zone, we were able to gain a broad overview of biological processes affected by Cd in each of the distinct developmental stages driving leaf growth. In addition, it stimulated further biochemical analyses of phytohormones, minerals and ROS related parameters. Here, we showed an increase in stress hormone levels (i.e. SA, ABA and ACC) and a decrease of growth promoting hormones (i.e. GA1 and trans-zeatin riboside). For GA1 were able to directly link the effect of Cd on the spatial distribution phytohormone levels to transcript levels of its key synthesis and degradation genes. Also, a potential new role for conjugated ACCs and specific cytokinins in the response to Cd was revealed. In addition, a broad overview of cadmium affected minerals in the maize leaf growth zone was provided and an important remark was made towards the affected dry-to-fresh weight ratio, which can affect the interpretation of mineral profiles obtained in Cd stressed tissue. Lastly, we extended the knowledge on oxidative stress, caused by Cd, by acquiring MDA and FRAP levels throughout the entire maize leaf growth zone for all three treatments, where we confirmed MDA and FRAP increases relative to Cd stress intensity. Indications for the involvement of the carbohydrate metabolism, revealed in our transcriptome study, were not addressed in this chapter, but will be the research topic of the next and final research chapter, chapter 5.

Author contributions

All authors participated in the conception of the topic. J.B. wrote the manuscript. G.B. edited the manuscript. J.B. made the figures and tables. The NGS was conducted by G.B. and K.S.. The transcriptome analysis was performed by J.B.. Samples for phytohormone measurements were prepared by J.B. and E.P., measurements were performed by E.P.. Mineral analysis was performed by J.B. and L.B.. Oxidative stress measurements were performed by J.B. and H.A.G..

Funding

This work was supported by the Research Foundation Flanders (FWO) by project funding for J.B. [G0B6716N].

Chapter 5

The role of the sucrose metabolism in the response of maize leaf growth to cadmium stress

Jonas Bertels[1], Hamada AbdElgawad[1], Wim Van den Ende[2], Ann Cuypers[3] and Gerrit T.S. Beemster[1]

[1] Laboratory for Integrated Molecular Plant Physiology Research (IMPRES), University of Antwerp, Groenenborgerlaan 171, 2020 Antwerpen, Belgium

[2] Moleculaire Biotechnologie van Planten en Micro-organismen, KU Leuven, Kasteelpark Arenberg 31 - bus 2434, 3001 Leuven

[3] Centre for Environmental Sciences (CMK), Hasselt University, Agoralaan Building D, 3590 Diepenbeek, Belgium

Abstract

In chapter 4, the transcriptome study indicated that cadmium (Cd) stress affected the carbohydrate metabolism in the maize leaf growth zone. We therefore studied the effect of Cd on the carbohydrate metabolism in the maize leaf growth zone. Our results show an increase of total soluble sugars, sucrose, glucose and fructose across the maize leaf growth zone. Through the use of published mutants in the sugar metabolism, we revealed a mutant with reduced cell wall invertase (CWI) activity that was hypersensitive to Cd. More specifically, we found that in the genetic background (W22) CWI activity and fructose levels increased under Cd stress, where the mutant was unable to elicit this increase. A cellular analysis showed that the extra sensitivity of the CWI mutant could be traced back to a severely reduced number of meristematic cells, in conjunction with an increase cell cycle duration. In addition, we showed that the mutant had a significantly reduced photosynthetic rate and stomatal conductance. A genome wide transcriptome analysis demonstrated that a broad range of biological processes (glucose catabolic process, nucleus organisation, cytoplasmic translation and photosynthesis, amongst others) are differentially affected in the CWI mutant under Cd stress. However, detailed studies of the reads mapping to the mutation (*mn1,* Zm00001d003776, a single nucleotide change at position 1383 (C to T) located in an exon, which would result in the substitution of a proline by a leucine amino acid) failed to confirm its presence. This suggests that other mutations in the same (and/or other) gene(s) may be present in the mutant. Nevertheless, our results suggest that the sugar metabolism and signalling play a key role in the control of genome-wide responses to Cd in the growth zone.

Introduction

Sucrose is a central molecule in the plant's energy metabolism. It is the primary sugar molecule that is exported from the photosynthetic source tissue to sinks throughout the plant, where it can be metabolised to provide energy. Besides energy provision, glucose and fructose, the hexoses it is composed of, also provide essential building blocks for plants to grow and function. A large amount of glucose is used to synthesize cellulose for the cell wall matrix in growing tissue (Keegstra, 2010). Fructose on the other hand, can be used as a building block for fructans, which are essential for osmoregulation (Singh *et al.*, 2015) and storage carbohydrates (Bieleski, 1993; Carvalho and Dietrich, 1993). Finally, these sugars can act as signals, interacting with plant hormone signalling, gene expression and translation (Rolland *et al*., 2006).

In the cytoplasm of the mesophyll cells of photosynthetically active leaves, photosynthesis delivers the building blocks for sucrose production, i.e. uridine diphosphate-glucose (UDP-glucose) and fructose 6-phosphate. Sucrose-phosphate synthase transfers the glucosyl moiety of UDP-glucose to fructose 6-phospate, producing the intermediate sucrose 6-phosphate. Sucrose-phosphate phosphatase then hydrolysis sucrose 6-phosphate to form sucrose. The produced sucrose is subsequently loaded into the phloem for transport to heterotrophic tissues (Ruan, 2014). Loading the sucrose into the phloem can be performed by a subfamily of SWEET sucrose efflux transporters. In *Arabidopsis thaliana* sucrose-phosphate synthase is typically co-expressed with AtSWEET11 and -12, coupling sucrose biosynthesis with its transport (Chen *et al.*, 2012). When sucrose arrives at the sink cells, it can be unloaded via the apoplastic or symplastic route. During symplastic uptake, it enters the cell through plasmodesmata, where cytoplasmatic invertases or sucrose synthases metabolise sucrose to glucose and fructose or UDP-glucose and fructose, respectively. Besides sucrose processing in the cytoplasm, it can be imported in into the vacuole, where vacuolar invertases hydrolyse it to glucose and fructose. The apoplastic route first involves sucrose loading into the cell wall matrix, after which cell wall invertases (CWI) hydrolyse sucrose, allowing membrane hexose transporters to import the

resulting glucose and fructose into the cell's cytoplasm. Apoplastic sucrose can also be directly taken up by cells though membrane bound sucrose transporters (Zeeman, 2015).

The invertases are not only important for the plant's energy metabolism, but also in its response to abiotic stress. For instance, under cold stress, cell wall invertases were upregulated in *Catharanthus roseus* (Nishanth *et al.*, 2018) and breakdown of sucrose into glucose and fructose related to invertase activity under cold stress was shown in Arabidopsis (Kaplan *et al.*, 2007). Under drought stress, a marked down-regulation of several cell wall invertases was shown in the anther and peduncle of rice, but remained unaffected in flag leaves, indicating organ specific responses related to *cwi* expression (Ji *et al.*, 2005). In addition, in tomato, ectopic overexpression of cell wall invertase markedly improved the plant tolerance to drought stress (Albacete *et al.*, 2015). Also metal stress induces changes in sucrose metabolism through altered CWI activity. Copper stress increased cell wall invertase activity in roots and young seeds of a metalliferous *Rumex dentatus* population, which was also linked to increased *cwi* transcript levels (Xu *et al.*, 2018). On the other hand, in roots of Rangpur lime, Cd caused a significant decrease in CWI and cytoplasmic invertase activity, while vacuolar invertase activity remained unaffected (Podazza *et al.*, 2006), resulting in higher apoplastic sucrose content in the Cd-exposed roots, while overall sucrose content reduced.

Clearly, besides having a central role in the plant's general metabolism, sucrose metabolism is also important for the plant's response to abiotic stress. In chapter 4, GO's like "response to glucose" (GO:0009749) and "fructose 6-phosphate metabolic process" (GO:0006002) were strongly overrepresented among differentially expressed downregulated genes in the meristem due to severe Cd stress, with fold enrichments of respectively 16.1 and 14.02 (FDR $p < 0.05$, chapter 4 - Table 1). Also, MapMan visualisations indicated sucrose metabolism to be affected by Cd (Chapter 4: Figure 6 and 17). We therefore hypothesize that sucrose metabolism in the maize leaf growth zone is strongly affected by Cd stress, resulting in altered sucrose, glucose and fructose

levels under Cd stress conditions. In addition, we hypothesize that maize mutants in sucrose metabolism are more sensitive to Cd stress. To verify this hypothesis, we tested the growth response of two carbohydrate related mutants to Cd and functionally characterized the effect of reduced CWI activity, found in the most strongly affected mutant.

Material and Methods

Seeds, soil preparation and growth conditions

We grew a cell wall invertase (CWI) mutant (Maize GDB stock record: 209F mn1-89 (Cheng *et al.*, 1996; Carlson *et al.*, 2000)), a sucrose synthase double mutant (Maize GDB stock record: 910K sh1 sus1) and their common genetic background, W22 (obtained from the North Central Regional Plant Introduction Station, Wisconsin, US) in a growth chamber under controlled conditions (16-h day/8-h night, 25°C/18°C day/night, 200 $\mu mol \cdot m^{-2} \cdot s^{-1}$ photosynthetically active radiation, provided by high-pressure sodium lamps). The cell wall invertase mutant (209F mn1-89) is reported to be mutated in a gene (*mn1,* Zm00001d003776, a single nucleotide change at position 1383 (C to T) located in an exon, which would result in the substitution of a proline by a leucine amino acid) encoding an endosperm-specific cell wall invertase protein (MN1) (Cheng *et al.*, 1996; Carlson *et al.*, 2000), yet we found its transcription to be significantly affected in the maize leaf growth zone under Cd stress (chapter 4), indicating is it also transcribed therein. The mutation resulted in low levels of CWI protein and enzymatic activity. The sucrose synthase double mutant (910K sh1 sus1) is mutated for two biochemically similar isozymes of sucrose synthase (*sh1,* Zm00001d045042 and *sus1,* Zm00001d047253) for which reduced sucrose synthase activity in the developing maize endosperm is already described (Chourey *et al.*, 1998).

Peat potting medium (57% soil water content, Jiffy Products International B.V., The Netherlands) was spiked with 10 ml distilled water (control treatment) or 10 ml CdSO4 solutions (3CdSO4·8H2O, mild (46.5 mg Cd/ kg dry soil) and severe (372.1 mg Cd/ kg dry soil) treatment, prepared in distilled water). Mild and severe treatment refers to the plant growth response, i.e. the reduction of leaf elongation rate, as described in chapter 3. It should be noted that mild stress is already relatively high compared to what is found in the environment. For instance, in the Campine region, Belgium, only high concentrations are found in the direct surroundings of sites of historical industrial activity (10-50 mg Cd / kg dry soil), where in the larger surrounding area, soil

contamination is mainly diffuse and moderate (< 5 mg Cd / kg dry soil, Schreurs et al. (2011)). However, the bioavailability may strongly depend on the soil-type and may be relatively low in our potting soil, containing a high fraction organic material. Therefore we selected concentrations that gave a clear growth response in the young maize seedling. A fixed mass (650 grams) of potting medium was used for each individual pot (2.0L) to which the Cd solutions were added dropwise under continuous mixing with a kitchen mixer (Kenwood kMix KMX50). Thereafter, it was mixed for an extra two minutes to obtain a homogenous distribution of Cd. Pots were watered daily with tap water to maintain the original soil water content.

Growth analysis of two mutants in sucrose metabolism

Five to six plants of each line described above were grown under the control, mild and severe treatment. The length of the fifth leaf of these plants was measured by ruler until it reached final leaf length. The leaf elongation rate (LER) of each plant was calculated by averaging the first three LERs (each determined over approximately 24h intervals).

Carbohydrate analysis and cell wall invertase activity

Leaf number 5 of each plant was dissected three days after emergence from the whorl of older leaves and the first 10 centimetres were divided in one-centimetre sections. The middle centimetre segment of the remaining blade was also collected and labelled blade tissue. Four biological replicates per treatment / genotype combination were obtained by pooling three to four one-centimetre segments and flash frozen in liquid nitrogen immediately after dissection. Tissue was then reduced to powder using a ball mill grinder MM 400 (Retsch, Haan, Germany), while frequently being cooled with liquid nitrogen to keep the leaf material frozen at all times. The ground plant material was mixed with extraction buffer, of which 100 µl was used to determine soluble sugar content, while the remainder was used to determine cell wall invertase activity. The 100 µl aliquot was heated for 15 minutes to 90 °C to denature any enzymes which could change soluble sugar content and centrifuged 5 minutes at 13200 rpm to pellet

the insoluble fraction. Of the supernatant, 50 µl was then loaded on top of a mixed bed Dowex column (300 ml Dowex H^+, 300 ml Dowex Ac^-; both 100-200 mesh; Acros Organics, Morris Plains, NJ, USA) and eluted six times with 150 µl distilled water. Hereafter, total soluble sugars were measured using 150 µl Anthrone reagent (0.1% in 98% sulfuric acid) and 50 µl of the eluent in a 96 well-plate (two technical replicates), using a glucose standard curve as reference (Hansen and Møller, 1975). In short, after adding the Anthrone reagent to the samples, the plate was placed 10 minutes on ice, followed by an incubation of 30 minutes at 80 °C in a hot air oven. The plates were allowed to cool for 20 minutes at room temperature, after which absorbance was measured at 620 nm.

In the Dowex column eluents, fructose, glucose and sucrose were separated by anion exchange chromatography and quantified by pulsed amperometric detection (Dionex, Sunnyvale Ca, USA) according to Vergauwen et al. (2000).

For the cell wall invertase activity analysis, meristem samples from both genotypes and all three treatments were used. In addition, the activity was determined in blade tissue of both control treated genotypes. The ground plant material was pelleted by centrifugation, after which it was washed three times with ice-cold 50 mM Na-acetate buffer, pH 5.0 and redissolved in this buffer. Aliquots of this suspension were used for cell wall activity determinations under continuous shaking at 30°C (500 rpm; Thermomixer, Eppendorf, Hamburg, Germany) to keep the cell walls in suspension. The reaction mixtures contained 100 µl cell wall suspension, 25 µl of sucrose as substrate (0.5M) and 125 µl of Na-acetate buffer (pH 5). Invertase activity was assayed by measuring the release of reducing sugars from sucrose over a 150 minute interval and expressed relative to protein (Lowry assay, (Lowry *et al.*, 1951)) content, according to Nelson-Somogyi method (Nelson, 1944). The reactions were stopped by the addition of copper tartrate reagent, a mix of 4mL of copper reagent A (2.54g anhydrous sodium carbonate, 2g sodium bicarbonate, 2.5g potassium sodium tartrate and 20g anhydrous sodium sulphate dissolved in 100mL Milli-Q water) and of 96 mL of copper reagent B (15% $CuSO_4$.5HzO containing one drop of concentrated sulfuric acid per 100

ml). The released reducing sugars were determined by the reactions with arsenomolybdate reagent (a mix of 2.5g ammonium molybdate and 2.5mL sulphuric acid in 45mL and 0.3g disodium hydrogen arsenate dissolved in 25mL water, which incubated at 37°C for 24 hours). CWI activity was measured as the amount of reducing sugar released from sucrose (= sucrose break down by CW invertase enzyme to reducing sugar glucose and fructose) and expressed as reducing sugar·min^{-1}·mg $protein^{-1}$.

Kinematic analysis

From the day of emergence from the sheet of leaf 4, the fifth leaf of six plants was measured daily until it reached its final leaf length, while for six other plants, the fifth leaf was measured 3 days, after it was dissected for the microscopy study and further kinematic analysis. For the microscopy study, cell length measurements throughout the growth zone and meristem size measurements based on the distribution of mitotic cells were obtained as described in Sprangers et al. (2016). All kinematic calculations were then performed with the *leafkin* package (Chapter 2). Cell length fits were obtained every 0.01 cm along the 10 cm growth zone using the default fit (bandwidth multiplier = 1).

Transcriptome analysis of the meristem

Next-Generation Sequencing

For each treatment, 9 plants were dissected of both W22 and the CWI mutant three days after emergence of the fifth leaf. During dissection, the fifth leaf was isolated and the first centimetre (i.e. meristematic tissue) of three plants was pooled, resulting in three biological replicates for each genotype/treatment combination (18 samples in total). Tissue was then ground using a ball mill grinder MM 400 (Retsch, Haan, Germany), while frequently being cooled with liquid nitrogen to keep the material frozen at all times. Hereafter, RNA extraction was performed with the RNeasy Plant Mini Kit (Qiagen, Hilden, Germany) after which purity was checked on the NanoDrop

ND-1000 UV-VIS Spectrophotometer (Thermo Scientific, USA, 260/280 ratio: 2.12 ± 0.02, 260/230 ratio: 2.00 ± 0.24). Paired-end 100 base pair next-generation sequencing with at least 20 million reads for each end of the fragment was performed by BGI (Copenhagen, Denmark). Further processing and analysis of the raw read fastq-files was performed on the usegalaxy.eu platform (Afgan *et al.*, 2018). Quality control was performed using FastQC (Andrews, 2012), after which the raw reads were trimmed using Trimmomatic (sliding window trimming: window size = 4, minimal average quality = 20; headcrop: 15 (Bolger *et al.*, 2014)), resulting in mainly 85 bp pair-end reads. Paired-end reads were mapped on the V4 maize genome, provided on ensemblgenomes.org (release 46) using HISAT2 (pair-end, default settings (Kim *et al.*, 2015)), aligning 91.1 to 92.2% of the reads in pairs. Counts per gene were then determined using featureCounts (fragments with both reads aligned, exon feature (Liao *et al.*, 2014)) together with the GTF-file provided on ensemblgenomes.org (release 46).

Statistics and count normalisation (DESeq2)

The raw counts were statistically analysed using DESeq2 package (v 1.28.1) in R (version 4.0.2) to determine which genes had an altered gene expression and to calculate log fold changes (Love *et al.*, 2014). The effect of plant line, treatment and their interaction was tested using the likelihood ratio to compare a full model against a reduced model, which allows to collect a p-value for terms removed in the reduced model. To compensate for multiple testing, Benjamini & Hochberg corrected p-values, defined as false discovery rates (FDRs), were calculated. The adjusted p-value cut-off used was 0.05 (alpha) for the selection of significantly altered gene expression. Hereafter, post-hoc statistics were performed for specific comparisons of interest, i.e. comparing the effect of specific treatments in each plant line and plant lines within each treatment, and log fold changes were obtained. Counts were transformed using regularized log (rlog) transformation (DESeq2).

Venn diagrams, cluster analysis and gene ontology overrepresentation analysis

Venn diagrams were created to obtain insight in the distribution of the significant genes across treatments and between the CWI mutant and its genetic background, W22 (Bardou *et al.*, 2014). Cluster analysis was performed in MultiExperimentViewer (v 4.9.0). Prior to clustering, the normalize gene/rows function was used on the rlog transformed counts data to obtain expression values for each gene in the same range, resulting in overlapping expression patterns during clustering. Next, genes were clustered using k-means clustering (Pearson correlation) to create four clusters of genes with similar expression patterns. Gene ontology overrepresentation for each cluster resulting from the k-means clustering were obtained through http://www.pantherdb.org/ (Thomas *et al.*, 2003), using the internal maize gene database as a background, a Fisher's exact test and false discovery rate p-value correction ($p < 0.05$).

Pathway visualisation through MapMap

Log-fold changes of significantly altered genes (FDR < 5%) for treatment contrasts in the meristem were visualised using MapMan. For gene ID compatibility, V4 gene IDs were replaced by V3 gene IDs using the v3_v4_xref.txt file from maizegdb.org.

Photosynthesis related parameters

One day prior to harvesting of the NGS plants, photosynthetic rate, stomatal conductance and photochemical efficiency (Fv/Fm) of noncyclic electron transport in photosystem II were collected on 5 to 7 plants (i.e. on mature tissue of the fifth leaf, 2nd day of emergence) for each treatment/genotype combination 6 to 9 hours into the photoperiod. Fv/Fm measurements were taken with the Plant Efficiency Analyzer (Hansatech Ltd, King's Lynn, Norfolk, UK) on 10-minute dark-adapted leaves. Photosynthetic rate and stomatal conductance were measured using a portable photosynthesis system (LI-6400, LI-COR Inc., Lincoln, NE, USA). The fifth leaf blade was first allowed to acclimatise in the measurement chamber for 10 minutes (photon flux

density: 1500 µmol m^{-2} s^{-1}, CO_2-flow: 400 µmol CO_2 mol^{-1}, temperature: 26°C), after which 13 to 14 measurements were taken with a 15 second interval (averages logged) on which the average value was calculated. It is important to note that the water content of the airflow in the chamber was not constant over de different measurement days, due to an error with the H_2O desiccant (Supplementary Figure 5.1). The impact of no and full H_2O removal in the air of the measurement chamber on photosynthetic rate and stomatal conductance was determined on one left-over plant of each treatment-genotype combination, indicating that short duration differences in H_2O content in the air had minimal impact on photosynthetic rate (-1.6 $\pm$ 7%, SD), but reduced stomatal conductance on average by 12.6 $\pm$ 8.6% (SD) (Supplementary Figures 5.2 and 5.3). This indicated that photosynthetic rate data can be interpreted with some certainty, but that caution is appropriate when interpreting stomatal conductance data.

Statistics

Statistical analysis of carbohydrate levels, cell wall invertase activity, kinematic analysis and photosynthesis related parameters was performed in R (v. 3.6.1 (R Core Team, 2014)). Segment, plant line and treatment effects were factored in. When normality and homoscedasticity assumptions were met, a two-way ANOVA was performed. When assumptions were not met, data were log_{10} transformed prior to ANOVA. Post-Hoc analysis for comparison of means was performed through Tukey's honestly significant difference testing in R. When differences between two means were statistically tested, a t-test was used.

Results

The effect of mutations in the sucrose metabolism on growth under optimal and Cd stress conditions

In chapter 4, transcriptome data indicated that Cd stress could affect carbohydrate metabolism in the maize leaf growth zone. We therefor grew a cell wall invertase (CWI) mutant (209F mn1-89; Cheng *et al.* (1996); Carlson *et al.* (2000)), a sucrose synthase mutant (910K sh1 sus1; Chourey *et al.* (1998)) and their common genetic background (W22) under control and Cd conditions (mild and severe; Figure 1). Under control conditions, the final leaf length of both mutants is significantly smaller than W22, demonstrating that a compromised sugar metabolism affects growth under optimal growth conditions. The impact of Cd on the sucrose synthase mutant was comparable to W22, while on the other hand, the final leaf length and the leaf elongation rate of the cell wall invertase mutant were reduced two-fold by Cd stress when compared to W22, especially at severe Cd stress (Figure 1; Supplementary Figure 5.4). This suggests that reduced cell wall invertase activity compromises the plants ability to regulate its growth in response to Cd.

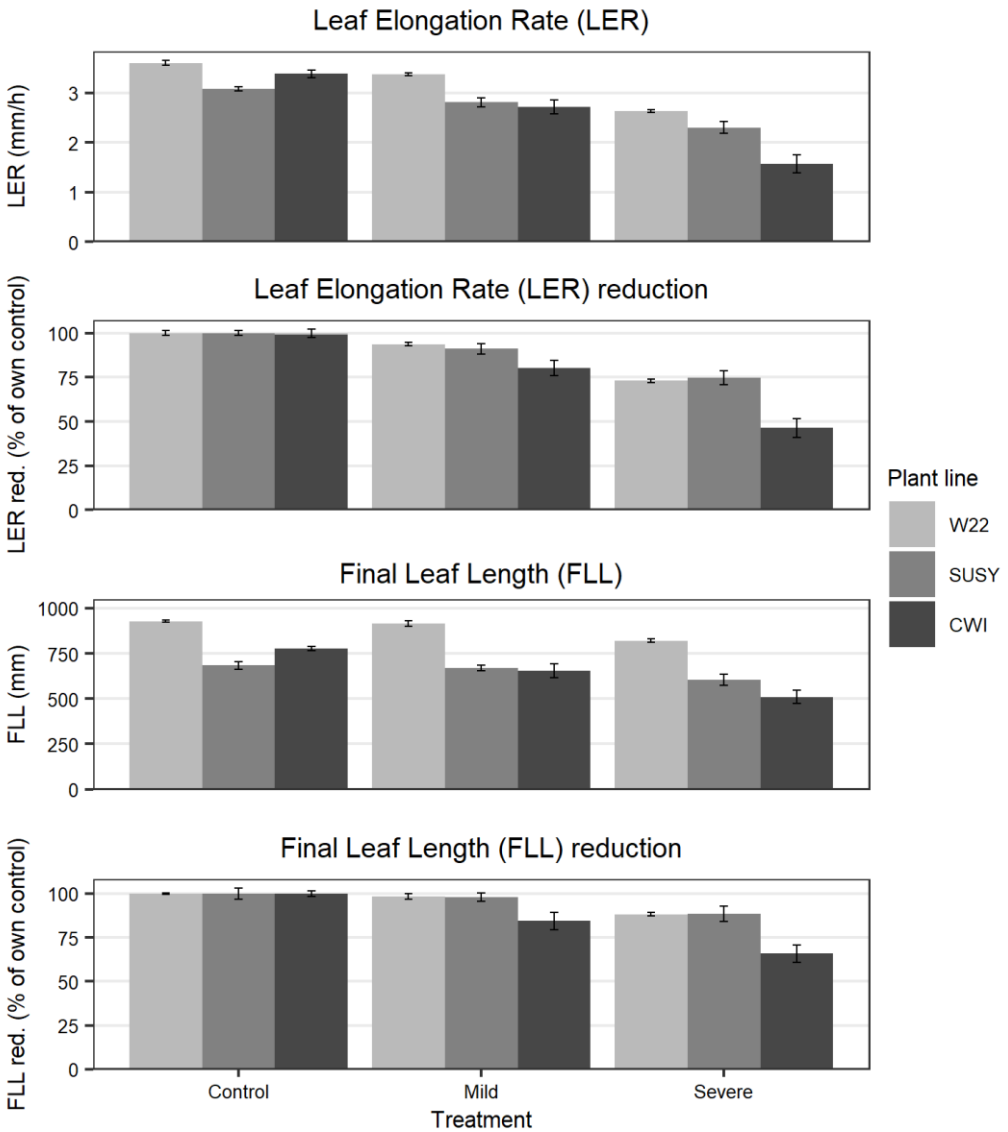

Figure 1. The effect of Cd on leaf growth of carbohydrate metabolism mutants in maize. Final leaf length and leaf elongation rate absolute values and relative values compared to control treated plants for the used cell wall invertase mutant (CWI), sucrose synthase mutant (SUSY) and their genetic background (W22). Values are averages ± SE (n = 5-6).

Cell wall invertase activity

To understand how CWI activity affects growth in response to Cd, we first set out to determine the effect of Cd stress on the overall cell wall invertase activity in the leaf growth zone. As expected, both in the meristem and mature part of the leaf, CWI activity was strongly reduced in the mutant, confirming its functional perturbation (Cheng *et al.*, 1996). In W22 under control conditions cell wall invertase activity was significantly lower in the meristem compared to mature tissue ($p = 0.028$). In the mutant, however, the activity did not differ significantly between these zones ($p = 0.37$). In the meristem of W22, Cd stress progressively increased CWI activity (Figure 2). In contrast, the mutant fails to exhibit a similar response and no significant increase in activity in response to Cd stress was observed. Thus, it seems that the mutant has reduced CWI activity and, in contrast to W22, is unable to upregulate this activity under Cd stress.

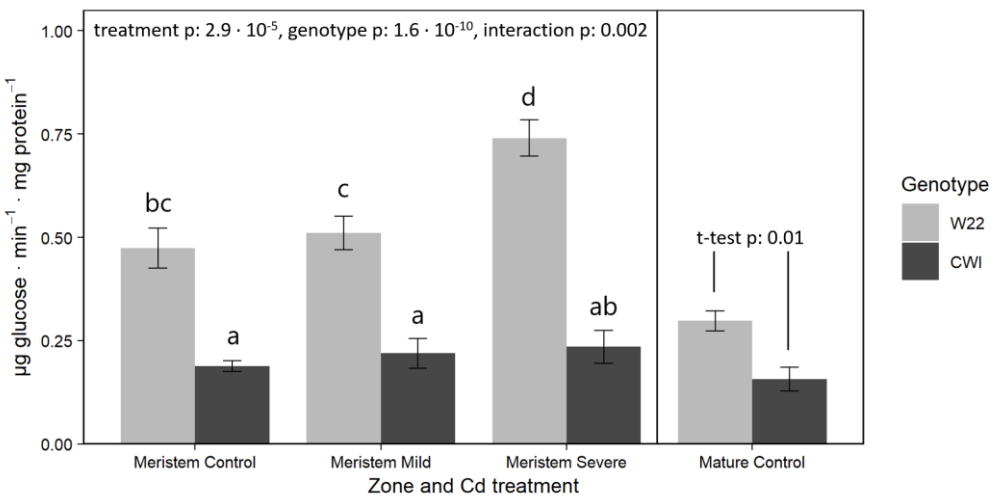

Figure 2. The effect of Cd on invertase activity in the maize leaf. Cell wall invertase activity was measured in the control plus Cd treated meristem tissue and in mature tissue of both the CWI mutant and its genetic background (W22) under control conditions. Data presented are means ± SE, letters are $p < 0.05$ for TukeyHSD ($n = 4$). P-values in main (left) panel indicate the effect of treatment, genotype and their interaction for the meristem (ANOVA), where the right panel P-value results from a t-test between mature leaf tissue of W22 and CWI mutant under control conditions.

Transcriptome study

The kinematics analysis, performed in B73 (chapter 3), indicated that reduced leaf elongation rate was mainly related to a reduced meristem cell number and an increased cell cycle duration. In addition, our transcriptome study (chapter 4) revealed changes in the sucrose metabolism, with the upregulation of sucrose synthases and downregulation of cell wall invertases in the leaf meristem in response to Cd. To reveal the molecular changes induced by Cd in the meristematic tissue of both W22 and mutant, we performed a genome wide transcriptome study on meristematic cells in the CWI mutant and W22 under control, mild and severe Cd stress conditions.

The mutation in CWI mutant 209F mn1-89 is a single nucleotide change at position 1383 (C to T) located in an exon, which would result in the substitution of a proline by a leucine amino acid (Carlson *et al.*, 2000). To confirm this, we first checked the mapping of the individual reads of W22 and mutant samples to this region of the B73 genome. Curiously, we did not find the mutation in the mutant (and W22; Supplementary Figure 5.5).

To obtain a global insight in the effect of Cd in W22 and the mutant, we performed a genome wide analysis of gene expression. As a first step clustered the samples using a PCA analysis. This analysis shows that largest differences in the transcriptome are determined by genotype (Figure 3). The genotypes are separated along PC1, which explains 91% of the variation in the transcriptome dataset.

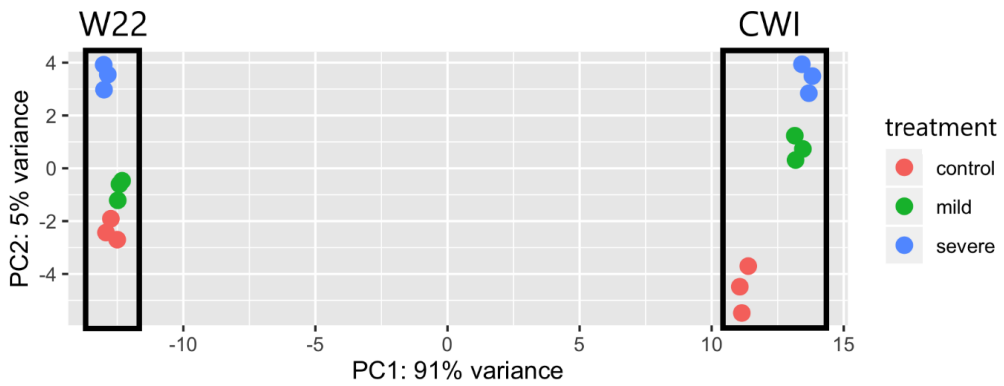

Figure 3. The effect of Cd treatment and lowered CWI activity on the transcriptome in the maize leaf meristem. Counts were normalized using variance stabilizing transformation. In color scale, control and Cd treatment are indicated (mild and severe). W22 is the genetic background of the CWI mutant.

The effect of the genotype on the transcriptome is further confirmed by the differential expression of genes. Here, we found around a third of all the genes in the genome (i.e. 16757 out of 46430 genes) to be differentially expressed (FDR < 0.05) when genotypes were compared, while the impact of Cd was limited to 8027 differentially expressed genes. In addition, 3669 genes showed a significant interaction effect (FDR < 0.05) implying that the response to the Cd treatment is also depended on the genotype (Figure 4).

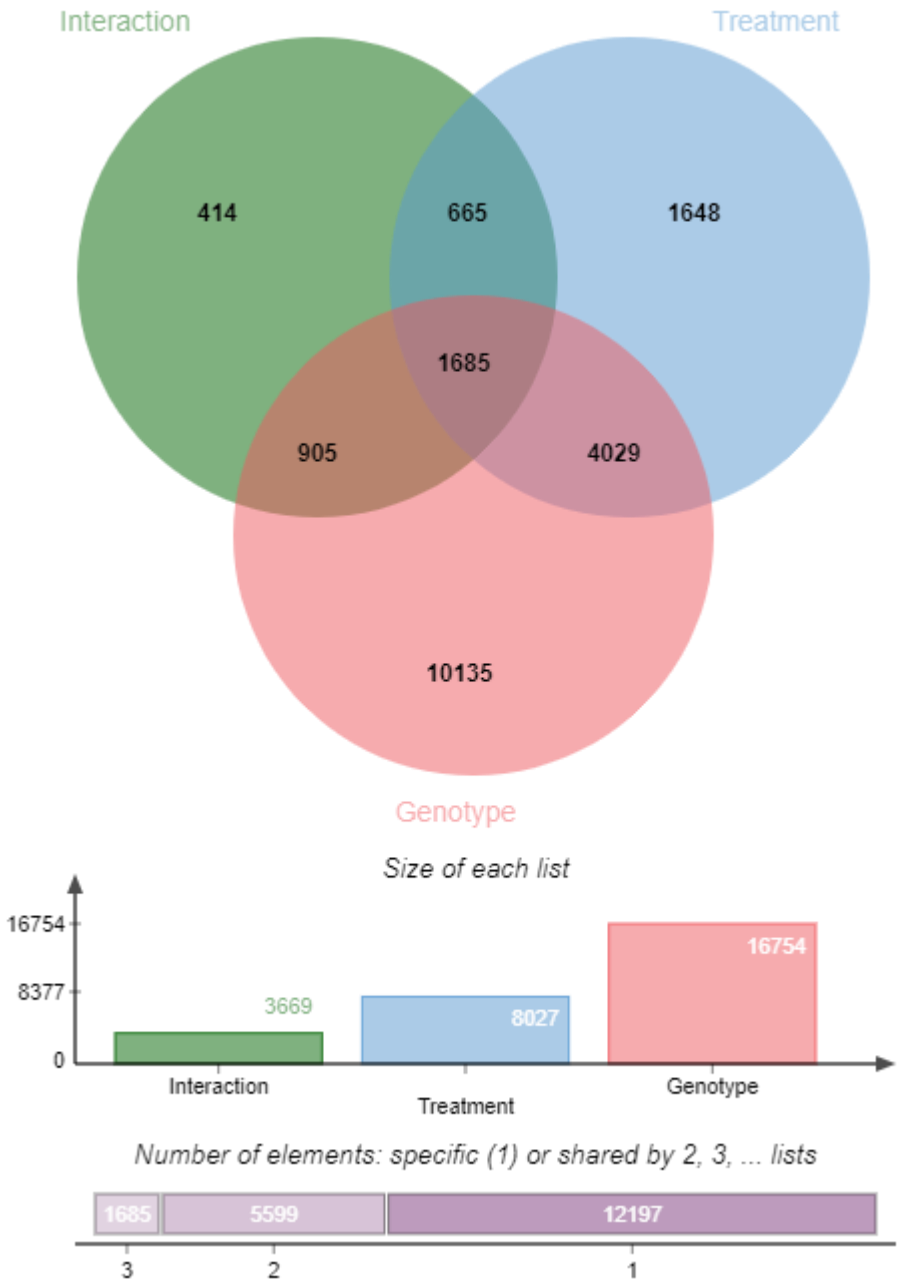

Figure 4. Overview of the number of differentially expressed genes in the maize leaf meristem in response to Cd treatment, genotype (CWI mutant or W22) or showing an interaction between Cd treatment and genotype. (FDR < 0.05)

Impact of Cd on the transcriptome

Increasing Cd levels progressively increased the number of differentially expressed genes (Figure 5). In W22, 362 and 3284 genes were differentially expressed in response to mild and severe Cd stress, respectively. In the CWI mutant, the response was stronger, where mild and severe stress affected 6566 and 8962 genes, respectively. The majority of the genes differentially expressed in W22 are also affected in the CWI mutant, confirming their significance.

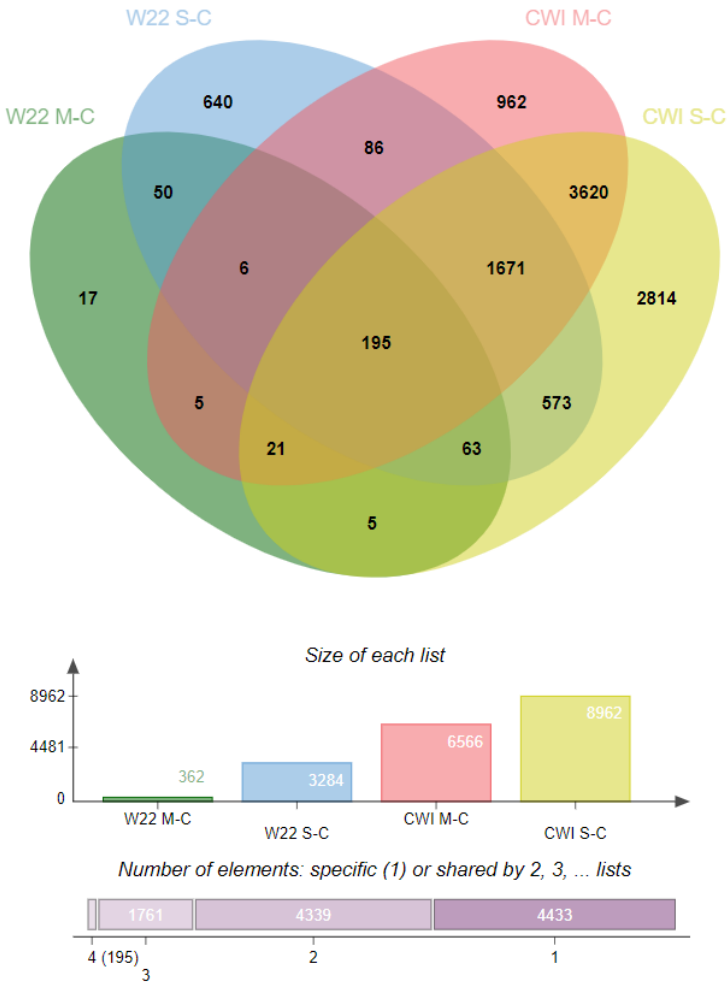

Figure 5. Overview of the number of differentially expressed genes in the mild versus control (M-C) and severe versus control (S-C) contrasts in the W22 and the CWI mutant maize leaf meristem. (FDR < 0.05)

Cell wall invertase expression values

Since we were unable to confirm the described mutation in our mutant, it is of interest to not only look at the alleged mutated cell wall invertase, but also at all other cell wall invertases known in maize (maizeGDB). When inspecting specific contrasts for the cell wall invertase gene that was claimed to be mutated (Carlson *et al.*, 2000) in the CWI mutant (*mn1*, Zm00001d003776, also referred to as *incw2*) in our Deseq2 statistical analysis, we were able to confirm the downregulation of the cell wall invertase gene under Cd stress, described in chapter 4, in both the mutant line and W22 (Figure 6). Under all treatments, the mutant has significantly higher expression levels of the *mn1* than W22.

For the 7 other described cell wall invertase genes, only cell wall invertase 5 (incw5, Zm00001d025354) was significantly upregulated in the mutant under both control, mild and severe stress conditions (Figure 6). Under severe Cd stress, this gene was significantly downregulated in both W22 and CWI mutant, with a significant upregulation in the mutant under mild Cd stress, thus showing a similar expression pattern to *mn1*. Two other cell wall invertases were also significantly downregulated by Cd stress, where *incw4* (Zm00001d001941) was downregulated under severe Cd stress in both mutant and W22, and *incw1* (Zm00001d016708) was downregulated in the mutant under severe Cd stress. All the other cell wall invertase expression contrasts were not significantly impacted.

In conclusion, Cd stress results in downregulation of cell wall invertase gene expression and an increased expression in the mutant when compared to W22, which is opposite the corresponding enzyme activities.

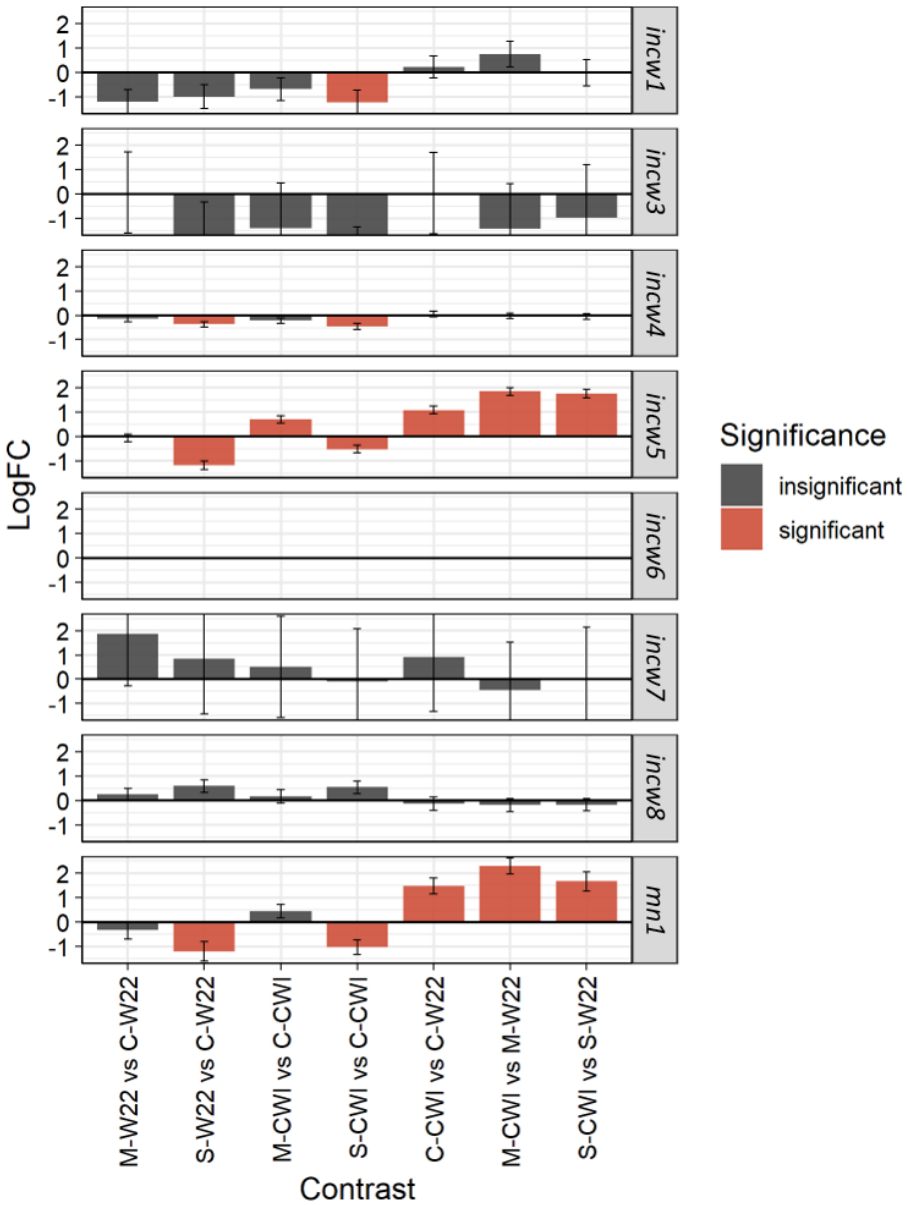

Figure 6. The effect of Cd on expression levels of cell wall invertase genes in the maize leaf meristem. LogFCs were obtained using contrasts in DESeq2, including the significance (FDR) and standard error. Gene symbol names of maize GDB were used to identify the cell wall invertases, where mn1 is the alleged mutated gene of the mutant used. W22 and CWI refer to the inbred line W22 and the mutant with reduced CWI activity, where C, M and S refer to the treatments used (i.e. control, mild and severe). Bars colored red are statistically significant (FDR < 0.05) LFCs. Y-scale was set to clearly present significant LFCs, causing some insignificant LFCs to be displayed only partially. For *incw6*, no reads were obtained, but is included to be complete.

K-means clustering, GO analysis and MapMan analysis

In order to find the dominant gene expression profiles across the samples we performed K-means clustering. For this, we selected genes that were significantly altered for at least one of the following factors: treatment, genotype or interaction between treatment-genotype. This resulted in a list of 19483 genes, which were grouped in four clusters (Figure 7).

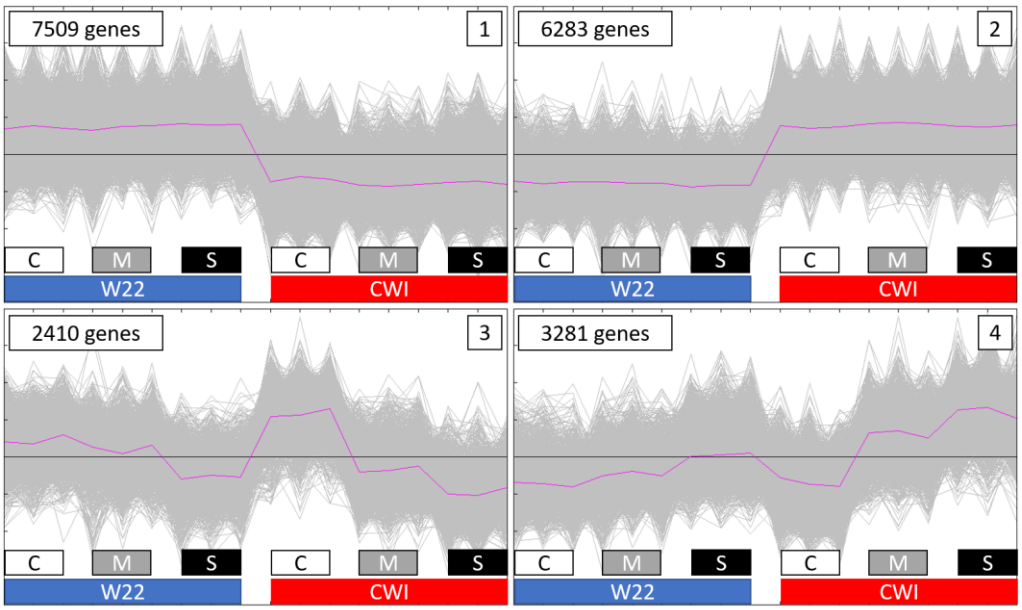

Figure 7. K-means clustering of differentially expressed genes in response to Cd in the meristem of the CWI mutant and W22 maize leaves. The genes either had a significant (FDR < 0.05) effect of Cd treatment, genotype, treatment-genotype interaction or a combination of the former. Transcription levels were rlog normalized using Deseq2 and the gene-row normalization of MeV. Three Cd treatments (C: control, M: mild, S: severe) were used on two genotypes (a cell wall invertase mutant, CWI, and its background, the W22 maize inbred). Every genotype/treatment combination encompasses three biological replicates.

Table 1. Biological processes significantly affected by Cd stress in the meristem of the CWI mutant and its genetic background (W22) for each K-means cluster (Figure 7). Only FDR significant (FDR < 0.05) GOs were selected and summarised (based on semantic similarity) using REViGO. The top 15 GOs of the summarised GOs of each cluster are presented in the table. CL: cluster number, FE: Fold enrichment.

CL	GO ID	GO DESCRIPTION	FE
1	GO:0000045	autophagosome assembly	2.69
1	GO:0007033	vacuole organization	2.51
1	GO:0006914	autophagy	2.32
1	GO:0007265	Ras protein signal transduction	2.24
1	GO:0007018	microtubule-based movement	2.21
1	GO:0006928	movement of cell or subcellular component	2.19
1	GO:0007034	vacuolar transport	2.1
1	GO:0007017	microtubule-based process	1.73
1	GO:0031399	regulation of protein modification process	1.67
1	GO:0051128	regulation of cellular component organization	1.59
1	GO:0051174	regulation of phosphorus metabolic process	1.58
1	GO:0022402	cell cycle process	1.44
1	GO:0023052	signaling	1.38
1	GO:0007154	cell communication	1.37
1	GO:0044283	small molecule biosynthetic process	1.34
2	GO:1902299	pre-replicative complex assembly involved in cell cycle DNA replication	3.71
2	GO:0045036	protein targeting to chloroplast	3.25
2	GO:0009793	embryo development ending in seed dormancy	2.41
2	GO:0009657	plastid organization	2.26
2	GO:0009658	chloroplast organization	2.2
2	GO:0001510	RNA methylation	2.14
2	GO:0071806	protein transmembrane transport	2.13
2	GO:0016072	rRNA metabolic process	2.1
2	GO:0034660	ncRNA metabolic process	1.94
2	GO:0042273	ribosomal large subunit biogenesis	1.89
2	GO:0006412	translation	1.74
2	GO:0006396	RNA processing	1.69
2	GO:0044085	cellular component biogenesis	1.68
2	GO:0010467	gene expression	1.64
2	GO:0043603	cellular amide metabolic process	1.63
3	GO:1902626	assembly of large subunit precursor of preribosome	13.99
3	GO:0000338	protein deneddylation	13.99
3	GO:0010499	proteasomal ubiquitin-independent protein catabolic process	11.66
3	GO:0006177	GMP biosynthetic process	11.2
3	GO:0034969	histone arginine methylation	11.2

CL	GO ID	GO DESCRIPTION	FE
3	GO:0006086	acetyl-CoA biosynthetic process from pyruvate	10.69
3	GO:0009561	megagametogenesis	10.33
3	GO:0051096	positive regulation of helicase activity	9.6
3	GO:0006007	glucose catabolic process	8.4
3	GO:0018195	peptidyl-arginine modification	8.4
3	GO:0046112	nucleobase biosynthetic process	7.42
3	GO:0080156	mitochondrial mRNA modification	6.72
3	GO:0002181	cytoplasmic translation	6.23
3	GO:0006997	nucleus organization	5.77
3	GO:0034982	mitochondrial protein processing	5.34
4	GO:0009773	photosynthetic electron transport in photosystem I	8.49
4	GO:0015969	guanosine tetraphosphate metabolic process	7.08
4	GO:0043467	regulation of generation of precursor metabolites and energy	5.75
4	GO:0009644	response to high light intensity	5.39
4	GO:0042402	cellular biogenic amine catabolic process	5.11
4	GO:0018298	protein-chromophore linkage	4.95
4	GO:0010119	regulation of stomatal movement	4.55
4	GO:0010027	thylakoid membrane organization	4.55
4	GO:0015979	photosynthesis	4.45
4	GO:0015994	chlorophyll metabolic process	4.33
4	GO:0005991	trehalose metabolic process	3.79
4	GO:0007623	circadian rhythm	3.68
4	GO:0048511	rhythmic process	3.68
4	GO:0033013	tetrapyrrole metabolic process	3.16
4	GO:0042908	xenobiotic transport	3.14

Cluster 1 and 2 are clusters where the expression profile is dominated by genotype and cannot be related to clear differences based on Cd treatment. The first cluster contained 7509 genes which were expressed at higher levels in W22, relative to the CWI mutant (Figure 7). Functional overrepresentation analysis revealed that this cluster was overrepresented for GO's related to microtubules, autophagy, vacuolar organisation/transport and Ras protein signal transduction, amongst others (Table 1). The second cluster, containing 6283 genes, exhibited the opposite profile compared to cluster 1, i.e. upregulation in the mutant (Figure 7). In this cluster, highest fold

enrichments were related to DNA replication, RNA processing, plastid organisation and translation (Table 1). Thus, these clusters broadly reflect effects of the mutation on wide range of biological processes in the meristem.

Clusters 3 and 4 related to the Cd treatments (Figure 7). Cluster 3 contained 2410 genes of which the transcription levels decreased with increasing Cd stress. The relative decrease in transcription was larger in the CWI mutant compared to W22. A diverse set of GOs was overrepresented, amongst which are assembly of large subunit precursor of preribosome, protein deneddylation, proteasomal ubiquitin-independent protein catabolic process, GMP biosynthetic process and glucose catabolic process (Table 1). The fourth and last cluster contained 3281 significantly affected genes, most of which are related to photosynthesis GOs. Here, genes were upregulated under increasing Cd stress, where this increase was relatively larger in the CWI mutant. The remaining gene ontologies in this cluster were associated with signalling, ion transport and process regulation, amongst others (Table 1).

With regards to the Cd upregulated genes related to photosynthesis in cluster 4, we confirmed the upregulation of genes related to light reactions in the MapMan metabolism overview for both W22 and mutant, which is rather unexpected in the meristem (Figure 8). In addition, in W22, secondary metabolism genes related to terpenes, flavonoids, phenylpropanoids and phenolics are upregulated in response to Cd. Starch and sucrose metabolism show mostly moderate changes in gene expression levels in response to Cd (Figure 8). Yet, in the mutant, the carbohydrate metabolism, starch degradation and sucrose synthesis are strongly upregulated under Cd stress (Figure 8).

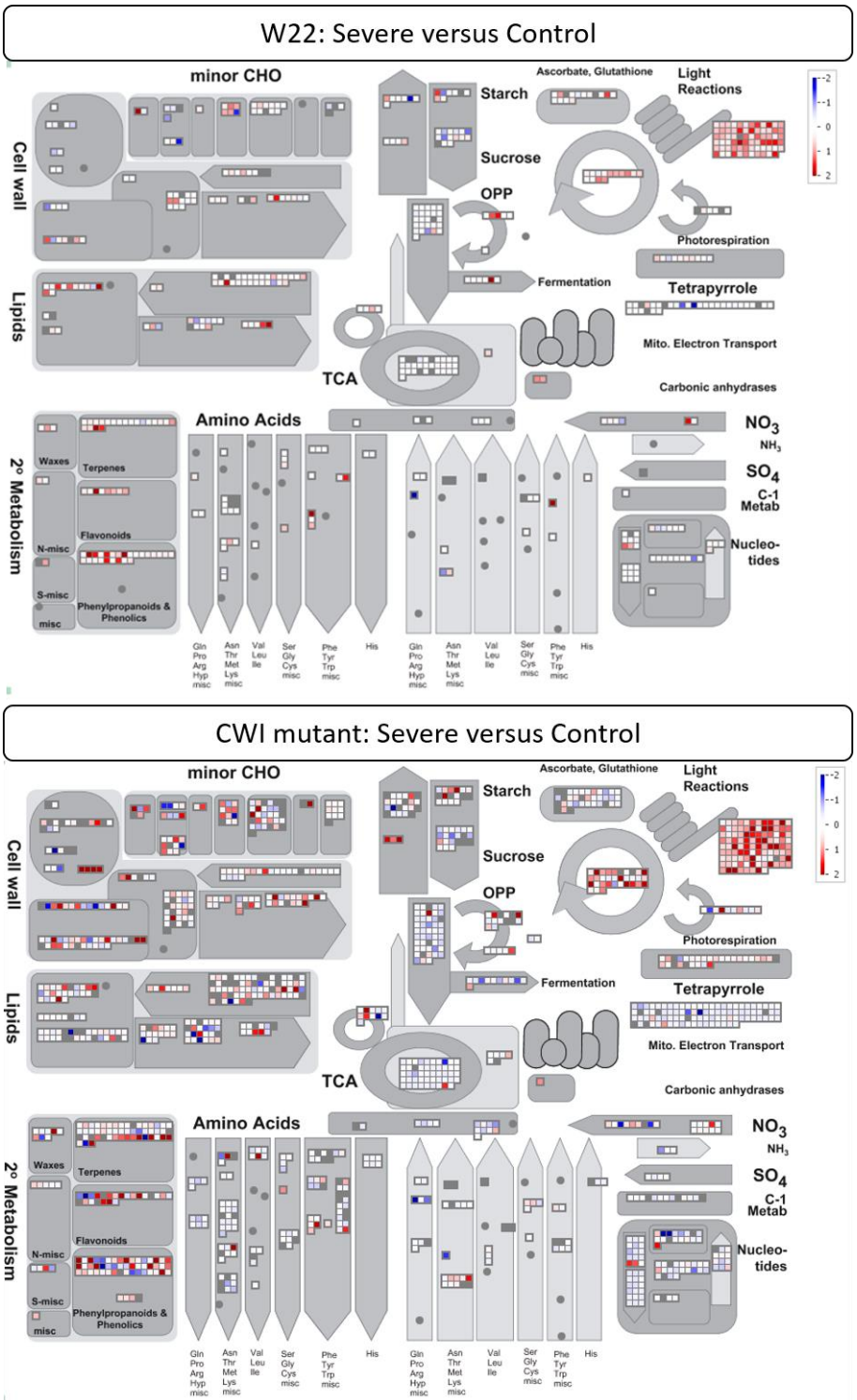

Figure 8. The effect of severe Cd stress on the metabolism in the maize leaf meristem in W22 and the CWI mutant. The MapMan metabolism overview is presented containing (*continues next page…*)

significant (FRD < 0.05) LFCs for severe versus control contrast of both genotypes. A color scale is used to visualize log_2 fold changes and indicates whether genes are upregulated (red) or downregulated (blue) under severe Cd stress when compared to control conditions. Log_2 fold changes were calculated by the Deseq2 package, which corrects counts for library size.

When inspecting MapMan mappings for specifically sucrose related metabolism, we are able to verify the low impact on this pathway at transcriptome level in W22 even in response to severe Cd stress (Figure 9). In the sucrose pathway, only two cell wall invertase genes are significantly downregulated (LFC: -1.2 and -1.2, resp. Zm00001d003776 and Zm00001d025354), where for starch degradation, the transcription of affected two beta-amylases rather ambiguous, with one up- (LFC 1.5, Zm00001d027619) and one down-regulated (LFC 1.1, Zm00001d029983). The reduced cell wall invertase gene expression levels do not match the increased activity, presented in Figure 2. In addition, due to the strongly altered sugar levels across the growth zone under Cd stress (Figure 10), we expected to find more significantly altered carbohydrate related genes. This suggests other regulatory mechanisms, such as translation and protein phosphorylation, potentially control enzyme activity.

In the CWI mutant, we noted a stronger impact of the mild and severe Cd treatment on the sucrose and starch metabolism related transcriptome in the MapMan metabolism overview (Figure 8). Related to sucrose, we found upregulation of genes encoding enzymes responsible for sucrose synthesis from fructose-6-phosphate and UDP-glucose (sucrose-phosphate synthase, Zm00001d048979 (LFC severe vs control: 1.8), sucrose phosphatase, Zm00001d024821 (LFC severe vs control: 1.2)). However, it seems like the export of sucrose is stimulated given a significant upregulation of sucrose transporters (LFC severe vs control: 2.0 and 1.6, resp. Zm00001d027854 and Zm00001d048311) (Figure 9). Related to sucrose degradation, the most downregulated genes are cell wall invertases, amongst which are Zm00001d016708 (LFC severe versus control: -1.2) and Zm00001d003776 (LFC severe vs control: -1.0, being the mutant gene). Due to the upregulation of sucrose production and export related genes and downregulation of cell wall invertase genes, it is hard to directly link the sucrose levels (Figure 10) to the differentially expressed genes (Figure 9).

We observe an upregulation of genes related to starch degradation (i.e. beta-amylases, LFC severe vs control: 0.8, 1.2, 2.6, resp.: Zm00001d047480, Zm00001d027619, Zm00001d029164) (Figure 9), potentially to free up glucose to compensate for the reduced activity of cell wall invertase (Figure 2). Since these genes are upregulated under both mild and severe stress conditions, it is difficult to link these transcript levels to the observed glucose levels (Figure 10), since these appear to be reduced under mild stress and increased under severe stress in the mutant.

Finally, we want to highlight interesting mappings of myo-inositol and raffinose. Here, it seems like both metabolites are favourited under Cd stress in the CWI mutant due to the upregulation of genes encoding enzymes which catalyse myo-inositol and raffinose production (Figure 11). More specifically, we found four myo-inositol phosphate synthases to be upregulated in both W22 and CWI mutant, where fold changes increased in proportion to the Cd stress level (average LFC for severe vs control, in W22 = 1.01 ± 0.11; in CWI mutant: 1.16 ± 0.28). In addition, 5 genes with galactinol-sucrose galactosyltransferase activity (related to raffinose production) were significantly affected for the severe versus control contrast, of which 3 were upregulated (LFC 2.24, 1.41, 0.97) and 2 were downregulated (LFC -1.01, -0.13). In W22, only 2 genes were significantly affected for the same contrast, where one was highly upregulated (LFC 2.21) and the other slightly downregulated (LFC -0.47). For CWI vs W22 contrast under control conditions, no less than 7 genes related to galactinol-sucrose galactosyltransferase activity are higher expressed in the CWI mutant (data not shown). Taken together, these results indicate that raffinose production could be affected by Cd stress and probably does not take precedence in W22 like it does in the CWI mutant (Figure 11).

In conclusion, we found a very diverse set of processes differing between both genotypes, making it hard to pinpoint exact differences between them based on the transcriptome. This huge difference could have been expected, given the large differences in transcriptome, described above. With regards to Cd stress, an interesting observation was the upregulation of photosynthesis related processes

already in the meristematic tissue. When inspecting impact of Cd on the pathways related to carbohydrate metabolism, we were unable to directly match changes in expression levels to our observations in the measured carbohydrates levels for both genotypes. Additionally, a potential role for myo-inositol and raffinose under Cd stress was revealed.

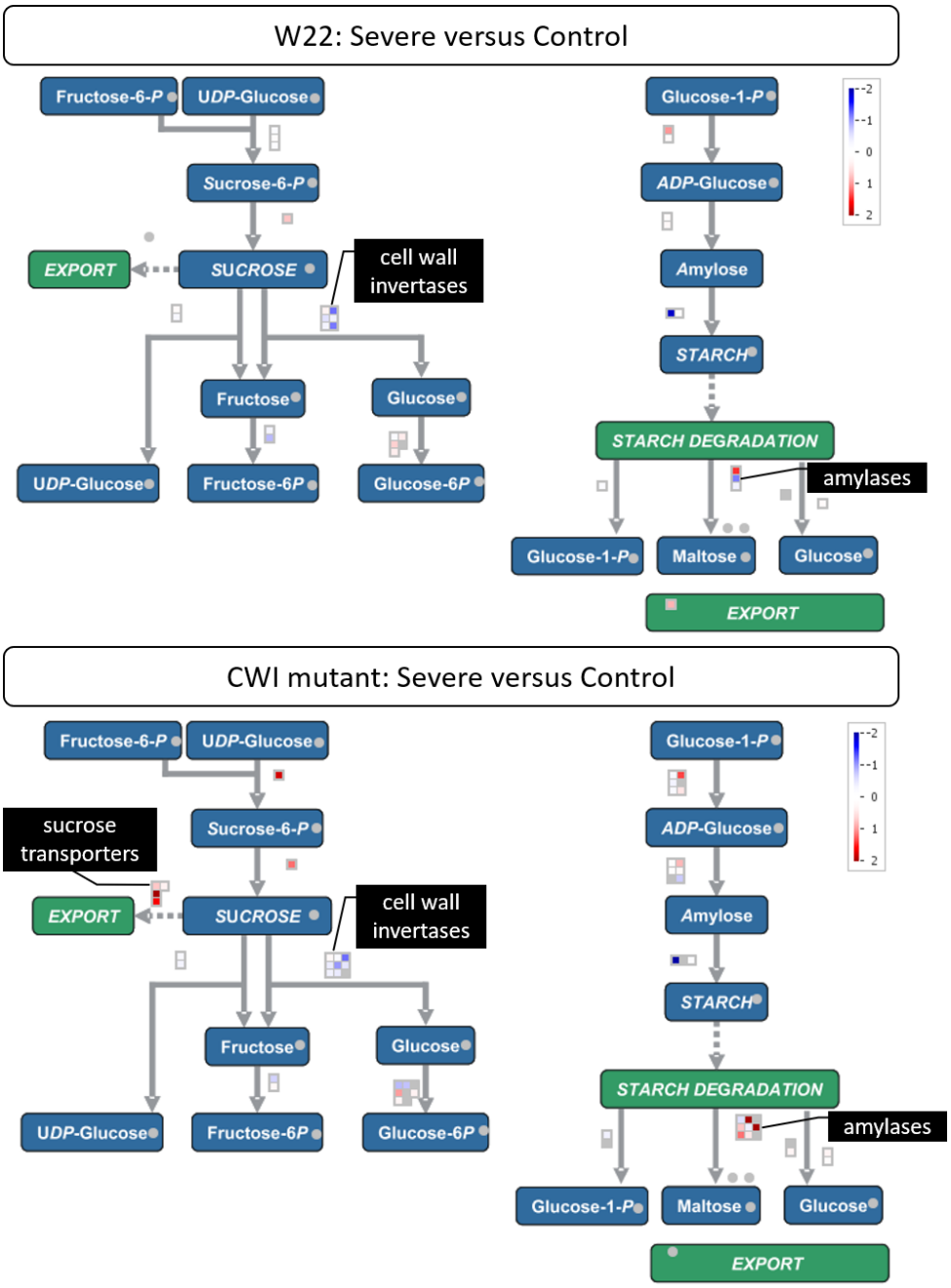

Figure 9. The effect of severe Cd stress on sucrose and starch metabolism gene expression in W22 (upper graph) and the CWI mutant (lower graph). The MapMan sucrose and starch metabolism overview is presented containing significant (FRD < 0.05) LFCs for severe versus control contrast of both genotypes. A color scale is used to visualize $\log_2$ fold changes and indicates whether genes are upregulated (red) or downregulated (blue) under mild and severe Cd stress when compared to control conditions. Log_2 fold changes were calculated by the Deseq2 package, which corrects counts for library size.

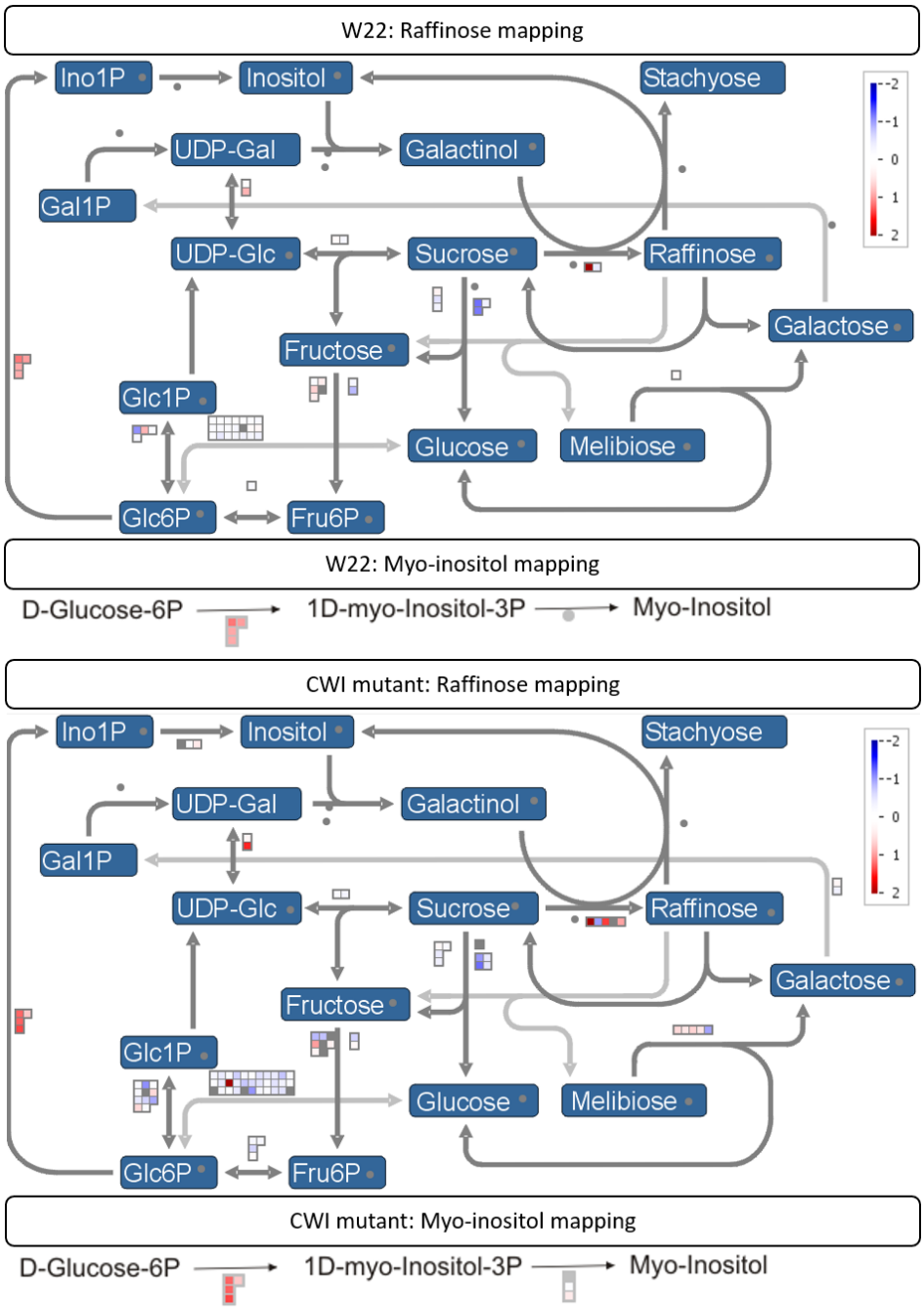

Figure 11. The effect of severe Cd stress on the raffinose and myo-inositol in the maize leaf meristem of W22 and the CWI mutant. The MapMan raffinose and myo-inositol mappings are presented containing significant (FRD < 0.05) LFCs for severe versus control contrast of both genotypes. A color scale (shared by both mappings) is used to visualize $\log_2$ fold changes and indicates whether genes are upregulated (red) or downregulated (blue) under mild and severe Cd stress when compared to control conditions. Log_2 fold changes were calculated by the Deseq2 package, which corrects counts for library size.

Sugar measurements

To functionally understand the role of CWI activity, we determined the levels of its substrate sucrose and products glucose and fructose in the maize leaf growth zone.

Under control conditions, no distinct differences between the total soluble sugars levels of W22 and the CWI mutant were found (Figure 10). For both lines, total soluble sugars decreased slightly from meristem to mature tissue under control conditions. Cadmium stress progressively increased total soluble sugar levels in the maize leaf growth zone of W22. In the mutant, total soluble sugar levels dropped below control levels under mild Cd stress and increased significantly under severe Cd stress.

When inspecting the individual carbohydrate measurements, we found that under control conditions, soluble sugars in the meristematic tissue are mainly composed out of sucrose, where glucose and fructose levels show a clear peak in the region between 2 and 7 cm from the leaf base (Figure 10). Under severe Cd stress, sucrose, glucose and fructose levels increase significantly in W22, where the mutant only shows an increase in sucrose and glucose, but fails to increase fructose levels in the first 5 cm of the growth zone. Under mild Cd stress, W22 only slightly increases sucrose and glucose levels above control level, where fructose levels remain unaffected. The CWI mutant failed to exhibit similar increases. On the contrary, particularly under mild stress, its sucrose, glucose and fructose levels are well below the control levels at most positions along the growth zone.

Taken together, carbohydrate levels are strongly affected by both treatment and cell wall invertase functionality. In W22 and the CWI mutant, carbohydrate levels are significantly increased under severe Cd stress, yet, both genotypes respond differently to mild Cd stress. In the meristem, carbohydrate levels are dominated by sucrose, where towards maturation, glucose levels take the upper hand. Fructose levels are generally low and reduced in the CWI mutant compared to W22 under all treatments.

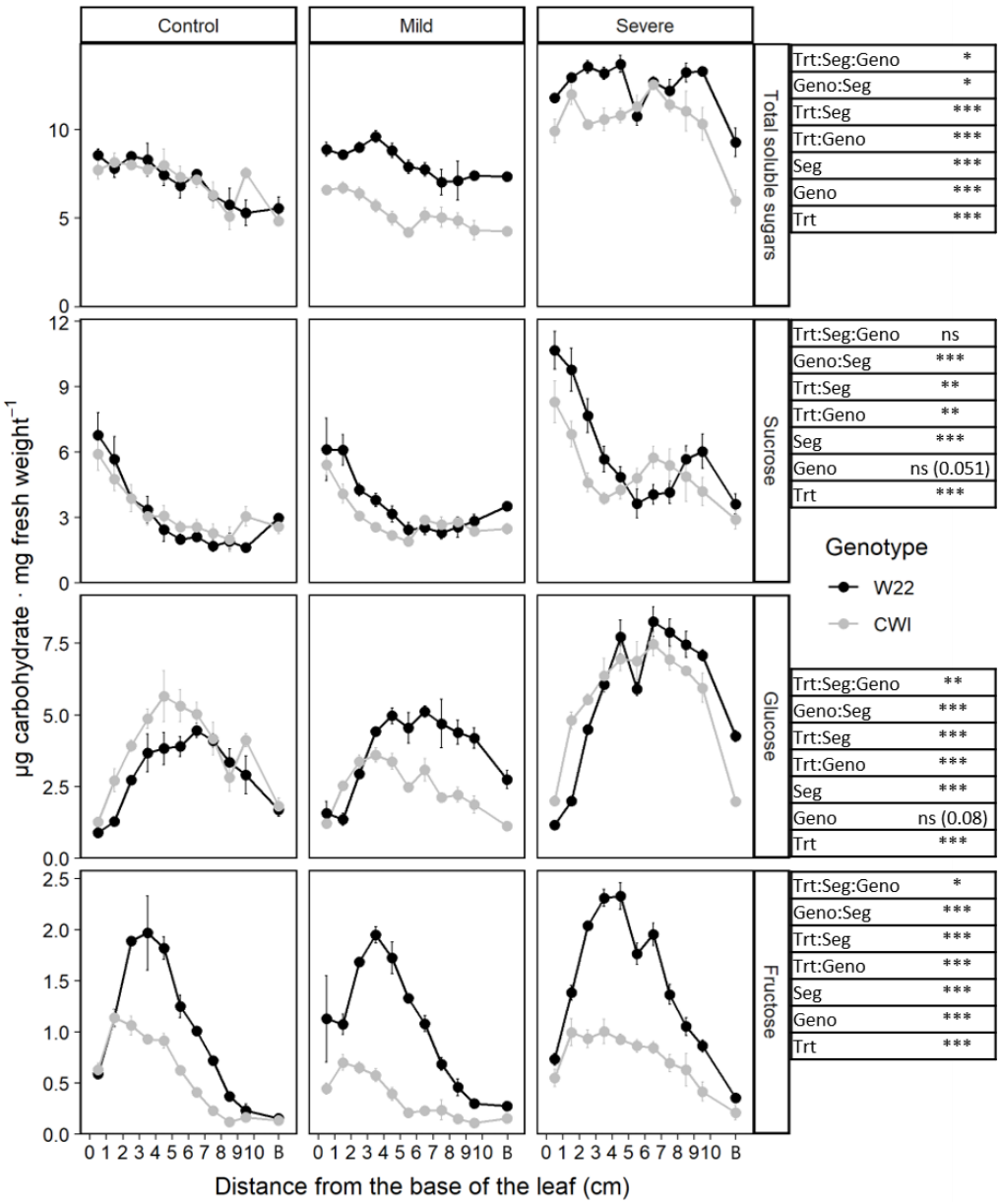

Figure 10. The effect of Cd on carbohydrate levels in the growth zone and mature blade (B) of wild-type and CWI plants. Total soluble sugar, sucrose, glucose and fructose levels were measured in a cell wall invertase mutant (CWI) and its genetic background (W22), both treated with a control treatment and two Cd treatments (mild and severe). Presented data are means ± SE (n = 3-4). A three-way ANOVA was performed to determine the interaction and individual effect of Cd treatment, segment in the maize leaf and genotype. Sucrose and fructose data were $\log_{10}$ transformed to better approximate the normal distribution. The significance of Cd treatment (Trt.), genotype (Geno.) and the interaction between them (Inter.) is indicated by asterisks (ns: not significant, * $p < 0.05$, ** $p < 0.01$, *** $p < 0.001$))

Kinematics

In order to study the cellular basis (i.e. cell division and elongation) of the increased growth inhibition in relation to the altered CWI activity and increased Cd sensitivity of the CWI mutant, we performed a kinematic analysis of both the mutant and its genetic background, W22.

Under control conditions, the smaller phenotype of the CWI mutant (Supplementary Figure 5.4) is related to a 23% reduction of final leaf length (Table 2). The shorter final leaf length is associated with a 13% lower leaf elongation rate, suggesting that a reduced duration of the growth phase (not determined) plays an additional role. Reduced leaf elongation rates, in turn can be explained mainly by a significantly reduced cell production rate in the mutant (25%). Lower cell production rates are presumably due to the combined effect of a reduction of the number of cells in the meristem and slower cell division rate, although neither is significant. Interestingly, the reduced cell production rate is partially compensated by an increased mature cell length (18%). The increase in mature cell length appears to result from an increased (27%, but not significant) length at which cells leave the meristem and start elongating, while time cells spent in the elongation zone and average relative cell elongation rate remain unaffected.

When comparing the CWI mutant to its background (W22) under Cd stress conditions, we were able to determine the cellular basis for the mutants increased sensitivity to Cd (Table 2). Leaf Elongation rate of W22 was reduced by 29% in response severe Cd stress. The CWI mutant on the other hand already showed 36% reduction under mild stress conditions. Under severe stress conditions, the mutant almost succumbed to the imposed Cd stress, having an LER of only 34% compared to control conditions. For both W22 and the CWI mutant, the reduction in LER could be related to a progressive reduction of cell production rate, which reduced by 7 and 29% in W22 and by 40 and 66% under mild and severe stress conditions in the CWI mutant, respectively. For W22, the reduction in cell production rate could be mainly related to an increased cell cycle

duration (11% and 50% under resp. mild and severe Cd stress), as meristematic cell number was mostly unaffected, where in the CWI mutant both processes were significantly negatively impacted: 24 and 69% increased cell cycle duration and 25 and 43% reduced meristematic cell number under mild and severe stress respectively. Mature cell length remained unaffected by Cd stress in W22. In the mutant, severe Cd stress did not affect mature cell length and mild stress conditions increased it slightly (12%).

In conclusion, we were able to relate the sensitivity of the CWI mutant to Cd to a stronger inhibition of cell cycle duration and a drastically reduced cell number in the meristem, closely mirrored by meristem size, while this parameter in W22 remained largely unaffected. Interestingly, we also found that the mutant had an increased mature cell length under control conditions when compared to W22.

Table 2. (*Next page*) Kinematic analysis of the effect of Cd on cell division and cell expansion in the growing maize leaf of a cell wall invertase mutant (CWI) and its genetic background (W22). Data are mean values ± SE (n = 12 for leaf elongation rate, n = 6 for final leaf length, n = 6-7 for the other parameters).The significance of Cd treatment (Trt.), genotype (Geno.) and the interaction between them (Inter.) determined by ANOVA is indicated by asterisks (ns: not significant, (*) $0.1 < p < 0.05$, * $p < 0.05$, ** $p < 0.01$, *** $p < 0.001$)). For the effect of genotype, the control treatment of both genotypes are compared against each other, while the impact of Cd on both genotypes is expressed by comparing mild and severe treatment against the control treatment of the same genotype. The resulting magnitude in change is expressed as percentages, of which the background is colored gray when significantly different (TukeyHSD, $p < 0.05$). Number of cells in the meristem, cell cycle duration, time in the elongation zone, time in the division zone, length of the cells leaving the meristem and relative cell elongation rate were $\log_{10}$ transformed to better approximate the normal distribution.

Parameters	W22			CWI			Inter.	Trt.	Geno.	C CWI / C W22	W22		CWI	
	C	M	S	C	M	S					M / C	S / C	M / C	S / C
Final leaf length (mm)	955 ± 13	883 ± 16	767 ± 8	737 ± 19	511 ± 32	387 ± 8	***	***	***	77%	92%	80%	69%	52%
Leaf elongation rate ($mm \cdot h^{-1}$)	3.3 ± 0.04	3.02 ± 0.04	2.36 ± 0.03	2.86 ± 0.07	1.85 ± 0.09	0.97 ± 0.05	***	***	***	87%	92%	71%	64%	34%
Length of the meristem (mm)	15.5 ± 0.5	16.6 ± 0.4	16.4 ± 0.3	13.5 ± 0.6	11.5 ± 1.1	9 ± 0.8	**	*	***	87%	107%	106%	86%	67%
Length of the elongation zone (mm)	47.9 ± 1.9	47.1 ± 2.4	39.3 ± 3	45.7 ± 4.4	39.5 ± 3.2	30.3 ± 2.7	ns	***	***	95%	98%	82%	87%	66%
Length of the growth zone (mm)	63.4 ± 2.1	63.7 ± 2.4	55.8 ± 3	59.1 ± 4.8	51.1 ± 3	39.3 ± 2.2	ns	***	*	93%	100%	88%	86%	66%
Length cells leaving meristem (µm)	17.3 ± 0.8	19.3 ± 0.8	20.2 ± 1.3	22 ± 0.5	29.4 ± 3.5	32 ± 5.1	ns	*	***	127%	112%	117%	134%	145%
Mature cell length (µm)	112 ± 3	112 ± 1	116 ± 4	132 ± 3	148 ± 4	137 ± 1	*	**	***	118%	100%	104%	112%	104%
Number of cells in meristem	875 ± 32	904 ± 61	929 ± 22	743 ± 25	555 ± 30	420 ± 26	***	***	***	85%	103%	106%	75%	57%
Number of cells in elongation zone	1061 ± 41	989 ± 38	750 ± 40	793 ± 49	524 ± 52	409 ± 43	ns	***	***	75%	93%	71%	66%	52%
Number of cells in total growth zone	1936 ± 59	1892 ± 63	1679 ± 41	1537 ± 65	1079 ± 41	829 ± 32	***	***	***	79%	98%	87%	70%	54%
Cell production rate ($cells \cdot h^{-1}$)	29.5 ± 1.4	27.5 ± 0.5	20.8 ± 0.6	22.1 ± 1	13.4 ± 0.8	7.6 ± 0.4	***	***	***	75%	93%	71%	60%	34%
Cell division rate ($cells \cdot cell^{-1} \cdot h^{-1}$)	0.034 ± 0.001	0.031 ± 0.003	0.022 ± 0.001	0.03 ± 0.001	0.024 ± 0.002	0.019 ± 0.002	ns	***	**	88%	93%	67%	82%	63%
Relative cell elongation rate ($\mu m \cdot \mu m^{-1} \cdot h^{-1}$)	0.052 ± 0.001	0.049 ± 0.001	0.049 ± 0.002	0.05 ± 0.003	0.043 ± 0.003	0.029 ± 0.002	***	***	***	97%	95%	94%	86%	57%
Cell cycle duration (h)	20.7 ± 0.9	23 ± 1.8	31.1 ± 1.2	23.4 ± 0.7	29.1 ± 1.9	39.6 ± 4.3	ns	***	**	113%	111%	150%	124%	169%
Time cells spend in the meristem (h)	203 ± 9	226 ± 20	307 ± 12	223 ± 6	266 ± 18	347 ± 41	ns	***	(*)	110%	112%	151%	119%	155%
Time cells spend in the elongation zone (h)	36.1 ± 1	36 ± 1.1	36.2 ± 1.9	35.9 ± 1.9	39.6 ± 4.1	54.1 ± 5.9	(*)	(*)	(*)	99%	100%	100%	110%	151%

Photosynthesis parameters

To better understand the increased carbohydrate levels in the growth zone in response to Cd exposure, and the CWI mutant failing to increase those to the same level, we determined the impact of both Cd and CWI functionality on the photosynthetic process. For this, we performed gas exchange measurements to determine photosynthetic rate and stomatal conductance and determined chlorophyll fluorescence (Fv/Fm), which is a good indication of the efficiency at which light is absorbed at photosystem II for use in photosynthesis.

Under control conditions photosynthetic rate was reduced by 14.5% in the CWI mutant compared to W22. Fv/Fm and stomatal conductance were somewhat lower in the CWI mutant, albeit not significantly (Figure 12).

The impact of Cd on the photosynthesis parameters, resembles the growth phenotype, where all three parameters progressively decrease in W22 with increasing Cd levels. The CWI mutant responded much stronger, even to mild stress levels (Figure 12). Fv/Fm in W22 remained unaffected by severe Cd stress, indicating that absorbed light was still efficiently used by photosystem II, while in the mutant it was reduced by 21% and 12.9% under mild and severe Cd stress. Photosynthetic rate and stomatal conductance were more sensitive to Cd. In W22 severe stress reduced these parameters by 21.5 and 23.2%, respectively. In the CWI mutant, photosynthetic rate and stomatal conductance already dropped strongly under mild Cd stress, by respectively 87.4 and 79.4%, where under severe Cd stress, interestingly, both parameters recovered slightly, yet still being reduced by respectively 67.7 and 58.6%.

In conclusion, while the reduced CWI activity has little effect under control conditions, it strongly increases the sensitivity of photosynthesis to Cd. These observations could explain the reduced sugar levels in the mutant compared to its genetic background under Cd stress, but not the increased levels in W22.

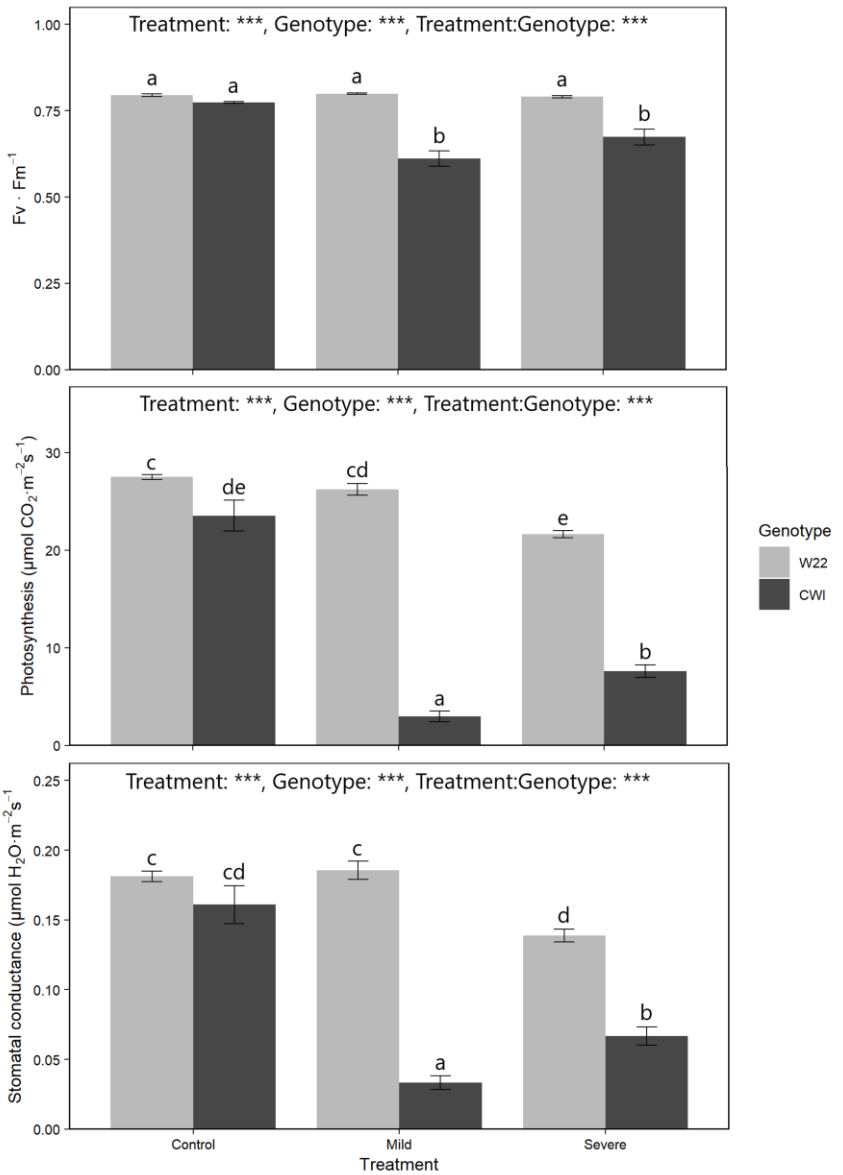

Figure 12. The effect of Cd on photosynthesis parameters in the 5th leaf of the CWI mutant and its genetic background (W22) in maize. Fv/Fm as an indicator of the maximum quantum yield of photosystem II chemistry), CO2 consumption as an indicator for photosynthesis driven assimilation rate and stomatal conductance as an indicator for stomatal opening. Leaves of both a cell wall invertase mutant (CWI) and its genetic background (W22) were emerged for two days from the whorl of older leaves and adapted to darkness for 10 minutes before Fv/Fm measurements were performed. Data presented are means ± SE (n = 5-7). Fv/Fm and photosynthesis data did not meet assumptions for the two-way ANOVA, yet log10 transformation was not performed since it worsened the distribution / homoscedasticity (***: $p < 0.001$). Letters result from a TukeyHSD test, where different letters indicate $p < 0.05$.

Discussion

Verification of the mutant

At the biochemical level, we were able to verify the reduced CWI activity in the mutant. Under control conditions, the activity of CWI's reduced by 39.8% in the mutant compared to W22, where in the blade tissue, the activity was reduced by 52.6%. In the CWI mutant however, where the activity of cell wall invertases was measured in the kernels, Cheng et al. (1996) found that only 6% of WT activity remained. Yet, it is hard to directly compare these activities, since tissue and methods used differ significantly (i.e. for Cheng et al. (1996) versus this study: kernel versus leaf and extraction of CWI out of pelleted tissue versus CWI activity measurement using the pelleted tissue directly).

The transcriptome study involves a word of caution, since we did not find the mutation described in Carlson et al. (2000). All transcriptome samples, originating from the CWI mutant, lacked the single nucleotide change at position 1383 (C to T), which would result in the substitution of proline by leucine. In addition, over 90% of the variation in transcriptome was attributed to the effect of genotype. With such large variation in the transcriptome, it is hard to believe that such pleiotropy in the transcriptome is caused by just one malfunctioning cell wall invertase, especially since it is known that up to 8 cell wall invertases genes are present in the maize genome. Alternatively, the reduced CWI activity does indeed lie at the basis of the observed phenotype, which indicates that carbohydrates (i.e. cell wall invertases) occupy such a central role in the plants metabolism of actively growing tissue that an altered carbohydrate metabolism therein might set a chain reaction in motion, resulting in a heavily affected transcriptome.

Additional research is required to confirm the link between the observed reduced cell wall invertase activity and the observed phenotype. If indeed the reduction in cell wall invertase activity is cause by one (or a few) single nucleotide polymorphism (SNP), bulked segregant RNA-sequencing mutation mapping could be used to locate the SNP

and identify candidate genes responsible for the reduced CWI activity (Hill *et al.*, 2013). The list of candidate genes could then be screened for cell wall invertases or other genes related to carbohydrate metabolism. In addition, a large set of mutants in carbohydrate metabolism can be tested for their tolerance to cadmium. Such an experiment could indicate whether Cd sensitivity can be found in other CWI mutants or perhaps is a trait commonly observed in this set of mutants. Alternatively, directed CRISPR-Cas9 mutagenesis of cell wall invertase genes could be elicited (Svitashev *et al.*, 2016), where the created mutants can be used to check reduced CWI activity and the link to Cd sensitivity.

Taken together, we believe that caution should be exercised when the results presented in this chapter are linked directly to reduced cell wall invertase activity. While our biochemical data support reduced cell wall invertase activities under both control and Cd stress conditions in the mutant, our transcriptome study also revealed that both genotypes differed strongly for a broad range of gene ontologies.

For now, the results will be discussed assuming that the reduced cell wall invertase activity of the mutant is the main cause for the observations made.

Cd stress affects carbohydrate levels in the leaf growth zone

In chapter 4, the transcriptome study indicated sucrose metabolism to be affected by Cd stress in the maize leaf growth zone. We therefore hypothesized that Cd would affect sucrose, glucose and fructose levels in this zone. Indeed, we found that Cd stress increased the level of all three of these carbohydrates and total soluble sugars in the W22 growth zone proportional to the imposed Cd stress level. The increase in soluble sugars seems to be a common response to Cd stress in leaves. In potato leaves and roots, 48-day Cd exposure (40 µM) resulted in increased total soluble sugar, fructose, glucose and sucrose content (Shahid *et al.*, 2019). Rice seedling exposed to 5 and 10 days Cd (100 µM) also had increased leaf sucrose and soluble sugar levels (Moya *et al.*, 1993). Cadmium stressed pea seedlings also showed elevated sucrose levels in the shoot, yet in roots, sucrose contents were not significantly affected (Devi *et al.*, 2007). Total soluble sugars increased in *Pinus Sylvestris* seedling shoots after growing in 10 and 100 mg Cd/kg soil. Yet, in roots, total soluble sugars increased under 10 mg Cd/kg treatment, but decreased under 100 mg Cd/kg treatment (Kim *et al.*, 2004). Also, decreasing levels of fructose, glucose and sucrose have been reported under Cd stress in both shoot and root of in vitro cultured *Lupinus albus* (Costa and Spitz, 1997).

Increased carbohydrate levels might help the plant to cope with Cd stress. Shi et al. (2015) have shown that exogenous glucose reduced shoot Cd concentration and rescued Cd-induced chlorosis in Arabidopsis. Also, in the roots, the content of hemicelluloses 1 and the amount of Cd retained by it was increased significantly by the increased glucose levels. In addition, more Cd was sequestered into the vacuoles when exogenous glucose was added to the growth medium. Increased sucrose levels might also be related to the oxidative stress, caused by Cd in the growth zone. Stoyanova et al. (2011) have demonstrated in vitro that sucrose has antioxidant properties and it was also suggested by Peshev and Van den Ende (2013) that accumulation of sucrose in vacuoles of some plant species, like sugarcane and sugar beet, might act as ROS scavengers in these organelles. Finally, through the close relationship of these carbohydrates with mitochondrial respiration and fatty acid beta-oxidation, soluble

sugars inherently occupy a central role in the cellular redox balance (Couée *et al.*, 2006; Keunen *et al.*, 2013).

CWI activity under control and Cd conditions

We hypothesised sucrose metabolism maize mutants to be more sensitive to Cd stress. In our mutant screen, we found the sucrose synthase double mutant to lack increased sensitivity to Cd stress, perhaps due to compensated activity by other sucrose synthases in the maize genome (i.e. 4 sucrose synthases present in the maize genome database). On the other hand, the mutant with reduced CWI activity did show higher sensitivity to Cd stress. Under mild Cd stress conditions, the total soluble sugar levels in the CWI mutant were lower compared to those under control conditions. This decrease was mainly caused by a decrease in glucose and fructose levels, since sucrose levels only reduced slightly. Under severe Cd stress, total soluble sugars in the mutant increased, however, they did not reach the same levels as in W22. This increase was mainly achieved by increased glucose and sucrose levels, as fructose levels remained at control levels. Under control conditions, we mainly found an impact on fructose levels, which were markedly lower in the CWI mutant compared to W22. Glucose levels, on the other hand, were slightly increased in the CWI mutant, whereas total soluble sugars and sucrose levels remained similar to each other. Taken together, this indicates that increased fructose levels might have an important function in plant resistance to Cd stress. In cold stressed pea leaves, increased fructose levels helped in coping with cold-induced oxidative stress (Bogdanović *et al.*, 2008). Perhaps, the lack of increased fructose levels in the CWI mutant can be related to an increased susceptibility to reactive oxygen species originating from Cd stress.

With regards to the reduced cell wall invertase activity in the mutant, one could expect increased amounts of available sucrose in the mutant, but this was not the case. Neither did the significant increase in CWI activity in the W22 meristem tissue under Cd stress cause reduced sucrose levels and increased glucose and fructose levels. Even though we are unable to make direct links between changes in CWI activity and

carbohydrate contents, these results still indicate that altered cell wall invertase activity could affect Cd stress susceptibility, which was shown by our phenotype analysis. Also previous studies link altered CWI activity to Cd stress. In roots of Rangpur lime, CWI activity decreased significantly under Cd stress, which could be linked to an increase in apoplastic sucrose content (Podazza *et al.*, 2006). In an ethylene insensitive Arabidopsis mutant, Zhou et al. (2019*a*) linked acquired tolerance to Cd a decrease in CWI activity. In addition, they reported that transcript levels of CWIs did not match the decrease in activity. This is also the case in our study, where we report increased CWI activities under Cd stress in W22, while cell wall invertase transcript levels are mostly reduced. Zhou et al. (2019*a*) therefore suggest other mechanisms than transcription to control CWI activity, such as proteinaceous inhibitors and protein (de)phosporylation. Other invertase activities also seem to be influenced by Cd exposure, where acidic and alkaline invertase activities were low in stressed pea seedlings (roots, shoot, cotyledon), with the exception of alkaline invertase in cotyledons (Devi *et al.*, 2007). Also, acidic invertase activity (vacuolar) decreased and neutral invertase activity increased with Cd stress in leaves of potato (Shahid *et al.*, 2019).

We also found cell wall invertase activity to be related to meristem function and energy provision therein. The main reason for the CWI mutant to grow worse under Cd stress, was the severely reduced meristem size, in addition to reduced cell division rates. Since sucrose is the main form of carbohydrate delivery to this sink tissue, hydrolysis of sucrose by CWI is required for the uptake of glucose and sucrose (Hartig and Beck, 2006). Changes in these hexose levels could then alter cell cycle progression, since a close correlation between glucose supply and the expression of certain cyclins (type D, A and B) was reported, suggesting glucose signalling to impact the whole cell cycle process (Wang and Ruan, 2013). Perhaps, the lowered glucose and fructose levels under mild stress and lowered fructose levels under severe stress might explain the reduction in meristem size and increased cell cycle duration of the CWI mutant.

Photosynthesis and stomatal conductance

The CWI mutant had a significantly reduced CO_2-assimilation rate under control conditions, indicating that the mutant might not be able provide energy and building blocks for growth at the same rate as W22, resulting in the observed reduced leaf elongation rate during control treatment. Nonetheless, total soluble sugars and sucrose levels remained quite similar between W22 and the CWI mutant, indicating a tight regulation of these carbohydrate levels in the maize leaf growth zone. This leads us to speculate that perhaps the reduced CWI activity at the meristem leads to reduced sucrose consumption at this sink tissue. This in turn might inhibit photosynthetic activity to maintain the tightly controlled sucrose levels under control conditions, related to sugar-mediated source-sink feedback inhibition of CO_2-assimilation (Podazza *et al.*, 2006).

Under Cd stress, total soluble sugar levels increased in both the CWI mutant and W22, while both had a significantly reduced CO_2-assimilation rate. Perhaps, soluble sugars could also accumulate because Cd slowed down growth, reducing sugar consumption at the growth zone. Reduced sugar consumption under Cd stress was also observed in *Lactuca sativa* (iceberg lettuce), where 10 µM Cd exposure resulted in an increase of soluble sugars, accompanied by a strong reduction of net CO_2-assimilation rate (Dias *et al.*, 2013).

CO_2-assimilation rate reduced several fold more in the CWI mutant compared to W22. The reason for this might be the significantly reduced maximal efficiency of excitation energy capture by PSII reaction centres, indicated by the Fv/Fm measurements, in the CWI mutant under Cd stress. We expected W22 to also have a reduced photosynthetic performance, since Fv/Fm is typically reduced in plants exposed to Cd stress, as was reported for cowpea (Santos *et al.*, 2018), iceberg lettuce (Dias *et al.*, 2013), sunflower (Azevedo *et al.*, 2005) and chamomile (Kummerová *et al.*, 2010), but under our conditions we did not observe a significant effect.

Related to photosynthesis, stomatal conductance reduced under severe Cd stress in both W22 and CWI mutant, where in the latter, it was also significantly affected under mild Cd stress. Reduced stomatal conductance under Cd stress seems to be the common response and was also reported in *A. thaliana* (Perfus-Barbeoch *et al.*, 2002), white lupin (Costa and Spitz, 1997) and pea (Sandalio *et al.*, 2001) plants. Reduced stomatal conductance could be induced by Cd itself. Cadmium can enter the guard cells through the Ca^{2+} channels, where it mimics intracellular Ca^{2+}, leading to stomatal closure (Perfus-Barbeoch *et al.*, 2002). In addition, stomatal closure is also frequently reported when plants experience osmotic stress, for instance under drought stress. In response to drought, plants also increase total soluble sugar levels to maintain water uptake and cell turgor (Camisón *et al.*, 2020). The increased total soluble sugar levels observed in response to Cd could therefor indicate that the plant is also experiencing osmotic stress. Disturbances in water relations under heavy metal stress seem to be common, since heavy metals can negatively impact water uptake by decreasing primary and secondary root growth and reducing root hair surface (Rucińska-Sobkowiak, 2016).

Transcriptome study

The transcriptome data globally confirmed the susceptibility of the CWI mutant, where the transcriptome of the mild treatment samples resembled more that of the severe treatment samples, instead of the control treated samples (Figure 3). Also at mild stress conditions, we found a large number of genes (i.e. 6566) to be affected in the CWI mutant, compared to only 362 genes in W22, confirming that the mutant was already responding strongly to mild Cd stress. The K-means clustering and gene-ontologies, related to these clusters, provide an overview of the affected processes (Figure 7 and Table 1). Yet, due to the large number and diversity of the reported ontologies, isolating one or a few processes is rather arbitrary and thus remained inconclusive.

Digging deeper into the transcriptome data, where we specifically looked for carbohydrate related processes, lead us to find an upregulation sucrose export in the

CWI mutant. Due to the severely reduced activity of CWI's in the mutant under Cd stress, we hypothesise that sucrose might not be degraded at sufficient rates, which could lead to the export of sucrose to regulate sucrose concentrations. In addition, since meristematic tissue preferentially takes up free hexoses (Hartig and Beck, 2006), which are less available due to the lowered CWI activity, the observed upregulated starch breakdown into maltose could indicate glucose release from starch (through its degradation into maltose) as an alternative source of glucose (Figure 9). This hypothesis is supported by the previous observation that deprivation of sucrose can trigger starch breakdown (Journet *et al.*, 1986).

We also found several upregulated genes that indicate raffinose synthesis under Cd stress in the maize leaf meristem (Figure 11). Raffinose is a trisaccharide, synthesised by raffinose synthase from galactinol and sucrose (galactinol-sucrose galactosyltransferase activity). Galactinol in turn is synthesized from myo-inositol and UDP-galactinol, catalysed by galactinol synthase (Van den Ende, 2013). Regarding myo-inositol synthesis, we found four myo-inositol phosphate synthases to be upregulated in both W22 and CWI mutant, where fold changes increased in proportion to the Cd stress level. Interestingly, three of these genes are also expressed higher in the CWI mutant under control conditions when compared to W22, indicating that in the mutant leaf meristem, perhaps higher amounts of myo-inositol are present already under control conditions.

In turn, this produced myo-inositol might be used in raffinose synthesis. For CWI vs W22 contrast under control conditions, no less than 7 genes related to galactinol-sucrose galactosyltransferase activity are higher expressed in the CWI mutant. Also, under Cd stress, more raffinose synthesis related genes were affected (both up- and down-regulate) in the CWI mutant. Taken together, this could indicate that reduced cell wall invertase activity could result in channelling more of the available sucrose towards raffinose production under both control and Cd stress conditions in the CWI mutant, when compared to W22.

Raffinose production in plants under salinity, drought and temperature stress is has been reported multiple times (reviewed by Sharma et al., 2014; Van den Ende, 2013). A limited number of reports have also described an increase in raffinose content when exposed to Cd stress. In in vitro cultured *Lupinus albus*, raffinose levels increased several fold in both shoots and roots in proportion to Cd treatment (Costa and Spitz, 1997). In poplar leaves, Cd stress significantly increased inositol, galactinol and sucrose, precursors for raffinose production. In turn, raffinose levels also increased significantly (Kieffer *et al.*, 2009). In Arabidopsis seedlings, exposed to mild (5 µM Cd) and severe (50 µM Cd) stress, Sun et al. (2010) have shown significantly increased raffinose contents, respectively a 2 and 4-fold increase under both stress conditions. The increase in raffinose content was suggested to protect the plant from osmotic stress (Kieffer *et al.*, 2009), but also hydroxyl radical scavenging proportions were assigned to raffinose to protect plant cells from oxidative damage (Sun *et al.*, 2010). Both suggestions are viable roles for raffinose production in the meristem, since we showed in chapter 4 that the meristem endures oxidative stress, where we show here, in chapter 5, that osmotic stress might be present as indicated by the reduced stomatal conductance and increased sugar levels.

Conclusion

This study reports that carbohydrate levels are increased by Cd throughout the maize leaf growth zone. Reduced cell wall invertase activity in the CWI mutant related to altered carbohydrate profiles. Here, in contrast to the genetic background W22, the mutant failed to increase fructose levels in response to Cd stress. Reduced CWI activity in the mutant was linked to increased sensitivity of leaf elongation rates to Cd stress. This growth response was related to a reduced meristematic cell number. Unfortunately, the causal mutation could not be verified. Therefore, to establish causality of the observed phenotype, additional analyses are required where the mutation(s) in the mutant are identified and/or additional mutants in carbohydrate metabolism are analyzed.

Author contributions

All authors participated in the conception of the topic. J.B. wrote the manuscript. G.B. edited the manuscript. J.B. made the figures and tables. J.B performed the kinematic analysis, photosynthesis related measurements and transcriptome data analysis. J.B., H.A.G. and W.V.d.E performed the sugar related measurements.

Acknowledgements

We want to thank Leen Vandenberghe and Geoffrey Hibbs for their assistance with the carbohydrate measurements and kinematic analysis.

Funding

This work was supported by the Research Foundation Flanders (FWO) by project funding for J.B. [G0B6716N].

Chapter 6

Conclusions and future perspectives

Contribution to the field

Prior to starting my PhD study, much was already known about the impact of cadmium (Cd) stress on plants and the plant's response to this form of abiotic stress (Chapter 1), Nevertheless, the impact of this heavy metal specifically on the growth processes in the leaf, i.e. cell division and expansion, received only little attention. The aim of my project was therefor to assess the impact of cadmium in the maize leaf growth zone and how the plant responds to Cd. We set out several research questions, which were investigated further in research chapters 2 to 5. These chapters present our key findings, which make a significant contribution to the field.

It is well accepted that Cd in the soil is taken up by the roots and transported to the shoot through the xylem sap stream (Fujimaki *et al.*, 2010). In the shoot, it is transferred to the phloem sap stream and preferentially transported to the growing leaves (Kobayashi *et al.*, 2013). However, up until now, the distribution of cadmium in the monocotyledonous growth zone was not yet studied. When studying the effect of cadmium on leaf growth, this data is particularly interesting, since it could indicate whether cadmium could have a local impact in the growth zone, or that perhaps only low to neglectable concentrations are present there, meaning that the impact of Cd on growth driving processes (i.e. cell division and elongation) has to come from outside the growth zone (e.g. long distance signals from roots or mature leaves).

I showed that Cd specifically accumulates in the maize leaf meristem, after which its concentration declines throughout the elongation zone and remains relatively low in the mature blade tissues of the growing leaf (Figure 1). In addition, I also found that Cd is mainly deposited in the growth zone (Figure 1). This finding could indicate that, during the water uptake required for cell growth in cell division and elongation, Cd enters these cells as well. However, since it was shown that calcium is also preferentially transported to growing leaves, but distributed throughout this leaf (Kobayashi *et al.*, 2013), perhaps specific transporters aid in the uptake of Cd of these dividing and elongating cells. In addition, the absence of a physical barrier (i.e.

secondary cell wall) in the meristem and elongation zone could allow easier passage into and through this developing tissue, facilitating its deposition therein. Finally, I found that the deposition of Cd in the growth zone, but also its competition for uptake and transport with other minerals (Qin *et al.*, 2020), affected mineral content in the growth zone, where most apparent and consistent were the reduced manganese levels throughout the growth zone under Cd stress (Figure 1).

The deposited Cd could induce oxidative stress by replacement of redox-active metals from their binding sites, in turn leading to increased reactive oxygen species levels and oxidative stress (Cuypers *et al.*, 2012; Huybrechts *et al.*, 2019). My PhD study is the first to shown the effect of this Cd induced oxidative damage as increased malondialdehyde levels throughout the growth zone. Interestingly, MDA levels increased with progressive tissue maturation, indicating that higher Cd concentration levels do not have to result in a proportional amount of oxidative damage. However, this MDA pattern throughout the maize growth zone under abiotic stress does not seem to be uncommon, since a similar gradient was also found in response to drought (Avramova *et al.*, 2015*b*, 2017). In the meristem transcriptome, I also found clues related to these increased MDA levels, where the GO *response to hydrogen peroxide* was enriched for genes which were upregulated under Cd stress in the meristematic tissue (Chapter 4, table 1, cluster 2). A stronger control of hydrogen peroxide levels could be required due to its suggested signalling role in the plant metal phytotoxicity response (Cuypers *et al.*, 2016). I have also shown an increased antioxidative potential in the meristem under control conditions through FRAP measurements, perhaps to intrinsically control ROS levels in this region.

Figure 1 (next page). Schematic overview of the most important conclusions made in this PhD study. An arrow up (↑) indicates higher values under Cd stress. An arrow down (↓) indicates lower values under Cd stress. Cd conc.: Cd concentration, Cd depo.: Cd deposition, SA: salicylic acid, ABA: abscisic acid, ACC: 1-aminocyclopropane-1-carboxylic acid, GA1: gibberellin 1, N_{mer}: number of cells in the meristem, l_{mer}: length of the meristem, cytok. O-gluc.: cytokinin O-glucosilation, t-ZR: trans-zeatin riboside, MDA: malondialdehyde, FRAP: ferric reducing antioxidant power, JA-ACC: jasmonyl-ACC.

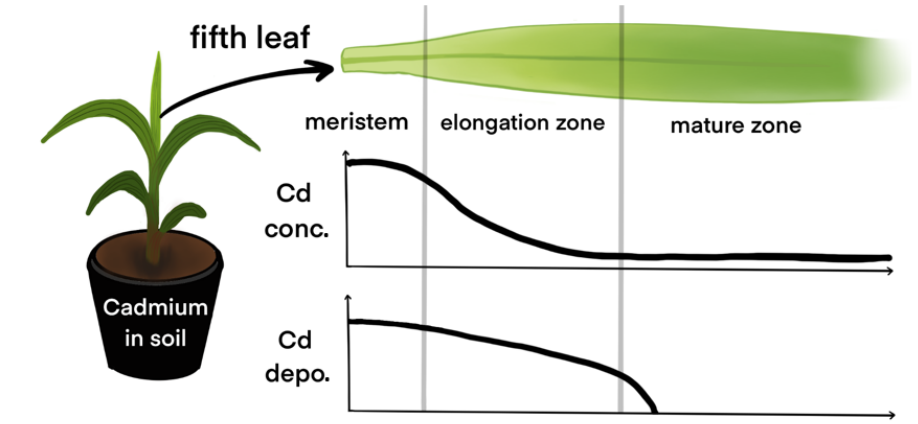

Meristem	Elongation zone	Mature zone
SA↑ ABA↑ ACC↑ ↓ ↓ ↓ negative impact on cell cycle + growth promoting hormones ↓ GA1↓ cytok. O-gluc. ↑ ↓ ↓ N_{mer}↓ t-ZR↓ ↓ ↓ I_{mer}↓ - cell cycle gene expr. ↓ - cells halted at G1/S transition - S-phase cells ↓ ↓ cell production ↓ ↓ growth inhibition	SA↑ ABA↑ ACC↑ ↓ ↓ polyploidy ↓ cell elongation rate ↓ ↓ + cell elongation time ↑ ↓ mature cell length unaffected	(osmotic stress) ↓ SA↑ ABA↑ ACC↑ ↓ ↓ ↓ Ethylene↑ ↓ stomatal conductance ↓ ↓ photosynthesis ↓ ↑ negative feedback on photosynthesis?

Additionally: - accumulation of soluble sugars throughout the growth zone
- → *active* defence to ROS?
- → *active* adaptation to osmotic stress?
- → *active* signalling function?
- → *consequence* of growth inhibition?

- MDA↑, FRAP↑
- Potential role for ACC conjugates as jasmonic acid sink (JA-ACC↑)
- Mineral content affected (reduction in Mn most consistent)

Our results show that growth response of the maize leaves to Cd could be caused by the locally deposited Cd in the growth zone, but we cannot exclude that also long-distance signals from other organs (roots, mature leaves) interact with this strictly local response. Regardless, the combination of these effects causes a complex of regulatory changes to occur in the growing tissues. I found that, in response to Cd, maize seedlings increased stress hormones salicylic acid (SA), abscisic acid (ABA) and ethylene precursor 1-aminocyclopropane-1-carboxylic acid (ACC) throughout the growth zone. Salicylic acid showed a dose- dependent response, ABA was only increased under Cd severe stress and ACC was increased to about the same level under both Cd stress conditions. Stress hormone jasmonic acid (JA) remained undetected in the growth zone. However, ACC conjugates acted as a potential sink for JA, since I observed increased JA-ACC conjugate levels relative to the imposed Cd stress.

In the meristematic region, the rise of these plant stress hormones could negatively impact the cell cycle (Figure 1). For instance, the shoot length of rice seedlings was drastically reduced by ABA treatment (Meguro and Sato, 2015), where an ABA inhibited cell cycle at the G1/S boundary was put forward as a possible explanation. In young proliferating leaves of *Arabidopsis thaliana* under osmotic stress, cell cycle arrest coincided with an increase in ACC levels and the activation of ethylene signalling (Skirycz *et al.*, 2011). Ethylene, the levels of which are believed to correlate with ACC levels, is also a well-accepted inhibitor of cell division (Dubois *et al.*, 2018). Finally, exogenous treatment of Arabidopsis roots with 50 µM SA or higher inhibited cell cycle progression (Pasternak *et al.*, 2019), however, in young rice seedlings, exogenous application of SA resulted in moderate promotion of shoot growth by antagonising ABA (Meguro and Sato, 2015).

Besides increased stress hormone levels, I also found a reduction in growth promoting hormones, which can be related to the reduced meristematic function under Cd stress (Figure 1). In the maize leaf growth zone, a clear gibberellin 1 (GA1) peak regulates the spatial control of cell division (Nelissen *et al.*, 2012). In response to the severe Cd treatment, I found that the maize seedling significantly reduced the GA1 peak at the

meristem-elongation zone transition area, which consequently could explain the reduction in meristem cell number and meristem size. Through the transcriptome data, I showed that GA1 levels were probably reduced though a reduction in GA20-oxidase transcript levels (enzyme required for GA1 synthesis) and an increase in GA2-oxidase transcript levels (enzyme required for GA1 breakdown). In addition, I found an increase in cytokinin O-glucosilation (i.e. essentially inactivating cytokinins), which could explain the reduced trans-zeatin riboside levels in the meristem under Cd stress. Cytokinins are known for their stimulating effect on the cell cycle (Schaller *et al.*, 2014). The reduction of active cytokinins in the plant's response to Cd could be linked to the observed inhibited G1/S transition leading to a reduced number of cells in the S-phase, and the reduction in cell cycle gene expression. When all of these results are taken together, I found a significantly reduced cell production, initiated by phytohormone changes, to lie at the basis of leaf growth inhibition in response to Cd.

In the elongation zone, I found the impact of Cd on cell elongation to be less important in explaining leaf growth inhibition, i.e. maize seedlings still tightly control the cell elongation process under Cd stress to maintain normal cell length. For the two tested non-mutant lines, B73 and W22, I found mature cell length (i.e. the end product of cell elongation) to be unaffected by Cd treatment. The B73 inbred line was however more sensitive to Cd stress. I found a significantly reduced relative cell expansion rate under severe Cd stress. Yet, the time cells spend in the elongation zone increased significantly, ensuring normal mature cell length was still obtained (Figure 1). In a meta-analysis, including a multitude of abiotic stress studies, Gázquez and Beemster (2017) showed that mature cell length can reduce by stress conditions, yet, these changes usually do not explain differences in growth.

The cause for the observed cell elongation rate could be the reduced polyploidy levels (Melaragno *et al.*, 1993; Sugimoto-Shirasu and Roberts, 2003). Yet, it could also be that the increased stress hormones levels negatively regulated the cell elongation process (Figure 1). As recently reviewed, the impact of ethylene on cell growth in leaves is almost exclusively negative, which could be linked with the observed increased ACC

levels in my study (Dubois *et al.*, 2018). Concerning ABA, it was shown in roots of Arabidopsis that ABA inhibits actin reorganisation required to initiate cell elongation, therefor inhibiting root growth (Takatsuka and Umeda, 2019). Abscisic acid also reduced hypocotyl elongation in Arabidopsis seedlings (Lorrai *et al.*, 2018), however, in ABA-deficient tomato seedlings, hypocotyl growth was reduced, where ABA supplementation could improve hypocotyl elongation, making it harder to link the observed cell expansion rate reduction to the increased ABA levels (Humplík *et al.*, 2015). The same contradiction is true for SA, where exogenous SA inhibited cell elongation, significantly reducing the length of the primary root (Pasternak *et al.*, 2019). Yet, in young rice seedlings, SA supplementation to the growth medium increased shoot length and even showed an antagonistic effect to ABA induced growth inhibition (Meguro and Sato, 2015).

After cells have elongated and reached their mature cell length, they become part of the blade where photosynthesis takes place. Regarding photosynthesis, I have found a significantly reduced photosynthetic rate in W22 under severe Cd stress (Figure 1). This reduction could be explained by a significantly reduced stomatal conductance. Interestingly, in the B73 phytohormone study, I have found ABA levels to be only increased under severe Cd stress, which matches well with the observed stomatal closure under the same stress condition in W22, since ABA induces stomatal closure (Mittelheuser and Van Steveninck, 1969). In addition, ethylene and SA have also shown to reduced stomatal conductance, limiting photosynthetic rate as a result (Pallas and Kays, 1982; Janda *et al.*, 2014).

Reduced photosynthesis could reduce sugar transport to the growth zone. In contrast to that idea, I found increased total soluble sugars levels throughout the growth zone. Therefore, although photosynthetic rate was reduced, I can now hypothesize that an even stronger reduction in growth probably limits carbohydrate consumption, causing them to accumulate (Figure 1). Alternatively, in response to Cd, the plant might also actively increase its soluble sugar levels, which in turn can limit photosynthetic rate due to negative feedback on the photosynthetic process (Paul and Foyer, 2001). The

observed accumulation of soluble sugars could be an active response to ROS (due to the potential antioxidative properties of sugars; Keunen *et al.*, 2013) or to osmotic stress (since an increase in soluble sugar levels lowers osmotic potential; Camisón *et al.*, 2020). Alternatively, they could act as a signal (Bolouri-Moghaddam *et al.*, 2010; Smeekens *et al.*, 2010; Ruan, 2012).

In conclusion, through the use of the maize leaf growth zone as a model to study Cd stress on leaf growth (Avramova *et al.*, 2015*c*), I found that Cd mainly inhibited maize leaf growth through an impaired cell cycle and a reduction in meristem cell number, which could be related to phytohormone changes. In addition, a role for carbohydrate metabolism in Cd stress tolerance was revealed.

Future perspectives

To quote Louis Pasteur: "*Science proceeds by successive answers to questions more and more subtle, coming nearer and nearer to the very essence of phenomena*." This is exactly what I experienced during my PhD study. We started by revealing how Cd affected growth at the cellular level, which prompted us to generate an overview of the Cd affected processes at the molecular level. This overview directed us to study several processes at the biochemical level (i.e. hormones, minerals, ROS and carbohydrates). Yet, there is still one biochemical topic in particular for which I did not have time to address and which I believe is quite promising in revealing why Cd slows down leaf growth.

As described, the transcriptome study (chapter 4) revealed GOs related to phenylalanine and cinnamic acid in the Cd upregulated gene cluster. I believe that these GOs potentially relate to lignin production, already in the maize leaf meristem. Typically, lignin synthesis would be expected to occur in mature cells during secondary cell wall formation. Functionally lignin could provide a protective physical barrier for the deposited Cd, increase the rigidity of the cell walls, slowing down cell growth of proliferating cells required for cells to divide in two new daughter cells. In addition, we also found the relative cell elongation rates in the elongation zone to be reduced, a finding that could also be related to reduced cell wall extensibility due to lignin deposition. I find support for this hypothesis in the meristem transcriptome data when searching for *brown midrib* (*bm*) genes, mutants of which are often linked to reduced lignin biosynthesis (reviewed by Christensen and Rasmussen (2019)). Out the five *bm* genes listed in the maize genetics and genomics database, three were significantly (FDR < 0.05) affected by the cadmium treatment in the meristem (*bm5* - Zm00001d015459, *bm1* - Zm00001d015618, *bm3* - Zm00001d049541), all of which were significantly upregulated in the severe versus control contrast (resp. LFCs: 0.82 ± 0.15, 0.84 ± 0.15, 0.53 ± 0.12). Increased lignin synthesis under cadmium stress is a well-accepted phenomenon, reported in multiple plant species and already linked to reduced growth (Schutzendubel *et al.*, 2001; Yang *et al.*, 2007; Elobeid *et al.*, 2012;

Wang *et al.*, 2018; Chiao *et al.*, 2019). Therefore, analysis of lignin contents throughout the maize leaf growth zone and perhaps the use of lignin mutants could increase our understanding in Cd inhibited leaf growth.

Chapter 4 also contains data on the content of several minerals across the maize leaf growth zone. Here, it is clear that some minerals show a similar profile as Cd, i.e. Mg, Zn, Cu and Ca, while others are more stable, i.e. Fe, K, Mn and Na. This raises the question how the deposition pattern of these minerals compares to, or differs from, Cd. It can be expected that minerals with similar concentration profiles show similar deposition profiles. However, small variations in concentrations can have strong effects on deposition rates. Although beyond the scope of the current thesis, the data offer the opportunity for future kinematic analyses to calculate deposition rates along the growth zone for all these minerals based on the distribution of their concentrations in combination with the tissue velocity profiles. These results could make a valuable contribution to the domain of plant mineral homeostasis under control and Cd stress conditions.

I also believe that there are opportunities to investigate the importance of carbohydrate metabolism in the plant's response to Cd stress. First of all, as indicated in chapter 5, we believe that CRISPR-Cas directed mutation of specific cell wall invertases could be important to confirm the observed sensitivity related to reduced CWI activity. In addition, cooperation with Prof. Hamada AbdElgawad, who is also part of the IMPRES research group and who maintains a set of carbohydrate maize mutants, could provide a good point of entry for the screening of more maize mutants. The expertise of Prof. AbdElgawad and Prof. Gerrit T.S. Beemster in maize sugar feeding experiments could also be utilized to perform sugar feeding experiments during Cd exposure which might reveal potential (signalling) functions of specific carbohydrates during Cd stress.

During the PhD study, also a set of 12 maize lines (5 commercial hybrids; KWS Benelux B.V., and 7 inbred lines) was screened for their sensitivity to Cd (data not presented).

Here, I found that the most sensitive line had its leaf elongation rate reduced by 58% under severe Cd stress (inbred B37), while the leaf elongation rate of commercial hybrid “Atletico” was only reduced by 20% under the same stress level, making it the most tolerant line of the screened set. This dataset could be used to select the more tolerant and sensitive lines for a comparative study, where molecular and biochemical traits, related to their sensitivity, might be revealed.

In parallel with my PhD study, Michiel Huybrechts performed a study on Cd exposed rice seedlings at Hasselt University. His kinematics data revealed a significantly reduced mature cell length under Cd stress (Huybrechts *et al.*, 2020), where I showed in two maize inbred lines that mature cell length remained unaffected under Cd stress. This difference intrigues me and makes me wonder whether these different results were there because of different experimental conditions (e.g. hydroponics, exposure timing) or different species used.

In addition, the experimental setup of Michiel (hydroponics where Cd can be administered at a time point of interest) allows one to tackle the response over time by sampling multiple time points after Cd administration. This could be used to study the directionality in the interactions between different parameters determined in this thesis (Figure 1). For example, it would be possible to see whether reduced photosynthesis occurs before, after or during the accumulation of carbohydrates in the sink tissue, which could reveal whether photosynthesis is reduced due to negative feedback from the sink or inherently inhibited by, or in response to, Cd.

Regarding the *leafkin* R package, I believe there is the possibility to expand the library with functions for the kinematic analysis of dicot leaves. During my PhD study, I did not obtain expertise with this type of kinematic analysis. However, when consulting the methodology (Nelissen *et al.*, 2013), it becomes clear that also this analysis requires repeatedly executing a set of calculations needs for individual plants. The integration of these calculations in the *leafkin* library, would make this library complete with regards to kinematic analysis of leaves.

Finally, with Cd being omnipresent in the environment, it is important to understand the response of plants to this heavy metal. Through my PhD study, it is my wish to have made a small, but significant, contribution to understanding leaf growth inhibition by Cd. Increasing our understanding at this fundamental level might be of use in applications to obtain more resistant plants to adverse environments, like Cd polluted soil. As presented above, my research also lead to new questions raised, where it is my hope that my findings and raised questions inspire other researchers in the quest to fully understand Cd inhibited growth.

Supplementary data

Supplementary data chapter 1

No supplementary data.

Supplementary data chapter 2

Supplementary File 2.1: *leafkin* user manual

An R package for automated kinematic data analysis of monocot leaves.

Preface

Growth is one of the most studied processes in plants. At the cellular level, plant growth is driven by cell division and cell expansion. Kinematic analysis, a method to quantify the contribution of these two cellular processes to organ level growth, has been developed and perfected over the past decades. To streamline the data analysis of the raw data, collected during the lab work involved, we have created ***leafkin***, an R-package to perform all the calculations in the kinematic analysis of monocot leaves using four functions. These functions support leaf elongation rate calculations, creating plots of fitted cell lengths, extraction of fitted cell lengths and execution of all kinematic equations.

The goal of this manual is to provide a step-by-step manual, with attention for technical aspects such as file paths and troubleshooting errors. The manual works closely with a tutorial script and sample data, which can be downloaded following the instructions in this manual.

Kinematic analysis summarised

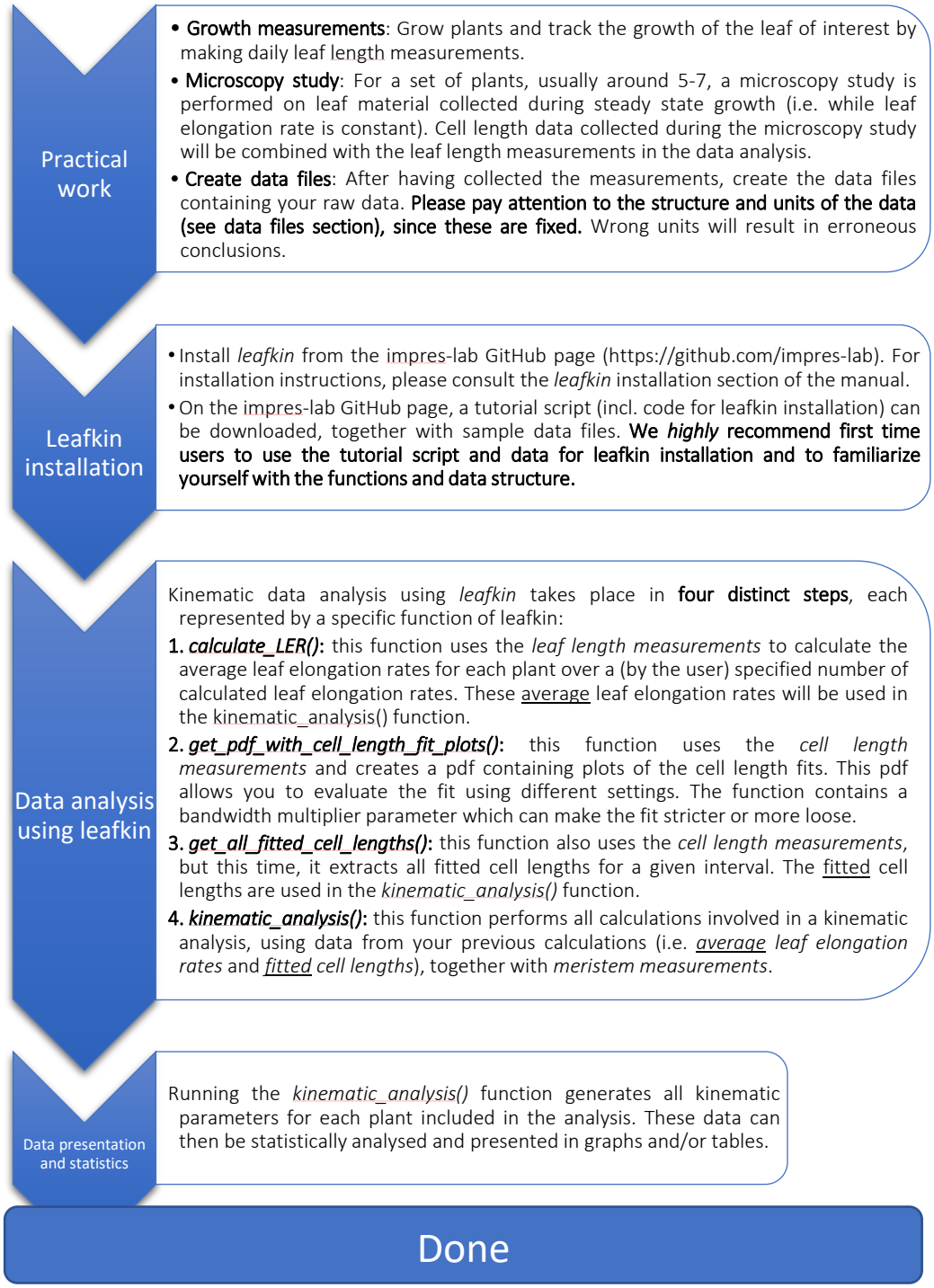

A brief introduction to the practical work involved in a kinematic analysis of monocot leaves

For those unfamiliar with the practical work involved in a kinematic analysis, we provide a brief introduction on the practical work involved. To fully understand each step and execute it with attention for the details, a more extensive protocol can be consulted (Sprangers *et al.*, 2016). Besides detailed written instructions, Sprangers *et al.* (2016) provides a video tutorial illustrating each step of the kinematic analysis.

Practical work involved in a kinematic analysis of monocot leaves:

1. Grow your monocotyledonous species of interest and select a leaf to study. In maize seedlings, the IMPRES lab (Antwerp University, Belgium) works on the fifth leaf to limit the duration of the experiment (ca 3 weeks), while the growth is no longer supported by seed reserves and treatments have sufficient time to establish and impact growth.
2. As soon as the leaf of interest emerges, measure it daily with a ruler (in mm). In our experience with maize, the fifth leaf is growing at a constant rate for at least three days from the time it emerges from the whorl of older leaves (steady state growth).
3. Three days after emergence, during the steady state growth, dissect the plant and isolate the entire leaf of interest form the other leaves. Pay special attention for the younger leaves already growing inside the leaf of interest. These need to be removed as well.
4. For the leaf of interest, retain the basal 11 cm, i.e. the part which was attached to the stem. One side of the blade (lateral of the mid vein) is used for cell length measurements, while the other side is used for meristem size measurements.
    a. For the meristem measurement, a 3 cm segment from the basal part, i.e. starting from where the leaf wat attached to the stem, is retained and stored in a 3:1 (v:v) absolute ethanol:acetic acid solution for at least 24h at 4 °C. Through DAPI staining and fluorescence microscopy, mitotic figures are visualised in the epidermis. The most distal mitotic figure (i.e. the one furthest away from the base of the leaf) is used as a reference for the meristem border. The distance from the leaf base to this mitotic figure is the meristem size (stored in µm for each plant).

b. For the cell length measurements, the other half of the leaf is used. It is first stored in denatured absolute ethanol at 4 °C to remove pigments. The absolute ethanol can be replaced several times in order to obtain a cleared leaf. When the leaf is as clear as possible, the absolute ethanol is replaced by pure lactic acid (wear gloves), which will make the leaf tissue flexible again (ethanol treatment makes it brittle). The leaf can be stored in the lactic acid at 4 °C for several months if needed. The first 10 cm of the 11 cm leaf is now dissected into 10 one-centimetre segments, in which cell length measurements are made (in µm). Dissecting the tissue in 10 one-centimetre segments will facilitate navigating and positioning your lens across the leaf, which it is less easy when using longer segments. Using a microscope equipped with differential interference contrast optics allows for visualisation of the cell walls. The cell walls can then be used to measure the cell size across the first (basal) 10 cm of the leaf.

Leaf length, meristem size and cell length measurements provide the input for the data analysis with *leafkin*.

Flowchart

Below, the relation between de data and the functions is shown. On the top, the raw data is presented in dark blue boxes. They are fed to functions, presented in the grey boxes. These functions produce the intermediate data in the light blue boxes, which can then be fed in the *kinematic_analysis()* function at the bottom to perform the final calculations and obtain the results for all the kinematic parameters for each plant. The dotted line and the green box represents a conclusion which can be made on the cell length fit plots in order to continue safely with the *get_all_fitted_cell_lengths()* function.

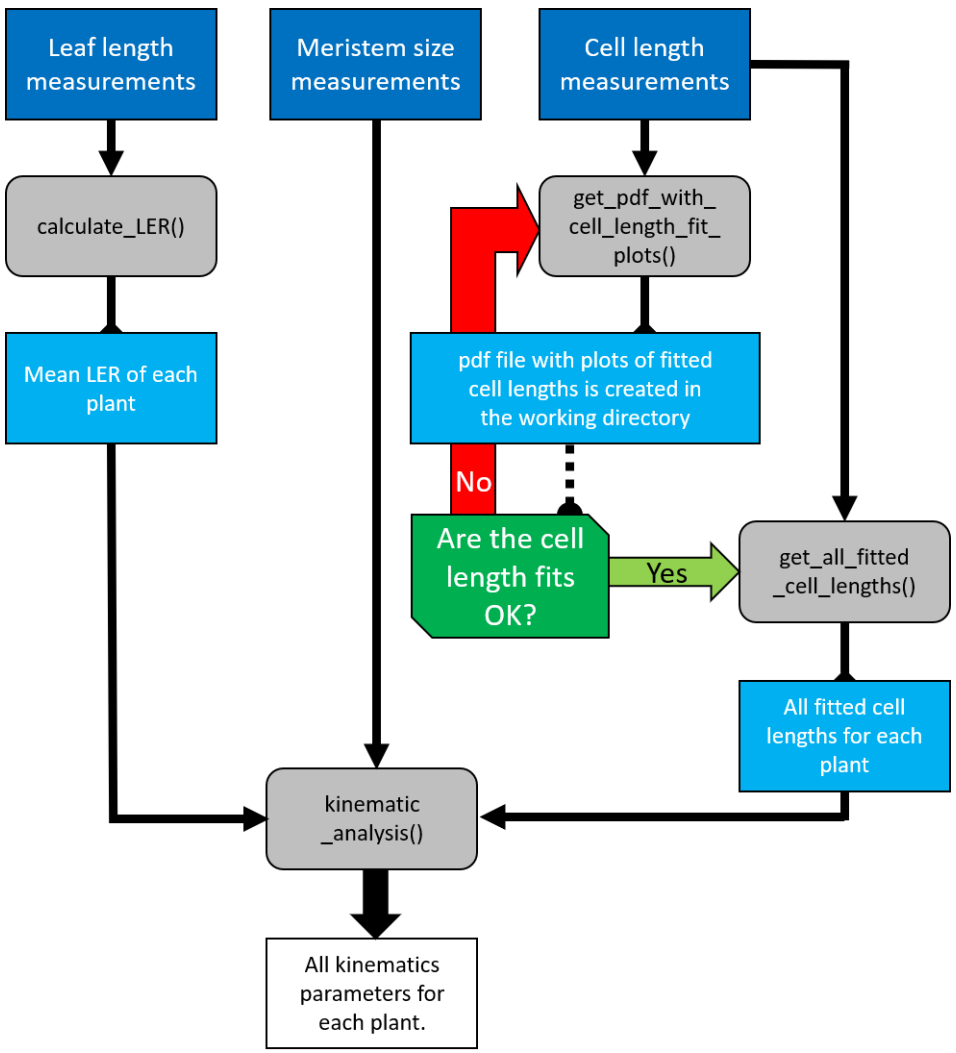

Requirements

The next sections contain information on the requirements in order to use the *leafkin* library:

- Required data files
- Required software
- *Leafkin* installation

Prior to *leafkin* installation, downloading the sample data and tutorial script is described. The tutorial script contains code to install *leafkin*.

Required data files

As introduced in the kinematic analysis overview, three datasets with raw data should be available after performing the practical work:

- Leaf length measurements
- Cell length measurements
- Meristem size measurements

We advise to prepare the raw data in a spread sheet program (e.g. Microsoft Excel), using the provided files as a template. The raw data should be saved as tab-delimited text files. We advise to use this format because importing Excel files directly into R transforms date-times into numbers and renders them unusable by the *leafkin* functions.

The data files should be structured in the following way:

- The leaf length data file (sample data: growth_measurements_millimetre.txt) requires a column with unique plant ID's, followed by multiple columns containing leaf length measurements, expressed in millimetres (Table 1A). The first row contains the headers, which should be *plant_id* for the first column, while the following column headers are in the date-time format *yyyy/mm/dd hh:mm* (or *yyyy/mm/dd hh:mm:ss*), indicating when measurements were made.
- The cell length measurements (sample data: cell_length_measurements_micrometre.txt) are organised in three columns (Table 1B). The first column (header = *plant_id*), holds the plant ID for each measurement. The second column (header = *position*) contains the position of the cell length measurements relative to the leaf base (in centimetres) and is followed by the cell lengths themselves (in micrometres) in the third column (header = *cell_length*). Cell length measurements of all plants are combined in these three columns.
- The third file (sample data: meristem_size_micrometre.txt) contains the meristem size measurements (Table 1C). The first column (header = *plant_id*), contains the unique plant ID's, whereas the second column (header = *mer_length_um*), contains meristem sizes (in micrometres).

Important notes:

- Units and column names should be strictly respected. Wrong units = Wrong conclusions
- Plant ID's should be identical across all three files since these are used to combine the data originating from the different measurements.
- When entering data, do not use NA or any other remark to replace missing data. Keep cells with missing data completely empty.

Table 1. Example data and column description for the datasets required for kinematic analysis using *leafkin.* A: Example of leaf length measurements data and column descriptions. B: Example of cell length measurements data and column descriptions. C: Example of meristem length measurements data and column descriptions. The types char, int and double refer to respectively characters (i.e. everything which includes letters, or numbers specified to be handled as letters), integers (i.e. numbers without decimals) and double (i.e. numbers which can contain decimals).

A. Leaf length measurements data and column descriptions

Example data

plant_id	2016/12/13 10:00	2016/12/14 10:00	2016/12/15 10:00	2016/12/16 10:16	2016/12/17 10:00
C.1	142	216	293		
C.2		142	212	296	
C.3		196	277	360	436
C.4		194	268	352	
…					

Column description

COL	HEADER	TYPE	BRIEF DESCRIPTION
1	plant_ID	char or int	Contains the plant ID for which leaf lengths were measured.
2-LAST	data time format yyyy/mm/dd hh:mm(:ss)	int or double	Contains leaf length measurements in millimetre on a certain day-time. Time can be in hh:mm or hh:mm:ss.

B. Cell length measurements data and column descriptions.

Example data

plant_id	position	cell_length
C.1	0.01	27.18
C.1	0.01	23.71
C.1	0.01	23.68
C.1	0.01	22.23
…	…	…

Column description

COL	HEADER	TYPE	BRIEF DESCRIPTION
1	plant_ID	char or int	Contains the plant ID for which cell lengths were measured.
2	position	int or double	Contains the position at which cell lengths were measured in centimetre.
3	cell_length	int or double	Contains cell length measurement in micrometre.

C. Meristem length measurements data and column descriptions.

Example data

plant_id	mer_length_um
C.1	12423
C.2	14792
C.4	12350
C.7	14568
…	…

Column description

COL	HEADER	TYPE	BRIEF DESCRIPTION
1	plant_ID	char or int	Contains the plant ID for which meristem lengths were measured.
2	mer_length_um	int or double	Contains the length of the meristem in micrometre.

R and RStudio installation

Leafkin requires the following to be installed:

- R, version 4.0.0 or higher.
    - The most recent version of R can be installed from the CRAN website, https://cran.r-project.org/.
    - Users already using an older version of R need to update to version 4.0.0 or higher.

We also strongly advise to install:

- RStudio
    - RStudio provides a graphical user interface which makes the use of R more convenient. The tutorial also assumes RStudio to be installed. Do note that its installation does not install R as well. For it to work, R must also be installed. With R and RStudio both installed, make sure to work within RStudio. You do not need to open R, since RStudio will take care of R for you.
    - A free open source edition of RStudio is available on https://rstudio.com/ (RStudio Team, 2015).
- Rtools40 (for Windows users)
    - Local compilation of *leafkin* on Windows systems will result in a warning when Rtools40 is not installed.
    - Rtools40 can be downloaded here: https://cran.r-project.org/bin/windows/Rtools/

Download sample data and tutorial script

FROM HERE AND ONWARD, THE USER MANUAL WILL FOLLOW A TURORIAL SCRIPT AND USE SAMPLE DATA AVAILABLE FROM THE IMPRES-lab GitHub page: https://github.com/impres-lab

The sample data files and tutorial script can be downloaded all together from the leafkin-sample-data-and-tutorial-script repository as instructed here below. The data provided in as sample data originates from a recent publication in which a kinematic analysis was performed (Bertels *et al.*, 2020).

Note that the content present on the print screens below might not match the current version.

On the impres-lab GitHub, open de leafkin-sample-data-and-tutorial-script repository.

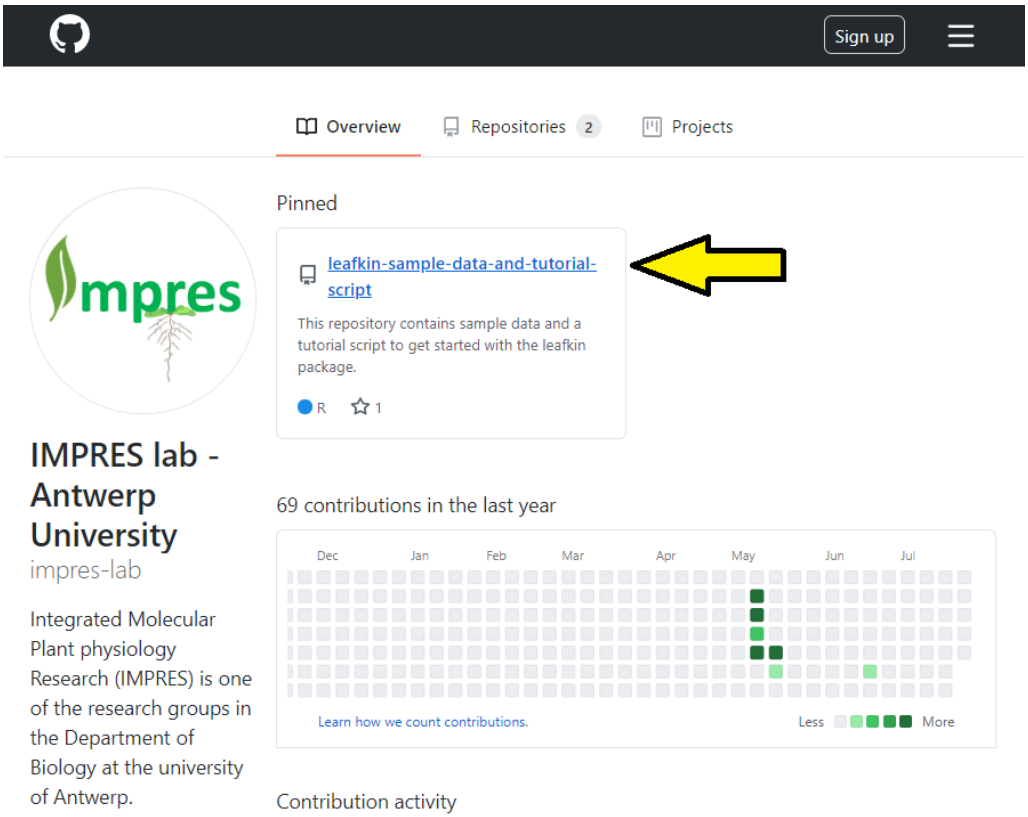
Sign up
Overview
Repositories 2
Projects
Pinned
leafkin-sample-data-and-tutorial-script
This repository contains sample data and a tutorial script to get started with the leafkin package.
R
1
IMPRES lab - Antwerp University
impres-lab
Integrated Molecular Plant physiology Research (IMPRES) is one of the research groups in the Department of Biology at the university of Antwerp.
69 contributions in the last year
Dec
Jan
Feb
Mar
Apr
May
Jun
Jul
Learn how we count contributions.
Less
More
Contribution activity

Within the leafkin-sample-data-and-tutorial-script repository, download its entire contents as a zipped folder. You can do this by clicking on the drop-down menu “Code” and select “Download ZIP”:

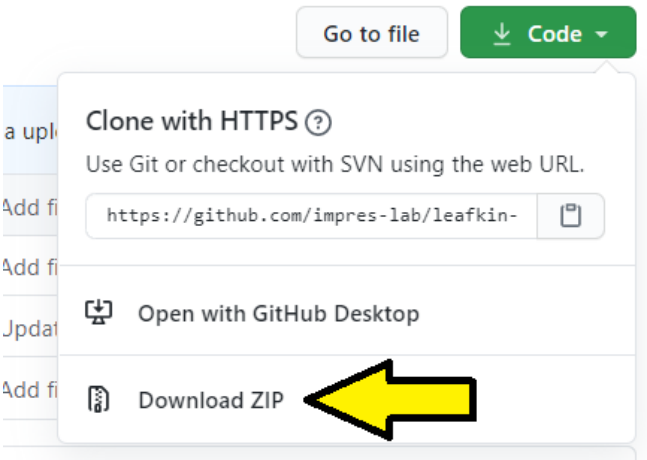

When downloaded, extract the zipped folder. **It is important that the folder is extracted**. Double clicking a zipped folder might allow you to view its contents, but will not allow proper functioning of the script which it contains.

Within the downloaded folder, the following files are present:

- An RStudio project file (.Rproj extension)
    - This file should be opened in RStudio (which should launch by default when trying to open this file).
- An R-script (.R extension)
    - From within the RStudio (with the project file opened therein), this R-script can be opened.
- A README file (.md extension)
    - This file contains information. Its primary function is to provide information on the GitHub repository page.
- A data files folder
    - This folder contains the sample data. Both the Excel files and the txt files are provided. Note that the txt files (tab delimited) are used by the R script. The excel files are just there to serve as an example.
        - cell_length_measurements_micrometre.txt
        - cell_length_measurements_micrometre.xlsx
        - growth_measurements_millimetre.txt
        - growth_measurements_millimetre.xlsx
        - meristem_size_micrometre.txt
        - meristem_size_micrometre.xlsx

When the files are extracted, open the R-project-file (.Rproj extension). This will automatically open RStudio for you. Within the Files tab (on the bottom right), you can now see the contents of the working directory. If you click on the R SCRIPT file, the R-script will be opened in RStudio:

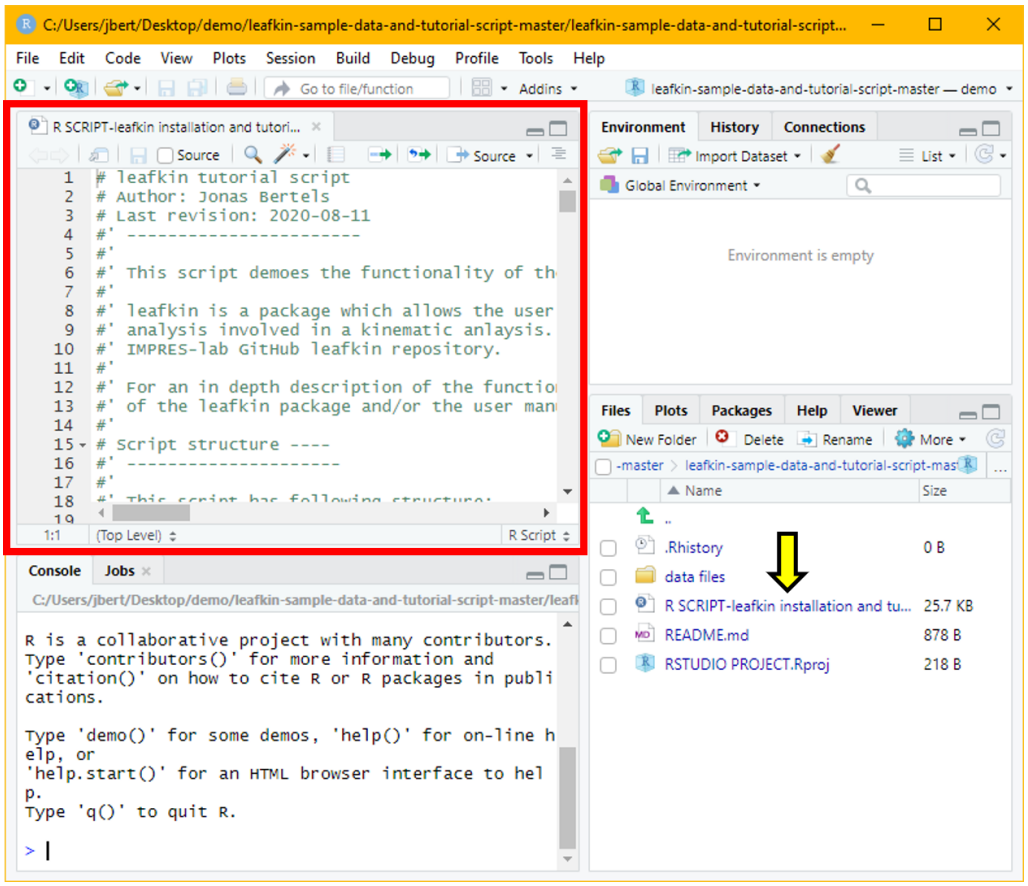

With the tutorial R script opened in the RStudio Project, the user is ready to install *leafkin* and to perform the kinematic data analysis. The tutorial script contains a quick start, containing all the steps of a kinematic data analysis with minimal explanation. This quick start is followed by a more elaborate code section, where each step of the kinematic analysis is addressed in more detail. At the end of the script, we highlight some extra functionalities.

Working with an R-project has a major advantage. The folder where the R-project file is positioned in, is automatically set up as the working directory. This means that R will look in this folder for files to use or that R will create files here when you order it to.

Explaining how to work within RStudio is beyond the scope of this manual, but, for those new to RStudio, the How To R YouTube channel has a nice video introduction on how to work within RStudio:

https://www.youtube.com/watch?v=lVKMsaWju8w

When you want to learn more about R, RStudio Education is a nice place to start:

https://education.rstudio.com/learn/beginner/

Install *leafkin*

Prior to installing *leafkin*, we install the tidyverse and devtools packages by running the following line of code:

```
install.packages(c("tidyverse", "devtools"))
```

The devtools package allows installing *leafkin* from the impres-lab GitHub page. The tidyverse is a collection of packages which are used by the tutorial script as well.

Next, we can install *leafkin*. During the intallation of *leafkin* using the following function, you might be prompted to install and/or update the packages used by the *leafkin* package. On you first try, you should choose to install/update all packages suggested by the function (first option, **1: All**, when prompted: "Enter one or more numbers, or an empty line to skip updates:").

- If, during installation, you are prompted with the question to compile packages or not (i.e. "Do you want to install from sources the package which needs compilation? (Yes/no/cancel)"), the most stable option here is to choose **no**, since local compilation

of the latest uncompiled packages sometimes results in an error. When you select **no**, the latest precompiled version of the packages is installed, which is just fine for *leafkin*.

- When you have tried this and there is still an error occurring during installation, you should skip updates of the remaining packages causing an error during installation (just hit your **ENTER** key when prompted: "Enter one or more numbers, or an empty line to skip updates:". This should install *leafkin*.

Run this line to install *leafkin*:

```
devtools::install_github("impres-lab/leafkin")
```

With *leafkin* and the tidyverse packages installed, we can now load the functions into the current RStudio session to make all of their functions available for use. Do this by running the following two lines:

```
library("leafkin")
```

```
library("tidyverse")
```

You are now ready to perform kinematic data analysis.

Kinematic data analysis using *leafkin*

For the manual, we will use the code in the quick start section of the sample script, but feel free to run the code with the more elaborate explanation in the second part of the script as well.

Step 1: Load your data / file paths

First, the data is loaded into our R session. The data provided in as sample data originates from a recent publication in which a kinematic analysis was performed (Bertels *et al.*, 2020). For this, we need to do two things for each file:

1. Create file path which to tell R where to find the files.
2. Give this file path to the *read_tsv()* function which will read the contents of the file and make it available in R.

To create the file path, we use the *file.path()* function to help us and store the created file path in a variable. For example, in our extracted folder, we find the data files folder. Within the data files folder are the data files we need to read into the R sessions. As mentioned previously, RStudio set the folder from which the R project file is opened as the working directory. Within the working directory, we want R to look for the data files in the data files folder. Therefore, we create the file path where we first have "data files", followed by the name of the file, for example "growth_measurements_millimetre.txt". The path is stored within a variable, different for each file. This variable is then used in the *read_tsv()* function to read the data from the files into the R session.

Running these lines will import the contents of the files:

```r
# 0.3 Load required data into R
#' Leaf length data
leaf_length_measurements_path <- file.path("data files",
                                           "growth_measurements_millimetre.txt")
leaf_length_measurements <- read_tsv(leaf_length_measurements_path)

#' Cell length data
cell_length_measurements_path <- file.path("data files",
                                           "cell_length_measurements_micrometre.txt")
cell_length_measurements <- read_tsv(cell_length_measurements_path)

#' Meristem size data
mersitem_length_measurements_path <- file.path("data files",
                                               "meristem_size_micrometre.txt")
meristem_size <- read_tsv(mersitem_length_measurements_path)
```

Of course it is possible to create file paths to any file on your computer. For this, we also advice to use the *file.path()* function, since file paths are operating system specific and the *file.path()* function automatically makes a path in the right format.

Looking into the details of a file on both Windows and MacOS systems will reveal you the file path. On MacOS, you can also easily copy the file path by right-clicking the file in the finder while holding down the option key. In the dropdown menu, the option to copy as pathname is now revealed. This file path can be used directly in R. Using Windows file paths directly in R is not possible since they have another format, we therefore advice to recreate the path yourself using the *file.path()* function.

After importing the data, you can see that the data is now imported in the Environment tab on the top right:

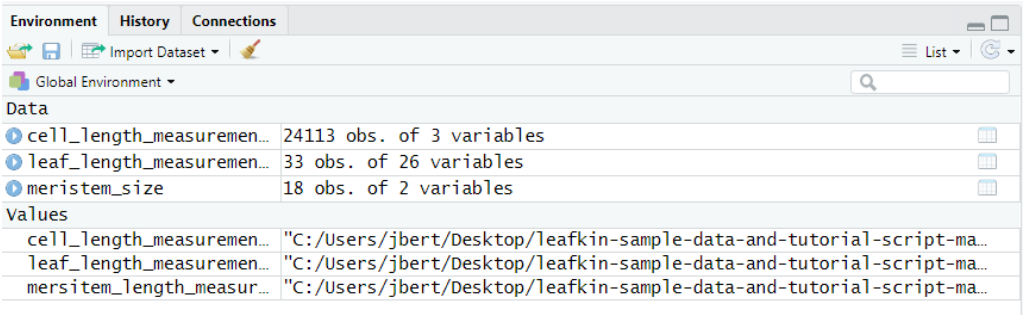

Step 2: Calculating the average leaf elongation rates

Next, we calculate the average leaf elongation rates during the interval of steady state growth and prior to the harvest of the leaves of each plant using the *calculate_LER()* function. We store the result in the *result_LER_means* variable.

```
# 0.4 Perform kinematic analysis
# 0.4.1 Average leaf elongation rates of each plant
result_LER_means <- calculate_LER(leaf_length_data = leaf_length_measurements,
                                  n_LER_for_mean = 2,
                                  output = "means")
view(result_LER_means)
```

For the first parameter of the function, we indicated that the *leaf_length_data* are stored in the *leaf_length_measurements* table. For the second parameter, i.e. *n_LER_for_mean*, we want the first two calculated leaf elongation rates (prior to the harvest of these leaves, for the cellular analysis below) to be used for the calculation of the mean. The last parameter determines the output, which in the kinematic analysis should be means. Notice the parenthesis around means: “means”. This is because means should be interpreted as text. If you do not use the parenthesis, R will not know what you are referring to (since we have not made a variable called means).

The view(*result_LER_means*) will open the results for you within RStudio, allowing you to inspect them visually. Notice that an extra line has appeared in the Environment tab of RStudio, now also including *result_LER_means*.

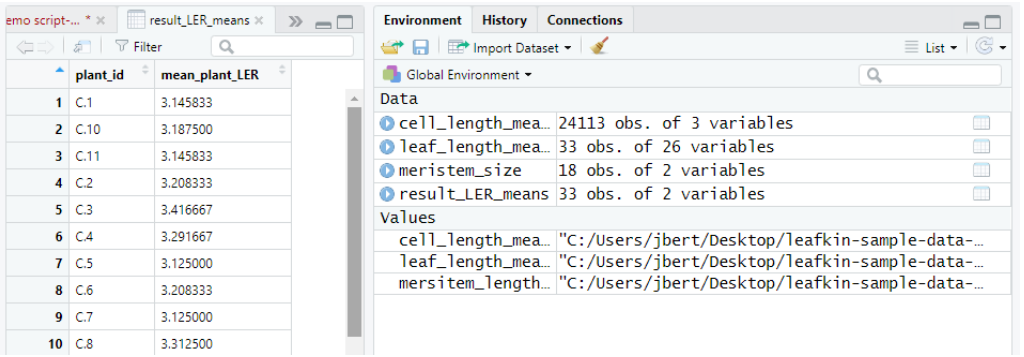

Step 3: Inspect the cell length fits

The *get_pdf_with_cell_length_fit_plots()* function will create a pdf file in your working directory with plots of fitted cell lengths. Also plots of the derivative of this curve will be printed into the pdf, visualising the slope of the fit.

Within this function, we indicate that the *cell_lenght_data* can be found in the *cell_length_measurements* parameter. Next, we set the *interval_in_cm* parameter to 0.1 for cell lengths to be estimated every 0.1 cm. In addition, we can control the fit of the function by setting the *bw_multiplier*. By default, the *bw_multiplier* is set to 1, which means that the calculated bandwidth is multiplied by 1 and thus not manipulated. We also want the function to return a tibble (see additional information for tibbles at the end of the manual) containing the calculated bandwidths. For this, we set *output_bw_tibble* to TRUE. These bandwidths can be used to provide an alternative bandwidth for plants which had a failed bandwidth calculation in the next step (step 4: Obtaining the fitted cell lengths).

```
# 0.4.2 Evaluate cell length fits and store bandwidths
#' A pdf file with the cell length fits will be created in the working directory.
bw_tibble <- get_pdf_with_cell_length_fit_plots(cell_length_data = cell_length_measurements,
                                                interval_in_cm = 0.1,
                                                bw_multiplier = 1,
                                                output_bw_tibble = TRUE)
```

After running this line, a pdf file with the fits has appeared in the working directory:

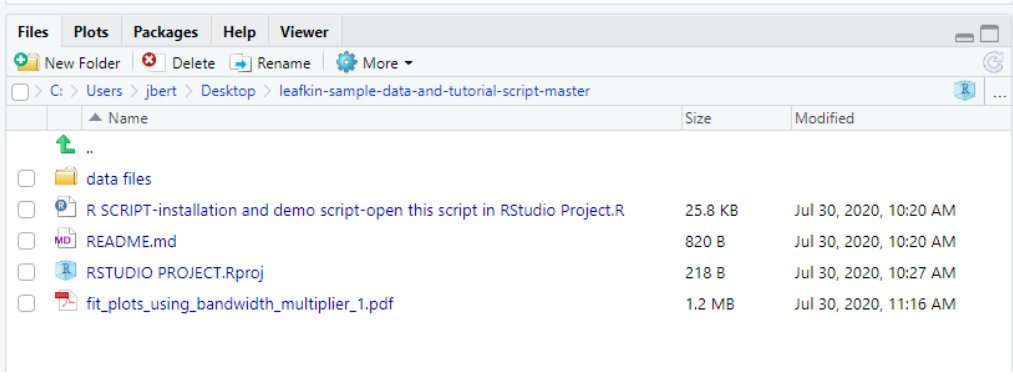

The created pdf-file with the plotted cell lengths and fit curves can be used to evaluate the cell length fits for each plant and to check the impact of set bandwidth multipliers

on these fits. A good fit does not overly follow minor local variations in cell length, but closely fits the global profile. When the *bw_multiplier* value was set too low, e.g. 0.3, too much local variation could be introduced in the fit, especially in the mature region, where cell length can be considered approximately constant (Figure 1A). Inversely, when the *bw_multiplier* value was set too high, e.g. 3, oversmoothing could occur, particularly affecting fitted cell sizes in the meristem.

In the created pdf file, also the calculated bandwidths for each individual plant are plotted in the last graph. If, for some plants, the function was unable to calculate the optimal bandwidth (for example when an insufficient number of cell length measurements was provided), there will be missing data in the bandwidth plot, but also will the concerned cell length fit plots have no fit and a warning message will be printed in the console of RStudio. In this case, when extracting all the fitted cell lengths in the next step, an alternative bandwidth should be provided in the *get_all_fitted_cell_lengths()* function (see next section).

The effect of the bandwidth parameter on cell length fits:

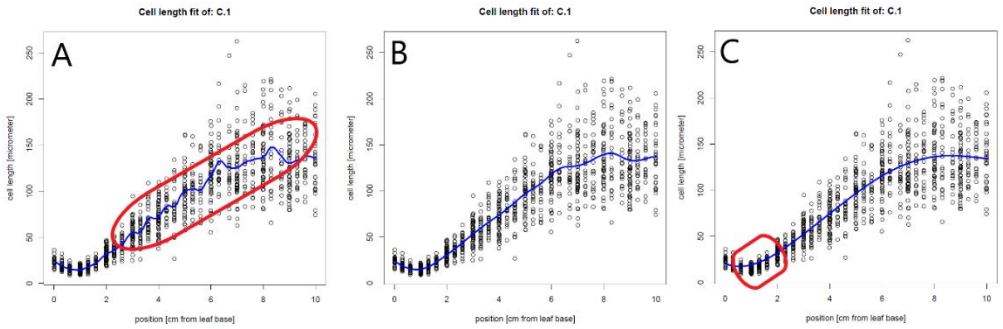

A) A very strict fit of the cell lengths by setting the *bw_multiplyer* to 0.3. A strict fit can result in too much variation (encircled in red). **B)** Fitted cell length data, using the calculated bandwidth (bandwidth multiplier = 1). **C)** A more loose fit of the cell lengths by setting the *bw_multiplyer* to 3. A loose fit can result in oversmoothing, poorly fitting cell sizes, especially at the end of the meristem (encircled in red) and/or the end of the growth zone.

If the fit is not good, vary the *bw_multiplier* parameter and asses each fit until you have found the most satisfying fit. Your ideal *bw_multiplier* value can then be used in the next step, where we extract the fitted cell lengths.

Extra:

In addition to the cell length fit plots, plots of the local first derivative (i.e. slope) are also printed (where in the y-axis label, dl/dx, l = cell length and x = position). These can be used to assess the smoothness of the fit.

The effect of the bandwidth parameter on the slope of the cell length fits:

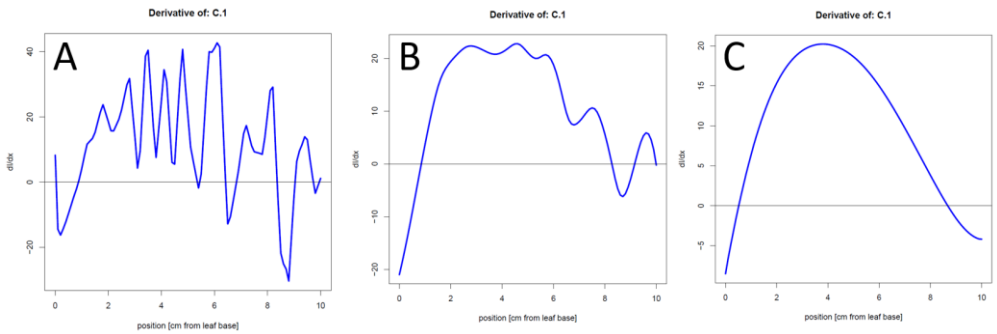

A) A very strict fit of the cell lengths by setting the *bw_multiplyer* to 0.3 results in a lot of variation in the slope. **B)** The unmanipulated calculated bandwidth (bandwidth multiplier = 1) resulted here in an acceptable amount of variation in the slope. **C)** A more loose fit of the cell lengths by setting the *bw_multiplyer* to 3 resulted in a slope which does not follow any variation in the data.

The last graph of the document, contains all calculated bandwidths:

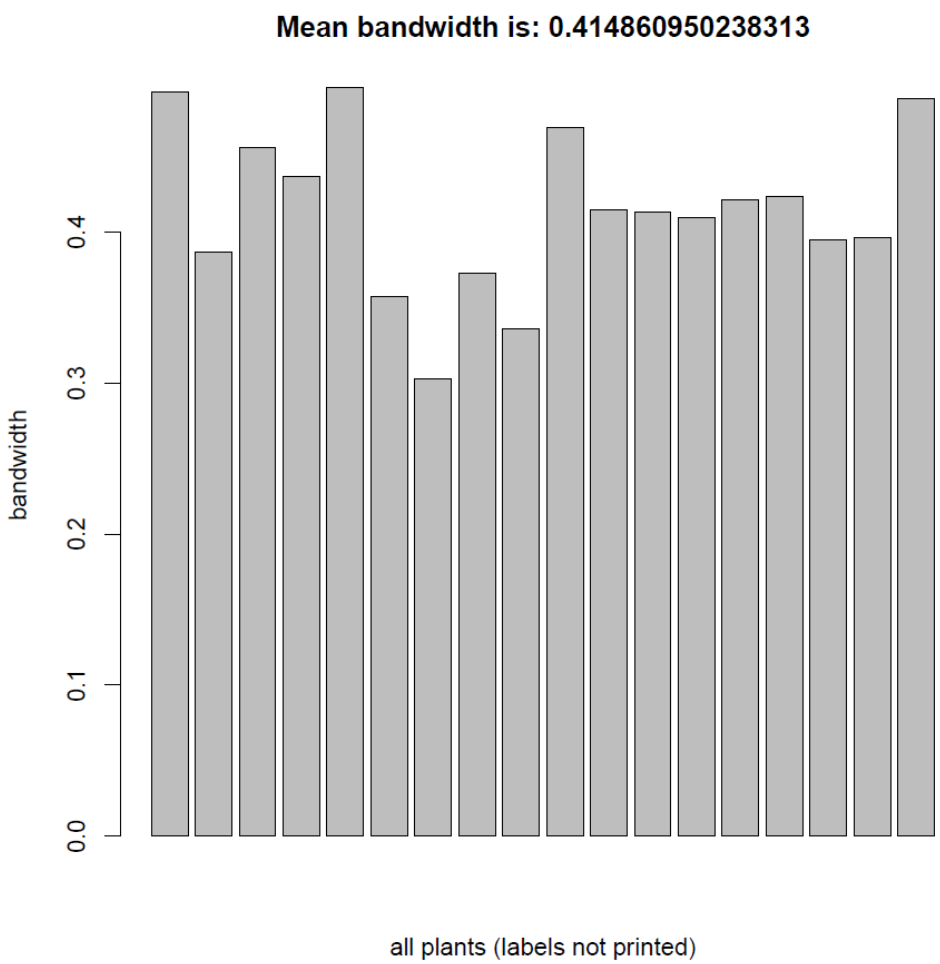

If, for some plants, the function was unable to calculate the optimal bandwidth (for example when an insufficient number of cell length measurements was provided), there will be missing data in the bandwidth plot, but also will the concerned cell length fit plots have no fit and a warning message will be printed in the console of RStudio.

Step 4: Obtaining the fitted cell lengths

During the microscopy study, it is impossible to obtain cell lengths at every possible location. However, a fit of the measured cell lengths will allow to obtain estimated cell lengths at every desired location.

With the *get_all_fitted_cell_lengths()* function, we obtain the fitted cell lengths for a user-set interval and store them in the *fitted_cell_lengths* variable.

```
# 0.4.3 Obtain fitted cell lengths.
fitted_cell_lengths <- get_all_fitted_cell_lengths(cell_length_data = cell_length_measurements,
                                                   interval_in_cm = 0.1,
                                                   bw_multiplier = 1,
                                                   alternative_bw = mean(bw_tibble$collected_bandwidths,
                                                                         na.rm = TRUE),
                                                   tidy_cell_lengths = TRUE)
```

As you can see, this function again requires you to supply the *cell_lenght_measurements* data to the *cell_length_data* parameter. Next, we set the interval at which cell lengths should be obtained, in this case every 0.1 cm. The bandwidth does not have to be manipulated, so we set the multiplier to 1 (this is the default value). All of our plants had a calculated bandwidth, but for the sake of completeness, we added here a line which calculates the mean of the *collected_bandwidths*, present in the *bw_tibble* (where na.rm = TRUE removes missing bandwidth values). Lastly, the most important line is the way we want the fitted cell lengths to be returned. It is important that they are returned in a tidy format (see addition information at the end of the document for more information on the tidy format), so we set *tidy_cell_lengths* to TRUE.

Inspecting the *fitted_cell_lengths* will show you the estimated cell length (µm) at every position (cm) of the given interval. Reducing the interval size is possible of course.

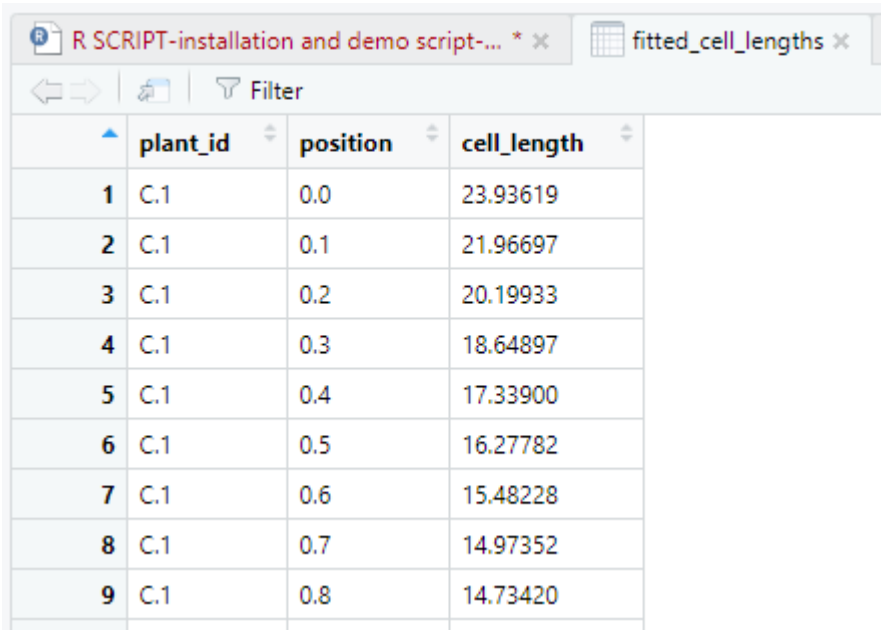

	plant_id	position	cell_length
1	C.1	0.0	23.93619
2	C.1	0.1	21.96697
3	C.1	0.2	20.19933
4	C.1	0.3	18.64897
5	C.1	0.4	17.33900
6	C.1	0.5	16.27782
7	C.1	0.6	15.48228
8	C.1	0.7	14.97352
9	C.1	0.8	14.73420

With the fitted cell lengths collected, we can now move on to the kinematic analysis calculations.

Step 5: Performing the kinematic analysis calculations

With the *kinematic_analysis()* function, the all the kinematic analysis calculations can be executed at once for every plant in the microscopy analysis. The results of the average leaf elongation rate calculations are supplied to the *LER_means* parameter, the fitted cell lengths are supplied to the *tidy_cell_lengths* parameter and the meristem sizes, which were imported as a simple table in the beginning, are assigned to the *meristem_size_micrometre* parameter. The result is stored in the *final_kinematic_analysis* variable.

```
# 0.4.4 Perform kinematic analysis
#' Remaining kinematics calculations, all at once.
final_kinematic_analysis <- kinematic_analysis(LER_means = result_LER_means,
                                               tidy_cell_lengths = fitted_cell_lengths,
                                               meristem_size_micrometre = meristem_size)
view(final_kinematic_analysis)
```

The contents of *final_kinematic_analysis* contains the values for all kinematic parameters for each plant:

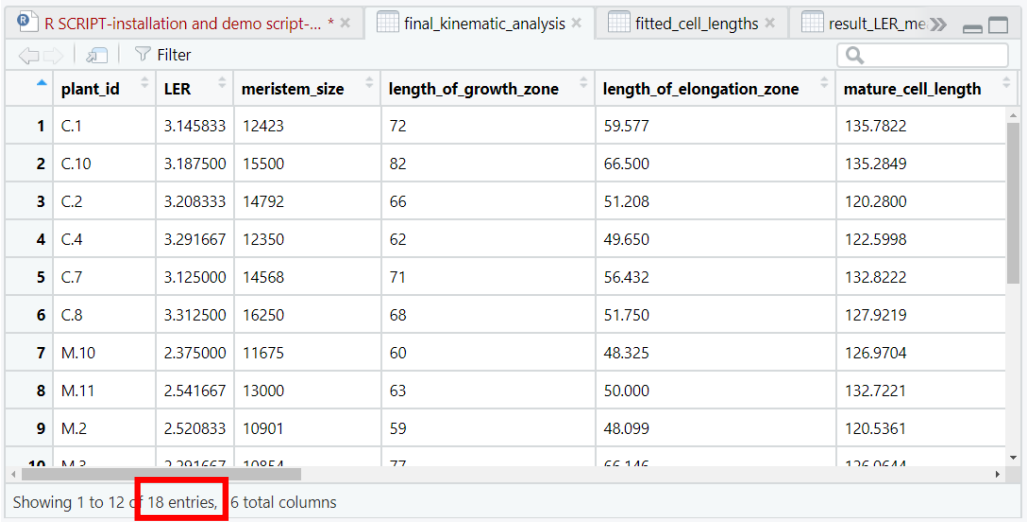

	plant_id	LER	meristem_size	length_of_growth_zone	length_of_elongation_zone	mature_cell_length
1	C.1	3.145833	12423	72	59.577	135.7822
2	C.10	3.187500	15500	82	66.500	135.2849
3	C.2	3.208333	14792	66	51.208	120.2800
4	C.4	3.291667	12350	62	49.650	122.5998
5	C.7	3.125000	14568	71	56.432	132.8222
6	C.8	3.312500	16250	68	51.750	127.9219
7	M.10	2.375000	11675	60	48.325	126.9704
8	M.11	2.541667	13000	63	50.000	132.7221
9	M.2	2.520833	10901	59	48.099	120.5361

Pay attention to the leaf elongation rates. In the results from the kinematic analysis function, the values of only the plants on which a microscopy study was performed are presented, while most often also additional leaf elongation rates are available for plants that have grown to obtain the final leaf length. All mean LERs for each plant are available in the previously obtained *result_LER_means*:

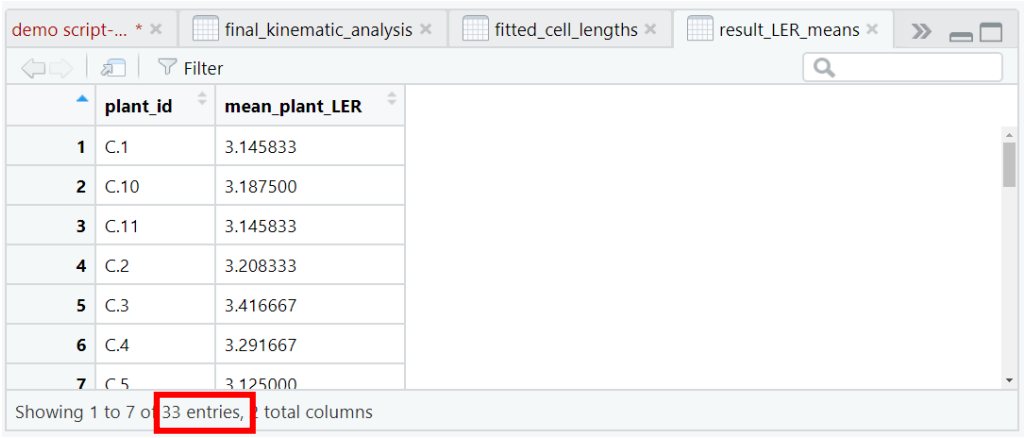

After these five steps, the kinematic analysis is completed and data for each kinematics parameter is now available with the following units:

KINEMATICS PARAMETER	UNIT
leaf elongation rate (LER)	$mm \cdot h^{-1}$
length of the meristem	mm
length of the elongation zone	mm
length of the growth zone	mm
length cells leaving meristem	µm
mature cell length	µm
number of cells in meristem	
number of cells in elongation zone	
number of cells in total growth zone	
cell production rate	$cells \cdot h^{-1}$
cell division rate	$cells \cdot cell^{-1} \cdot h^{-1}$
relative cell elongation rate	$\mu m \cdot \mu m^{-1} \cdot h^{-1}$
cell cycle duration	h
time cells spend in the meristem	h
time cells spend in the elongation zone	h

For more information on the formulas used, we refer to formula section at the end of the manual. To use the calculated parameters outside R, the results can be exported to a tab-delimited .txt file with the following code:

```
# DONE
#' All calculation involved are done. You can opt to write the results to a
#' txt-file:
write_tsv(final_kinematic_analysis, "kinematic_analysis_results.txt")
```

This command generates a txt file (kinematic_analysis_results.txt) with the values is now available in the working directory:

Additional code

In the tutorial script, also code to inspect all the individually calculated LERs and to recreate the cell length plot is available. Feel free to play around with this code to familiarize yourself with these types of functionality in R.

Errors and troubleshooting

Known errors of difficulties users might encounter are listed here below. An updated version of this list is maintained on the GitHub leafkin repository: https://github.com/impres-lab/leafkin. The known difficulties and errors upon the release of *leafkin* are presented here below:

Installation of *leafkin*.

- Starting with R 4.0.0 (released April 2020), R for **Windows** uses a new toolchain bundle called Rtools40. Rtools40 is advised for *leafkin* installation through GitHub on Windows and can be downloaded from https://cran.r-project.org/bin/windows/Rtools/.

Extra columns could be added through the use of Excel when creating the .txt file.

The use of Excel to enter data can, whilst being convenient, sometimes be the cause of errors in R. Excel sometimes adds extra tabs, resulting in extra rows without headers and data. These extra columns get named by R with default names, usually starting with an X. The *leafkin* functions rely on datasets with the right format. Therefore, these extra columns will result in an error when running the *leafkin* functions. A way to solve this issue is to select only the columns you are interested using the select function, provided by the dplyr package of the tidyverse. The following line will for instance only select 6 columns, starting with the first one, up until the sixth:

```
leaf_length_measurements %>% select(1:6)
```

If you make sure that the selected columns contain your data and not any extra column, processing of the data should now be errorless.

Error when creating the pdf containing cell length fit plots: cannot open file

This means that you have a pdf opened with exactly the same name as the one the *get_pdf_with_cell_length_fit_plots()* function is trying to create. This happens for

instance when you create a pdf file with the *get_pdf_with_cell_length_fit_plots()* function, open the created pdf and run the function again with the pdf file still open. With the pdf file still open, R cannot replace the old file by the new file. Just close the pdf file and you should be able to run the function again.

Error when fitting cell lengths related to gridsize: Binning grid too coarse for current (small) bandwidth.

There are limits to the interval which can be chosen. An interval that is too coarse will result in an error related to the gridsize. Very small intervals will slow down the function. In our experience, the 10-centimetre growth zone of a maize leaf is ideally analysed with an interval of 0.1 or 0.01 centimetre (i.e. resulting in 101 or 1001 datapoints respectively). It is also important to note that an insufficient number of cell length measurements could result in a failed bandwidth calculation (though tests revealed that only extreme borderline disruptions in the data resulted in an error). In that case, cell lengths are not fitted, and a warning is printed after executing the function, indicating the number of plants for which no bandwidth could be calculated.

Additional information

Tidy and wide data

We use the concept of tidy as defined by Hadley Wickham (Wickham, 2014). In tidy data, each variable is saved in its own column and each observation is saved in its own row:

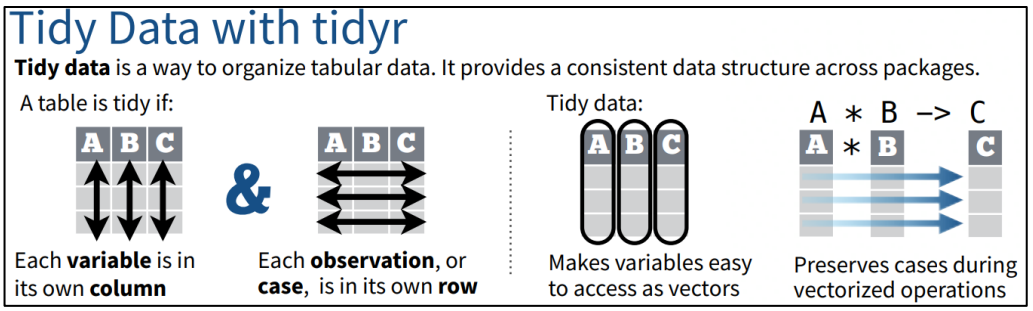

Figure 1. Snippet from the Data Import cheat sheet related to tidy data, available on: https://rstudio.com/resources/cheatsheets/.

Tidy data can be *spread* out in a wide format, where variables are spread out over multiple columns. A wide format is harder to work with in data analysis, but could be more human readable. When transforming the wide dataset back to a tidy format, it is called *melting* it (Wickham, 2014).

As an example, we will demonstrate tidy and wide tables with daily leaf length measurements. When taking measurements, one could opt to note them down in a wide format (which is often more convenient for humans):

plant_id	2020/07/20 10:40	2020/07/21 9:43	2020/07/22 10:12
plant1	121	153	186
plant2	93	130	169
plant3	112	146	180

Yet, the same data could also be presented in a tidy format, where each variable is in its own column and each observation is in its own row:

plant_id	date	leaf_length
plant1	2020/07/20 10:40	121
plant1	2020/07/21 9:43	153
plant1	2020/07/22 10:12	186
plant2	2020/07/20 10:40	93
plant2	2020/07/21 9:43	130
plant2	2020/07/22 10:12	169
plant3	2020/07/20 10:40	112
plant3	2020/07/21 9:43	146
plant3	2020/07/22 10:12	180

For data analysis, tidy date is easier to handle, since the user can now work easily with the dates and leaf lengths. The user can now also access each measurement individually with all measured variables linked to it in the same row.

Tibbles

Tibbles are an updated version of data.frames and are a way to story data as a table in R. For more information on tibbles, please visit: https://tibble.tidyverse.org/.

Formulas used by *leafkin*

Below we present the formulas used by the *leafkin* functions:

$$LER = \frac{LL_2 - LL_1}{t_2 - t_1} \qquad (1)$$

Leaf elongation rate formula (*LER*), with LL_x being the leaf length measurement x (in mm) and t_x being the time at which LL_x was taken (in data time format yyyy/mm/dd hh:mm(:ss)).

$$CCN_p = CCN_{p-1} + \frac{position_p - position_{p-1}}{\left(\frac{cell\ length_{p-1} + cell\ length_p}{2}\right)} \qquad (2)$$

Cumulative cell number (*CCN*) is a formula used internally by the kinematic analysis function to determine the cumulative number of cells at every position (*p*) by adding the cumulative cell number in the previous interval to the estimated number of cells in the current interval. The number of cells in the current interval uses the current and previous position to determine the size of the interval, which is divided by the average cell length in this interval (calculated by using the current and previous cell size).

$$P95_p = 0.95 \times \frac{\sum_{i=p}^{n} cell\ length_i}{n - p} \qquad (3)$$

The 95-percent value (P95) formula is used internally by the kinematic analysis function at every position (p) and multiplies 0.95 by the mean cell length for cell sizes starting at the current position up until the last determined cell length (n).

$$L_{gz} = \min\left(position_{(cell\ size > P95_{cell\ size})}\right) \qquad (4)$$

The growth zone size (L_{gz}) is the first position where cell size exceeds the 95-percent value of the cell sizes.

$$l_{mat} = \frac{\sum_{i=p}^{n} cell\ length_i}{n - p} \qquad (5)$$

The mature cell length (l_{mat}) is the average cell length between the first position after the growth zone (p) and the final measurement (n).

$$P = \frac{LER}{l_{mat}} \qquad (6)$$

The cell production rate (*P*) is calculated by dividing the leaf elongation rate (*LER*) by the mature cell length l_{mat}.

$$N_{mer} = CCN_i + \left((CCN_{i+1} - CCN_i) \times (L_{mer} \bmod interval\ size)\right) \qquad (7)$$

The number of cells in the meristem (N_{mer}) is determined by the cumulative cell number (CCN) at position *i*, where *i* is the last position which is still located within the meristem size, plus the difference in CNN between position *i* and *i+1*, multiplied by the meristem length (L_{mer}) modulo interval size.

$$l_{mer} = cell\ length_i + \left((cell\ length_{i+1} - cell\ length_i) \times (L_{mer} \bmod interval\ size)\right) \qquad (8)$$

The length of the cells leaving the meristem (l_{mer}) is determined by the cell length at position *i*, where *i* is the last position which is still located within the meristem size, plus the difference in cell length between position *i* and *i+1*, multiplied by the meristem length (L_{mer}) modulo interval size.

$$N_{gz} = CCN_i \qquad (9)$$

The number of cells in the growth zone (N_{gz}) is equal to the cumulative cell number at position *i*, where *i* is the position at which the length of the growth zone L_{gz} was determined.

$$N_{el} = N_{gz} - N_{mer} \qquad (10)$$

The number of cells in the meristem (N_{mer}) is determined by subtracting the number of cells in the growth zone (N_{gz}) by the number of cells in the meristem (N_{mer}).

$$D = \frac{P}{N_{mer}} \qquad (11)$$

The average cell division rate (*D*) is determined by dividing the cell production rate (*P*) by the number of cells in the meristem (N_{mer}).

$$T_c = \frac{\ln 2}{D} \qquad (12)$$

The cell cycle duration (T_c) is determined by dividing the natural logarithm of 2 by the average cell division rate (*D*).

$$T_{el} = \frac{N_{el}}{P} \qquad (13)$$

The time in the elongation zone (T_{el}) is determined by dividing the number of cells in the elongation zone (N_{el}) by the cell production rate (P).

$$T_{div} = \log_2 N_{mer} \times T_c \qquad (14)$$

The time cells spend in the meristem (division zone, T_{div}) is determined by the log2 of the number of cell in the meristem (N_{mer}) multiplied by the cell cycle duration (T_c).

$$R_{el} = \frac{\ln l_{mat} - \ln l_{div}}{T_{el}} \qquad (15)$$

The relative cell elongation rate (R_{el}) is determined by the difference in the natural logarithm of mature cell length (l_{mat}) and the natural logarithm of the lengths of the cells leaving the meristem (l_{div}), divided by the time cells spend in the elongation zone (R_{el}).

Supplementary data chapter 3

Supplementary Table 3.1. Average Cт values for the 4 tested housekeeping genes with their standard deviation. The number of quantitative real-time PCR reactions per run, combined with high number of samples originating from the thorough sectioning of the growth zone, limited the number of house genes to be used during each run to 1. In order to select the most appropriate housekeeping gene, the expression of 4 candidate housekeeping genes wat tested for 2 plants of each treatment in segments 0.5-1, 1.5-2, 4-5 and mature blade. Cт values closer to each other resemble more equal expression levels between segments.

Potential housekeeping gene	Gramene gene description	Mean Cт value ± SD
Zm00001d053296	Ubiquitin-conjugating enzyme E2 variant 1C	23.7 ± 1.5
Zm00001d013367	Tubulin alpha-4 chain	19.0 ± 2.7
Zm00001d015962	Prolyl oligopeptidase family protein	27.2 ± 1.6
Zm00001d036201	Unknown (Hypothetical protein which is found to be a very stable housekeeping gene in maize (Lin *et al.*, 2014))	22.7 ± 1.2

Supplementary Table 3.2. Primers used for quantitative real-time PCR. The first column contains the gene ID for the v4 B73 gene model. The second column shows the gene symbol according to the maize genetics and genomics database (Maize GDB). The third column contains the description of the gene obtained at http://ensembl.gramene.org/Zea_mays.

Gene ID	Gene Symbol	Gene description	Forward primer 5' → 3'	Reverse primer 5' → 3'
Zm00001d053998	*wee1*	Putative wee1-like protein kinase	TTCTTCTGCACCCCGGACTA	GAGGGTTCGCTGACTTCTCC
Zm00001d036360	*cyc3*	Cyclin-B2-4	GCCCTCAGCGACATCAAGAA	GCGAATTTCCTGGTGACTGG
Zm00001d044540	*mcm4*	DNA replication licensing factor MCM4	GAAATTCATATGCACGAACTCCG	AAGGAAGTGGCGGGTTGGA

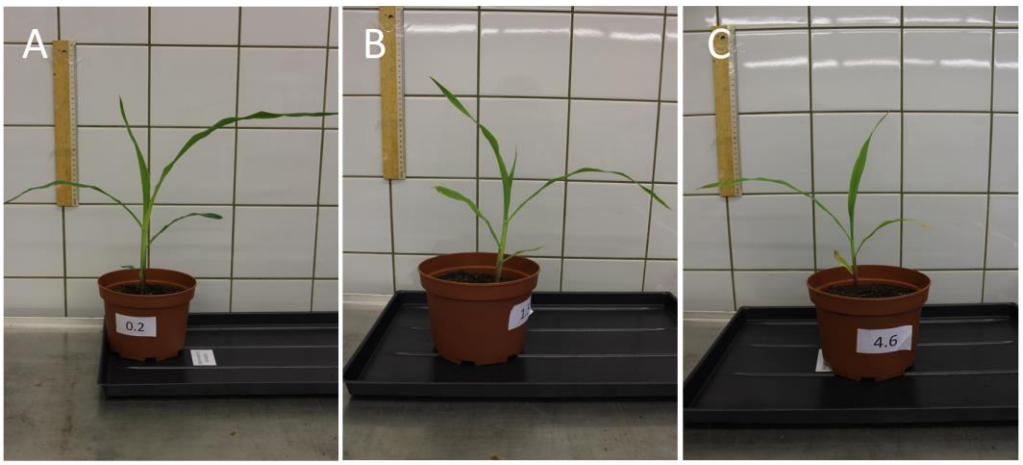

Supplementary Figure 3.1. The effect of cadmium on the overall seedling phenotype. Representative plants exposed to A. control, B. mild (46.5 mg Cd · kg^{-1} dry soil) and C. severe cadmium (372 mg Cd · kg^{-1} dry soil) treatments at 24 days after sowing. Under control and mild stress conditions, plants are in the 5^{th} leaf stage. Under severe stress conditions, they are in the fourth leaf stage. The ruler indicates 30 cm.

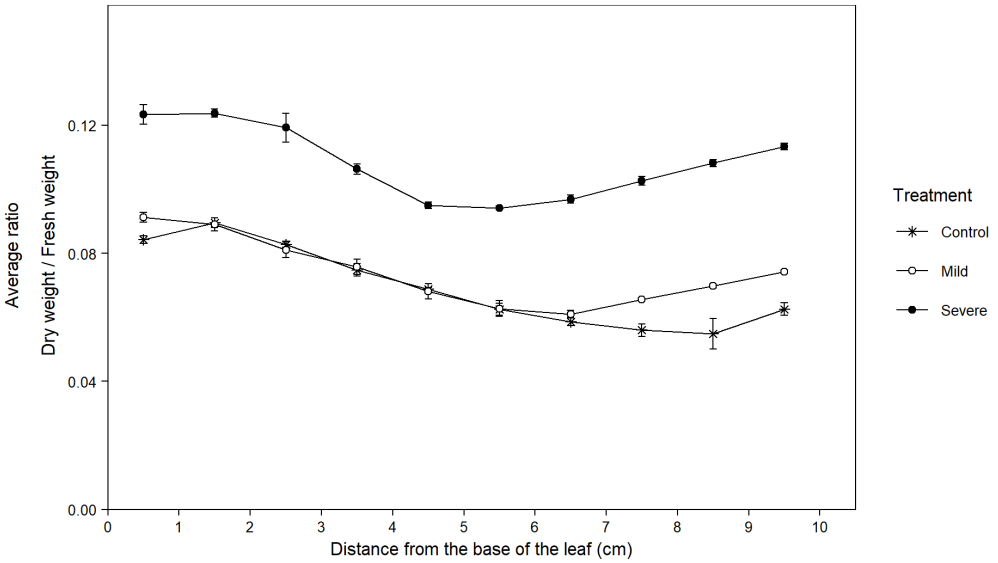

Supplementary Figure 3.2. Dry to fresh weight ratio across the maize leaf growth. This figure illustrates the relative increase in dry weight under severe Cd stress conditions. This increase masks the increased amount of Cd in the growth zone, which can be seen when Cd concentrations are expressed on fresh weight basis. Data shown are means ± SE (n = 5).

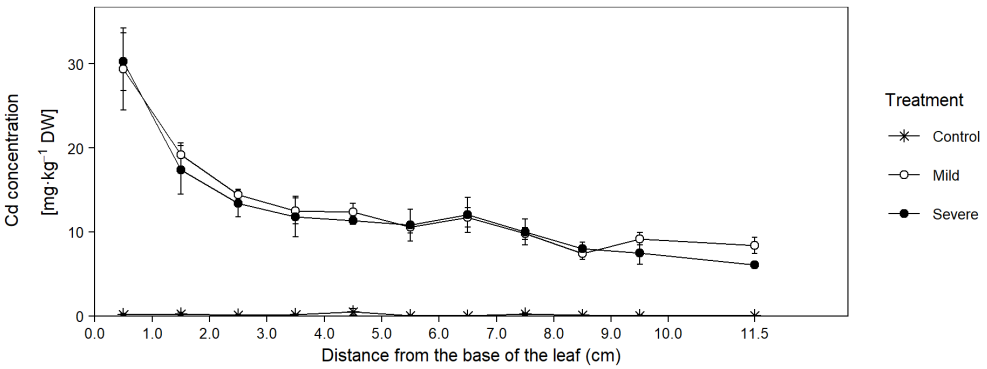

Supplementary Figure 3.3. Cadmium concentration relative to tissue dry weight in the maize leaf growth zone. Data originates from the same samples as in figure 2.A, where Cd concentration is expressed on fresh weight tissue basis. The maize leaf growth zone was subdivided in 10 one-centimetre segments, starting from the base of the leaf. Data shown are mean values ± SE (n = 5). Statistics: Treatment $p = 0.0004$, Segment $p < 0.001$, Interaction: not significant.

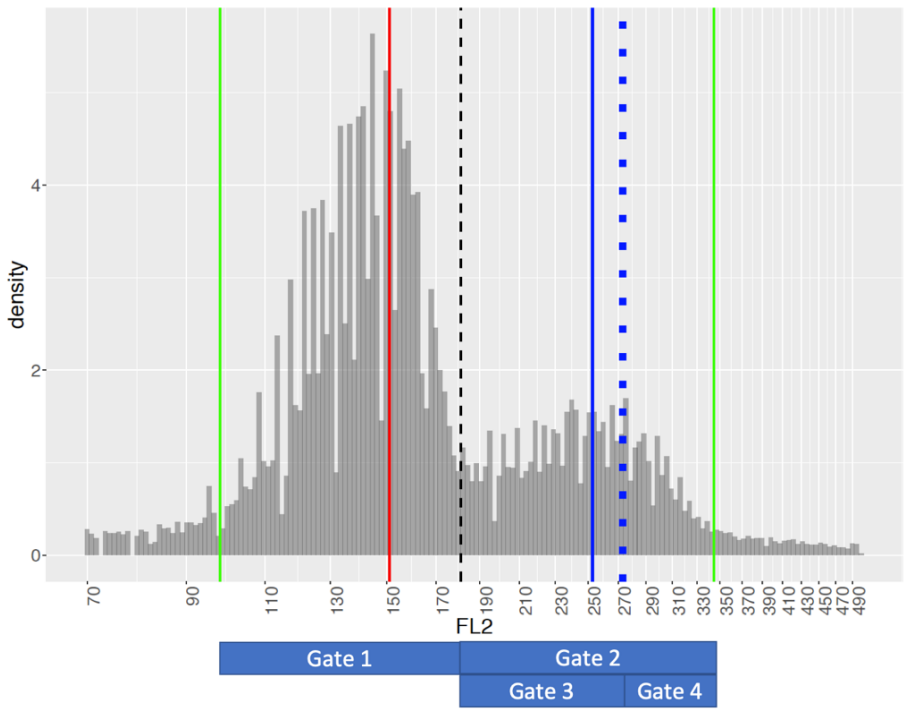

Supplementary Figure 3.4. Flow cytometry gates illustration. Full red and full blue line, 2C and 4C peak respectively, were positioned using the density curve from geom_density (ggplot2) with kernel set to Gaussian and bandwidth set to nrd0 (default bandwidth). Green lines: First and second green line define the start and stop of 2C and 4C respectively. Black dashed line: Defines the end of the steep decline of the 2C peak. Blue dotted line: the calculated 4C peak. The calculation uses the relative 4C peak distance to the 2C peak based on the blade samples (i.e. 1.81 ± 0.007) times the FL2 value of the 2C peak, based on blade samples.) Calculation of the true position of the 4C peak is necessary when estimating the proportion of nuclei in the S-phase since nuclei in the S-phase mask the real 4C peak when using a lower resolution flow cytometer. Visually assigning the position of the 4C peak in segments with a large proportion of cells in the S-phase would shift the 4C peak position towards the 2C peak, resulting in an underestimation of cells in the S-phase. Gate 1 and 2 encompass 2C nuclei and 4C nuclei (+ nuclei in the S-phase), respectively. Gate 3 starts at end of 2C peak, ends at the calculated 4C peak and therefore contains a small portion of 2C nuclei, cells in the S-phase and part of the 4C nuclei. Gate 4 starts at the calculated 4C peak and ends at the end of the 4C peak and therefore encloses mainly 4C nuclei. Gate 1 and 2 were used to determine the 4C/2C ratio (i.e. ratio 4C/2C nuclei = Gate 2 · Gate 1^{-1}), whereas all gates were used to estimate the proportion of cells in the S-phase (i.e. proportion of nuclei in S-phase = (Gate 3 – Gate 4) · (Gate 1 + Gate 2)$^{-1}$).

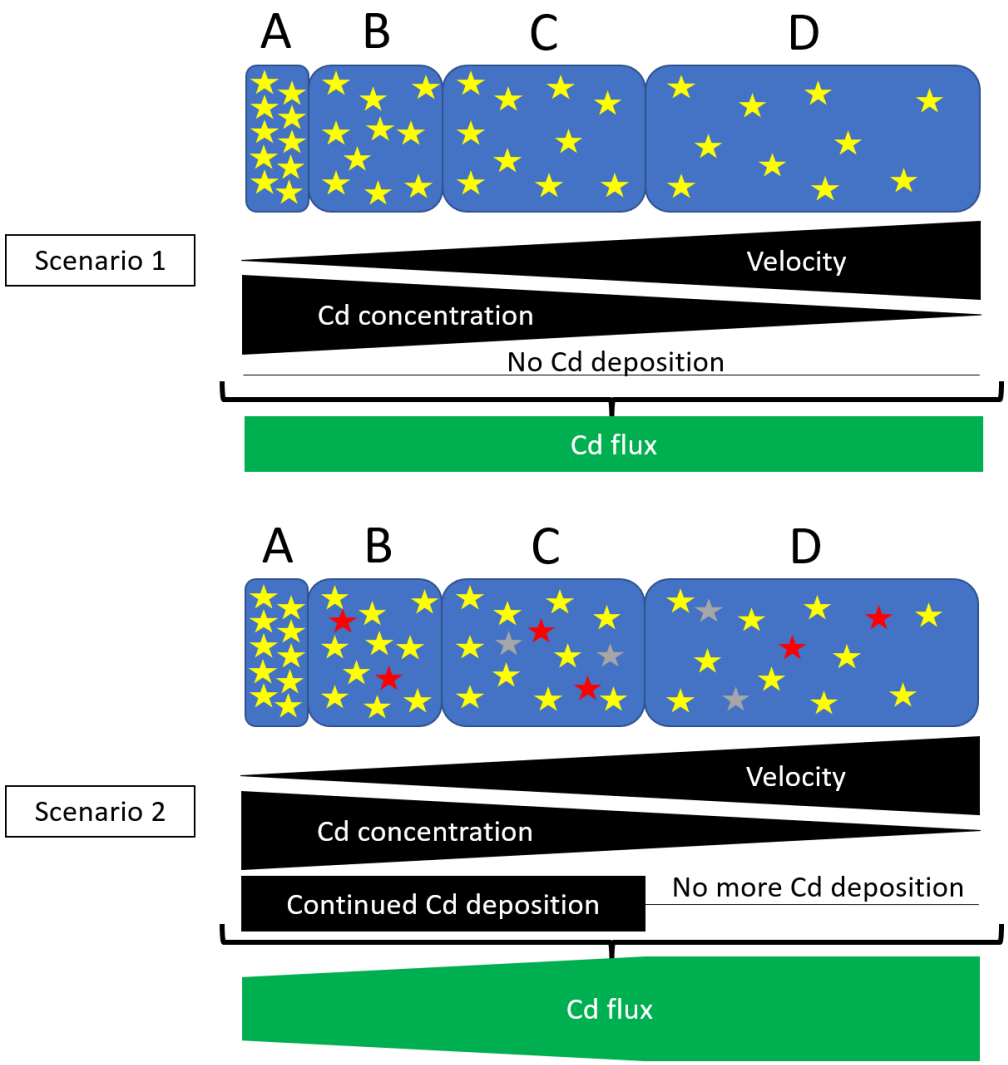

Supplementary Figure 3.5. Illustration of whether or not Cd deposition occurs in the growth zone. Depicted are cells along the growth zone, where **cells A** are meristematic cells at the meristem boundary, **cells B and C** are elongating cells and **cells D** are mature cells. The stars indicate Cd ions. In each cell, the number of yellow Cd ions is constant. Red and grey Cd ions are deposited at distinct locations and giving them a different colour, allows for tracking of these ions in the cells. **Scenario 1.** Cadmium deposition occurs only in the meristem (A). As cells start to grow and take up water, the Cd is diluted (B to D). Yet, as also velocity increases during cell elongation, the amount of Cd passing by each second at each location in the elongation zone therefore remains constant (constant flux) and its dilution (decrease in Cd flux) is proportional to the increase in velocity (increase in Cd flux). **Scenario 2.** Deposition in the meristem (A)

and elongating cells (B and C). Deposition in the elongating cells causes the Cd flux to continue to increase. The derivative of this increased flux is a positive number, which resembles Cd deposition.

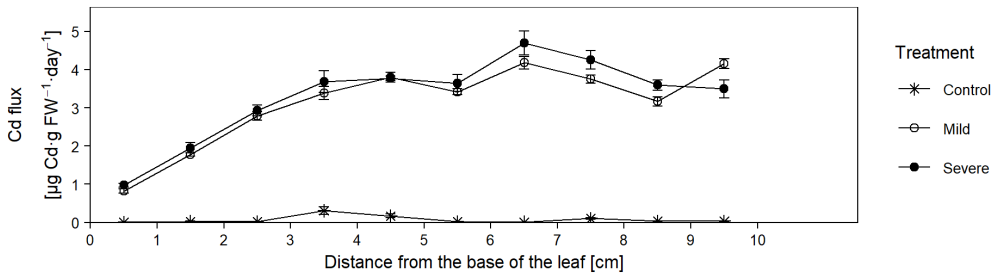

Supplementary Figure 3.6. Cadmium flux based on tissue mass in the maize leaf growth zone. This parameter illustrates the amount of Cd passing through a segment in the growth zone per second for each gram of fresh weight.

Supplementary data chapter 4

Supplementary Table 4.1. All 58 significantly (FDR) affected genes in the meristem for the mild versus control contrast. Genes are sorted in descending LFC size (absolute value). Gene descriptions were obtained from NCBI and were manually curated to obtain concise gene descriptions. When no NCBI description was available, the description on Gramene was obtained. If only a description based on homology was available, the species used is also indicated.

V4 ID	FDR p-val.	LFC and SE	Description of the gene.
Zm00001d023332	7.42E-12	4.5 ± 0.6	WRKY-type transcription factor
Zm00001d046676	0.012533	2.2 ± 0.5	tryptophan synthase beta type 2
Zm00001d048643	0.00079	1.9 ± 0.4	Cyclopropane-fatty-acyl-phospholipid synthase
Zm00001d013725	1.17E-09	-1.6 ± 0.2	gibberellin 20 oxidase 2|gibberellin 20-oxidase4
Zm00001d003760	0.000244	1.4 ± 0.3	Bifunctional inhibitor/lipid-transfer protein/seed storage 2S albumin superfamily protein
Zm00001d024000	0.012095	1.4 ± 0.3	non-cyanogenic beta-glucosidase|beta-glucosidase3
Zm00001d002801	0.047854	1.3 ± 0.4	GT-2-like 1
Zm00001d020137	0.006738	1.3 ± 0.3	putative WRKY DNA-binding domain superfamily protein
Zm00001d024027	0.001104	-1.2 ± 0.3	proline rich cell wall protein 1
Zm00001d042697	0.001712	1.2 ± 0.3	photosystem II subunit PsbS1
Zm00001d021336	0.02239	-1.2 ± 0.3	Serine/threonine-protein kinase STY17
Zm00001d025623	0.049556	1.1 ± 0.3	Vacuolar iron transporter 1
Zm00001d002346	4.83E-05	1.1 ± 0.2	cinnamyl alcohol dehydrogenase 1
Zm00001d012725	0.001419	1 ± 0.2	Transcription factor TCP4
Zm00001d029923	0.006072	-1 ± 0.2	ctenidin-1|extensin-like protein
Zm00001d003757	0.000225	1 ± 0.2	Bifunctional inhibitor/lipid-transfer protein/seed storage 2S albumin superfamily protein
Zm00001d032386	0.006738	-0.9 ± 0.2	phosphofructose kinase2
Zm00001d033369	0.019292	0.9 ± 0.2	gibberellin-regulated protein 1
Zm00001d031344	0.036655	-0.9 ± 0.2	no description available
Zm00001d035001	0.035805	0.9 ± 0.2	adrenodoxin, mitochondrial|chloroplast ferredoxin 1
Zm00001d026160	0.00022	0.8 ± 0.2	cortical cell-delineating protein|gibberellin responsive 2
Zm00001d031441	0.048839	0.8 ± 0.2	DNA binding protein|putative HLH DNA-binding domain superfamily protein
Zm00001d041819	0.000501	0.8 ± 0.2	photosystem I reaction center subunit N, chloroplastic
Zm00001d015008	0.00022	-0.8 ± 0.1	UTP-glucose-1-phosphate uridylyltransferase 1
Zm00001d049387	0.000225	0.7 ± 0.1	photosystem II 10 kDa polypeptide, chloroplastic|zinc finger protein 3
Zm00001d006110	0.019428	0.6 ± 0.2	Description+A1:D2
Zm00001d037453	0.039732	0.6 ± 0.2	Reticulon-like protein
Zm00001d028759	0.000798	-0.6 ± 0.1	pyruvate decarboxylase 3
Zm00001d033799	0.033594	0.6 ± 0.2	phytochrome A1 apoprotein

V4 ID	FDR p-val.	LFC and SE	Description of the gene.
Zm00001d039081	0.006738	0.6 ± 0.1	CTP synthase family protein
Zm00001d051080	0.041743	-0.6 ± 0.2	Adenine phosphoribosyltransferase 2
Zm00001d043423	0.007525	0.6 ± 0.1	Transcription factor TCP4
Zm00001d016691	0.012533	0.6 ± 0.1	Copper transport protein CCH
Zm00001d042695	0.012533	-0.6 ± 0.1	Serine/threonine-protein kinase SRK2A|SnRK2.4
Zm00001d020353	0.000244	0.6 ± 0.1	Cyclin-D1-1
Zm00001d011051	0.046057	-0.6 ± 0.1	ACT domain-containing protein ACR9
Zm00001d003252	0.028683	-0.5 ± 0.1	glucose-6-phosphate 1-dehydrogenase, cytoplasmic isoform
Zm00001d029365	0.02837	0.5 ± 0.1	non-specific lipid transfer protein-like 1|putative bifunctional inhibitor/LTP/seed storage protein family|xylogen protein 1
Zm00001d033383	2.27E-05	-0.5 ± 0.1	hydroxymethylpyrimidine phosphate synthase1|thiamine biosynthesis protein thiC
Zm00001d039914	0.009086	0.5 ± 0.1	metallothionein-like protein 2A
Zm00001d002261	0.023004	-0.5 ± 0.1	Peroxisomal (S)-2-hydroxy-acid oxidase GLO1
Zm00001d020910	0.006738	-0.5 ± 0.1	induced stolen tip protein TUB8
Zm00001d017121	0.003835	-0.5 ± 0.1	cytosolic glyceroldehyde-3-phosphate dehydrogenase GAPC4
Zm00001d045431	0.000244	-0.4 ± 0.1	enolase 1|2-phospho-D-glycerate hydro-lyase 1|2-phosphoglycerate dehydratase 1
Zm00001d040027	0.006401	-0.4 ± 0.1	Bowman-Birk type wound-induced proteinase inhibitor WIP1
Zm00001d024633	8.77E-06	-0.4 ± 0.1	Monodehydroascorbate reductase 5 mitochondrial
Zm00001d043049	0.035928	0.4 ± 0.1	Non-specific lipid-transfer protein 1
Zm00001d016166	0.019643	-0.4 ± 0.1	phosphoenolpyruvate carboxylase2
Zm00001d053453	0.02295	-0.4 ± 0.1	phosphoenolpyruvate carboxylase 1
Zm00001d047516	0.012806	-0.4 ± 0.1	WEB family protein|putative DUF827 domain containing family protein
Zm00001d033931	0.025598	-0.4 ± 0.1	alcohol dehydrogenase 1
Zm00001d038891	0.040035	-0.3 ± 0.1	Phosphoethanolamine N-methyltransferase 3
Zm00001d048461	0.049041	-0.3 ± 0.1	blue fluorescent 1|blue fluorescent1
Zm00001d039131	0.006738	-0.3 ± 0.1	glucose-1-phosphate adenylyltransferase large subunit 2, chloroplastic/amyloplastic|ADP glucose pyrophosphorylase2
Zm00001d031891	0.041743	-0.3 ± 0.1	Peptidase M1 family protein
Zm00001d026291	0.038148	-0.3 ± 0.1	DNA (cytosine-5)-methyltransferase 1
Zm00001d045069	0.043195	-0.3 ± 0.1	putative 60S ribosomal protein L19-3 family protein
Zm00001d049409	0.013589	-0.3 ± 0.1	aconitase1|Arabidopsis thaliana: Aconitate hydratase 3, mitochondrial

Supplementary Table 4.2. Top 60 significantly (FDR) affected genes in the meristem for the severe versus control contrast. Genes are sorted in descending LFC size (absolute value). Gene descriptions were obtained from NCBI and were manually curated to obtain concise gene descriptions. When no NCBI description was available, the description on Gramene was obtained. If only a description based on homology was available, the species used is also indicated.

V4 ID	FDR pval.	LFC and SE	Description of the gene.
Zm00001d046234	1.66E-07	-7.5 ± 1.2	Inositol oxygenase 2
Zm00001d025055	1.06E-06	6.2 ± 1.1	2C-type protein phosphatase protein
Zm00001d032253	0.000819	6 ± 1.4	putative inositol polyphosphate phosphatase (synaptogenin-like) family protein
Zm00001d016590	3.09E-24	5.7 ± 0.5	sugars will eventually be exported transporter15b
Zm00001d034259	0.001286	-5.5 ± 1.3	probable nucleolar protein 5-1
Zm00001d048694	0.001753	5.4 ± 1.3	no description available
Zm00001d041670	4.76E-06	5.1 ± 0.9	phytase2
Zm00001d032138	0.0067	5 ± 1.4	no description available
Zm00001d019163	4.89E-10	4.9 ± 0.7	alkaline alpha galactosidase 1|stachyose synthase
Zm00001d007341	8.45E-09	4.9 ± 0.7	HVA22-like protein e
Zm00001d025665	0.001201	4.8 ± 1.2	putative amino acid permease 7
Zm00001d050577	3.50E-06	4.6 ± 0.8	sugars will eventually be exported transporter15a
Zm00001d029654	3.61E-07	4.5 ± 0.8	trehalase1
Zm00001d037909	0.017487	4.4 ± 1.3	NRR repressor homolog 1
Zm00001d039364	0.000617	4.3 ± 1	4-methyl-5-thiazole monophosphate biosynthesis protein
Zm00001d042862	8.68E-14	4.3 ± 0.5	Lipid binding protein
Zm00001d045036	0.001388	4.2 ± 1	dnaJ homolog subfamily B member 3|Chaperone DnaJ-domain superfamily protein
Zm00001d037894	0.001395	4.1 ± 1	dehydrin DHN1|responsive to abscisic acid17
Zm00001d003760	9.98E-59	4.1 ± 0.2	lipid binding protein|Bifunctional inhibitor/lipid-transfer protein/seed storage 2S albumin superfamily protein
Zm00001d036965	3.14E-53	3.9 ± 0.2	Zinc transporter 4
Zm00001d016255	3.36E-13	3.8 ± 0.5	heat shock factor protein 1|Heat stress transcription factor C-1
Zm00001d038997	0.014585	-3.8 ± 1.1	no description available
Zm00001d023332	1.12E-08	3.6 ± 0.6	WRKY-type transcription factor
Zm00001d020552	0.039496	3.6 ± 1.2	senescence-associated protein DH|Tetraspanin-7
Zm00001d023443	0.000662	3.5 ± 0.8	light-inducible protein CPRF2|Basic-leucine zipper (bZIP) transcription factor family protein
Zm00001d042541	0.004078	3.5 ± 0.9	linoleate 9S-lipoxygenase1
Zm00001d045883	0.023852	3.4 ± 1.1	sodium/hydrogen exchanger 4
Zm00001d047418	0.000496	3.4 ± 0.8	Cytochrome P450 709B2
Zm00001d029038	2.52E-06	-3.4 ± 0.6	HAD superfamily subfamily IIIB acid phosphatase
Zm00001d015905	6.74E-13	3.3 ± 0.4	sugars will eventually be exported transporter4a
Zm00001d011687	0.000507	3.2 ± 0.7	IAA-amino acid hydrolase ILR1-like 4

V4 ID	FDR pval.	LFC and SE	Description of the gene.
Zm00001d020717	2.00E-21	3.2 ± 0.3	abscisic acid 8'-hydroxylase4|putative cytochrome P450 superfamily protein
Zm00001d034558	5.05E-05	3.2 ± 0.6	Remorin
Zm00001d008983	5.20E-05	3.1 ± 0.6	P-loop containing nucleoside triphosphate hydrolases superfamily protein
Zm00001d018838	0.004543	3.1 ± 0.8	*Oryza sativa Japonica Group*: Similar to B0616E02-H0507E05.5 protein
Zm00001d013725	2.28E-30	-3.1 ± 0.3	gibberellin 20 oxidase 2|gibberellin 20-oxidase4
Zm00001d003776	0.042664	-3.1 ± 1.1	miniature seed 1|cell wall invertase 2
Zm00001d039194	0.002767	3.1 ± 0.8	RNA polymerase sigma factor sigE, chloroplastic/mitochondrial
Zm00001d005996	0.003377	3.1 ± 0.8	photosystem I reaction center subunit V
Zm00001d019228	0.000846	3 ± 0.7	ZIP zinc/iron transport family protein
Zm00001d042922	4.69E-14	3 ± 0.4	heat shock 70 kDa protein-like|putative mediator of RNA polymerase II transcription subunit 37c
Zm00001d052063	2.43E-05	3 ± 0.6	Transmembrane amino acid transporter family protein
Zm00001d041853	0.040845	3 ± 1	transcription factor MYB8
Zm00001d046937	2.89E-13	-3 ± 0.4	Basic leucine zipper 9|bZIP transcription factor|light-inducible protein CPRF-2
Zm00001d031325	0.037418	2.9 ± 1	25.3 kDa heat shock protein chloroplastic
Zm00001d003757	6.37E-62	2.9 ± 0.2	Bifunctional inhibitor/lipid-transfer protein/seed storage 2S albumin superfamily protein
Zm00001d024000	4.08E-16	2.9 ± 0.3	non-cyanogenic beta-glucosidase|beta-glucosidase3
Zm00001d018298	1.55E-37	2.9 ± 0.2	17.4 kDa class III heat shock protein
Zm00001d050099	0.044134	2.9 ± 1	no description available
Zm00001d001915	0.03574	2.9 ± 1	metal ion binding protein
Zm00001d047659	0.000746	2.8 ± 0.7	nitric oxide synthase interacting protein|phosphoinositide binding
Zm00001d028588	0.04556	2.8 ± 1	*Arabidopsis thaliana*: Fes1A
Zm00001d028561	0.029244	2.8 ± 0.9	class I heat shock protein 3|17.4 kDa class I heat shock protein
Zm00001d014816	0.022268	2.8 ± 0.9	Senescence-associated protein DIN1
Zm00001d040545	0.000346	2.8 ± 0.6	no description available
Zm00001d022069	0.000458	2.8 ± 0.6	ninja-family protein 5|putative DUF1675 domain containing family protein
Zm00001d029853	4.69E-19	-2.7 ± 0.3	proline oxidase
Zm00001d041827	1.58E-05	-2.7 ± 0.5	peroxidase 43|Peroxidase superfamily protein
Zm00001d038913	2.63E-11	2.7 ± 0.4	nonspecific lipid-transfer protein AKCS9|lipid transfer protein1
Zm00001d031934	0.018959	2.7 ± 0.8	Chlorophyllase-1

Supplementary Table 4.3. Top 60 significantly (FDR) affected genes in the meristem for the severe versus mild contrast. Genes are sorted in descending LFC size (absolute value). Gene descriptions were obtained from NCBI and were manually curated to obtain concise gene descriptions. When no NCBI description was available, the description on Gramene was obtained. If only a description based on homology was available, the species used is also indicated.

V4 ID	FDR pval.	LFC and SE	Description of the gene.
Zm00001d046234	8.59E-06	-6.8 ± 1.2	Inositol oxygenase 2
Zm00001d025055	2.07E-06	6.1 ± 1.1	probable protein phosphatase 2C 37
Zm00001d019704	0.003755	5.7 ± 1.4	*Triticum turgidum* subsp. *durum*: vamp/synaptobrevin-associated protein 27-2 G
Zm00001d044124	0.004108	5.6 ± 1.4	SNF1-related protein kinase regulatory subunit gamma-1
Zm00001d050577	5.49E-05	5.6 ± 1.1	sugars will eventually be exported transporter15a
Zm00001d048694	0.004673	5.3 ± 1.3	no description available
Zm00001d010373	0.021382	5.1 ± 1.5	stem 28 kDa glycoprotein|Stem glycoprotein
Zm00001d016590	6.37E-27	4.8 ± 0.4	sugars will eventually be exported transporter15b
Zm00001d038997	0.001879	-4.8 ± 1.1	*Triticum turgidum* subsp. *durum*: Clavata3/ESR (CLE) gene family member G
Zm00001d041670	7.60E-06	4.6 ± 0.8	phytase2
Zm00001d042541	0.000619	4.5 ± 1	linoleate 9S-lipoxygenase1
Zm00001d032253	0.044982	4.1 ± 1.3	putative inositol polyphosphate phosphatase (synaptogenin-like) family protein
Zm00001d037894	0.00375	4.1 ± 1	dehydrin DHN1|responsive to abscisic acid17
Zm00001d019163	2.04E-09	4.1 ± 0.6	alkaline alpha galactosidase 1|stachyose synthase
Zm00001d011687	0.000534	4 ± 0.9	IAA-amino acid hydrolase ILR1-like 4
Zm00001d029038	3.33E-08	-3.9 ± 0.6	acid phosphatase 1|HAD superfamily subfamily IIIB acid phosphatase
Zm00001d019110	0.004597	3.9 ± 1	60S ribosomal protein L10a
Zm00001d007341	5.95E-08	3.5 ± 0.5	HVA22-like protein e
Zm00001d037769	4.56E-11	3.4 ± 0.5	C3H39 C3H type transcription factor|Zinc finger CCCH domain-containing protein 23
Zm00001d042862	2.66E-11	3.3 ± 0.4	Lipid binding protein
Zm00001d016255	4.93E-09	3.1 ± 0.5	heat shock factor protein 1|Heat stress transcription factor C-1
Zm00001d037724	0.018679	3.1 ± 0.9	gibberellin 2-beta-dioxygenase
Zm00001d029654	8.89E-06	3.1 ± 0.6	trehalase1
Zm00001d019228	0.002189	3 ± 0.7	ZIP zinc/iron transport family protein
Zm00001d009626	0.026794	3 ± 0.9	2C-type protein phosphatase protein
Zm00001d022069	0.000546	2.9 ± 0.7	ninja-family protein 5|putative DUF1675 domain containing family protein
Zm00001d008983	0.00028	2.9 ± 0.6	P-loop containing nucleoside triphosphate hydrolases superfamily protein
Zm00001d033797	0.048694	2.9 ± 0.9	alpha/beta-Hydrolases superfamily protein
Zm00001d025354	6.28E-14	-2.9 ± 0.3	Beta-fructofuranosidase insoluble isoenzyme CWINV2
Zm00001d042540	2.51E-07	2.9 ± 0.5	Linoleate 9S-lipoxygenase 1
Zm00001d036965	2.17E-37	2.9 ± 0.2	Zinc transporter 4

V4 ID	FDR pval.	LFC and SE	Description of the gene.
Zm00001d028838	0.003735	2.8 ± 0.7	long cell-linked locus protein
Zm00001d023443	0.006472	2.8 ± 0.7	light-inducible protein CPRF2|Basic-leucine zipper (bZIP) transcription factor family protein
Zm00001d040028	6.82E-14	2.8 ± 0.3	*Zea mays*: Bowman-Birk type wound-induced proteinase inhibitor WIP1
Zm00001d035646	0.020452	-2.7 ± 0.8	protein kinase|putative DUF26 domain family protein
Zm00001d029087	5.08E-06	2.7 ± 0.5	sucrose synthase 4|Sucrose synthase 3
Zm00001d003760	1.08E-39	2.7 ± 0.2	lipid binding protein|Bifunctional inhibitor/lipid-transfer protein/seed storage 2S albumin superfamily protein
Zm00001d042768	0.026084	-2.7 ± 0.8	hevamine-A
Zm00001d046937	4.10E-10	-2.7 ± 0.4	Basic leucine zipper 9|bZIP transcription factor|light-inducible protein CPRF-2
Zm00001d020717	8.40E-16	2.6 ± 0.3	abscisic acid 8'-hydroxylase4|putative cytochrome P450 superfamily protein
Zm00001d039936	0.028842	2.6 ± 0.8	16.9 kDa class I heat shock protein 1|17.4 kDa class I heat shock protein
Zm00001d025665	0.019261	2.6 ± 0.7	putative amino acid permease 7
Zm00001d023592	0.018672	-2.6 ± 0.7	amino acid permease 3|Amino acid permease 2
ENSRNA049469775	1.29E-08	-2.5 ± 0.4	Early nodulin 40
Zm00001d052063	0.000517	2.5 ± 0.6	Transmembrane amino acid transporter family protein
Zm00001d018195	6.37E-08	-2.4 ± 0.4	WAT1-related protein
Zm00001d045036	0.042933	2.4 ± 0.8	dnaJ homolog subfamily B member 3|Chaperone DnaJ-domain superfamily protein
Zm00001d041827	0.000526	-2.4 ± 0.5	peroxidase 43|Peroxidase superfamily protein
Zm00001d029853	1.72E-13	-2.4 ± 0.3	proline oxidase
Zm00001d052947	0.001613	2.4 ± 0.6	DNAJ heat shock N-terminal domain-containing protein
Zm00001d047259	0.001622	2.3 ± 0.6	no description available
Zm00001d042922	2.88E-08	2.3 ± 0.4	heat shock 70 kDa protein-like|putative mediator of RNA polymerase II transcription subunit 37c
Zm00001d018751	0.003842	-2.3 ± 0.6	Amino acid permease 6
Zm00001d028793	0.000585	-2.3 ± 0.5	abscisic acid receptor PYL4-like|Abscisic acid receptor PYL5|pyrabactin resistance-like protein
Zm00001d015905	9.95E-08	2.2 ± 0.4	sugars will eventually be exported transporter4a
Zm00001d044300	0.019142	2.2 ± 0.6	PIF / Ping-Pong family of plant transposases
Zm00001d038913	4.97E-08	2.2 ± 0.3	nonspecific lipid-transfer protein AKCS9|lipid transfer protein1
Zm00001d022518	1.85E-10	-2.1 ± 0.3	Thioredoxin-like 1-1 chloroplastic|pco089198(579)|putative thioredoxin superfamily protein|thioredoxin-like 1
Zm00001d052537	0.049186	2.1 ± 0.7	ZCN6 protein|RCN1 - Corn Centroradialis/TFL1-like protein|RCN1-Corn Centroradialis/TFL1-like protein
Zm00001d044301	6.42E-19	2.1 ± 0.2	2C-type protein phosphatase protein|protein phosphatase 2C ABI2

Supplementary Table 4.4. Top 60 significantly (FDR) affected genes in the elongation zone for the mild versus control contrast. Genes are sorted in descending LFC size (absolute value). Gene descriptions were obtained from NCBI and were manually curated to obtain concise gene descriptions. When no NCBI description was available, the description on Gramene was obtained. If only a description based on homology was available, the species used is also indicated.

V4 ID	FDR	LFC and SE	Description of the gene.
Zm00001d032253	0.044269	4.1 ± 1.3	Type IV inositol polyphosphate 5-phosphatase 9
Zm00001d038163	2.09E-06	2.9 ± 0.5	pyruvate, phosphate dikinase 1, chloroplastic
Zm00001d023332	2.32E-05	2.9 ± 0.6	WRKY-type transcription factor
Zm00001d039617	1.33E-05	-2.2 ± 0.4	kinesin-like protein KIN-14A|P-loop nucleoside triphosphate hydrolase superfamily protein with CH (Calponin Homology) domain
Zm00001d013150	0.042472	-2.2 ± 0.7	Protein JASON
Zm00001d048020	0.006135	-2 ± 0.5	class 1 nonsymbiotic hemoglobin|reversible oxygen binding
Zm00001d005775	0.027195	2 ± 0.6	cellulose synthase A catalytic subunit 9|Cellulose synthase A catalytic subunit 7|cellulose synthase catalytic subunit 13
Zm00001d048593	1.53E-07	2 ± 0.3	ribulose bisphosphate carboxylase/oxygenase activase, chloroplastic|RUBISCO activase2
Zm00001d029290	3.99E-10	2 ± 0.3	cytochrome P450 709B2
Zm00001d017711	2.52E-06	1.9 ± 0.3	Phosphoribulokinase
Zm00001d017065	0.025004	1.9 ± 0.6	putative dnaJ chaperone family protein
Zm00001d028367	0.000591	-1.9 ± 0.4	Purple acid phosphatase 3|purple acid phosphatase 1
Zm00001d027431	2.29E-05	1.8 ± 0.4	homeobox protein HD1|knotted related homeobox1|putative knotted-like transcription factor family protein
Zm00001d047276	0.003569	1.8 ± 0.5	brittle stalk-2COBRA-like protein 4
Zm00001d008737	0.015268	-1.8 ± 0.5	acyl-protein thioesterase 2
Zm00001d028195	0.002157	-1.8 ± 0.4	TPX2 (targeting protein for Xklp2) protein family
Zm00001d027589	0.001387	-1.8 ± 0.4	nucleolin-like
Zm00001d031224	0.000575	-1.8 ± 0.4	uncharacterized protein
Zm00001d025762	0.002306	-1.8 ± 0.4	*Oryza sativa Japonica Group*: Similar to H0306B06.4 protein
Zm00001d015623	0.034535	1.8 ± 0.6	limonoid UDP-glucosyltransferase
Zm00001d033193	0.000514	-1.7 ± 0.4	Serine-threonine protein kinase plant-type
Zm00001d042498	0.011483	-1.7 ± 0.5	QWRF motif-containing protein 6
Zm00001d013716	0.016691	1.7 ± 0.5	putative RING zinc finger domain superfamily protein|putative E3 ubiquitin-protein ligase ARI2
Zm00001d032828	0.04717	1.7 ± 0.6	Citrate transporter family protein
Zm00001d003751	3.03E-08	1.7 ± 0.3	NDR1/HIN1-like 1|VAMP protein SEC22
Zm00001d039638	9.81E-07	-1.7 ± 0.3	*Brassica napus*: BnaA01g28640D protein
Zm00001d019462	0.005918	-1.7 ± 0.4	rac GTPase activating protein
Zm00001d042527	0.000211	-1.7 ± 0.4	*Oryza sativa Japonica Group*: Similar to JHL23J11.5 protein
Zm00001d014319	8.27E-08	-1.7 ± 0.3	transcriptional regulatory protein algP
Zm00001d023450	0.000252	1.7 ± 0.4	Cationic amino acid transporter 6 chloroplastic
Zm00001d018552	0.031044	-1.6 ± 0.5	*Oryza sativa Japonica Group*: Similar to SKIP interacting protein 16

V4 ID	FDR	LFC and SE	Description of the gene.
Zm00001d025580	0.026842	1.6 ± 0.5	somatic embryogenesis receptor-like kinase 1|putative leucine-rich repeat receptor-like protein kinase family protein
Zm00001d032805	0.003566	-1.6 ± 0.4	shugoshin-1
Zm00001d040126	0.005172	1.6 ± 0.4	no description available
Zm00001d002939	5.09E-10	1.6 ± 0.2	multiple C2 and transmembrane domain-containing protein 2-like|C2 calcium/lipid-binding plant phosphoribosyltransferase family protein
Zm00001d015863	0.001069	-1.6 ± 0.4	mitotic spindle checkpoint component mad3
Zm00001d051362	1.21E-11	1.6 ± 0.2	aquaporin TIP2-1|tonoplast intrinsic protein 2-1|tonoplast membrane integral protein ZmTIP2-1
Zm00001d025869	0.034535	1.6 ± 0.5	integral membrane protein like protein|Nucleotide/sugar transporter family protein
Zm00001d004626	0.003012	1.6 ± 0.4	Probable beta-D-xylosidase 7
Zm00001d051110	4.25E-12	-1.6 ± 0.2	GDSL esterase/lipase LTL1|anther-specific proline-rich protein APG
Zm00001d048299	0.042257	-1.5 ± 0.5	*Zea mays*: Polyadenylate-binding protein RBP47B'
Zm00001d047853	0.028082	1.5 ± 0.5	putative serine/threonine-protein kinase
Zm00001d006237	0.001621	-1.5 ± 0.4	Protein POLLENLESS 3-LIKE 2
Zm00001d011486	4.15E-06	-1.5 ± 0.3	CTP synthase
Zm00001d030101	0.004674	-1.5 ± 0.4	*Arabidopsis thaliana*: Chalcone-flavanone isomerase family
Zm00001d032776	0.001296	1.5 ± 0.4	cellulose synthase catalytic subunit 10
Zm00001d021583	4.35E-06	-1.5 ± 0.3	Protein TPX2
Zm00001d022254	0.049479	1.5 ± 0.5	Haloacid dehalogenase-like hydrolase (HAD) superfamily protein
Zm00001d053272	0.008372	-1.5 ± 0.4	Reticulon-like protein B17
Zm00001d015802	7.97E-08	-1.5 ± 0.2	*Triticum turgidum* subsp. *durum*: Pesticidal crystal cry8Ba G
Zm00001d043413	4.26E-06	-1.5 ± 0.3	Putative uncharacterized protein
Zm00001d014495	0.019932	-1.5 ± 0.4	*Oryza sativa Japonica Group*: Similar to OSIGBa0115M15.5 protein
Zm00001d036360	0.000156	-1.5 ± 0.3	Cyclin-B2-4
Zm00001d035003	1.69E-05	1.5 ± 0.3	ferredoxin-2, chloroplastic
Zm00001d023559	7.23E-14	1.5 ± 0.2	Fructose-bisphosphate aldolase
Zm00001d052368	0.031606	-1.5 ± 0.5	Expressed protein
Zm00001d043451	0.002721	-1.4 ± 0.4	Dynamin-related protein 5A
Zm00001d024199	0.000244	1.4 ± 0.3	ATP binding protein|putative protein kinase superfamily protein|putative receptor-like serine/threonine-protein kinase
Zm00001d011661	5.84E-05	1.4 ± 0.3	GDSL esterase/lipase APG
Zm00001d052910	0.004715	1.4 ± 0.4	*Triticum turgidum* subsp. *durum*: Elongation factor 4 G

Supplementary Table 4.5. Top 60 significantly (FDR) affected genes in the elongation zone for the severe versus control contrast. Genes are sorted in descending LFC size (absolute value). Gene descriptions were obtained from NCBI and were manually curated to obtain concise gene descriptions. When no NCBI description was available, the description on Gramene was obtained. If only a description based on homology was available, the species used is also indicated.

V4 ID	FDR pval.	LFC and SE	Description of the gene.
Zm00001d010586	3.21E-09	8.2 ± 1.3	PEBP (phosphatidylethanolamine-binding protein) family protein
Zm00001d032253	2.17E-06	6.9 ± 1.3	putative inositol polyphosphate phosphatase (synaptogenin-like) family protein|Type IV inositol polyphosphate 5-phosphatase 9
Zm00001d037894	0.001274	6.7 ± 1.7	dehydrin DHN1|responsive to abscisic acid17
Zm00001d045456	2.10E-06	6.7 ± 1.3	Zinc finger (C3HC4-type RING finger) family protein
Zm00001d027870	9.95E-05	6.2 ± 1.4	AP2-EREBP transcription factor|Dehydration-responsive element-binding protein 2F
Zm00001d030305	3.98E-47	-5.4 ± 0.4	Proline-rich protein 2
Zm00001d030316	3.45E-10	-5.3 ± 0.8	Proline-rich protein 2
Zm00001d038997	0.000972	-5.3 ± 1.4	*Triticum turgidum* subsp. *durum*: Clavata3/ESR (CLE) gene family member G
Zm00001d004626	2.09E-05	-5.3 ± 1.1	Probable beta-D-xylosidase 7
Zm00001d029087	0.000122	5.2 ± 1.2	sucrose synthase 4|Sucrose synthase 3|putative sucrose synthase family protein
Zm00001d032144	0.001213	-5.2 ± 1.3	AP2-EREBP transcription factor|putative AP2/EREBP transcription factor superfamily protein
Zm00001d014971	5.12E-07	-5.1 ± 0.9	MDIS1-interacting receptor like kinase 1|Leucine-rich repeat receptor-like protein kinase PXL1
Zm00001d027627	0.003145	5.1 ± 1.4	subtilisin-like protease SBT1.2
Zm00001d052684	0.002275	-5.1 ± 1.4	O-methyltransferase ZRP4
Zm00001d010655	0.002121	-5 ± 1.4	WAT1-related protein
Zm00001d024734	0.002229	-4.9 ± 1.3	Peroxidase 2|putative class III secretory plant peroxidase family protein
Zm00001d020955	0.004706	-4.8 ± 1.4	WAK80 - OsWAK receptor-like protein kinase
Zm00001d024982	0.005468	-4.8 ± 1.4	ricin B-like lectin EULS3
Zm00001d035907	0.01118	-4.7 ± 1.5	Homeobox protein BEL1-like protein|putative POX domain/homeobox DNA-binding domain family protein
Zm00001d049625	0.009489	-4.6 ± 1.4	Protein LSD1
Zm00001d002679	0.008271	-4.6 ± 1.4	mechanosensitive ion channel protein 6
Zm00001d036366	0.00873	-4.6 ± 1.4	Basic endochitinase B
Zm00001d013448	6.33E-08	-4.3 ± 0.7	chemocyanin
Zm00001d014583	0.013919	-4.3 ± 1.4	putative protein kinase superfamily protein
Zm00001d036237	3.47E-13	-4.3 ± 0.5	alpha-L-fucosidase 2|GDSL esterase/lipase
Zm00001d026401	1.33E-13	4.2 ± 0.5	Protein EPIDERMAL PATTERNING FACTOR 2
Zm00001d003760	1.34E-22	4.2 ± 0.4	lipid binding protein|Bifunctional inhibitor/lipid-transfer protein/seed storage 2S albumin superfamily protein
Zm00001d045495	0.016581	-4.2 ± 1.4	short-chain dehydrogenase TIC 32, chloroplastic-like|NAD(P)-binding Rossmann-fold superfamily protein
Zm00001d048471	0.025019	-4.1 ± 1.4	Putative knotted-like transcription factor family protein|homeobox protein HD1
Zm00001d024839	1.73E-18	-4.1 ± 0.4	glutathione S-transferase 4

V4 ID	FDR pval.	LFC and SE	Description of the gene.
Zm00001d047799	6.91E-05	4 ± 0.9	Heat shock 70 kDa protein 5
Zm00001d015477	2.34E-09	4 ± 0.6	Protein ECERIFERUM 3
Zm00001d004921	4.76E-06	-4 ± 0.8	O-methyltransferase ZRP4|benzoxazinone synthesis14
Zm00001d040659	0.017311	4 ± 1.4	late embryogenesis abundant protein Lea5-D-like|Late embryogenesis abundant protein Lea5
Zm00001d047437	0.017567	-4 ± 1.3	putative protein kinase superfamily protein
Zm00001d014055	0.003605	-4 ± 1.1	Protein ECERIFERUM 1
Zm00001d046234	1.01E-47	-4 ± 0.3	Inositol oxygenase 2
Zm00001d020613	0.002425	4 ± 1.1	*Triticum turgidum* subsp. *durum*: Erect panicle 2 protein G
Zm00001d040089	5.08E-14	-3.9 ± 0.5	nodulin-like protein|nodulin MtN21 /EamA-like transporter family protein
Zm00001d043538	1.37E-08	-3.9 ± 0.6	BURP domain protein RD22
Zm00001d022518	1.10E-23	-3.9 ± 0.4	Thioredoxin-like 1-1 chloroplastic
Zm00001d038891	3.07E-158	3.9 ± 0.1	Phosphoethanolamine N-methyltransferase 3
Zm00001d022233	0.028657	-3.8 ± 1.4	*Triticum turgidum* subsp. *durum*: 50S ribosomal protein L17 G
Zm00001d003301	0.042072	-3.8 ± 1.5	C2 and GRAM domain-containing protein At5g50170
Zm00001d014996	0.041403	-3.8 ± 1.4	phytosulfokine receptor 1|putative phytosulfokine receptor (LRR repeat-containing protein kinase) family protein
Zm00001d038692	0.04313	-3.8 ± 1.4	no description available
Zm00001d044685	2.91E-11	-3.8 ± 0.5	Non-specific lipid-transfer protein|nonspecific lipid-transfer protein 3
Zm00001d037468	0.015311	-3.7 ± 1.2	phosphate transporter PHO1-3|phosphate transporter4
Zm00001d021813	7.37E-08	-3.7 ± 0.6	pco107293(576)
Zm00001d019163	4.63E-08	3.7 ± 0.6	alkaline alpha galactosidase 1|stachyose synthase
Zm00001d031878	0.000229	3.7 ± 0.9	proline-rich family protein|AC186231.4_FGT002
Zm00001d008983	1.38E-06	3.7 ± 0.7	P-loop containing nucleoside triphosphate hydrolases superfamily protein
Zm00001d023664	0.022515	3.7 ± 1.3	ABA-responsive protein
Zm00001d042768	0.016073	-3.7 ± 1.2	Hevamine-A
Zm00001d052532	4.36E-06	-3.7 ± 0.7	Major facilitator superfamily protein
Zm00001d048694	3.56E-15	3.7 ± 0.4	no description available
Zm00001d028505	0.000144	-3.7 ± 0.8	Phospholipase A2-alpha|phospholipase A2
Zm00001d008248	0.013048	-3.6 ± 1.2	*Triticum turgidum* subsp. *durum*: Transcription factor jumonji (jmjC) domain-containing protein G
Zm00001d032608	9.14E-13	3.6 ± 0.5	alpha-galactosidase
Zm00001d022380	0.015257	-3.6 ± 1.2	Glycosyltransferase family 61 protein

Supplementary Table 4.6. Top 60 significantly (FDR) affected genes in the elongation zone for the severe versus mild contrast. Genes are sorted in descending LFC size (absolute value). Gene descriptions were obtained from NCBI and were manually curated to obtain concise gene descriptions. When no NCBI description was available, the description on Gramene was obtained. If only a description based on homology was available, the species used is also indicated.

V4 ID	FDR pval.	LFC and SE	Description of the gene.
Zm00001d010586	6.99E-09	7.9 ± 1.3	PEBP (phosphatidylethanolamine-binding protein) family protein
Zm00001d037894	0.000232	7.3 ± 1.7	dehydrin DHN1|responsive to abscisic acid17
Zm00001d015477	4.29E-07	6.9 ± 1.2	Protein ECERIFERUM 3
Description of the gene.A1:C2	1.90E-06	-6.9 ± 1.3	Peroxidase 2|putative class III secretory plant peroxidase family protein
Zm00001d004626	4.46E-09	-6.8 ± 1.1	Probable beta-D-xylosidase 7
Zm00001d030316	3.13E-16	-6.7 ± 0.8	Proline-rich protein 2
Zm00001d026401	2.50E-08	6.5 ± 1.1	Protein EPIDERMAL PATTERNING FACTOR 2
Zm00001d030305	2.53E-64	-6.3 ± 0.4	Proline-rich protein 2
Zm00001d052684	7.35E-05	-6.1 ± 1.4	O-methyltransferase ZRP4
Zm00001d032144	5.20E-05	-6.1 ± 1.3	AP2-EREBP transcription factor
Zm00001d010655	5.73E-05	-6.1 ± 1.3	WAT1-related protein
Zm00001d003301	0.000161	-6 ± 1.4	C2 and GRAM domain-containing protein
Zm00001d038997	9.51E-05	-5.9 ± 1.3	*Triticum turgidum* subsp. *durum*: Clavata3/ESR (CLE) gene family member G
Zm00001d002679	0.000366	-5.7 ± 1.4	mechanosensitive ion channel protein 6
Zm00001d048471	0.000503	-5.6 ± 1.4	AY106075_IDP|Putative knotted-like transcription factor family protein|homeobox protein HD1
Zm00001d042030	0.000133	5.6 ± 1.3	*Triticum turgidum* subsp. *durum*: HPr kinase/phosphorylase G
Zm00001d028229	0.000688	5.6 ± 1.4	myosin-related
Zm00001d030328	1.83E-08	5.5 ± 0.9	acyl-[acyl-carrier-protein] desaturase 6, chloroplastic-like|stearoyl-acyl-carrier-protein desaturase4
Zm00001d040659	0.001139	5.5 ± 1.5	late embryogenesis abundant protein Lea5-D-like
Zm00001d035907	0.001785	-5.4 ± 1.5	Homeobox protein BEL1-like protein|putative POX domain/homeobox DNA-binding domain family protein
Zm00001d042656	1.74E-05	5.3 ± 1.1	beta-galactosidase 7|Beta-galactosidase 16
Zm00001d049625	0.001311	-5.3 ± 1.4	protein LOL4|Protein LSD1
Zm00001d044604	0.002459	-5.3 ± 1.5	Putative serine/threonine-protein kinase-like protein CCR3|receptor protein kinase CRINKLY4
Zm00001d036237	4.80E-21	-5.3 ± 0.5	alpha-L-fucosidase 2|GDSL esterase/lipase
Zm00001d047437	0.000554	-5.3 ± 1.3	putative protein kinase superfamily protein
Zm00001d008934	0.004616	-5.2 ± 1.5	GDSL esterase/lipase At1g28640
Zm00001d042141	0.001431	-5.1 ± 1.4	lichenase-2
Zm00001d005293	0.000627	5.1 ± 1.3	*Arabidopsis thaliana*: Cyclin-D3-1
Zm00001d044685	2.66E-21	-5.1 ± 0.5	nonspecific lipid-transfer protein 3
Zm00001d041377	0.003265	-5.1 ± 1.5	no description available
Zm00001d023984	0.001174	5.1 ± 1.4	GDSL-motif lipase/hydrolase-like protein
Zm00001d029270	0.003711	5.1 ± 1.5	Heat stress transcription factor B-4

V4 ID	FDR pval.	LFC and SE	Description of the gene.
Zm00001d048421	0.005364	5.1 ± 1.5	*Triticum turgidum* subsp. *durum*: DUF639 family protein
Zm00001d038202	0.005657	-5.1 ± 1.5	no description available
Zm00001d038726	0.003735	-5.1 ± 1.5	GDSL esterase/lipase At4g18970
Zm00001d014055	7.68E-05	-5 ± 1.1	Protein ECERIFERUM 1|Arabidopsis thaliana: Fatty acid hydroxylase superfamily
Zm00001d013448	4.39E-11	-5 ± 0.7	chemocyanin
Zm00001d037550	0.00605	5 ± 1.5	peroxidase 5
Zm00001d035604	0.004976	-5 ± 1.5	putative MYB DNA-binding domain superfamily protein
Zm00001d014971	8.18E-07	-5 ± 0.9	MDIS1-interacting receptor like kinase 1|Leucine-rich repeat receptor-like protein kinase PXL1
Zm00001d033063	0.008543	-5 ± 1.6	protein DETOXIFICATION 40|putative MATE efflux family protein
Zm00001d027870	0.002307	4.9 ± 1.4	AP2-EREBP transcription factor|Dehydration-responsive element-binding protein 2F
Zm00001d021813	1.24E-13	-4.9 ± 0.6	*Triticum turgidum* subsp. *durum*: Leucine-rich repeat protein kinase family protein G
Zm00001d033709	0.004997	4.9 ± 1.5	Basic blue protein
Zm00001d040089	1.03E-22	-4.9 ± 0.5	nodulin-like protein|nodulin MtN21 /EamA-like transporter family protein
Zm00001d005190	0.003742	-4.9 ± 1.4	cadmium/zinc-transporting ATPase HMA3|Cadmium/zinc-transporting ATPase HMA2|putative inactive cadmium/zinc-transporting ATPase HMA3
Zm00001d003751	1.18E-28	-4.9 ± 0.4	NDR1/HIN1-like 1|VAMP protein SEC22
Zm00001d031426	0.007119	-4.8 ± 1.5	protein kinase|putative protein kinase superfamily protein
Zm00001d053094	0.008489	-4.8 ± 1.5	tartrate-resistant acid phosphatase type 5|Purple acid phosphatase 3
Zm00001d032740	5.14E-06	-4.8 ± 0.9	protein NRT1/ PTR FAMILY 5.2
Zm00001d008983	5.54E-06	4.8 ± 0.9	P-loop containing nucleoside triphosphate hydrolases superfamily protein
Zm00001d018803	0.021331	-4.8 ± 1.7	putative inositol transporter 2
Zm00001d027627	0.004862	4.7 ± 1.4	subtilisin-like protease SBT1.2|putative subtilase family protein|subtilisin-like protease SDD1
Zm00001d014958	0.017769	-4.7 ± 1.6	putative cytochrome P450 superfamily protein|cytochrome P450 family 87 subfamily A polypeptide 6
Zm00001d030220	0.021198	-4.7 ± 1.7	monoglyceride lipase|alpha/beta-Hydrolases superfamily protein
Zm00001d041376	0.010008	-4.7 ± 1.5	putative transcription factor KAN4
Zm00001d003354	0.00842	-4.7 ± 1.5	ABC transporter G family member 51|ABC transporter G family member 31|pleiotropic drug resistance protein 13
Zm00001d002939	1.28E-41	-4.7 ± 0.3	multiple C2 and transmembrane domain-containing protein 2-like|C2 calcium/lipid-binding plant phosphoribosyltransferase family protein
Zm00001d022233	0.00336	-4.7 ± 1.4	*Triticum turgidum* subsp. *durum*: 50S ribosomal protein L17 G
Zm00001d021720	0.014449	-4.7 ± 1.6	*Triticum turgidum* subsp. *durum*: DNA-directed RNA polymerase subunit beta' G

Supplementary Table 4.7. Top 60 significantly (FDR) affected genes in the mature zone for the mild versus control contrast. Genes are sorted in descending LFC size (absolute value). Gene descriptions were obtained from NCBI and were manually curated to obtain concise gene descriptions. When no NCBI description was available, the description on Gramene was obtained. If only a description based on homology was available, the species used is also indicated.

V4 ID	FDR pval.	LFC and SE	Description of the gene.
Zm00001d027810	0.040954	6.9 ± 2.5	glycerol-3-phosphate acyltransferase 5
Zm00001d040265	8.71E-05	6.8 ± 1.5	glycerol-3-phosphate acyltransferase 1
Zm00001d029708	9.79E-06	-6.8 ± 1.3	glutathione S-transferase GST 30
Zm00001d020492	1.29E-05	6.5 ± 1.3	WRKY transcription factor
Zm00001d035854	1.86E-05	5.8 ± 1.1	fatty acid alpha-dioxygenase
Zm00001d043837	1.02E-07	-5.6 ± 0.9	transcription factor MYB4|MYB36
Zm00001d030314	7.01E-12	-4.8 ± 0.6	proline-rich protein
Zm00001d044765	0.013978	4.7 ± 1.4	anthranilate O-methyltransferase 2
Zm00001d044402	0.043571	4.6 ± 1.6	chlorophyll a-b binding protein of LHCII type 1
Zm00001d029816	0.003375	4.6 ± 1.2	Pollen Ole e 1 allergen and extensin family protein
Zm00001d030670	0.014698	4.5 ± 1.4	calcium binding EF-hand protein|putative peroxygenase 4
Zm00001d042940	0.009678	4.5 ± 1.3	plant-specific domain TIGR01589 family protein expressed
Zm00001d007349	0.022326	4.4 ± 1.4	Expressed protein
Zm00001d048694	0.0005	4.4 ± 1	no description available
Zm00001d030305	0.005938	-4.3 ± 1.2	Proline-rich protein 2
Zm00001d002158	0.016581	-4.3 ± 1.3	Wound-responsive family protein|wound induced protein
Zm00001d023443	0.045765	4.1 ± 1.5	light-inducible protein CPRF2|Basic-leucine zipper (bZIP) transcription factor family protein
Zm00001d032721	0.013789	4.1 ± 1.3	long-chain-alcohol oxidase FAO1|FAO4B
Zm00001d002564	0.039577	3.9 ± 1.4	Protein DMR6-LIKE OXYGENASE 2|1
Zm00001d035390	1.45E-05	3.8 ± 0.7	thioredoxin H-type
Zm00001d029645	0.004998	3.7 ± 1	putative polyol transporter 1
Zm00001d023984	1.70E-25	3.7 ± 0.3	GDSL-motif lipase/hydrolase-like protein
Zm00001d032788	0.028069	-3.6 ± 1.2	anther-specific proline-rich protein APG|GDSL esterase/lipase LTL1
Zm00001d037794	0.003565	3.6 ± 1	Sec14p-like phosphatidylinositol transfer family protein|transporter-like protein
Zm00001d038465	0.002116	3.6 ± 0.9	protein NUCLEAR FUSION DEFECTIVE 4
Zm00001d022320	0.015991	3.6 ± 1.1	putative carboxylesterase 18
Zm00001d012069	0.019551	-3.6 ± 1.1	DUF506 family protein
Zm00001d038930	1.09E-07	-3.5 ± 0.6	R2R3MYB-domain protein|Transcription factor MYB36
Zm00001d034722	0.044483	-3.5 ± 1.2	*Triticum turgidum* subsp. *durum*: Glucuronoxylan 4-O-methyltransferase 1 G
Zm00001d009622	0.000349	3.5 ± 0.8	ethylene-responsive transcription factor ERF061|putative AP2/EREBP transcription factor superfamily protein
Zm00001d051194	2.06E-05	3.4 ± 0.7	arginine decarboxylase
Zm00001d031586	0.000231	-3.4 ± 0.8	RING/U-box superfamily protein

V4 ID	FDR pval.	LFC and SE	Description of the gene.
Zm00001d016947	0.014294	3.4 ± 1.1	no description available
Zm00001d039101	0.048018	-3.4 ± 1.2	nucleic acid binding f|Zinc finger CCCH domain-containing protein 14
Zm00001d002755	0.040776	3.4 ± 1.2	adenylyltransferase and sulfurtransferase MOCS3
Zm00001d004187	1.16E-07	-3.4 ± 0.6	UDP-glycosyltransferase 92A1
Zm00001d043579	2.66E-06	-3.4 ± 0.6	anther-specific proline-rich protein APG|GDSL esterase/lipase
Zm00001d012956	0.045484	-3.4 ± 1.2	cyclin-dependent protein kinase inhibitor SMR4
Zm00001d037909	3.30E-08	3.4 ± 0.5	NRR repressor homolog 1
Zm00001d001960	0.000342	3.3 ± 0.8	Naringenin2-oxoglutarate 3-dioxygenase|flavanone 3-beta-hydroxylase
Zm00001d025477	0.003751	-3.3 ± 0.9	dehydration-responsive element-binding protein 1D|Ethylene-responsive transcription factor ERF021
Zm00001d003867	0.000984	3.3 ± 0.8	extensin
Zm00001d038891	2.69E-82	3.2 ± 0.2	Phosphoethanolamine N-methyltransferase 3
Zm00001d045221	0.008565	-3.2 ± 0.9	thiol protease SEN102
Zm00001d020306	0.001202	3.2 ± 0.8	strictosidine synthase 3
Zm00001d002278	1.04E-11	-3.2 ± 0.4	OSJNBa0058K23.15-like protein
Zm00001d040152	2.08E-07	3.2 ± 0.5	transcription factor bHLH162|basic helix-loop-helix (bHLH) DNA-binding superfamily protein
Zm00001d021895	0.042842	3.2 ± 1.1	beta-hexosaminidase
Zm00001d032230	2.27E-08	3.1 ± 0.5	terpene synthase 7
Zm00001d050039	0.031143	-3.1 ± 1	NAC domain-containing protein 30|putative NAC domain transcription factor superfamily protein
Zm00001d045560	2.33E-16	-3.1 ± 0.3	transcription factor MYB2|typical P-type R2R3 Myb protein
Zm00001d041437	0.03829	3.1 ± 1.1	IQ-domain 19
Zm00001d051333	1.08E-23	-3.1 ± 0.3	blue copper protein
Zm00001d028125	3.50E-05	3 ± 0.6	UPF0496 protein 1
Zm00001d003719	3.67E-09	3 ± 0.5	putative UPF0496 protein 2
Zm00001d037914	3.04E-06	3 ± 0.6	*Triticum turgidum* subsp. *durum*: NRR repressor homolog 1
Zm00001d019976	0.003489	3 ± 0.8	phosphoglucosamine mutase family protein
Zm00001d024897	1.60E-05	2.9 ± 0.6	Triticum turgidum subsp. durum: Shikimate dehydrogenase (NADP(+)) G
Zm00001d031257	0.001349	-2.9 ± 0.7	blue copper protein|Cupredoxin superfamily protein
Zm00001d012294	0.002933	2.9 ± 0.8	transcription factor LG2-like|liguleless related sequence1|putative bZIP transcription factor superfamily protein

Supplementary Table 4.8. Top 60 significantly (FDR) affected genes in the mature zone for the severe versus control contrast. Genes are sorted in descending LFC size (absolute value). Gene descriptions were obtained from NCBI and were manually curated to obtain concise gene descriptions. When no NCBI description was available, the description on Gramene was obtained. If only a description based on homology was available, the species used is also indicated.

V4 ID	FDR pval.	LFC and SE	Description of the gene.
Zm00001d048694	2.85E-18	9.2 ± 1	no description available
Zm00001d020492	1.54E-08	7.8 ± 1.2	WRKY transcription factor
Zm00001d043709	1.60E-07	7.4 ± 1.3	Late embryogenesis abundant protein, group 3
Zm00001d033872	4.70E-11	7.3 ± 1	peptidase, M50 family
Zm00001d030670	9.79E-07	7.3 ± 1.3	calcium binding EF-hand protein|putative peroxygenase 4
Zm00001d033369	1.44E-07	7.2 ± 1.2	gibberellin-regulated protein 1|pco104919(665)
Zm00001d005454	1.51E-42	6.8 ± 0.5	rRNA N-glycosidase
Zm00001d025055	0.001539114	6.8 ± 1.8	probable protein phosphatase 2C 37
Zm00001d016076	1.18E-05	6.6 ± 1.3	*Triticum turgidum* subsp. *durum*: HTH-type transcriptional repressor AllR G
Zm00001d024893	2.39E-05	6.5 ± 1.3	*Triticum turgidum* subsp. *durum*: Shikimate dehydrogenase (NADP(+)) G
Zm00001d032608	5.37E-08	6.5 ± 1.1	alpha-galactosidase
Zm00001d010840	0.037480625	6.4 ± 2.4	triacylglycerol lipase-like 1
Zm00001d024897	1.99E-29	6.4 ± 0.5	*Triticum turgidum* subsp. *durum*: Shikimate dehydrogenase (NADP(+)) G
Zm00001d051478	6.37E-18	-6.3 ± 0.7	histone H4
Zm00001d045456	6.68E-05	6.3 ± 1.4	Zinc finger (C3HC4-type RING finger) family protein
Zm00001d038891	0	6.3 ± 0.2	Phosphoethanolamine N-methyltransferase 3
Zm00001d023984	1.59E-82	6.2 ± 0.3	GDSL esterase/lipase|GDSL-motif lipase/hydrolase-like protein
Zm00001d014083	0.02004171	6.2 ± 2.1	beta-amylase
Zm00001d047705	5.47E-05	-6.2 ± 1.3	cyclase/dehydrase family protein|pyrabactin resistance-like protein
Zm00001d020332	0.000113746	6.1 ± 1.4	ubiquitin-protein ligase
Zm00001d016255	5.90E-22	6.1 ± 0.6	heat shock factor protein 1|Heat stress transcription factor C-1
Zm00001d044680	0.00014364	6.1 ± 1.4	putative WRKY transcription factor 38
Zm00001d045454	0.000216216	6 ± 1.4	Zinc finger (C3HC4-type RING finger) family protein
Zm00001d010586	7.54E-05	5.9 ± 1.3	PEBP (phosphatidylethanolamine-binding protein) family protein
Zm00001d023443	0.000280974	5.9 ± 1.4	light-inducible protein CPRF2|Basic-leucine zipper (bZIP) transcription factor family protein
Zm00001d019163	1.19E-41	5.9 ± 0.4	alkaline alpha galactosidase 1|stachyose synthase
Zm00001d027760	3.56E-12	-5.8 ± 0.8	Histone H2A
Zm00001d049218	0.000697281	5.8 ± 1.5	calcium-activated outward-rectifying potassium channel 1|Two-pore potassium channel 1
Zm00001d003482	0.000574588	5.7 ± 1.4	no description available
Zm00001d029366	4.43E-08	5.5 ± 0.9	Transducin/WD40 repeat-like superfamily protein
Zm00001d032256	0.00194903	5.5 ± 1.5	dynamin-2A

V4 ID	FDR pval.	LFC and SE	Description of the gene.
Zm00001d024898	1.04E-14	5.5 ± 0.7	macrodontain-1|Cysteine proteinases superfamily protein
Zm00001d037769	7.28E-21	5.4 ± 0.5	C3H39 C3H type transcription factor|Zinc finger CCCH domain-containing protein 23
Zm00001d042940	0.000376056	5.4 ± 1.3	plant-specific domain TIGR01589 family protein expressed
Zm00001d020495	0.003261319	5.4 ± 1.5	WRKY transcription factor|WRKY62 - superfamily of TFs having WRKY and zinc finger domains
Zm00001d031344	1.87E-19	-5.4 ± 0.6	no description available
Zm00001d015126	0.00272995	-5.3 ± 1.5	response to low sulfur 3
Zm00001d037468	0.001808165	-5.3 ± 1.4	phosphate transporter PHO1-3|4
Zm00001d003530	0.003045752	5.2 ± 1.5	Serine carboxypeptidase-like 19
Zm00001d010616	0.008700797	5.2 ± 1.6	probable WRKY transcription factor 62
Zm00001d012313	0.001406136	5.1 ± 1.4	starch binding domain containing protein
Zm00001d012320	0.005427722	-5.1 ± 1.5	Cell division control protein 6 homolog B
Zm00001d038870	0.00680264	5 ± 1.5	late embryogenesis abundant protein, group 3
Zm00001d031677	0.006953567	5 ± 1.5	MtN19-like protein
Zm00001d032253	6.33E-56	5 ± 0.3	putative inositol polyphosphate phosphatase (synaptogenin-like) family protein|Type IV inositol polyphosphate 5-phosphatase 9
Zm00001d008983	0.000251438	5 ± 1.2	P-loop containing nucleoside triphosphate hydrolases superfamily protein
Zm00001d022226	0.002184507	-5 ± 1.4	origin recognition complex subunit 6
Zm00001d020100	0.000283782	4.9 ± 1.2	2C-type protein phosphatase protein
Zm00001d006197	0.007738196	4.9 ± 1.5	Kinesin-like protein KIN-7G
Zm00001d002564	0.002390912	4.9 ± 1.3	Protein DMR6-LIKE OXYGENASE 2|1
Zm00001d027500	0.005444465	-4.9 ± 1.5	flower-specific gamma-thionin
Zm00001d040152	5.03E-19	4.9 ± 0.5	transcription factor bHLH162|basic helix-loop-helix (bHLH) DNA-binding superfamily protein
Zm00001d003164	0.003944619	-4.9 ± 1.4	Ribonucleoside-diphosphate reductase small chain C
Zm00001d002940	1.99E-16	4.8 ± 0.6	putative 1-phosphatidylinositol-4-phosphate 5-kinase/ zinc ion binding family
Zm00001d005748	0.000396391	4.8 ± 1.2	CBL-interacting protein kinase|CIPK-like protein 1
Zm00001d040979	5.57E-117	4.8 ± 0.2	Methylsterol monooxygenase 1-2
Zm00001d030314	8.03E-15	-4.7 ± 0.6	proline-rich protein
Zm00001d050577	1.75E-14	4.7 ± 0.6	sugars will eventually be exported transporter15a
Zm00001d009008	0.009932705	-4.7 ± 1.5	disease resistance protein PIK6-NP
Zm00001d044317	0.01073793	-4.6 ± 1.5	actin cytoskeleton-regulatory complex protein pan-1

Supplementary Table 4.9. Top 60 significantly (FDR) affected genes in the mature zone for the severe versus mild contrast. Genes are sorted in descending LFC size (absolute value). Gene descriptions were obtained from NCBI and were manually curated to obtain concise gene descriptions. When no NCBI description was available, the description on Gramene was obtained. If only a description based on homology was available, the species used is also indicated.

V4 ID	FDR pval.	LFC and SE	Description of the gene.
Zm00001d043709	1.53E-06	7.1 ± 1.3	Late embryogenesis abundant protein, group 3
Zm00001d008983	4.79E-05	6.5 ± 1.3	P-loop containing nucleoside triphosphate hydrolases superfamily protein
Zm00001d025055	0.004987745	6.5 ± 1.8	probable protein phosphatase 2C 37|2C-type protein phosphatase protein
Zm00001d037894	0.000354126	6.1 ± 1.4	dehydrin DHN1|responsive to abscisic acid17
Zm00001d045221	1.74E-08	5.9 ± 0.9	thiol protease SEN102
Zm00001d016076	0.001091208	5.4 ± 1.3	*Triticum turgidum* subsp. *durum*: HTH-type transcriptional repressor AllR G
Zm00001d047705	0.0020342	-5.3 ± 1.4	cyclase/dehydrase family protein|pyrabactin resistance-like protein
Zm00001d032608	9.48E-08	5.2 ± 0.8	alpha-galactosidase
Zm00001d033872	7.24E-15	5.1 ± 0.6	peptidase, M50 family
Zm00001d032253	6.01E-50	4.9 ± 0.3	putative inositol polyphosphate phosphatase (synaptogenin-like) family protein|Type IV inositol polyphosphate 5-phosphatase 9
Zm00001d010586	0.000651452	4.9 ± 1.2	PEBP (phosphatidylethanolamine-binding protein) family protein
Zm00001d048694	2.27E-55	4.8 ± 0.3	no description available
Zm00001d016255	8.44E-23	4.6 ± 0.4	heat shock factor protein 1|Heat stress transcription factor C-1
Zm00001d023973	2.90E-06	4.6 ± 0.8	thiol protease SEN102|Cysteine proteinases superfamily protein
Zm00001d033369	1.48E-08	4.5 ± 0.7	gibberellin-regulated protein 1
Zm00001d005454	7.48E-43	4.4 ± 0.3	rRNA N-glycosidase
Zm00001d027760	2.78E-06	-4.3 ± 0.8	Histone H2A
Zm00001d051478	2.27E-07	-4.2 ± 0.7	histone H4
Zm00001d019163	5.46E-24	4.2 ± 0.4	alkaline alpha galactosidase 1|stachyose synthase
Zm00001d011968	0.005189451	4.2 ± 1.2	no description available
Zm00001d023873	0.007718273	-4.1 ± 1.2	putative glutaredoxin-C14|Glutaredoxin-C13
Zm00001d003190	2.84E-06	4 ± 0.7	endochitinase A|seed chitinase A
Zm00001d002158	0.034089679	4 ± 1.4	Wound-responsive family protein|wound induced protein
Zm00001d012069	0.006961807	3.9 ± 1.1	DUF506 family protein
Zm00001d050577	2.04E-10	3.9 ± 0.6	sugars will eventually be exported transporter15a
Zm00001d020100	0.002220524	3.9 ± 1	2C-type protein phosphatase protein|putative protein phosphatase 2C family protein
Zm00001d031778	0.000662375	3.9 ± 0.9	carbonic anhydrase
Zm00001d028574	1.29E-11	3.8 ± 0.5	2C-type protein phosphatase protein|Protein phosphatase 2C 37
Zm00001d048192	7.70E-12	-3.7 ± 0.5	AIR12
Zm00001d017422	0.000184017	3.7 ± 0.8	homeobox-leucine zipper protein ATHB-6

V4 ID	FDR pval.	LFC and SE	Description of the gene.
Zm00001d002940	3.17E-13	3.7 ± 0.5	putative 1-phosphatidylinositol-4-phosphate 5-kinase/ zinc ion binding family
Zm00001d003760	8.77E-19	3.7 ± 0.4	lipid binding protein|Bifunctional inhibitor/lipid-transfer protein/seed storage 2S albumin superfamily protein
Zm00001d029366	2.57E-07	3.7 ± 0.6	Transducin/WD40 repeat-like superfamily protein
Zm00001d007160	2.45E-10	-3.6 ± 0.5	plasma membrane-bound peroxidase 3-2
Zm00001d037769	2.56E-16	3.5 ± 0.4	C3H39 C3H type transcription factor|Zinc finger CCCH domain-containing protein 23
Zm00001d029341	0.03403795	-3.5 ± 1.2	aldose 1-epimerase
Zm00001d052063	2.92E-20	3.5 ± 0.3	Transmembrane amino acid transporter family protein
Zm00001d023664	0.000597707	3.5 ± 0.8	ABA-responsive protein
Zm00001d024897	2.72E-25	3.5 ± 0.3	*Triticum turgidum* subsp. *durum*: Shikimate dehydrogenase (NADP(+)) G
Zm00001d032788	0.043503174	3.4 ± 1.2	anther-specific proline-rich protein APG|GDSL esterase/lipase LTL1
Zm00001d024893	0.007108505	3.4 ± 1	*Triticum turgidum* subsp. *durum*: Shikimate dehydrogenase (NADP(+)) G
Zm00001d028838	0.002540316	3.4 ± 0.9	long cell-linked locus protein
Zm00001d038642	6.64E-10	-3.3 ± 0.5	pollenless 3|Protein SULFUR DEFICIENCY-INDUCED 1
Zm00001d031344	8.95E-07	-3.3 ± 0.6	no description available
Zm00001d049926	0.001042402	3.3 ± 0.8	conserved domain PLN02947-containing
Zm00001d052918	0.002023793	-3.3 ± 0.8	ubiquitin-protein ligase/ zinc ion binding protein
Zm00001d018531	6.41E-05	-3.3 ± 0.7	Replication protein A 32 kDa subunit A
Zm00001d024898	6.06E-12	3.3 ± 0.4	macrodontain-1|Cysteine proteinases superfamily protein
Zm00001d017019	0.02834469	-3.2 ± 1.1	ATFP4
Zm00001d025354	0.03403795	-3.1 ± 1.1	Beta-fructofuranosidase insoluble isoenzyme CWINV2
Zm00001d032307	0.010689235	3.1 ± 0.9	no description available
Zm00001d024886	4.86E-19	3.1 ± 0.3	Zinc finger (C3HC4-type RING finger) family protein|protein binding protein
Zm00001d047814	1.39E-41	3.1 ± 0.2	Catalytic/ hydrolase
Zm00001d045877	0.000802986	-3.1 ± 0.7	glycine-rich cell wall structural protein
Zm00001d007027	1.63E-05	3.1 ± 0.6	ubiquitin-protein ligase CIP8|putative RING zinc finger domain superfamily protein
Zm00001d038891	2.77E-114	3.1 ± 0.1	Phosphoethanolamine N-methyltransferase 3
Zm00001d050061	0.008003488	-3.1 ± 0.9	Putative SWI/SNF-related matrix-associated actin-dependent regulator of chromatin subfamily A member 3-like 3
Zm00001d005748	0.007295234	3 ± 0.9	CBL-interacting protein kinase
Zm00001d017989	1.75E-05	3 ± 0.6	GDSL esterase/lipase
Zm00001d051420	5.22E-12	3 ± 0.4	dehydrin|DHN2-like protein|drought-inducible

Supplementary Table 4.10. Genes (24 in total) in the overrepresented metal ion transport GO for meristem cluster 2. Genes are sorted in descending LFC size (absolute value). Gene descriptions were kept from panther and were similar to those of NCBI. When no panther description was available, the description from NCBI was used when available. The FDR p-value and LFC, plus standard error (SE) were provided for the severe vs control contrast.

V4 ID	FDR pval.	LFC and SE	Gene description	Panther family
Zm00001d036965	3.14E-53	3.9 ± 0.2	Zinc transporter 4	PROTEIN ZNTC (PTHR11040:SF44)
Zm00001d045883	0.023852	3.4 ± 1.1	Sodium/hydrogen exchanger	SODIUM/HYDROGEN EXCHANGER 4 (PTHR10110:SF179)
Zm00001d019228	0.000846	3 ± 0.7	ZIP zinc/iron transport family protein	ZINC TRANSPORTER 1 (PTHR11040:SF35)
Zm00001d001915	0.03574	2.9 ± 1	metal ion binding protein (NCBI)	Not Available
Zm00001d019227	0.021602	2.6 ± 0.8	Uncharacterized protein	ZINC TRANSPORTER 1 (PTHR11040:SF35)
Zm00001d025623	2.75E-09	2 ± 0.3	Vacuolar iron transporter 1	PROTEIN CCC1 (PTHR31851:SF52)
Zm00001d016691	4.80E-23	1.5 ± 0.1	Copper transport protein CCH	COPPER CHAPERONE HOMOLOG CCH (PTHR22814:SF315)
Zm00001d004138	0.001042	1.3 ± 0.3	Heavy metal-associated isoprenylated plant protein 27	OSJNBA0091C12.3 PROTEIN (PTHR22814:SF168)
Zm00001d023223	7.58E-07	1.3 ± 0.2	Ferritin	FERRITIN (PTHR11431:SF75)
Zm00001d034035	0.000743	1 ± 0.2	Glutathione transporter1	OLIGOPEPTIDE TRANSPORTER 3 (PTHR22601:SF47)
Zm00001d052457	0.003127	0.9 ± 0.2	Calcium-transporting ATPase	CALCIUM-TRANSPORTING ATPASE (PTHR24093:SF456)
Zm00001d037756	8.18E-09	0.9 ± 0.1	Zinc transporter 4	ZINC TRANSPORTER 7 (PTHR11040:SF52)
Zm00001d028093	0.000645	0.7 ± 0.2	Calcium-transporting ATPase	CALCIUM-TRANSPORTING ATPASE 1 (PTHR24093:SF474)
Zm00001d042939	0.013509	0.7 ± 0.2	Metal tolerance protein 11	METAL TOLERANCE PROTEIN 11 (PTHR43840:SF5)
Zm00001d022504	0.000617	0.7 ± 0.2	Sodium/hydrogen exchanger	SODIUM/HYDROGEN EXCHANGER (PTHR10110:SF176)
Zm00001d031543	0.000206	0.6 ± 0.1	Calcium-transporting ATPase	CALCIUM-TRANSPORTING ATPASE 10, PLASMA MEMBRANE-TYPE (PTHR24093:SF472)
Zm00001d048411	0.01465	0.6 ± 0.2	Metal ion binding protein	HEAVY METAL-ASSOCIATED DOMAIN CONTAINING PROTEIN, EXPRESSED (PTHR46413:SF4)
Zm00001d014669	0.005058	0.5 ± 0.1	Cadmium/zinc-transporting ATPase HMA2	CADMIUM/ZINC-TRANSPORTING ATPASE HMA2 (PTHR48085:SF5)
Zm00001d027884	0.000278	0.5 ± 0.1	Copper-transporting ATPase PAA2 chloroplastic	COPPER-TRANSPORTING ATPASE PAA2, CHLOROPLASTIC (PTHR43520:SF19)
Zm00001d008515	2.65E-06	0.5 ± 0.1	Heavy metal transport/detoxification superfamily protein	HEAVY METAL-ASSOCIATED ISOPRENYLATED PLANT PROTEIN 37 (PTHR45868:SF19)
Zm00001d024300	0.006847	0.5 ± 0.1	Potassium transporter	POTASSIUM TRANSPORTER 12-RELATED (PTHR30540:SF93)
Zm00001d029072	9.20E-05	0.5 ± 0.1	Potassium transporter	POTASSIUM TRANSPORTER 2 (PTHR30540:SF6)
Zm00001d052316	0.000327	0.5 ± 0.1	Ferritin	FERRITIN (PTHR11431:SF75)

V4 ID	FDR pval.	LFC and SE	Gene description	Panther family
Zm00001d002396	0.000951	0.4 ± 0.1	Calcium-transporting ATPase	CALCIUM-TRANSPORTING ATPASE 5, PLASMA MEMBRANE-TYPE (PTHR24093:SF430)

Supplementary Table 4.11. Genes (5 in total) in the overrepresented L-phenylalanine catabolic process GO for meristem cluster 2. All genes were shared for by the cinnamic acid biosynthetic process GO, except for Zm00001d045610. Genes are sorted in descending LFC size (absolute value). Gene descriptions were kept from panther and were similar to those of NCBI. The FDR p-value and LFC, plus standard error (SE) were provided for the severe vs control contrast.

V4 ID	FDR pval.	LFC and SE	Gene description	Panther family
Zm00001d017279	5.87E-06	1.8 ± 0.3	Phenylalanine ammonia-lyase	PHENYLALANINE AMMONIA-LYASE (PTHR10362:SF34)
Zm00001d045610	0.035457773	0.8 ± 0.3	Homogentisate 12-dioxygenase	HOMOGENTISATE 1,2-DIOXYGENASE (PTHR11056:SF0)
Zm00001d003016	6.78E-06	0.7 ± 0.1	Phenylalanine ammonia-lyase	PHENYLALANINE AMMONIA-LYASE (PTHR10362:SF54)
Zm00001d017275	0.001196191	0.7 ± 0.2	Phenylalanine ammonia-lyase	HAL-LIKE PROTEIN DDB_G0273787/DDB_G0273081 (PTHR10362:SF35)
Zm00001d017274	1.41E-05	0.7 ± 0.1	Phenylalanine ammonia-lyase	PHENYLALANINE AMMONIA-LYASE (PTHR10362:SF11)

Supplementary Table 4.12. Genes (5 in total) in the overrepresented response to hydrogen peroxide GO for meristem cluster 2. Genes are sorted in descending LFC size (absolute value). Gene descriptions were kept from panther and were similar to those of NCBI. The FDR p-value and LFC, plus standard error (SE) were provided for the severe vs control contrast.

V4 ID	FDR pval.	LFC and SE	Gene description	Panther family
Zm00001d018298	1.55E-37	2.9 ± 0.2	17.4 kDa class III heat shock protein	17.4 KDA CLASS III HEAT SHOCK PROTEIN (PTHR11527:SF297)
Zm00001d028561	0.029244	2.8 ± 0.9	17.4 kDa class I heat shock protein	18.1 KDA CLASS I HEAT SHOCK PROTEIN (PTHR11527:SF321)
Zm00001d039936	0.044527	2 ± 0.7	16.9 kDa class I heat shock protein 1	16.9 KDA CLASS I HEAT SHOCK PROTEIN 2 (PTHR11527:SF315)
Zm00001d028557	0.00041	1.3 ± 0.3	17.4 kDa class I heat shock protein	17.4 KDA CLASS I HEAT SHOCK PROTEIN 3 (PTHR11527:SF265)
Zm00001d039566	0.007264	1.2 ± 0.3	17.5 kDa class II heat shock protein	18.0 KDA CLASS II HEAT SHOCK PROTEIN (PTHR11527:SF260)

Supplementary Table 4.13. Genes (16 in total) in the overrepresented cell cycle related GOs for meristem cluster 3. Genes from different GOs were combined to one list. Genes are sorted in descending LFC size (absolute value). Gene descriptions were kept from panther and were similar to those of NCBI. When no panther description was available, the description from NCBI was used when available. The FDR p-value and LFC, plus standard error (SE) were provided for the severe vs control contrast.

V4 ID	FDR pval.	LFC and SE	Gene description	Panther family	Panther protein class
Zm00001d051995	0.001201	-0.4 ± 0.1	Proliferating cell nuclear antigen	PROLIFERATING CELL NUCLEAR ANTIGEN (PTHR11352:SF0)	DNA polymerase processivity factor(PC00015)
Zm00001d021706	0.000372	-0.4 ± 0.1	Histone H2A	HISTONE H2A.6 (PTHR23430:SF286)	histone(PC00118)
Zm00001d006547	0.012025	-0.4 ± 0.1	Histone H2A	HISTONE H2A.1-RELATED (PTHR23430:SF95)	histone(PC00118)
Zm00001d025234	0.06326	-0.4 ± 0.1	DNA primase large subunit	DNA PRIMASE LARGE SUBUNIT (PTHR10537:SF3)	primase(PC00189)
Zm00001d002510	0.064252	-0.3 ± 0.1	Regulator of nonsense transcripts 1-like protein (NCBI: DNA replication ATP-dependent helicase/nuclease JHS1)	DNA REPLICATION ATP-DEPENDENT HELICASE/NUCLEASE DNA2 (PTHR10887:SF433)	RNA helicase(PC00032);DNA helicase(PC00011)
Zm00001d045649	0.066954	-0.3 ± 0.1	Ribonucleoside-diphosphate reductase small chain	RIBONUCLEOSIDE-DIPHOSPHATE REDUCTASE SMALL CHAIN (PTHR23409:SF38)	reductase(PC00198)
Zm00001d018415	0.03286	-0.3 ± 0.1	Proliferating cell nuclear antigen	PROLIFERATING CELL NUCLEAR ANTIGEN (PTHR11352:SF0)	DNA polymerase processivity factor(PC00015)
Zm00001d036322	0.063146	-0.3 ± 0.1	Ribonucleoside-diphosphate reductase	RIBONUCLEOSIDE-DIPHOSPHATE REDUCTASE LARGE SUBUNIT (PTHR11573:SF6)	reductase(PC00198)
Zm00001d033421	0.182392	-0.2 ± 0.1	Deoxyuridine 5'-triphosphate nucleotidohydrolase	DEOXYURIDINE 5'-TRIPHOSPHATE NUCLEOTIDOHYDROLASE (PTHR11241:SF12)	phosphatase(PC00181)
Zm00001d002601	0.084429	-0.2 ± 0.1	Histone H1	OS04G0253000 PROTEIN (PTHR11467:SF101)	histone(PC00118)
Zm00001d038667	0.508791	-0.2 ± 0.1	Protein BREAST CANCER SUSCEPTIBILITY 1-like protein	BREAST CANCER TYPE 1 SUSCEPTIBILITY PROTEIN (PTHR13763:SF0)	ubiquitin-protein ligase(PC00234)
Zm00001d032239	0.299496	-0.2 ± 0.1	HMG-Y-related protein A	HMG-Y-RELATED PROTEIN A (PTHR11467:SF103)	histone(PC00118)
Zm00001d006548	0.299943	-0.2 ± 0.1	Histone H2A	HISTONE H2A.3-RELATED (PTHR23430:SF277)	histone(PC00118)
Zm00001d039498	0.334768	-0.2 ± 0.1	Aurora b kinase1	AURORA A (PTHR24350:SF0)	non-receptor serine/threonine protein kinase(PC00167)

V4 ID	FDR pval.	LFC and SE	Gene description	Panther family	Panther protein class
Zm00001d018531	0.528554	-0.1 ± 0.1	Replication protein A 32 kDa subunit A	REPLICATION PROTEIN A 32 KDA SUBUNIT A (PTHR13989:SF41)	NA
Zm00001d045192	0.453872	-0.1 ± 0.1	Ribonucleoside-diphosphate reductase	RIBONUCLEOSIDE-DIPHOSPHATE REDUCTASE LARGE SUBUNIT (PTHR11573:SF6)	reductase(PC00198)

Supplementary Table 4.14. Genes (3 in total) in the overrepresented positive regulation of superoxide dismutase activity GO for mature zone cluster 1. Genes are sorted in descending LFC size (absolute value). Gene descriptions were kept from panther and were similar to those of NCBI or more informative. The FDR p-value and LFC, plus standard error (SE) were provided for the severe vs control contrast.

V4 ID	FDR pval.	LFC and SE	Gene description	Panther family
Zm00001d052101	7.93E-14	-0.8 ± 0.1	Chaperonin10	OS02G0781400 PROTEIN (PTHR10772:SF26)
Zm00001d045025	1.15E-11	-0.7 ± 0.1	20 kDa chaperonin chloroplastic	20 KDA CHAPERONIN, CHLOROPLASTIC (PTHR10772:SF32)
Zm00001d005812	9.39E-05	-0.5 ± 0.1	Sterile alpha motif (SAM) domain-containing protein	DNA CROSS-LINK REPAIR 1A PROTEIN (PTHR23240:SF6)

Supplementary Table 4.15. Genes (3 in total) in the overrepresented cinnamic acid biosynthetic process GO for mature zone cluster 3. Genes are sorted in descending LFC size (absolute value). Gene descriptions were kept from panther and were similar to those of NCBI or more informative. The FDR p-value and LFC, plus standard error (SE) were provided for the severe vs control contrast.

V4 ID	FDR pval.	LFC and SE	Gene description	Panther family
Zm00001d051161	0.000513	-0.7 ± 0.2	Phenylalanine ammonia-lyase	PHENYLALANINE AMMONIA-LYASE (PTHR10362:SF11)
Zm00001d017275	9.00E-05	-0.6 ± 0.1	Phenylalanine ammonia-lyase	HAL-LIKE PROTEIN DDB_G0273787/DDB_G0273081 (PTHR10362:SF35)
Zm00001d017274	0.023615	-0.4 ± 0.1	Phenylalanine ammonia-lyase	PHENYLALANINE AMMONIA-LYASE (PTHR10362:SF11)

Supplementary Table 4.16. Genes (30 in total) presented in the MapMan regulation (figure 7) overview which were related to phytohormones for the meristem. Genes are sorted based on hormone class and within hormone class in descending absolute LFC value. Gene descriptions of NCBI were used and complemented with those from gramene.org when NCBI descriptions were unavailable. The FDR p-value and LFC, plus standard error (SE) were provided for the severe vs control contrast. Phytohormone is indicated in the first column: IAA: related to indole-3-acetic acid , ABA: abscisic acid, BA: 6-benzyladenine, Cytokinin, Jasmonate, SA: salicylic acid and GA: gibberellic acid.

Hormone	V4 ID	FDR pval.	LFC and SE	Gene description
ABA	Zm00001d007341	8.45E-09	4.9 ± 0.7	HVA22-like protein e
ABA	Zm00001d018178	0.001830791	1.3 ± 0.3	ABSCISIC ACID-INSENSITIVE 5-like protein 5|bZIP transcription factor ABI5|putative bZIP transcription factor superfamily protein
ABA	Zm00001d047710	0.048713816	1.2 ± 0.4	No description available
ABA	Zm00001d037170	0.034017579	0.8 ± 0.3	ABSCISIC ACID-INSENSITIVE 5-like protein 5|Putative bZIP transcription factor superfamily protein|bZIP transcription factor family protein
ABA	Zm00001d050018	0.029754323	0.7 ± 0.2	ABSCISIC ACID-INSENSITIVE 5-like protein 5|bZIP transcription factor|putative bZIP transcription factor superfamily protein
ABA	Zm00001d031790	0.038549248	0.5 ± 0.2	bZIP transcription factor TRAB1|ABSCISIC ACID-INSENSITIVE 5-like protein 5|putative bZIP transcription factor superfamily protein
BA	Zm00001d013035	9.12E-05	0.9 ± 0.2	cycloartenol-C-24-methyltransferase 1
BA	Zm00001d042362	0.000321827	-0.9 ± 0.2	leucine-rich repeat receptor protein kinase MSP1|Leucine-rich repeat receptor protein kinase EMS1|leucine-rich repeat receptor protein kinase EXS
BA	Zm00001d019139	0.017187048	-0.3 ± 0.1	(S)-adenosyl-L-methionine:delta 24-sterol methyltransferase|cycloartenol-C-24-methyltransferase 1|endosperm C-24 sterol methyltransferase|sterol methyltransferase1
Cytokinin	Zm00001d012005	0.042549648	0.4 ± 0.1	Putative histidine kinase family protein
Cytokinin	Zm00001d042312	0.011944001	0.4 ± 0.1	histidine kinase 2|histidine kinase2
GA	Zm00001d013725	2.28E-30	-3.1 ± 0.3	gibberellin 20 oxidase 2|gibberellin 20-oxidase4
GA	Zm00001d033369	4.69E-33	2.6 ± 0.2	gibberellin-regulated protein 1
GA	Zm00001d037724	0.025736385	2.4 ± 0.8	gibberellin 2-beta-dioxygenase
GA	Zm00001d033680	0.001695636	-0.5 ± 0.1	DELLA protein DWARF8|Protein dwarf-8|dwarf plant8|gibberelin response modulator dwarf 8|gibberellin response modulator
IAA	Zm00001d011687	0.000506614	3.2 ± 0.7	IAA-amino acid hydrolase ILR1-like 4
IAA	Zm00001d031555	0.004978457	1.5 ± 0.4	Membrane protein
IAA	Zm00001d049786	0.017487033	1.3 ± 0.4	cytochrome b561 and DOMON domain-containing protein
IAA	Zm00001d049141	0.028423615	0.8 ± 0.3	AUX/IAA transcription factor|Auxin-responsive protein IAA26
IAA	Zm00001d052493	1.10E-09	-0.8 ± 0.1	stem-specific protein TSJT1|aluminum induced protein with YGL and LRDR motifs
IAA	Zm00001d034433	0.00045785	0.6 ± 0.1	Heat stress transcription factor A-6b
IAA	Zm00001d002302	0.036348173	0.4 ± 0.1	Auxin responsive protein
Jasmonate	Zm00001d042541	0.004077761	3.5 ± 0.9	linoleate 9S-lipoxygenase1

Hormone	V4 ID	FDR pval.	LFC and SE	Gene description
Jasmonate	Zm00001d033623	2.29E-26	2.4 ± 0.2	linoleate 9S-lipoxygenase3
Jasmonate	Zm00001d053675	2.87E-19	1.9 ± 0.2	linoleate 13S-lipoxygenase10
Jasmonate	Zm00001d048021	1.75E-12	1.5 ± 0.2	allene-oxide synthase1|putative cytochrome P450 superfamily protein
Jasmonate	Zm00001d028282	8.60E-05	0.7 ± 0.1	allene-oxide synthase2|cytochrome P450 CYP74A19|putative cytochrome P450 superfamily protein
Jasmonate	Zm00001d040842	0.018378535	-0.6 ± 0.2	12-oxophytodienoate reductase6|12-oxo-phytodienoic acid reductase 6|12-oxo-phytodienoic acid reductase6
Jasmonate	Zm00001d047340	0.048171511	0.6 ± 0.2	allene-oxide cyclase2|Allene oxide cyclase 3 chloroplastic|allene oxide cyclase 4
SA	Zm00001d035767	1.31E-05	2.2 ± 0.4	Jasmonate O-methyltransferase

Supplementary Table 4.17. Genes (86 in total) presented in the MapMan regulation (figure 15) overview which were related to phytohormones for the mature zone. Genes are sorted based on hormone class and within hormone class in descending absolute LFC value. Gene descriptions of NCBI were used and complemented with those from gramene.org when NCBI descriptions were unavailable. The FDR p-value and LFC, plus standard error (SE) were provided for the severe vs control contrast. Phytohormone is indicated in the first column: IAA: related to indole-3-acetic acid , ABA: abscisic acid, BA: 6-benzyladenine, Cytokinin, Jasmonate, SA: salicylic acid and GA: gibberellic acid.

Hormone	V4 ID	FDR pval.	LFC and SE	Gene description
ABA	Zm00001d007341	8.43E-09	3.8 ± 0.6	HVA22-like protein e
ABA	Zm00001d011753	0.040029942	-2.8 ± 1	HVA22-like protein f
ABA	Zm00001d023664	0.000808464	2.8 ± 0.7	ABA-responsive protein
ABA	Zm00001d018178	3.51E-14	2.2 ± 0.3	ABSCISIC ACID-INSENSITIVE 5-like protein 5|bZIP transcription factor ABI5|putative bZIP transcription factor superfamily protein
ABA	Zm00001d044940	0.000304595	1.7 ± 0.4	bZIP transcription factor 46|ABSCISIC ACID-INSENSITIVE 5-like protein 6|bZIP transcription factor 23|putative bZIP transcription factor superfamily protein
ABA	Zm00001d034388	4.96E-13	1.5 ± 0.2	indole-3-acetaldehyde oxidase-like|aldehyde oxidase4
ABA	Zm00001d050018	0.000456844	1.3 ± 0.3	ABSCISIC ACID-INSENSITIVE 5-like protein 5|bZIP transcription factor|putative bZIP transcription factor superfamily protein
ABA	Zm00001d031773	0.040386535	1.1 ± 0.4	protein HVA22
ABA	Zm00001d047710	0.011352084	1.1 ± 0.4	no description available
ABA	Zm00001d031790	0.006496343	1 ± 0.3	bZIP transcription factor TRAB1|ABSCISIC ACID-INSENSITIVE 5-like protein 5|putative bZIP transcription factor superfamily protein
ABA	Zm00001d018869	0.018372898	0.8 ± 0.3	indole-3-acetaldehyde oxidase-like
ABA	Zm00001d018869	0.018372898	0.8 ± 0.3	indole-3-acetaldehyde oxidase-like
ABA	Zm00001d023459	0.046824659	0.8 ± 0.3	HVA22-like protein j
ABA	Zm00001d025362	0.00263783	-0.8 ± 0.2	Pathogenicity protein PATH531-like protein
ABA	Zm00001d028429	0.009411797	0.8 ± 0.2	HVA22-like protein i|receptor expression-enhancing protein 3
ABA	Zm00001d034385	0.028805191	-0.7 ± 0.3	aldehyde oxidase3
ABA	Zm00001d034387	0.000396103	0.7 ± 0.2	indole-3-acetaldehyde oxidase|IAA oxidase|aldehyde oxidase|aldehyde oxidase1
ABA	Zm00001d025545	0.003979538	0.4 ± 0.1	zeaxanthin epoxidase2
BA	Zm00001d013035	0.040352381	2.2 ± 0.8	cycloartenol-C-24-methyltransferase 1
BA	Zm00001d037745	0.000936985	-1.9 ± 0.5	cytochrome P450 90D2|cytochrome P450 CYP90D10.b|putative cytochrome P450 superfamily protein
BA	Zm00001d042843	0.002739196	-1.1 ± 0.3	steroid reductase DET2|nana plant1
BA	Zm00001d026064	8.72E-06	1 ± 0.2	polyprenol reductase 1|Polyprenol reductase 2
BA	Zm00001d027548	0.004848784	-0.9 ± 0.3	sterol methyl transferase 2|sterol methyl transferase2
BA	Zm00001d008569	2.29E-07	0.8 ± 0.1	delta-7-sterol-C5|Delta(7)-sterol-C5(6)-desaturase 1
BA	Zm00001d048356	0.008045706	-0.8 ± 0.3	24-methylenesterol C-methyltransferase 2

Hormone	V4 ID	FDR pval.	LFC and SE	Gene description
BA	Zm00001d002600	0.032484307	0.6 ± 0.2	Polyprenol reductase 2
BA	Zm00001d044673	0.020584768	0.4 ± 0.1	cytochrome P450-like protein|Sterol 14-demethylase
Cytokinin	Zm00001d032664	0.030206006	-2.8 ± 1	cytokinin dehydrogenase 6|cytokinin oxidase6
Cytokinin	Zm00001d005344	8.60E-12	1.4 ± 0.2	histidine-containing phosphotransfer protein 2|Histidine-containing phosphotransfer protein 1|ZmHP2 3'untrans|histidine-containing phosphotransfer protein2
Cytokinin	Zm00001d012005	7.46E-06	0.9 ± 0.2	Putative histidine kinase family protein
Cytokinin	Zm00001d033786	2.66E-06	0.9 ± 0.2	histidine kinase|putative histidine kinase family protein
Cytokinin	Zm00001d042312	0.031327293	0.5 ± 0.2	histidine kinase 2|gpm789a|histidine kinase2
Ethylene	Zm00001d029636	2.60E-11	-2.5 ± 0.3	Protein SRG1|cl945_1(263)|leucoanthocyanidin dioxygenase
Ethylene	Zm00001d007718	2.56E-07	2.4 ± 0.4	1-aminocyclopropane-1-carboxylate oxidase|benzoxazinone synthesis13
Ethylene	Zm00001d037487	0.016681809	1.8 ± 0.6	2-oxoglutarate (2OG) and Fe(II)-dependent oxygenase superfamily protein
Ethylene	Zm00001d024853	1.18E-07	-1.4 ± 0.2	1-aminocyclopropane-1-carboxylate oxidase15|acc oxidase
Ethylene	Zm00001d002200	0.039576955	1.2 ± 0.5	uncharacterized protein LOC100383774|Transcription factor bHLH112|putative HLH DNA-binding domain superfamily protein
Ethylene	Zm00001d019216	0.034300895	1 ± 0.4	ethylene-responsive transcription factor ABI4|AP2-EREBP transcription factor|putative AP2/EREBP transcription factor superfamily protein
Ethylene	Zm00001d043248	0.033497334	1 ± 0.4	uncharacterized protein LOC100277655|Transcription factor bHLH112
Ethylene	Zm00001d037604	0.04875303	0.7 ± 0.3	probable ethylene response sensor 2|Ethylene response sensor 1
Ethylene	Zm00001d004354	0.000192692	0.6 ± 0.1	cystathionin beta synthase protein|CBS domain-containing protein CBSX1 chloroplastic
Ethylene	Zm00001d050130	0.00219863	-0.5 ± 0.1	IMP dehydrogenase
GA	Zm00001d033369	1.44E-07	7.2 ± 1.2	gibberellin-regulated protein 1|pco104919(665)
GA	Zm00001d038056	0.000275156	3.6 ± 0.8	gibberellin-regulated protein 6-like|GAST1 protein|Gibberellin-regulated protein 13
GA	Zm00001d037724	2.96E-09	3.4 ± 0.5	gibberellin 2-beta-dioxygenase
GA	Zm00001d013725	7.77E-05	-1.5 ± 0.3	conserved domain cl26046-containing|gibberellin 20 oxidase 2|gibberellin 20-oxidase4
GA	Zm00001d029648	0.03973648	-1.4 ± 0.5	ent-copalyl diphosphate synthase AN2, chloroplastic|CPP synthase 2|Ent-CPP synthase|Ent-copalyl diphosphate synthase AN2, chloroplastic|Protein ANTHER EAR 2|anther ear2
GA	Zm00001d046344	4.82E-09	1.3 ± 0.2	putative cytochrome P450 superfamily protein
GA	Zm00001d032961	0.00048874	0.9 ± 0.2	ent-copalyl diphosphate synthase AN1, chloroplastic|CPP synthase 1|Ent-CPP synthase|Ent-copalyl diphosphate synthase AN1, chloroplastic|Ent-kaurene synthase A|Protein ANTHER EAR 1
IAA	Zm00001d048192	4.19E-11	-3.5 ± 0.5	AIR12

Hormone	V4 ID	FDR pval.	LFC and SE	Gene description
IAA	Zm00001d026530	0.008150967	-2 ± 0.6	indole-3-acetic acid-induced protein ARG7|SAUR-like auxin-responsive protein family
IAA	Zm00001d031556	3.02E-09	-1.9 ± 0.3	AIR12
IAA	Zm00001d032088	1.01E-10	-1.6 ± 0.2	SAUR33 - auxin-responsive SAUR family member
IAA	Zm00001d012362	0.002635964	1.3 ± 0.4	uncharacterized protein|O-fucosyltransferase family protein
IAA	Zm00001d014774	0.011925572	-1.3 ± 0.4	Auxin-responsive protein SAUR32
IAA	Zm00001d038263	0.001793399	1.3 ± 0.4	O-fucosyltransferase 19
IAA	Zm00001d032475	0.009008937	1.2 ± 0.4	SAUR56 - auxin-responsive SAUR family member|SAUR56-auxin-responsive SAUR family member
IAA	Zm00001d034433	1.83E-12	1.2 ± 0.2	Heat stress transcription factor A-6b
IAA	Zm00001d026632	0.000420624	-1.1 ± 0.3	stem-specific protein TSJT1
IAA	Zm00001d044212	0.020531942	0.9 ± 0.3	putative aldo-keto reductase 4|putative oxidoreductase, aldo/keto reductase family protein
IAA	Zm00001d014562	0.02791146	0.8 ± 0.3	IAA-amino acid hydrolase ILR1-like 6
IAA	Zm00001d018024	3.47E-05	-0.8 ± 0.2	auxin efflux carrier component 1a|PIN-formed protein2
IAA	Zm00001d007357	0.001422747	0.7 ± 0.2	transport inhibitor response 1 protein|Protein AUXIN SIGNALING F-BOX 3
IAA	Zm00001d017906	0.043986978	-0.7 ± 0.3	rhamnogalacturonan I rhamnosyltransferase 1
IAA	Zm00001d010174	0.014558043	-0.6 ± 0.2	COV1-like protein|Protein LIKE COV 2
IAA	Zm00001d011363	0.010083099	0.6 ± 0.2	auxin-induced protein PCNT115|putative oxidoreductase, aldo/keto reductase family protein
IAA	Zm00001d044766	0.024421615	0.6 ± 0.2	O-fucosyltransferase 15
IAA	Zm00001d052493	4.57E-05	-0.6 ± 0.1	stem-specific protein TSJT1|aluminum induced protein with YGL and LRDR motifs
IAA	Zm00001d053004	0.019298063	-0.6 ± 0.2	auxin transporter-like protein 3
IAA	Zm00001d021016	0.037175494	-0.5 ± 0.2	cytochrome b561 and DOMON domain-containing protein At3g25290
IAA	Zm00001d019881	0.041117472	0.4 ± 0.1	auxin transport protein BIG
Jasmonate	Zm00001d044908	0.044580122	3.3 ± 1.3	12-oxo-phytodienoate reductase1|12-oxo-phytodienoic acid reductase 1|12-oxophytodienate reductase 1|12-oxophytodienate reductase1|PCO079165|Zmcoi6.12
Jasmonate	Zm00001d033623	2.53E-08	3.1 ± 0.5	linoleate 9S-lipoxygenase3|lipoxygenase|lipoxygenase3
Jasmonate	Zm00001d042541	1.39E-06	2.1 ± 0.4	linoleate 9S-lipoxygenase1|lipoxygenase 2|lipoxygenase1
Jasmonate	Zm00001d053675	2.60E-27	1.6 ± 0.1	linoleate 13S-lipoxygenase10
Jasmonate	Zm00001d013493	8.70E-16	1.5 ± 0.2	linoleate 9S-lipoxygenase5|lipoxygenase|lipoxygenase5
Jasmonate	Zm00001d028282	5.40E-13	1.1 ± 0.1	allene-oxide synthase2|cytochrome P450 CYP74A19|putative cytochrome P450 superfamily protein
Jasmonate	Zm00001d002000	2.46E-11	0.8 ± 0.1	linoleate 9S-lipoxygenase6|lipoxygenase6

Hormone	V4 ID	FDR pval.	LFC and SE	Gene description
Jasmonate	Zm00001d013185	0.029086171	-0.7 ± 0.2	allene oxide synthase 1, chloroplastic|Allene oxide synthase chloroplastic|putative cytochrome P450 superfamily protein
Jasmonate	Zm00001d033624	0.045442577	-0.7 ± 0.3	linoleate 9S-lipoxygenase4|9-lipoxygenase|lipoxygenase4
Jasmonate	Zm00001d004354	0.000192692	0.6 ± 0.1	cystathionin beta synthase protein|CBS domain-containing protein CBSX1 chloroplastic
Jasmonate	Zm00001d050130	0.00219863	-0.5 ± 0.1	IMP dehydrogenase
SA	Zm00001d029620	3.65E-07	1.9 ± 0.3	indole-3-acetate beta-glucosyltransferase
SA	Zm00001d052827	4.81E-07	1.3 ± 0.2	jasmonate O-methyltransferase|Salicylate/benzoate carboxyl methyltransferase
SA	Zm00001d044763	0.000569577	0.9 ± 0.2	anthranilate O-methyltransferase 3|Benzoate O-methyltransferase|O-methyltransferase 3|Salicylate O-methyltransferas|Salicylate/benzoate carboxyl methyltransferase|anthranilic acid methyltransferase 3
SA	Zm00001d035767	0.001273398	0.7 ± 0.2	Jasmonate O-methyltransferase

Supplementary Table 4.18. Genes (34 in total) presented in the MapMan cellular response (figure 15) overview which were related to abiotic stress-heat for the meristem. Genes are sorted in descending LFC size (absolute value). Gene descriptions of NCBI were used and complemented with those from gramene.org when NCBI descriptions were unavailable. The FDR p-value and LFC, plus standard error (SE) were provided for the severe vs control contrast.

V4 ID	FDR pval.	LFC and SE	Gene description
Zm00001d045036	0.001388453	4.2 ± 1	dnaJ homolog subfamily B member 3|Chaperone DnaJ-domain superfamily protein
Zm00001d016255	3.36E-13	3.8 ± 0.5	heat shock factor protein 1|Heat stress transcription factor C-1
Zm00001d042922	4.69E-14	3 ± 0.4	heat shock 70 kDa protein-like|putative mediator of RNA polymerase II transcription subunit 37c
Zm00001d031325	0.037417791	2.9 ± 1	25.3 kDa heat shock protein chloroplastic
Zm00001d018298	1.55E-37	2.9 ± 0.2	17.4 kDa class III heat shock protein|17.5 kDa class II heat shock protein
Zm00001d028561	0.029244052	2.8 ± 0.9	class I heat shock protein 3|17.4 kDa class I heat shock protein
Zm00001d048073	5.35E-15	2.5 ± 0.3	heat shock 70 kDa protein 1|heat shock protein 1
Zm00001d028630	3.04E-05	2.2 ± 0.4	heat shock cognate 70 kDa protein 2|hsp70 protein
Zm00001d039936	0.044527453	2 ± 0.7	16.9 kDa class I heat shock protein 1|17.4 kDa class I heat shock protein
Zm00001d038806	1.42E-05	1.9 ± 0.4	101 kDa heat shock protein|Chaperone protein ClpB1
Zm00001d044874	0.014584778	-1.8 ± 0.5	23.6 kDa heat shock protein mitochondrial
Zm00001d052947	0.008436962	1.8 ± 0.5	DNAJ heat shock N-terminal domain-containing protein
Zm00001d046299	1.52E-08	1.4 ± 0.2	heat shock factor protein 3|HSF28 HSF type transcription factor
Zm00001d028557	0.000409581	1.3 ± 0.3	17.9 kDa class I heat shock protein|17.4 kDa class I heat shock protein|17.7 kDa class I heat shock protein
Zm00001d012420	2.09E-05	1.2 ± 0.2	heat shock protein 1|Heat shock 70 kDa protein
Zm00001d016070	1.78E-14	1.2 ± 0.1	BAG family molecular chaperone regulator 6|phosphate regulatory homolog1
Zm00001d039566	0.00726447	1.2 ± 0.3	17.5 kDa class II heat shock protein|18kDa heat shock protein
Zm00001d010529	2.86E-07	1 ± 0.2	heat shock 70 kDa protein|heat shock protein 1|heat shock protein 70 kDa|putative mediator of RNA polymerase II transcription subunit 37c
Zm00001d052194	0.022217207	1 ± 0.3	low molecular weight heat shock protein precursor|23.6 kDa heat shock protein mitochondrial|heat shock 22 kDa protein
Zm00001d032923	1.90E-05	0.9 ± 0.2	heat shock factor protein HSF30|Heat stress transcription factor A-6b
Zm00001d014486	1.21E-08	0.8 ± 0.1	phosphosulfolactate synthase-related protein|phosphosulfolactate synthase protein
Zm00001d020898	3.33E-10	0.8 ± 0.1	Heat shock protein 90-2|putative heat shock protein 90 family protein
Zm00001d018297	0.006044215	0.7 ± 0.2	Chaperone DnaJ-domain superfamily protein
Zm00001d034433	0.00045785	0.6 ± 0.1	Heat stress transcription factor A-6b
Zm00001d018335	0.035492063	0.5 ± 0.2	protein SMAX1-like|Protein SUPPRESSOR OF MAX2 1
Zm00001d033210	4.70E-09	0.5 ± 0.1	chaperone DNA J2|Chaperone protein dnaJ 3
Zm00001d015839	0.000582468	-0.5 ± 0.1	chaperone protein dnaJ 6
Zm00001d025136	0.03381295	0.4 ± 0.1	protein SMAX1-LIKE 4

V4 ID	FDR pval.	LFC and SE	Gene description
Zm00001d013669	0.000115037	0.3 ± 0.1	Chaperone protein dnaJ 3|putative dnaJ chaperone family protein
Zm00001d006036	0.002426651	-0.3 ± 0.1	heat shock 70 kDa protein|Heat shock 70 kDa protein 9 mitochondrial|heat shock protein
Zm00001d052855	0.002518172	-0.3 ± 0.1	HSP protein|putative heat shock protein 90 family protein
Zm00001d037700	0.001578847	-0.3 ± 0.1	Heat shock protein 4
Zm00001d034368	0.018561024	0.3 ± 0.1	putative dnaJ chaperone family protein|chaperone DNA J homolog1
Zm00001d002823	0.35519606	0.2 ± 0.1	Hsp70-Hsp90 organizing protein 3

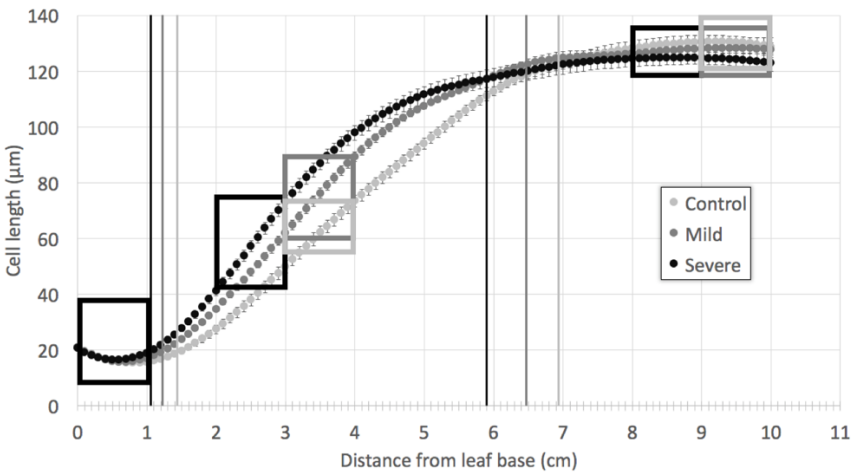

Supplementary Figure 4.1. Segment selection for transcriptome analysis. Not every cm was used for the transcriptome study. Using the data from the kinematic analysis, the location of the meristem and the elongation zone was determined. From each of these zones, and from the subsequent mature zone, a one cm sample from each leaf was collected. For the meristem, the first cm of the leaf was used. For the following zones, the sizes differs according to the treatment (see kinematic analysis chapter 3). To ensure the centre of the elongation zone was used (i.e. where elongation is in full swing), the third cm for leaves of the severe treatment was used, where for the control and mild treatment, the fourth cm segment of the leaves was used. For mature tissue, the ninth cm of the severe treatment was sampled for the severe treatment, where the 10 cm was sampled for the control and mild treatment.

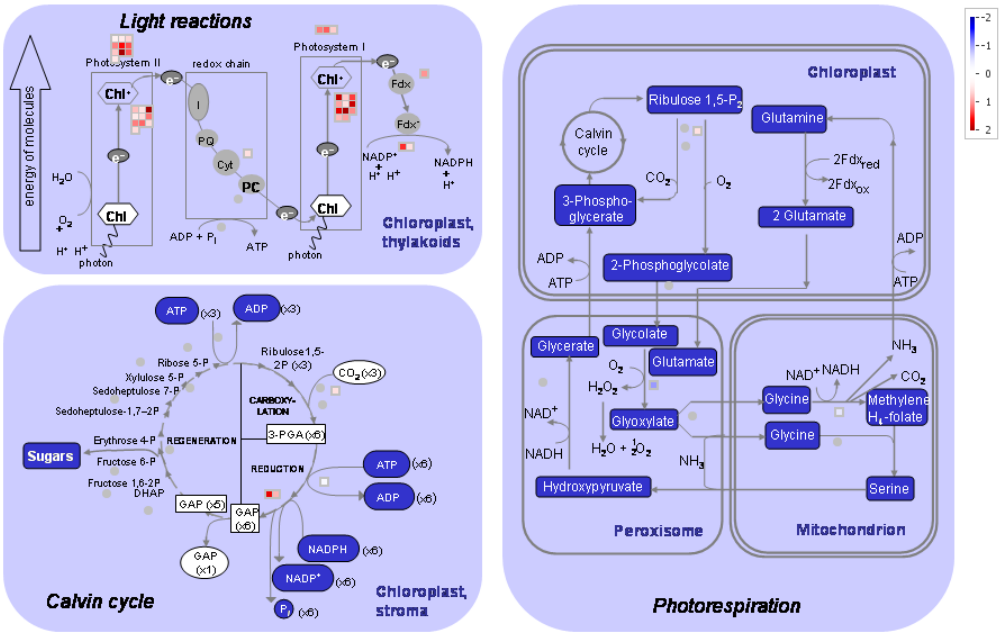

Supplementary Figure 4.2. Photosynthesis MapMan overview for the severe vs control contrast in the meristem. Colour gradient represents LFC. The coloured boxes besides arrows represent LFCs of genes, coding enzymes relevant for that process.

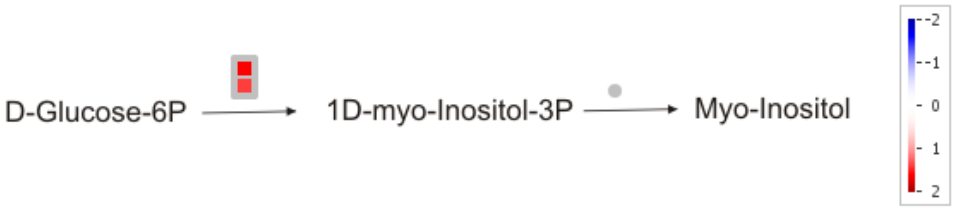

Supplementary Figure 4.3. Myo-inositol synthesis MapMan pathway for severe vs control contrast in the meristem. Colour gradient represents LFC. The coloured boxes besides arrows represent LFCs of genes, coding enzymes relevant for that process.

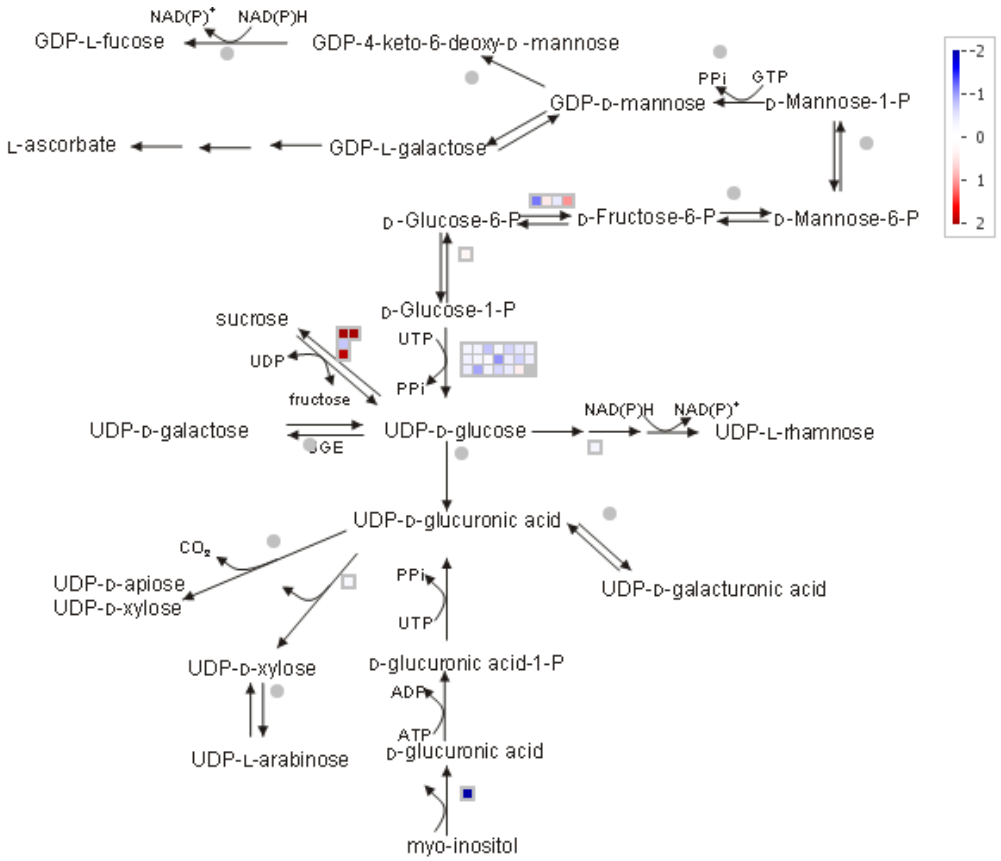

Supplementary Figure 4.4. Cell wall precursors MapMan overview for severe vs control contrast in the meristem. Colour gradient represents LFC. The coloured boxes besides arrows represent LFCs of genes, coding enzymes relevant for that process. Note the highly downregulated inositol oxygenase 2 (LFC -7.5, Zm00001d046234) at the bottom, indicating that myo-inositol serving as a cell wall precursor is less likely.

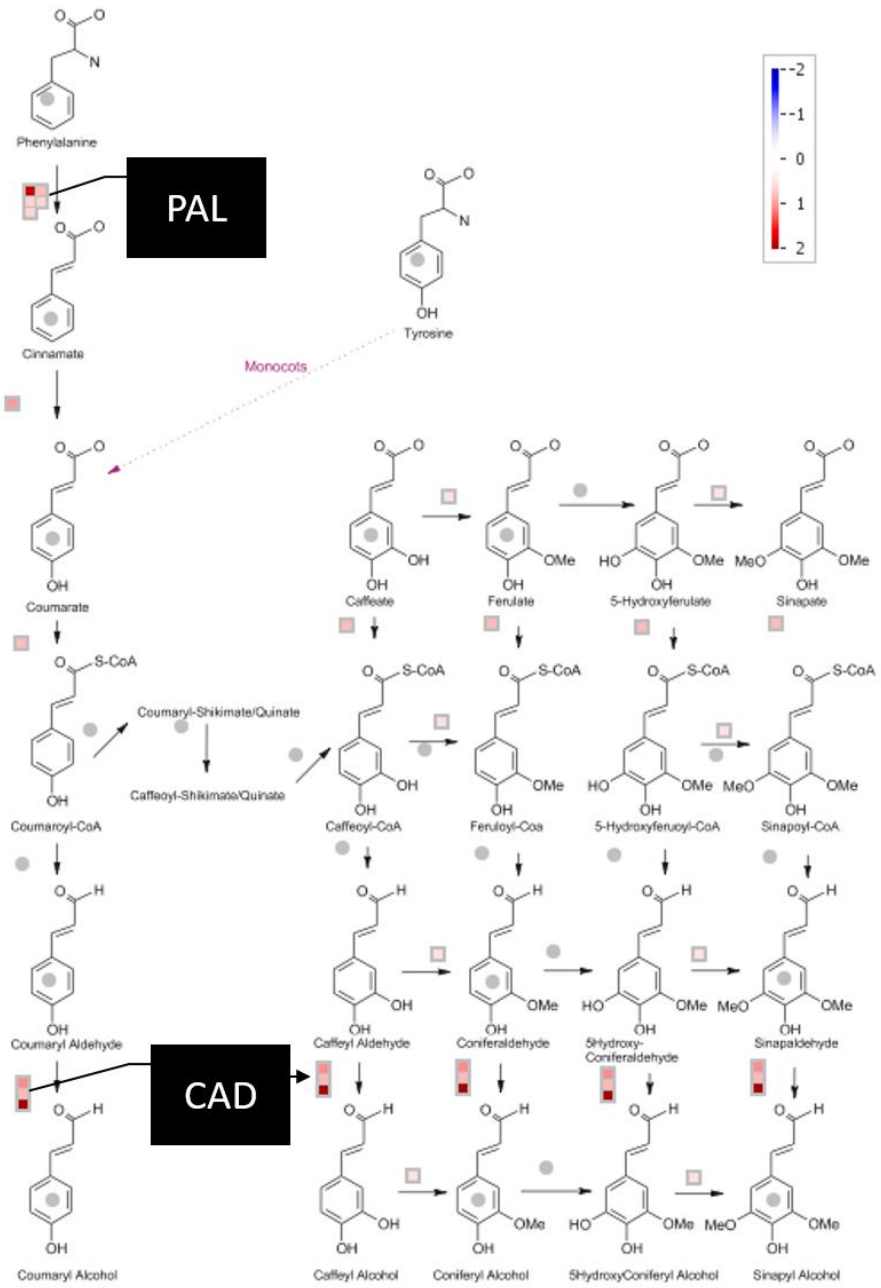

Supplementary Figure 4.5. Phenylpropanoid MapMan pathway for severe vs control contrast in the meristem. Colour gradient represents LFC. The coloured boxes besides arrows represent LFCs of genes, coding enzymes relevant for that process. PAL: phenylalanine ammonia-lyase, CAD: cinnamyl alcohol dehydrogenase

Mild vs control:

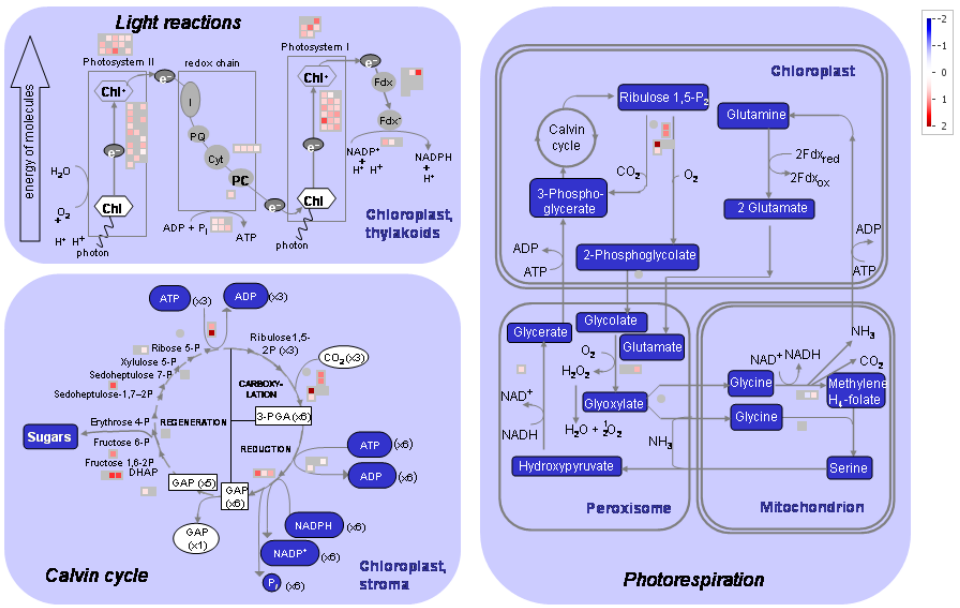

Severe vs control:

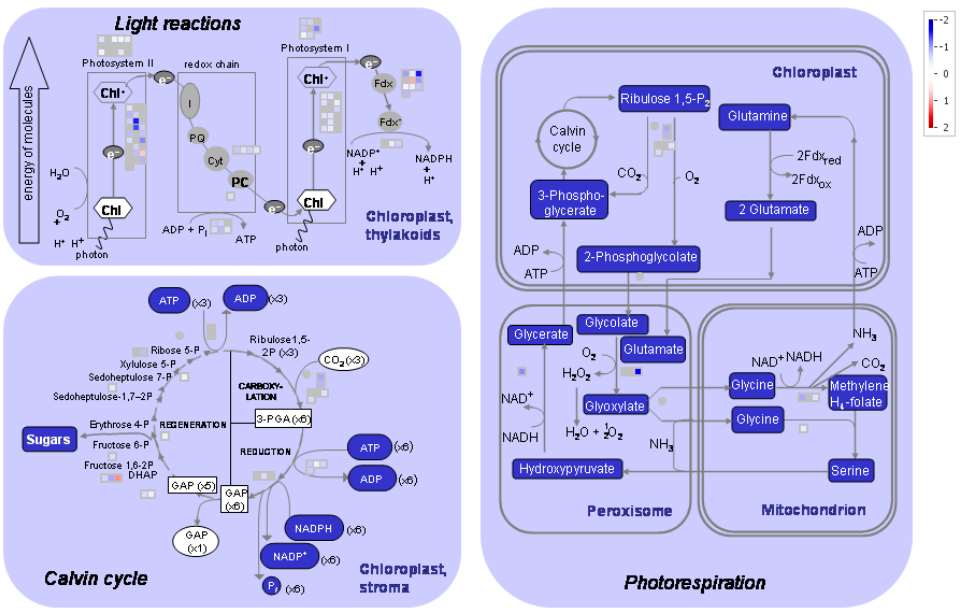

Supplementary Figure 4.6. Photosynthesis MapMan overview for the mild vs control and severe vs control contrast in the elongation zone. Colour gradient represents LFC. The coloured boxes besides arrows represent LFCs of genes, coding enzymes relevant for that process.

Mild vs control:

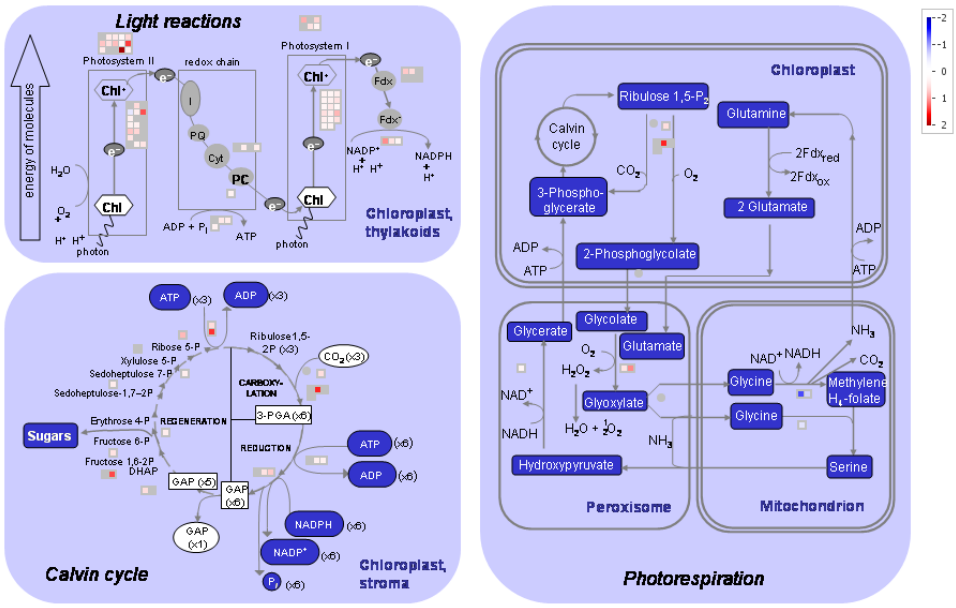

Severe vs control:

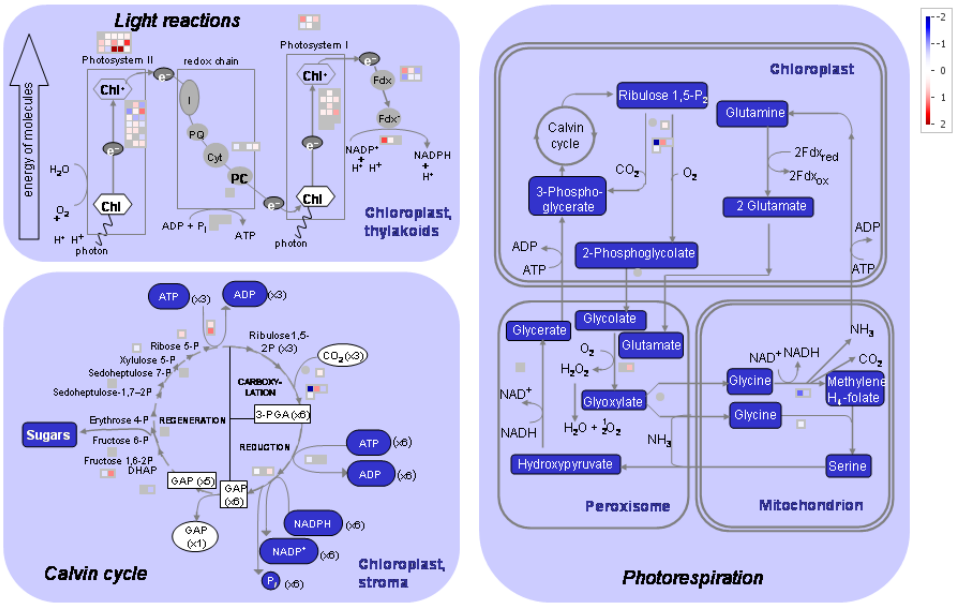

Supplementary Figure 4.7. Photosynthesis MapMan overview for the mild vs control and severe vs control contrast in the mature zone. Colour gradient represents LFC. The coloured boxes besides arrows represent LFCs of genes, coding enzymes relevant for that process.

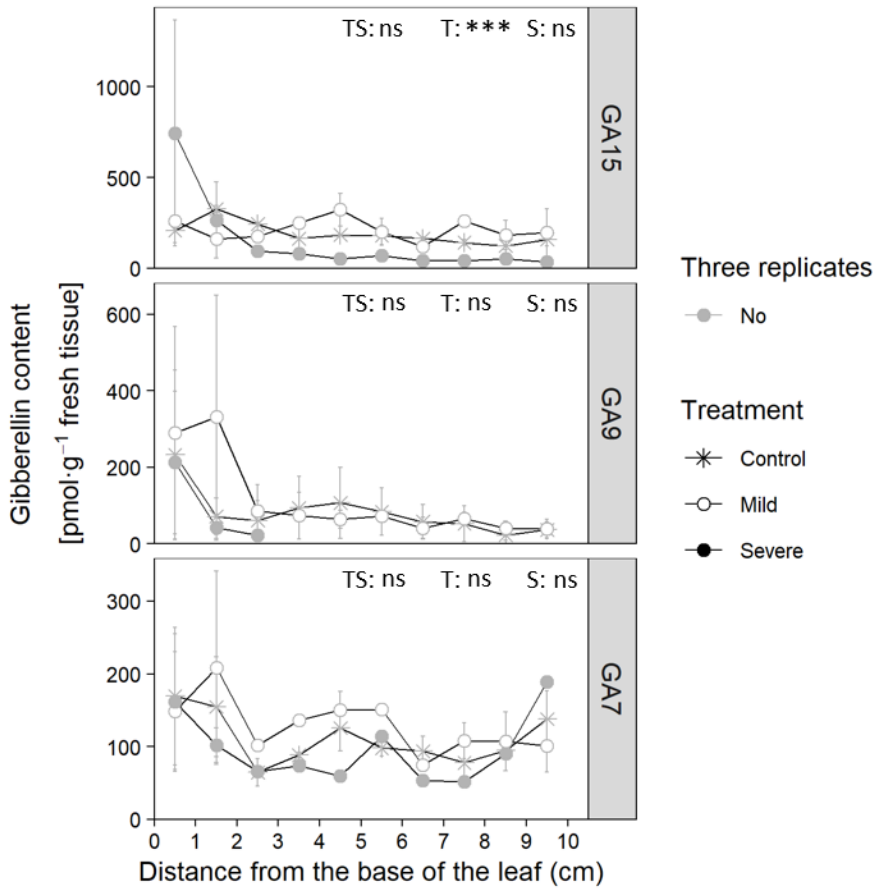

Supplementary Figure 4.8. Gibberellin content and gibberellin oxidase gene expression in the cadmium exposed maize leaf growth zone. Values are mean (n = 3), error bars are standard errors. When less than three measurements were available, the error bar and point is coloured grey. When grey and no error bar is present, only one measurement was available. TS: interaction treatment-segment p-value, T: treatment p-value, S: segment p-value. ns: not significant, * $p < 0.05$, ** $p < 0.01$, *** $p < 0.001$. Note: GA7, GA9 and GA15 were not normally distributed and/or heteroscedastic, even after log10 transformation.

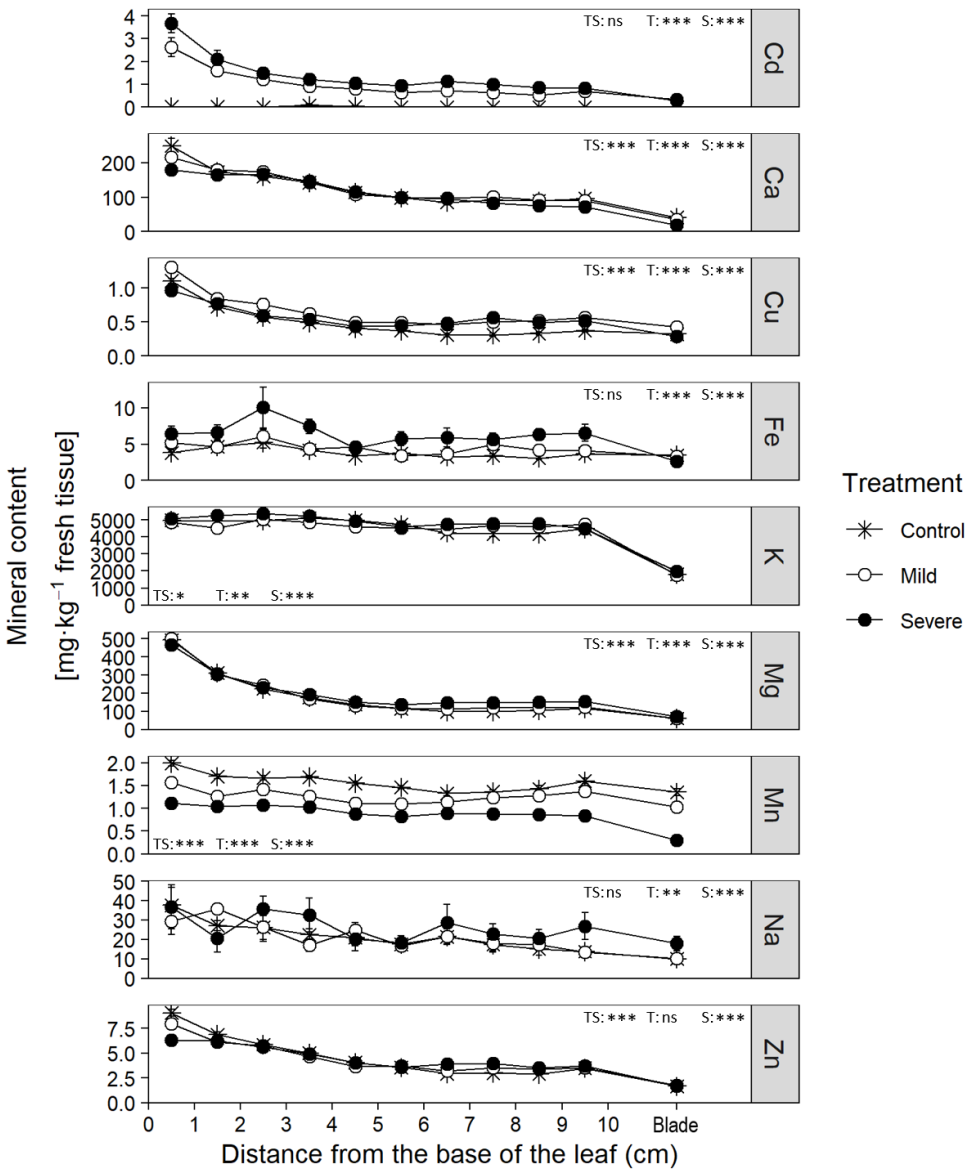

Supplementary Figure 4.9. The effect of Cd on mineral levels in the maize leaf growth zone, expressed on fresh mass of the tissue. Values are mean (n = 5), error bars are standard errors. When less than five measurements were available, the error bar and point is coloured grey. When no error bar is present, only one measurement was available. Do note that for most measurements, the error bars is too small to be visible beyond the point (i.e. the black points with seemingly no error bar). The following minerals were not detected or removed due to contamination: Co, Mo, Ni, Si and B. Note: Cd, Ca, Fe and K were not normally distributed after log10 transformation. TS: interaction treatment-segment p-value, T: treatment p-value, S: segment p-value. ns: not significant, * $p < 0.05$, ** $p < 0.01$, *** $p < 0.001$.

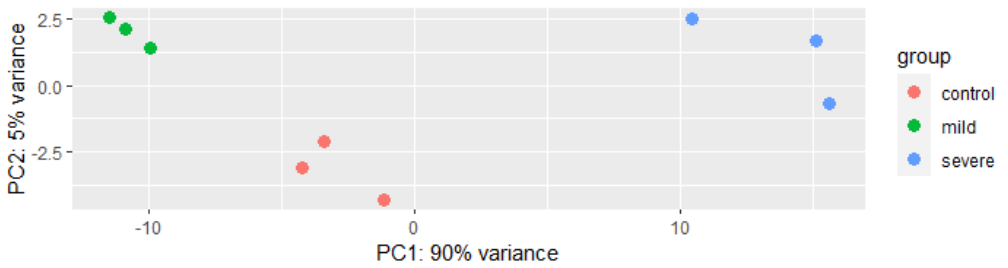

Supplementary Figure 4.10. The impact of developmental stage on the transcriptome profile in the elongation zone, presented through a principle component analysis. Each dot represents the entire transcriptome of a sample, where the distance between dots indicates the differences between the transcriptomes. Samples are grouped based on treatment (i.e. control, mild and severe). Clearly, mild and severe Cd treatments samples differ most from each other, since they are clearly separated by principle component 1 which explains 90% of the variation present in the datasets.

Supplementary data chapter 5

During the LICOR measurements, the majority of measurements were performed whilst scrubbing the air for water removal. This was not supposed to happen since it causes an extra from of stress on the plants, i.e. dry air. Over the five measurement days, water scrubbing was not constant (Supplementary Figure 5.1). One can see that scrubbing was performed on three of the five days (RH_R_in = 0), where on the third day, air was partially scrubbed. After it has passed by the leaf surface, humidity increased again (RH_S_in).

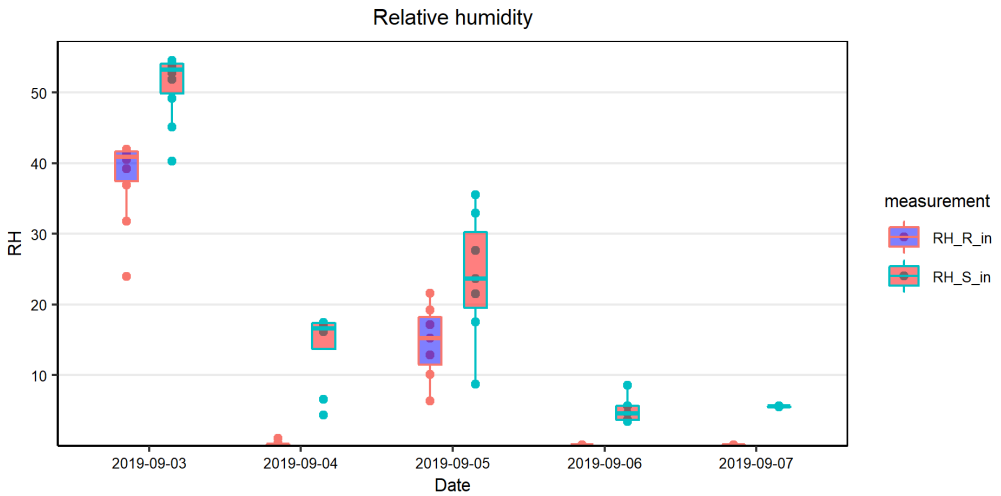

Supplementary Figure 5.1. Relative humidity (RH, %) across the five days of measurements. RH_R_in is the internal relative humidity before it reaches the sample, where RH_S_in is the internal relative humidity after it has been passed through the chamber with the leaf.

This dry air could affect stomatal conductance and photosynthetic activity. Therefore, with the remainder of plants, the effect of scrubbing the air for water was tested. Here, we can see that stomatal conductance was slightly affected, where it reduced due to scrubbing (Supplementary Figure 5.2). Yet, the response in photosynthetic rate on scrubbing seems rather unaffected within the small time frame of scrubbing (Supplementary Figure 5.3).

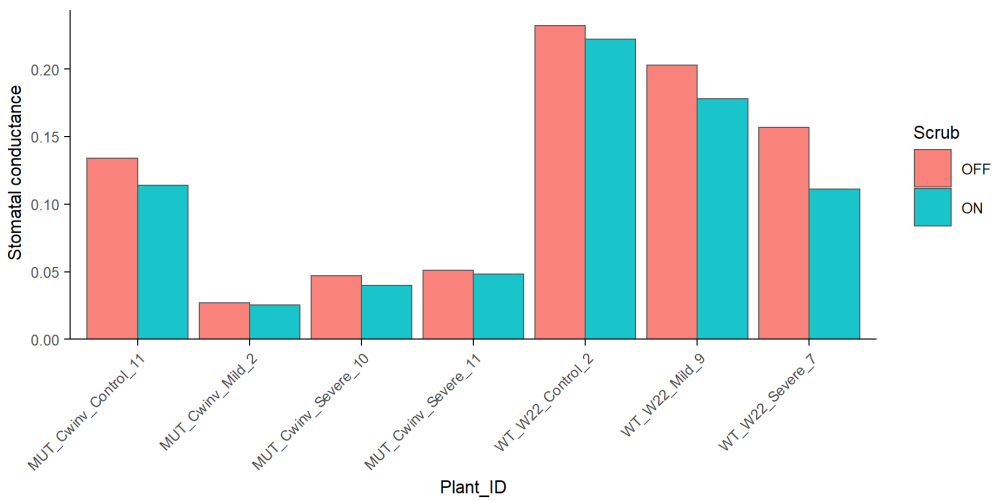

Supplementary Figure 5.2. The effect of scrubbing of the air for water on stomatal conductance before it is passed into the leaf measurement chamber of the LICOR.

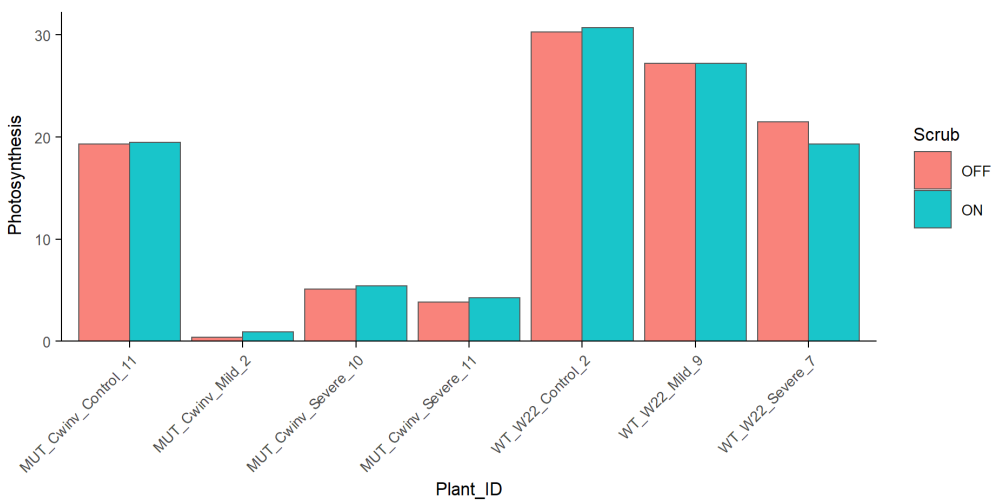

Supplementary Figure 5.3. The effect of scrubbing of the air for water on photosynthetic rate before it is passed into the leaf measurement chamber of the LICOR.

Supplementary Figure 5.4. Illustration of W22 and CWI mutant phenotype under control and Cd growth conditions (mild and severe) 4 weeks after sowing. Plants originate from the kinematic analysis experiment. The scale above is in total 30 cm, with ticks at 0, 10, 20 and 30 cm.

Supplementary Figure 5.5. Cell wall invertase transcriptome reads. The described mutation (CCG → CTG) is absent (top figure: W22, bottom figure: CWI mutant). A proline is still coded by the mRNA.

Supplementary data chapter 6

No supplementary data.

References

AbdElgawad H, Zinta G, Hamed BA, Selim S, Beemster G, Hozzein WN, Wadaan MAM, Asard H, Abuelsoud W. 2020. Maize roots and shoots show distinct profiles of oxidative stress and antioxidant defense under heavy metal toxicity. Environmental Pollution **258**, 113705.

Afgan E, Baker D, Batut B, *et al.* 2018. The Galaxy platform for accessible, reproducible and collaborative biomedical analyses: 2018 update. Nucleic Acids Research **46**, 537–544.

Akhtar T, Zia-ur-Rehman M, Naeem A, Nawaz R, Ali S, Murtaza G, Maqsood MA, Azhar M, Khalid H, Rizwan M. 2016. Photosynthesis and growth response of maize (*Zea mays* L.) hybrids exposed to cadmium stress. Environmental Science and Pollution Research, 5521–5529.

Albacete A, Cantero-Navarro E, Großkinsky DK, *et al.* 2015. Ectopic overexpression of the cell wall invertase gene CIN1 leads to dehydration avoidance in tomato. Journal of Experimental Botany **66**, 863–878.

Alves LR, Monteiro CC, Carvalho RF, Ribeiro PC, Tezotto T, Azevedo RA, Gratão PL. 2017. Cadmium stress related to root-to-shoot communication depends on ethylene and auxin in tomato plants. Environmental and Experimental Botany **134**, 102–115.

Alyemeni MN, Ahanger MA, Wijaya L, Alam P, Bhardwaj R, Ahmad P. 2018. Selenium mitigates cadmium-induced oxidative stress in tomato (*Solanum lycopersicum* L.) plants by modulating chlorophyll fluorescence, osmolyte accumulation, and antioxidant system. Protoplasma **255**, 459–469.

Andrews S. 2012. FastQC A Quality Control tool for High Throughput Sequence Data.

Andriankaja M, Dhondt S, DeBodt S, *et al.* 2012. Exit from Proliferation during Leaf Development in Arabidopsis thaliana: A Not-So-Gradual Process. Developmental Cell **22**, 64–78.

Arduini I, Masoni A, Mariotti M, Ercoli L. 2004. Low cadmium application increase miscanthus growth and cadmium translocation. Environmental and Experimental Botany **52**, 89–100.

Asgher M, Khan MIR, Anjum NA, Khan NA. 2015. Minimising toxicity of cadmium in plants—role of plant growth regulators. Protoplasma **252**, 399–413.

Avramova V, AbdElgawad H, Guisez Y, Asard H, Beemster GTS. 2015*a*. The growth zone of maize leaves is an ideal model system for systems biology approaches to investigate the effects of drought stress on organ growth regulation. Procedia Environmental Sciences **29**, 258.

Avramova V, AbdElgawad H, Vasileva I, Petrova AS, Holek A, Mariën J, Asard H, Beemster GTS. 2017. High Antioxidant Activity Facilitates Maintenance of Cell Division in Leaves of Drought Tolerant Maize Hybrids. Frontiers in Plant Science **8**, 84.

Avramova V, AbdElgawad H, Zhang Z, *et al.* 2015*b*. Drought induces distinct growth response, protection, and recovery mechanisms in the maize leaf growth zone. Plant Physiology **169**, 1382–1396.

Avramova V, Sprangers K, Beemster GTS. 2015*c*. The Maize Leaf: Another Perspective on Growth Regulation. Trends in Plant Science **20**, 787–797.

Awad F, Römheld V. 2000. Mobilization of heavy metals from contaminated calcareous soils by plant born, microbial and synthetic chelators and their uptake by wheat plants. Journal of Plant Nutrition **23**, 1847–1855.

Azevedo H, Pinto CGG, Fernandes J, Loureiro S, Santos C. 2005. Cadmium effects on sunflower growth and photosynthesis. Journal of Plant Nutrition **28**, 2211–2220.

Bali AS, Sidhu GPS, Kumar V. 2020. Root exudates ameliorate cadmium tolerance in plants: A review. Environmental Chemistry Letters **18**, 1243–1275.

Baliardini C, Corso M, Verbruggen N. 2016. Transcriptomic analysis supports the role of CATION EXCHANGER 1 in cellular homeostasis and oxidative stress limitation during cadmium stress. Plant Signaling and Behavior **11**, 1–5.

Barbier de Reuille P, Routier-Kierzkowska A-L, Kierzkowski D, *et al.* 2015. MorphoGraphX: A platform for quantifying morphogenesis in 4D. eLife **4**, 1–20.

Bardou P, Mariette J, Escudié F, Djemiel C, Klopp C. 2014. jvenn: an interactive Venn diagram viewer. BMC Bioinformatics **15**, 293.

Baryla A, Carrier P, Franck F, Coulomb C, Sahut C, Havaux M. 2001. Leaf chlorosis in oilseed rape plants (*Brassica napus*) grown on cadmium-polluted soil: Causes and consequences for photosynthesis and growth. Planta **212**, 696–709.

Bashir S, Zhu J, Fu Q, Hu H. 2018. Cadmium mobility, uptake and anti-oxidative response of water spinach (*Ipomoea aquatic*) under rice straw biochar, zeolite and rock phosphate as amendments. Chemosphere **194**, 579–587.

Basso MC, Cerrella EG, Cukierman AL. 2005. Cadmium Uptake by Lignocellulosic Materials: Effect of Lignin Content. Separation Science and Technology **39**, 1163–1175.

Beemster GTS, Baskin TI. 1998. Analysis of Cell Division and Elongation Underlying the Developmental Acceleration of Root Growth in *Arabidopsis thaliana*. Plant Physiology **116**, 1515–1526.

Beemster GTS, Fiorani F, Inzé D. 2003. Cell cycle: the key to plant growth control? Trends in Plant Science **8**, 154–158.

Benáková M, Ahmadi H, Dučaiová Z, Tylová E, Clemens S, Tůma J. 2017. Effects of Cd and Zn on physiological and anatomical properties of hydroponically grown *Brassica napus* plants. Environmental Science and Pollution Research **24**, 20705–20716.

Benzie IFF, Strain JJ. 1999. Ferric reducing/antioxidant power assay: Direct measure of total antioxidant activity of biological fluids and modified version for simultaneous measurement of total antioxidant power and ascorbic acid concentration. Methods in Enzymology **299**, 15–27.

Bertels J, Huybrechts M, Hendrix S, Bervoets L, Cuypers A, Beemster GTS. 2020. Cadmium inhibits cell cycle progression and specifically accumulates in the maize leaf meristem. Journal of Experimental Botany **71**, 6418–6428.

Bi Y, Chen W, Zhang W, Zhou Q, Yun L, Xing D. 2009. Production of reactive oxygen species, impairment of photosynthetic function and dynamic changes in mitochondria are early events in cadmium-induced cell death in *Arabidopsis thaliana*. Biology of the Cell **101**, 629–643.

Bieleski RL. 1993. Fructan hydrolysis drives petal expansion in the ephemeral daylily flower. Plant Physiology **103**, 213–219.

Binenbaum J, Weinstain R, Shani E. 2018. Gibberellin Localization and Transport in Plants. Trends in Plant Science **23**, 410–421.

Bišová K, Hendrychová J, Cepák V, Zachleder V. 2003. Cell growth and division processes are differentially sensitive to cadmium in *Scenedesmus quadricauda*. Folia Microbiologica **48**, 805–816.

Blackman VH. 1919. The Compound Interest Law and Plant Growth. Annals of Botany **os**-**33**, 353–360.

Bogdanović J, Mojović M, Milosavić N, Mitrović A, Vučinić Ž, Spasojević I. 2008. Role of fructose in the adaptation of plants to cold-induced oxidative stress. European Biophysics Journal **37**, 1241–1246.

Bolger AM, Lohse M, Usadel B. 2014. Trimmomatic: A flexible trimmer for Illumina sequence data. Bioinformatics **30**, 2114–2120.

Bolouri-Moghaddam MR, Le Roy K, Xiang L, Rolland F, Van Den Ende W. 2010. Sugar signalling and antioxidant network connections in plant cells. FEBS Journal **277**, 2022–2037.

Bruno L, Pacenza M, Forgione I, Lamerton LR, Greco M, Chiappetta A, Bitonti MB. 2017. In *Arabidopsis thaliana* Cadmium Impact on the Growth of Primary Root by Altering SCR Expression and Auxin-Cytokinin Cross-Talk. Frontiers in Plant Science **8**, 1–13.

Bücker-Neto L, Paiva ALS, Machado RD, Arenhart RA, Margis-Pinheiro M. 2017. Interactions between plant hormones and heavy metals responses. Genetics and Molecular Biology **40**, 373–386.

Cai K, Yu Y, Zhang M, Kim K. 2019. Concentration, source, and total health risks of cadmium in multiple media in densely populated areas, China. International Journal of Environmental Research and Public Health **16**.

Camisón Á, Ángela Martín M, Dorado FJ, Moreno G, Solla A. 2020. Changes in carbohydrates induced by drought and waterlogging in *Castanea sativa*. Trees - Structure and Function **34**, 579–591.

Cao X, Wang H, Zhuang D, *et al.* 2018. Roles of MSH2 and MSH6 in cadmium-induced G2/M checkpoint arrest in Arabidopsis roots. Chemosphere **201**, 586–594.

Cao Y, Zhao X, Liu Y, *et al.* 2019. Genome-wide identification of ZmHMAs and association of natural variation in ZmHMA2 and ZmHMA3 with leaf cadmium accumulation in maize. PeerJ **2019**, 1–21.

Carlson SJ, Shanker S, Chourey PS. 2000. A point mutation at the *Miniature1* seed locus reduces levels of the encoded protein, but not its mRNA, in maize. Molecular and General Genetics **263**, 367–373.

Carvalho MEA, Castro PRC, Kozak M, Azevedo RA. 2020. The sweet side of misbalanced nutrients in cadmium-stressed plants. Annals of Applied Biology, aab.12569.

Carvalho MAM, Dietrich SMC. 1993. Variation in fructan content in the underground organs of *Vernonia herbacea* (Veil.) Rusby at different phenological phases. New Phytologist **123**, 735–740.

Çatav ŞS, Genç TO, Oktay MK, Küçükakyüz K. 2019. Cadmium Toxicity in Wheat: Impacts on Element Contents, Antioxidant Enzyme Activities, Oxidative Stress, and Genotoxicity. Bulletin of Environmental Contamination and Toxicology **104**, 71–77.

Cerretani L, Bendini A. 2010. Rapid Assays to Evaluate the Antioxidant Capacity of Phenols in Virgin Olive Oil. Elsevier Inc.

Chen C, Cao Q, Jiang Q, Li J, Yu R, Shi G. 2019. Comparative transcriptome analysis reveals gene network regulating cadmium uptake and translocation in peanut roots under iron deficiency. BMC Plant Biology **19**, 1–14.

Chen D, Guo H, Li R, Li L, Pan G, Chang A, Joseph S. 2016. Low uptake affinity cultivars with biochar to tackle Cd-tainted rice — A field study over four rice seasons in Hunan, China. Science of the Total Environment **541**, 1489–1498.

Chen LQ, Qu XQ, Hou BH, Sosso D, Osorio S, Fernie AR, Frommer WB. 2012. Sucrose efflux mediated by SWEET proteins as a key step for phloem transport. Science **335**, 207–211.

Cheng WH, Taliercio EW, Chourey PS. 1996. The *Miniature1* Seed Locus of Maize Encodes a Cell Wall Invertase Required for Normal Development of Endosperm and Maternal Cells in the Pedicel. The Plant Cell **8**, 971–983.

Chiao WT, Yu CH, Juang KW. 2019. The variation of rice cultivars in Cd toxicity and distribution of the seedlings and their root histochemical examination. Paddy and Water Environment **17**, 605–618.

Chourey PS, Taliercio EW, Carlson SJ, Ruan YL. 1998. Genetic evidence that the two

isozymes of sucrose synthase present in developing maize endosperm are critical, one for cell wall integrity and the other for starch biosynthesis. Molecular and General Genetics **259**, 88–96.

Christensen CSL, Rasmussen SK. 2019. Low Lignin Mutants and Reduction of Lignin Content in Grasses for Increased Utilisation of Lignocellulose. Agronomy **9**, 256.

Clemens S. 2006. Toxic metal accumulation, responses to exposure and mechanisms of tolerance in plants. Biochimie **88**, 1707–1719.

Clemens S. 2019. Safer food through plant science: reducing toxic element accumulation in crops. Journal of Experimental Botany **70**, 5537–5557.

Clemens S, Aarts MGM, Thomine S, Verbruggen N. 2013. Plant science: The key to preventing slow cadmium poisoning. Trends in Plant Science **18**, 92–99.

Cobbett CS. 2000. Phytochelatin biosynthesis and function in heavy-metal detoxification. Current Opinion in Plant Biology **3**, 211–216.

Considine MJ, Foyer CH. 2014. Redox regulation of plant development. Antioxidants & redox signaling **21**, 1305–1326.

Cools T, Iantcheva A, Weimer AK, Boens S, Takahashi N, Maes S, Van den Daele H, Van Isterdael G, Schnittger A, De Veylder L. 2011. The Arabidopsis thaliana checkpoint kinase WEE1 protects against premature vascular differentiation during replication stress. The Plant Cell **23**, 1435–1448.

Corbesier L, Prinsen E, Jacqmard A, Lejeune P, Van Onckelen H, Périlleux C, Bernier G. 2003. Cytokinin levels in leaves, leaf exudate and shoot apical meristem of Arabidopsis thaliana during floral transition. Journal of Experimental Botany **54**, 2511–2517.

Costa G, Spitz E. 1997. Influence of cadmium on soluble carbohydrates, free amino acids, protein content of in vitro cultured *Lupinus albus*. Plant Science **128**, 131–140.

Couée I, Sulmon C, Gouesbet G, El Amrani A. 2006. Involvement of soluble sugars in reactive oxygen species balance and responses to oxidative stress in plants. Journal of Experimental Botany **57**, 449–459.

Crick F. 1970. Central Dogma of Molecular Biology. Nature **227**, 561–563.

Crowell EF, Timpano H, Desprez T, Franssen-Verheijen T, Emons A-M, Höfte H, Vernhettes S. 2011. Differential regulation of cellulose orientation at the inner and outer face of epidermal cells in the Arabidopsis hypocotyl. The Plant Cell **23**, 2592–2605.

Cui W, Wang H, Song J, *et al.* 2017. Cell cycle arrest mediated by Cd-induced DNA damage in Arabidopsis root tips. Ecotoxicology and Environmental Safety **145**, 569–574.

Cuypers A, Hendrix S, Reis RA dos, *et al.* 2016. Hydrogen peroxide, signaling in disguise during metal phytotoxicity. Frontiers in Plant Science **7**, 46.

Cuypers A, Keunen E, Bohler S, *et al.* 2012. Cadmium and copper stress induce a cellular oxidative challenge leading to damage versus signalling. Metal Toxicity in Plants: Perception, Signaling and Remediation. Berlin, Heidelberg: Springer Berlin Heidelberg, 65–90.

Cuypers A, Plusquin M, Remans T, *et al.* 2010. Cadmium stress: An oxidative challenge. BioMetals **23**, 927–940.

Dauthieu M, Denaix L, Nguyen C, Panfili F, Perrot F, Potin-Gautier M. 2009. Cadmium uptake and distribution in *Arabidopsis thaliana* exposed to low chronic concentrations depends on plant growth. Plant and Soil **322**, 239–249.

Demecsová L, Zelinová V, Liptáková Ľ, Tamás L. 2020. Mild cadmium stress induces auxin synthesis and accumulation, while severe cadmium stress causes its rapid depletion in barley root tip. Environmental and Experimental Botany **175**.

Dempsey DA, Vlot AC, Wildermuth MC, Klessig DF. 2011. Salicylic Acid Biosynthesis and Metabolism. The Arabidopsis Book **9**.

Devi R, Munjral N, Gupta AK, Kaur N. 2007. Cadmium induced changes in carbohydrate status and enzymes of carbohydrate metabolism, glycolysis and pentose phosphate pathway in pea. Environmental and Experimental Botany **61**, 167–174.

Dias MC, Monteiro C, Moutinho-Pereira J, Correia C, Gonçalves B, Santos C. 2013. Cadmium toxicity affects photosynthesis and plant growth at different levels. Acta Physiologiae Plantarum **35**, 1281–1289.

Dronnet VM, Renard CMGC, Axelos MAV, Thibault JF. 1996. Heavy metals binding by pectins: selectivity, quantification and characterisation. Progress in Biotechnology **14**, 535–540.

Dubey S, Shri M, Gupta A, Rani V, Chakrabarty D. 2018. Toxicity and detoxification of heavy metals during plant growth and metabolism. Environmental Chemistry Letters **16**, 1169–1192.

Dubois M, Van den Broeck L, Inzé D. 2018. The Pivotal Role of Ethylene in Plant Growth. Trends in Plant Science **23**, 311–323.

Elobeid M, Göbel C, Feussner I, Polle A. 2012. Cadmium interferes with auxin physiology and lignification in poplar. Journal of Experimental Botany **63**, 1413–1421.

Emamverdian A, Ding Y, Xie Y. 2020. The role of new members of phytohormones in plant amelioration under abiotic stress with an emphasis on heavy metals. Polish Journal of Environmental Studies **29**, 1009–1020.

Van den Ende W. 2013. Multifunctional fructans and raffinose family oligosaccharides. Frontiers in Plant Science **4**, 1–11.

Erickson RO. 1976. Modeling of Plant Growth. Annual Review of Plant Physiology **27**, 407–434.

Erickson RO, Sax KB. 1956. Rates of Cell Division and Cell Elongation in the Growth of

the Primary Root of *Zea mays*. Proc. Am. Phil. Soc. **100**, 499–514.

Eriksson J. E. 1989. The influence of pH, soil type and time on adsorbtion and uptake by plants of Cd added to soil. Water, Air, and Soil Pollution, 317–335.

Fang Y, Deng X, Lu X, Zheng J, Jiang H, Rao Y, Zeng D, Hu J, Zhang X, Xue D. 2019. Differential phosphoproteome study of the response to cadmium stress in rice. Ecotoxicology and Environmental Safety **180**, 780–788.

Feng J, Shi Y, Yang S, Zuo J. 2017. Cytokinins. Hormone Metabolism and Signaling in Plants, 77–106.

Finger-Teixeira A, Lucio Ferrarese M de L, Ricardo Soares A, da Silva D, Ferrarese-Filho Osvaldo O. 2010. Cadmium-induced lignification restricts soybean root growth. Ecotoxicology and Environmental Safety **73**, 1959–1964.

Fischer S, Spielau T, Clemens S. 2017. Natural variation in *Arabidopsis thaliana* Cd responses and the detection of quantitative trait loci affecting Cd tolerance. Scientific Reports **7**, 1–14.

Fujimaki S, Suzui N, Ishioka NS, Kawachi N, Ito S, Chino M, Nakamura S. 2010. Tracing cadmium from culture to spikelet: noninvasive imaging and quantitative characterization of absorption, transport, and accumulation of cadmium in an intact rice plant. Plant Physiology **152**, 1796–1806.

Fujita M, Fujita Y, Noutoshi Y, Takahashi F, Narusaka Y, Yamaguchi-Shinozaki K, Shinozaki K. 2006. Crosstalk between abiotic and biotic stress responses: a current view from the points of convergence in the stress signaling networks. Current Opinion in Plant Biology **9**, 436–442.

Fusconi A, Gallo C, Camusso W. 2007. Effects of cadmium on root apical meristems of *Pisum sativum* L.: Cell viability, cell proliferation and microtubule pattern as suitable markers for assessment of stress pollution. Mutation Research - Genetic Toxicology and Environmental Mutagenesis **632**, 9–19.

Fusconi A, Repetto O, Bona E, Massa N, Gallo C, Dumas-Gaudot E, Berta G. 2006. Effects of cadmium on meristem activity and nucleus ploidy in roots of *Pisum sativum* L. cv. Frisson seedlings. Environmental and Experimental Botany **58**, 253–260.

Gandar PW. 1980. The Analysis of Growth and Cell Production in Root Apices. Botanical Gazette **141**, 131–138.

Gázquez A, Beemster GTS. 2017. What determines organ size differences between species? A meta-analysis of the cellular basis. New Phytologist **215**, 299–308.

Goodwin RH, Stepka W. 1945. Growth and differentiation in the root tip of *Phleum pratense*. American Journal of Botany **32**, 36–46.

Green PB. 1962. Mechanism for Plant Cellular Morphogenesis. Science **138**, 1404–1405.

Grossmann K, Retzlaff G. 1997. Bioregulatory effects of the fungicidal strobilurin

kresoxim-methyl in wheat (*Triticum aestivum*). Pesticide Science **50**, 11–20.

Gruening BA. 2014. Multi Join.

Gu L, Zhao M, Ge M, Zhu S, Cheng B, Li X. 2019. Transcriptome analysis reveals comprehensive responses to cadmium stress in maize inoculated with arbuscular mycorrhizal fungi. Ecotoxicology and Environmental Safety **186**, 109744.

Gul F, Arfan M, Shahbaz MS, Basra MA. 2020. Salicylic acid seed priming modulates morphology, nutrient relations and photosynthetic attributes of wheat grown under cadmium stress. International Journal of Agriculture and Biology **23**, 197–204.

Guo Z, Gibson M, Sitha S, Chu S, Mohanty U. 2011. Role of large thermal fluctuations and magnesium ions in t-RNA selectivity of the ribosome. Proceedings of the National Academy of Sciences of the United States of America **108**, 3947–3951.

Guo B, Liu C, Liang Y, Li N, Fu Q. 2019*a*. Salicylic Acid Signals Plant Defence against Cadmium Toxicity. International Journal of Molecular Sciences **20**, 2960.

Guo J, Qin S, Rengel Z, Gao W, Nie Z, Liu H, Li C, Zhao P. 2019*b*. Cadmium stress increases antioxidant enzyme activities and decreases endogenous hormone concentrations more in Cd-tolerant than Cd-sensitive wheat varieties. Ecotoxicology and Environmental Safety **172**, 380–387.

Hadi F, Ali N, Ahmad A. 2014. Enhanced phytoremediation of cadmium-contaminated soil by *Parthenium hysterophorus* plant: Effect of gibberellic acid (GA3) and synthetic chelator, alone and in combinations. Bioremediation Journal **18**, 46–55.

Hahne F, LeMeur N, Brinkman RR, Ellis B, Haaland P, Sarkar D, Spidlen J, Strain E, Gentleman R. 2009. flowCore: a Bioconductor package for high throughput flow cytometry. BMC Bioinformatics **10**, 106.

Hansen J, Møller I. 1975. Percolation of starch and soluble carbohydrates from plant tissue for quantitative determination with anthrone. Analytical Biochemistry **68**, 87–94.

Harris NS, Taylor GJ. 2013. Cadmium uptake and partitioning in durum wheat during grain filling. BMC Plant Biology **13**, 1–16.

Hartig K, Beck E. 2006. Crosstalk between auxin, cytokinins, and sugars in the plant cell cycle. Plant Biology **8**, 389–396.

Hasan SA, Fariduddin Q, Ali B, Hayat S, Ahmad A. 2009. Cadmium: Toxicity and tolerance in plants. Journal of Environmental Biology March J. Environ. Biol **30**, 165–174.

Hawkes SJ. 1997. What Is a 'Heavy Metal'? Journal of Chemical Education **74**, 1374.

He F, Liu Q, Zheng L, Cui Y, Shen Z, Zheng L. 2015. Rna-seq analysis of rice roots reveals the involvement of post-transcriptional regulation in response to cadmium stress. Frontiers in Plant Science **6**, 1–16.

Hendrix S, Keunen E, Mertens AIG, Beemster GTS, Vangronsveld J, Cuypers A. 2018. Cell cycle regulation in different leaves of *Arabidopsis thaliana* plants grown under control and cadmium-exposed conditions. Environmental and Experimental Botany **155**, 441–452.

Hepler PK. 1994. The role of calcium in cell division. Cell Calcium **16**, 322–330.

Hill JT, Demarest BL, Bisgrove BW, Gorsi B, Su YC, Yost HJ. 2013. MMAPPR: Mutation Mapping Analysis Pipeline for Pooled RNA-seq. Genome Research **23**, 687–697.

Hluska T, Dobrev PI, Tarkowská D, *et al.* 2016. Cytokinin metabolism in maize: Novel evidence of cytokinin abundance, interconversions and formation of a new trans-zeatin metabolic product with a weak anticytokinin activity. Plant Science **247**, 127–137.

Hodges DM, DeLong JM, Forney CF, Prange RK. 1999. Improving the thiobarbituric acid-reactive-substances assay for estimating lipid peroxidation in plant tissues containing anthocyanin and other interfering compounds. Planta **207**, 604–611.

Hoffman NE, Fa Yang S. 1980. Changes of 1-Aminocyclopropane-1-carboxylic Acid Content in Ripening Fruits in Relation to their Ethylene Production Rates 1. J. Amer. Soc. Hort. Sci **105**, 492–495.

Hsu YT, Kao CH. 2003. Role of abscisic acid in cadmium tolerance of rice (Oryza sativa L.) seedlings. Plant, Cell and Environment **26**, 867–874.

Hu Z, Cools T, De Veylder L. 2016. Mechanisms used by plants to cope with DNA damage. Annual Review of Plant Biology **67**, 439–462.

Hu YF, Zhou G, Na XF, Yang L, Nan W Bin, Liu X, Zhang YQ, Li JL, Bi YR. 2013. Cadmium interferes with maintenance of auxin homeostasis in Arabidopsis seedlings. Journal of Plant Physiology **170**, 965–975.

Huang Y, Chen H, Reinfelder JR, Liang X, Sun C, Liu C, Li F, Yi J. 2019*a*. A transcriptomic (RNA-seq) analysis of genes responsive to both cadmium and arsenic stress in rice root. Science of the Total Environment **666**, 445–460.

Huang D, Gong X, Liu Y, *et al.* 2017. Effects of calcium at toxic concentrations of cadmium in plants. Planta **245**, 863–873.

Huang L, Li WC, Tam NFY, Ye Z. 2019*b*. Effects of root morphology and anatomy on cadmium uptake and translocation in rice (*Oryza sativa* L.). Journal of Environmental Sciences **75**, 296–306.

Humplík JF, Bergougnoux V, Jandová M, Šimura J, Pěnčík A, Tomanec O, Rolčík J, Novák O, Fellner M. 2015. Endogenous abscisic acid promotes hypocotyl growth and affects endoreduplication during dark-induced growth in tomato (*Solanum lycopersicum* L.). PLoS ONE **10**, 1–23.

Huybrechts M, Cuypers A, Deckers J, Iven V, Vandionant S, Jozefczak M, Hendrix S. 2019. Cadmium and plant development: an agony from seed to seed. International

Journal of Molecular Sciences **20**, 3971.

Huybrechts M, Hendrix S, Bertels J, Beemster GTS, Vandamme D, Cuypers A. 2020. Spatial analysis of the rice leaf growth zone under controlled and cadmium-exposed conditions. Environmental and Experimental Botany **177**, 104120.

Jalmi SK, Bhagat PK, Verma D, Noryang S, Tayyeba S, Singh K, Sharma D, Sinha AK. 2018. Traversing the Links between Heavy Metal Stress and Plant Signaling. Frontiers in Plant Science **9**, 1–21.

Janda T, Gondor OK, Yordanova R, Szalai G, Pál M. 2014. Salicylic acid and photosynthesis: signalling and effects. Acta Physiologiae Plantarum **36**, 2537–2546.

Järup L. 2003. Hazards of heavy metal contamination. British Medical Bulletin **68**, 167–182.

Javed MT, Akram MS, Tanwir K, Javed Chaudhary H, Ali Q, Stoltz E, Lindberg S. 2017. Cadmium spiked soil modulates root organic acids exudation and ionic contents of two differentially Cd tolerant maize (*Zea mays* L.) cultivars. Ecotoxicology and Environmental Safety **141**, 216–225.

Ji XM, Raveendran M, Oane R, Ismail A, Lafitte R, Bruskiewich R, Cheng SH, Bennett J. 2005. Tissue-specific expression and drought responsiveness of cell-wall invertase genes of rice at flowering. Plant Molecular Biology **59**, 945–964.

Jomova K, Baros S, Valko M. 2012. Redox active metal-induced oxidative stress in biological systems. Transition Metal Chemistry **37**, 127–134.

Joshi R, Pareek A, Singla-Pareek SL. 2015. Plant Metallothioneins: Classification, Distribution, Function, and Regulation. Plant Metal Interaction: Emerging Remediation Techniques, 239–261.

Journet EP, Bligny R, Douce R. 1986. Biochemical changes during sucrose deprivation in higher plant cells. Journal of Biological Chemistry **261**, 3193–3199.

Jozefczak M, Keunen E, Schat H, Bliek M, Hernández LE, Carleer R, Remans T, Bohler S, Vangronsveld J, Cuypers A. 2014. Differential response of Arabidopsis leaves and roots to cadmium: Glutathione-related chelating capacity vs antioxidant capacity. Plant Physiology and Biochemistry **83**, 1–9.

Kanter U, Usadel B, Guerineau F, Li Y, Pauly M, Tenhaken R. 2005. The inositol oxygenase gene family of Arabidopsis is involved in the biosynthesis of nucleotide sugar precursors for cell-wall matrix polysaccharides. Planta **221**, 243–254.

Kaplan F, Kopka J, Sung DY, Zhao W, Popp M, Porat R, Guy CL. 2007. Transcript and metabolite profiling during cold acclimation of Arabidopsis reveals an intricate relationship of cold-regulated gene expression with modifications in metabolite content. Plant Journal **50**, 967–981.

Kavanová M, Lattanzi FA, Grimoldi AA, Schnyder H. 2006. Phosphorus deficiency decreases cell division and elongation in grass leaves. Plant Physiology **141**, 766–775.

Keegstra K. 2010. Plant cell walls. Plant Physiology **154**, 483–486.

Keunen E, Peshev D, Vangronsveld J, Van Den Ende W, Cuypers A. 2013. Plant sugars are crucial players in the oxidative challenge during abiotic stress: Extending the traditional concept. Plant, Cell and Environment **36**, 1242–1255.

Keunen E, Schellingen K, Vangronsveld J, Cuypers A. 2016. Ethylene and Metal Stress: Small Molecule, Big Impact. Frontiers in plant science **7**, 23.

Keunen E, Truyens S, Bruckers L, Remans T, Vangronsveld J, Cuypers A. 2011. Survival of Cd-exposed *Arabidopsis thaliana*: Are these plants reproductively challenged? Plant Physiology and Biochemistry **49**, 1084–1091.

Khaliq MA, James B, Chen YH, Ahmed Saqib HS, Li HH, Jayasuriya P, Guo W. 2019. Uptake, translocation, and accumulation of Cd and its interaction with mineral nutrients (Fe, Zn, Ni, Ca, Mg) in upland rice. Chemosphere **215**, 916–924.

Khoubnasabjafari M, Ansarin K, Jouyban A. 2015. Reliability of malondialdehyde as a biomarker of oxidative stress in psychological disorders. BioImpacts **5**, 123–127.

Kieffer P, Planchon S, Oufir M, Ziebel J, Dommes J, Hoffmann L, Hausman JF, Renaut J. 2009. Combining proteomics and metabolite analyses to unravel cadmium stress-response in poplar leaves. Journal of Proteome Research **8**, 400–417.

Kim D, Langmead B, Salzberg SL. 2015. HISAT: A fast spliced aligner with low memory requirements. Nature Methods **12**, 357–360.

Kim CG, Power SA, Bell JNB. 2004. Effects of host plant exposure to cadmium on mycorrhizal infection and soluble carbohydrate levels of *Pinus sylvestris* seedlings. Environmental Pollution **131**, 287–294.

Kobayashi NI, Tanoi K, Hirose A, Nakanishi TM. 2013. Characterization of rapid intervascular transport of cadmium in rice stem by radioisotope imaging. Journal of Experimental Botany **64**, 507–517.

Kocsy G, Tari I, Vanková R, Zechmann B, Gulyás Z, Poór P, Galiba G. 2013. Redox control of plant growth and development. Plant Science **211**, 77–91.

Kreszies T, Schreiber L, Ranathunge K. 2018. Suberized transport barriers in Arabidopsis, barley and rice roots: From the model plant to crop species. Journal of Plant Physiology **227**, 75–83.

Krupa Z. 1988. Cadmium-induced changes in the composition and structure of the light-harvesting chlorophyll a/b protein complex II in radish cotyledons. Physiologia Plantarum **73**, 518–524.

Krupa Z. 1999. Cadmium against Higher Plant Photosynthesis - a Variety of Effects and Where Do They Possibly Come From? Zeitschrift fur Naturforschung - Section C Journal of Biosciences **54**, 723–729.

Krzesłowska M. 2011. The cell wall in plant cell response to trace metals: Polysaccharide remodeling and its role in defense strategy. Acta Physiologiae

Plantarum **33**, 35–51.

Kuliková ZL, Lux A. 2010. Silicon influence on maize, *Zea mays* L., hybrids exposed to cadmium treatment. Bulletin of Environmental Contamination and Toxicology **85**, 243–250.

Kummerová M, Zezulka Š, Král'ová K, MASAROVIČOVÁ E. 2010. Effect of zinc and cadmium on physiological and production characteristics in *Matricaria recutita*. Biologia Plantarum **54**, 308–314.

Küpper H, Parameswaran A, Leitenmaier B, Trtílek M, Šetlík I. 2007. Cadmium-induced inhibition of photosynthesis and long-term acclimation to cadmium stress in the hyperaccumulator *Thlaspi caerulescens.* New Phytologist **175**, 655–674.

Kuthanova A, Fischer L, Nick P, Opatrny Z. 2008. Cell cycle phase-specific death response of tobacco BY-2 cell line to cadmium treatment. Plant, Cell & Environment **31**, 1634–1643.

Lan XY, Yan YY, Yang B, Li XY, Xu FL. 2018. Differential expression of proteins in the leaves and roots of cadmium-stressed *Microsorum pteropus*, a novel potential aquatic cadmium hyperaccumulator. Science of the Total Environment **642**, 1369–1377.

Leverrier P, Montigny C, Garrigos M, Champeil P. 2007. Metal binding to ligands: Cadmium complexes with glutathione revisited. Analytical Biochemistry **371**, 215–228.

Li M, Wang G, Li J, Cao F. 2016. Foliar application of betaine alleviates cadmium toxicity in maize seedlings. Acta Physiologiae Plantarum **38**.

Li SW, Zeng XY, Leng Y, Feng L, Kang XH. 2018. Indole-3-butyric acid mediates antioxidative defense systems to promote adventitious rooting in mung bean seedlings under cadmium and drought stresses. Ecotoxicology and Environmental Safety **161**, 332–341.

Liang Y, Dong X, Ni X, Wang Q, Sahu SK, Hou J, Liang M, Chen L, Zhang G. 2018. Genotyping by sequencing of 270 Indica rice varieties revealed genetic markers probably related to heavy metal accumulation. Plant Breeding **137**, 691–697.

Liao Y, Smyth GK, Shi W. 2014. FeatureCounts: An efficient general purpose program for assigning sequence reads to genomic features. Bioinformatics **30**, 923–930.

Lin F, Jiang L, Liu Y, Lv Y, Dai H, Zhao H. 2014. Genome-wide identification of housekeeping genes in maize. Plant Molecular Biology **86**, 543–554.

Lin L, Ma Q, Wang J, *et al.* 2018. Effects of indole-3-butytric acid (IBA) on growth and cadmium accumulation in the accumulator plant *Stellaria media.* Environmental Progress and Sustainable Energy **37**, 733–737.

Liu Z, Ding Y, Wang F, Ye Y, Zhu C. 2016. Role of salicylic acid in resistance to cadmium stress in plants. Plant Cell Reports **35**, 719–731.

Liu S, Li Y, Liu L, Min J, Liu W, Li X, Pan X, Lu X, Deng Q. 2019. Comparative Proteomics in Rice Seedlings to Characterize the Resistance to Cadmium Stress by High-

Performance Liquid Chromatography–Tandem Mass Spectrometry (HPLC-MS/MS) with Isobaric Tag for Relative and Absolute Quantitation (iTRAQ). Analytical Letters **0**, 1–14.

Liu Y, Wang X, Zeng G, Qu D, Gu J, Zhou M, Chai L. 2007. Cadmium-induced oxidative stress and response of the ascorbate-glutathione cycle in *Bechmeria nivea* (L.) Gaud. Chemosphere **69**, 99–107.

Liu H, Xie Y, Li J, Zeng G, Li H, Xu F, Feng S, Xu H. 2020. Effect of Serratia sp. K3 combined with organic materials on cadmium migration in soil-*Vetiveria zizanioides* L. system and bacterial community in contaminated soil. Chemosphere **242**, 125164.

Liu S, Yang C, Xie W, Xia C, Fan P. 2012. The Effects of Cadmium on Germination and Seedling Growth of *Suaeda salsa*. Procedia Environmental Sciences **16**, 293–298.

Livak KJ, Schmittgen TD. 2001. Analysis of relative gene expression data using real-time quantitative PCR and the 2-ΔΔCT method. Methods **25**, 402–408.

Loewus FA, Murthy PPN. 2000. myo-Inositol metabolism in plants. Plant Science **150**, 1–19.

Loix C, Huybrechts M, Vangronsveld J, Gielen M, Keunen E, Cuypers A. 2017. Reciprocal interactions between cadmium-induced cell wall responses and oxidative stress in plants. Frontiers in Plant Science **8**, 1–19.

Lorrai R, Boccaccini A, Ruta V, Possenti M, Costantino P, Vittorioso P. 2018. Abscisic acid inhibits hypocotyl elongation acting on gibberellins, DELLA proteins and auxin. AoB PLANTS **10**, 1–10.

Love MI, Huber W, Anders S. 2014. Moderated estimation of fold change and dispersion for RNA-seq data with DESeq2. Genome Biology **15**, 1–21.

Lowry OH, Rosebrough NJ, Farr AL, Randall RJ. 1951. Protein measurement with the Folin phenol reagent. The Journal of biological chemistry **193**, 265–75.

Lu L, Tian S, Zhang M, Zhang J, Yang X, Jiang H. 2010. The role of Ca pathway in Cd uptake and translocation by the hyperaccumulator *Sedum alfredii*. Journal of Hazardous Materials **183**, 22–28.

Ludwig-Müller J. 2011. Auxin conjugates: Their role for plant development and in the evolution of land plants. Journal of Experimental Botany **62**, 1757–1773.

Lv W, Yang L, Xu C, Shi Z, Shao J, Xian M, Chen J. 2017. Cadmium Disrupts the Balance between Hydrogen Peroxide and Superoxide Radical by Regulating Endogenous Hydrogen Sulfide in the Root Tip of *Brassica rapa*. Frontiers in Plant Science **8**, 1–13.

Maksymiec W. 2007. Signaling responses in plants to heavy metal stress. Acta Physiologiae Plantarum **29**, 177–187.

Mansour MM, Kamel EAR. 2005. Interactive effect of heavy metals and gibberellic acid on mitotic activity and some metabolic changes of *Vicia faba* L. plants. Cytologia **70**, 275–282.

Marilena R, Diego P, Laura F, *et al.* 2019. Auxin-jasmonate crosstalk in *Oryza sativa* L. root system formation after cadmium and/or arsenic exposure. Environmental and Experimental Botany **165**, 59–69.

Masai H, Matsumoto S, You Z, Yoshizawa-Sugata N, Oda M. 2010. Eukaryotic chromosome DNA replication: where, when, and how? Annual Review of Biochemistry **79**, 89–130.

Masood A, Khan MIR, Fatma M, Asgher M, Per TS, Khan NA. 2016. Involvement of ethylene in gibberellic acid-induced sulfur assimilation, photosynthetic responses, and alleviation of cadmium stress in mustard. Plant Physiology and Biochemistry **104**, 1–10.

Meguro A, Sato Y. 2015. Salicylic acid antagonizes abscisic acid inhibition of shoot growth and cell cycle progression in rice. Scientific Reports **4**, 4555.

Meiri A, Silk WK, Läuchli A. 1992. Growth and deposition of inorganic nutrient elements in developing leaves of Zea mays L. Plant Physiology **99**, 972–978.

Melaragno JE, Mehrotra B, Coleman AW. 1993. Relationship between endopolyploidy and cell size in epidermal tissue of Arabidopsis. The Plant Cell **5**, 1661–1668.

Merchante C, Stepanova AN, Alonso JM. 2017. Translation regulation in plants: an interesting past, an exciting present and a promising future. Plant Journal **90**, 628–653.

Meyer CL, Juraniec M, Huguet S, Chaves-Rodriguez E, Salis P, Isaure MP, Goormaghtigh E, Verbruggen N. 2015. Intraspecific variability of cadmium tolerance and accumulation, and cadmium-induced cell wall modifications in the metal hyperaccumulator *Arabidopsis halleri*. Journal of Experimental Botany **66**, 3215–3227.

Mittelheuser CJ, Van Steveninck RFM. 1969. Stomatal Closure and Inhibition of Transpiration induced by (RS)-Abscisic Acid. Nature **221**, 281–282.

Monteiro C, Santos C, Pinho S, Oliveira H, Pedrosa T, Dias MC. 2012. Cadmium-induced cyto- and genotoxicity are organ-dependent in lettuce. Chemical Research in Toxicology **25**, 1423–1434.

Moya JL, Ros R, Picazo I. 1993. Influence of cadmium and nickel on growth, net photosynthesis and carbohydrate distribution in rice plants. Photosynthesis Research **36**, 75–80.

Muller B, Reymond M, Tardieu F. 2001. The elongation rate at the base of a maize leaf shows an invariant pattern during both the steady-state elongation and the establishment of the elongation zone. Journal of Experimental Botany **52**, 1259–1268.

Nada E, Ferjani BA, Ali R, Bechir BR, Imed M, Makki B. 2007. Cadmium-induced growth inhibition and alteration of biochemical parameters in almond seedlings grown in solution culture. Acta Physiologiae Plantarum **29**, 57–62.

Nagajyoti PC, Lee KD, Sreekanth TVM. 2010. Heavy metals, occurrence and toxicity for plants: a review. Environmental Chemistry Letters **8**, 199–216.

Nazir F, Fariduddin Q, Khan TA. 2020. Hydrogen peroxide as a signalling molecule in plants and its crosstalk with other plant growth regulators under heavy metal stress. Chemosphere **252**, 126486.

Nelissen H, Rymen B, Coppens F, Dhondt S, Fiorani F, Beemster GTS. 2013. Kinematic Analysis of Cell Division in Leaves of Mono- and Dicotyledonous Species: A Basis for Understanding Growth and Developing Refined Molecular Sampling Strategies. Plant Organogenesis: Methods and Protocols.247–264.

Nelissen H, Rymen B, Jikumaru Y, Demuynck K, Van Lijsebettens M, Kamiya Y, Inzé D, Beemster GTS. 2012. A local maximum in gibberellin levels regulates maize leaf growth by spatial control of cell division. Current Biology **22**, 1183–1187.

Nelson N. 1944. A photometric adaptation of the Somogyi method for the determination of glucose. The Journal of Biological Chemistry **153**, 375–380.

Nishanth MJ, Sheshadri SA, Rathore SS, Srinidhi S, Simon B. 2018. Expression analysis of Cell wall invertase under abiotic stress conditions influencing specialized metabolism in *Catharanthus roseus*. Scientific Reports **8**, 1–15.

Opdenakker K, Remans T, Keunen E, Vangronsveld J, Cuypers A. 2012. Exposure of *Arabidopsis thaliana* to Cd or Cu excess leads to oxidative stress mediated alterations in MAPKinase transcript levels. Environmental and Experimental Botany **83**, 53–61.

Ortega-Villasante C, Sobrino-Plata J, Carpena-Ruiz RO, Verbruggen N, Escobar C, Hernández LE. 2011. Oxidative Stress Induced by Cadmium in Transgenic *Nicotiana tabacum* Over-expressing a Plastidial Mn-Superoxide Dismutase.

Pallas JE, Kays SJ. 1982. Inhibition of Photosynthesis by Ethylene—A Stomatal Effect. Plant Physiology **70**, 598–601.

Pan C, Lu H, Liu J, Yu J, Wang Q, Li J, Yang J, Hong H, Yan C. 2020*a*. SODs involved in the hormone mediated regulation of H2O2 content in *Kandelia obovata* root tissues under cadmium stress. Environmental Pollution **256**, 113272.

Pan W, You Y, Shentu JL, Weng YN, Wang ST, Xu QR, Liu HJ, Du ST. 2020*b*. Abscisic acid (ABA)-importing transporter 1 (AIT1) contributes to the inhibition of Cd accumulation via exogenous ABA application in Arabidopsis. Journal of Hazardous Materials **391**, 122189.

Parrotta L, Guerriero G, Sergeant K, Cai G, Hausman J-F. 2015. Target or barrier? The cell wall of early- and later-diverging plants vs cadmium toxicity: differences in the response mechanisms. Frontiers in plant science **6**, 133.

Pasternak T, Groot EP, Kazantsev F V., Teale W, Omelyanchuk N, Kovrizhnykh V, Palme K, Mironova V V. 2019. Salicylic acid affects root meristem patterning via auxin distribution in a concentration-dependent manner. Plant Physiology **180**, 1725–1739.

Paul MJ, Foyer CH. 2001. Sink regulation of photosynthesis. Journal of Experimental Botany **52**, 1383–1400.

Pena LB, Barcia RA, Azpilicueta CE, Méndez AAE, Gallego SM. 2012. Oxidative post translational modifications of proteins related to cell cycle are involved in cadmium toxicity in wheat seedlings. Plant Science **196**, 1–7.

Peng H, He X, Gao J, Ma H, Zhang Z, Shen Y, Pan G, Lin H. 2015. Transcriptomic changes during maize roots development responsive to Cadmium (Cd) pollution using comparative RNAseq-based approach. Biochemical and Biophysical Research Communications **464**, 1040–1047.

Pérez Chaca M V., Vigliocco A, Reinoso H, Molina A, Abdala G, Zirulnik F, Pedranzani H. 2014. Effects of cadmium stress on growth, anatomy and hormone contents in *Glycine max* (L.) Merr. Acta Physiologiae Plantarum **36**, 2815–2826.

Perfus-Barbeoch L, Leonhardt N, Vavasseur A, Forestier C. 2002. Heavy metal toxicity: Cadmium permeates through calcium channels and disturbs the plant water status. Plant Journal **32**, 539–548.

Peshev D, Van Den Ende W. 2013. Crop Improvement Under Adverse Conditions (N Tuteja and SS Gill, Eds.). New York, NY: Springer Science+Business Media.

Philipps GR. 1970. Binding of transfer ribonucleic acid to ribosomes. Comparison of the nonenzymatic binding of aminoacylated and deacylated transfer ribonucleic acid. The Journal of biological chemistry **245**, 859–68.

Podazza C, Rosa M, González JA, Hilal M, Prado FE. 2006. Cadmium induces changes in sucrose partitioning, invertase activities, and membrane functionality in roots of rangpur lime (*Citrus limonia* L. Osbeck). Plant Biology **8**, 706–714.

Poorter H, Garnier E. 1996. Plant growth analysis: an evaluation of experimental design and computational methods. Journal of Experimental Botany **47**, 1343–1351.

Pound MP, French AP, Wells DM, Bennett MJ, Pridmorea TP. 2012. CellSeT: Novel software to extract and analyze structured networks of plant cells from confocal images. Plant Cell **24**, 1353–1361.

Qiao K, Liang S, Wang F, Wang H, Hu Z, Chai T. 2019. Effects of cadmium toxicity on diploid wheat (*Triticum urartu*) and the molecular mechanism of the cadmium response. Journal of Hazardous Materials **374**, 1–10.

Qin S, Liu H, Nie Z, Rengel Z, Gao W, Li C, Zhao P. 2020. Toxicity of cadmium and its competition with mineral nutrients for uptake by plants: A review. Pedosphere **30**, 168–180.

R Core Team. 2014. R: A language and environment for statistical computing.

Rafique M, Ortas I, Rizwan M, Sultan T, Chaudhary HJ, Işik M, Aydin O. 2019. Effects of Rhizophagus clarus and biochar on growth, photosynthesis, nutrients, and cadmium (Cd) concentration of maize (*Zea mays*) grown in Cd-spiked soil. Environmental Science and Pollution Research **26**, 20689–20700.

Rahman A, Nahar K, Hasanuzzaman M, Fujita M. 2016. Manganese-induced cadmium

stress tolerance in rice seedlings: Coordinated action of antioxidant defense, glyoxalase system and nutrient homeostasis. Comptes Rendus - Biologies **339**, 462–474.

Rajewska I, Talarek M, Bajguz A. 2016. Brassinosteroids and Response of Plants to Heavy Metals Action. Frontiers in Plant Science **7**.

Redjala T, Zelko I, Sterckeman T, Legué V, Lux A. 2011. Relationship between root structure and root cadmium uptake in maize. Environmental and Experimental Botany **71**, 241–248.

Repetto O, Massa N, Gianinazzi-Pearson V, Dumas-Gaudot E, Berta G. 2007. Cadmium effects on populations of root nuclei in two pea genotypes inoculated or not with the arbuscular mycorrhizal fungus *Glomus mosseae*. Mycorrhiza **17**, 111–120.

Rizvi A, Khan MS. 2019. Heavy metal-mediated toxicity to maize: oxidative damage, antioxidant defence response and metal distribution in plant organs. International Journal of Environmental Science and Technology **16**, 4873–4886.

Rizwan M, Ali S, Adrees M, Ibrahim M, Tsang DCW, Zia-ur-Rehman M, Zahir ZA, Rinklebe J, Tack FMG, Ok YS. 2017. A critical review on effects, tolerance mechanisms and management of cadmium in vegetables. Chemosphere **182**, 90–105.

Rizwan M, Ali S, Adrees M, Rizvi H, Zia-ur-Rehman M, Hannan F, Qayyum MF, Hafeez F, Ok YS. 2016. Cadmium stress in rice: toxic effects, tolerance mechanisms, and management: a critical review. Environmental Science and Pollution Research **23**, 17859–17879.

Robinson JT, Thorvaldsdóttir H, Winckler W, Guttman M, Lander ES, Getz G, Mesirov JP. 2011. Integrative Genome Viewer. Nature Biotechnology **29**, 24–6.

Rodda MS, Li G, Reid RJ. 2011. The timing of grain Cd accumulation in rice plants: The relative importance of remobilisation within the plant and root Cd uptake post-flowering. Plant and Soil **347**, 105–114.

Rodríguez-Serrano M, Romero-Puertas MC, Pazmiño DM, Testillano PS, Risueño MC, del Río LA, Sandalio LM. 2009. Cellular Response of Pea Plants to Cadmium Toxicity: Cross Talk between Reactive Oxygen Species, Nitric Oxide, and Calcium. Plant Physiology **150**, 229–243.

Rolland F, Baena-Gonzalez E, Sheen J. 2006. Sugar sensing and signaling in plants: Conserved and novel mechanisms. Annual Review of Plant Biology **57**, 675–709.

Ronzan M, Piacentini D, Fattorini L, Della Rovere F, Eiche E, Riemann M, Altamura MMM, Falasca G. 2018. Cadmium and arsenic affect root development in *Oryza sativa* L. negatively interacting with auxin. Environmental and Experimental Botany **151**, 64–75.

Rosa M, Prado C, Podazza G, Interdonato R, González JA, Hilal M, Prado FE. 2009. Soluble sugars-metabolism, sensing and abiotic stress a complex network in the life of

plants. Plant Signaling and Behavior **4**, 388–393.

Rozov A, Khusainov I, El Omari K, Duman R, Mykhaylyk V, Yusupov M, Westhof E, Wagner A, Yusupova G. 2019. Importance of potassium ions for ribosome structure and function revealed by long-wavelength X-ray diffraction. Nature Communications **10**, 1–12.

RStudio Team. 2015. RStudio: Integrated Development for R. RStudio, Inc.

Ruan YL. 2012. Signaling role of sucrose metabolism in development. Molecular Plant **5**, 763–765.

Ruan YL. 2014. Sucrose metabolism: Gateway to diverse carbon use and sugar signaling. Annual Review of Plant Biology **65**, 33–67.

Rucińska-Sobkowiak R. 2016. Water relations in plants subjected to heavy metal stresses. Acta Physiologiae Plantarum **38**, 257.

Ruppert D, Sheather SJ, Wand MP. 1995. An Effective Bandwidth Selector for Local Least Squares Regression. Journal of the American Statistical Association **90**, 1257–1270.

Rymen B, Coppens F, Dhondt S, Fiorani F, Beemster GTS. 2010. Kinematic Analysis of Cell Division and Expansion. Plant Developmental Biology.203–227.

Sakakibara H. 2006. CYTOKININS: Activity, Biosynthesis, and Translocation. Annual Review of Plant Biology **57**, 431–449.

Saleh SR, Kandeel MM, Ghareeb D, Ghoneim TM, Talha NI, Alaoui-Sossé B, Aleya L, Abdel-Daim MM. 2020. Wheat biological responses to stress caused by cadmium, nickel and lead. Science of the Total Environment **706**.

Sandalio LM, Dalurzo HC, Gómez M, Romero-Puertas MC, del Río LA. 2001. Cadmium-induced changes in the growth and oxidative metabolism of pea plants. Journal of Experimental Botany **52**, 2115–2126.

Santos LR, Batista BL, Lobato AKS. 2018. Brassinosteroids mitigate cadmium toxicity in cowpea plants. Photosynthetica **56**, 591–605.

Dos Santos WD, Ferrarese MDLL, Finger A, Teixeira ACN, Ferrarese-Filho O. 2004. Lignification and related enzymes in *Glycine max* root growth-inhibition by ferulic acid. Journal of Chemical Ecology **30**, 1203–1212.

Sasaki A, Yamaji N, Yokosho K, Ma JF. 2012. Nramp5 is a major transporter responsible for manganese and cadmium uptake in rice. Plant Cell **24**, 2155–2167.

Sayed S, Gadallah M. 2019. Hydrogen peroxide supplementation alleviates the deleterious effects of cadmium on photosynthetic pigments and oxidative stress and improves growth, yield and pods quality of pea (*Pisum sativum* L.) plants. Acta Physiologiae Plantarum **41**, 1–12.

Scarpella E, Barkoulas M, Tsiantis M. 2010. Control of leaf and vein development by

auxin. Cold Spring Harbor perspectives in biology **2**, 1–18.

Schaller GE, Street IH, Kieber JJ. 2014. Cytokinin and the cell cycle. Current Opinion in Plant Biology **21**, 7–15.

Schellingen K, Van Der Straeten D, Remans T, Loix C, Vangronsveld J, Cuypers A. 2015. Ethylene biosynthesis is involved in the early oxidative challenge induced by moderate Cd exposure in *Arabidopsis thaliana*. Environmental and Experimental Botany **117**, 1–11.

Schellingen K, Van Der Straeten D, Vandenbussche F, Prinsen E, Remans T, Vangronsveld J, Cuypers A. 2014. Cadmium-induced ethylene production and responses in *Arabidopsis thaliana* rely on ACS2 and ACS6 gene expression. BMC Plant Biology **14**, 1–14.

Scherer G, Barkemeyer H. 1983. Cadmium concentrations in tobacco and tobacco smoke. Ecotoxicology and Environmental Safety **7**, 71–78.

Schnable PS, Ware D, Fulton RS, *et al.* 2009. The B73 Maize Genome: Complexity, Diversity, and Dynamics. Science **326**, 1112–1115.

Schnyder H, Nelson CJ. 1987. Growth Rates and Carbohydrate Fluxes within the Elongation Zone of Tall Fescue Leaf Blades. Plant Physiology **85**, 548–553.

Schnyder H, Seo S, Rademacher IFF, Kühbauch W. 1990. Spatial distribution of growth rates and of epidermal cell lengths in the elongation zone during leaf development in *Lolium perenne* L. Planta **181**, 423–431.

Scholes DR, Paige KN. 2015. Plasticity in ploidy: a generalized response to stress. Trends in Plant Science **20**, 165–175.

Schreurs E, Voets T, Thewys T. 2011. GIS-based assessment of the biomass potential from phytoremediation of contaminated agricultural land in the Campine region in Belgium. Biomass and Bioenergy **35**, 4469–4480.

Schutzendubel A, Schwanz P, Teichmann T, Gross K, Langenfeld-Heyser R, Godbold DL, Polle A. 2001. Cadmium-Induced Changes in Antioxidative Systems, Hydrogen Peroxide Content, and Differentiation in Scots Pine Roots. Plant Physiology **127**, 887–898.

Scofield S, Jones A, Murray JAH. 2014. The plant cell cycle in context. Journal of Experimental Botany **65**, 2557–2562.

Shahid MA, Balal RM, Khan N, Zotarelli L, Liu GD, Sarkhosh A, Fernández-Zapata JC, Martínez Nicolás JJ, Garcia-Sanchez F. 2019. Selenium impedes cadmium and arsenic toxicity in potato by modulating carbohydrate and nitrogen metabolism. Ecotoxicology and Environmental Safety **180**, 588–599.

Shalaby S, Horwitz BA. 2015. Plant phenolic compounds and oxidative stress: integrated signals in fungal–plant interactions. Current Genetics **61**, 347–357.

Sharma R, Bhardwaj R, Thukral AK, Handa N, Kaur R, Kumar V. 2014. *Osmolyte*

Dynamics: New Strategies for Crop Tolerance to Abiotic Stress Signals. Elsevier Inc.

Sharma A, Sidhu GPS, Araniti F, Bali AS, Shahzad B, Tripathi DK, Brestic M, Skalicky M, Landi M. 2020. The role of salicylic acid in plants exposed to heavy metals. Molecules **25**, 1–22.

Shi J, Li L, Pan G. 2009. Variation of grain Cd and Zn concentrations of 110 hybrid rice cultivars grown in a low-Cd paddy soil. Journal of Environmental Sciences **21**, 168–172.

Shi GL, Li DJ, Wang YF, Liu CH, Hu ZB, Lou LQ, Rengel Z, Cai QS. 2019. Accumulation and distribution of arsenic and cadmium in winter wheat (*Triticum aestivum* L.) at different developmental stages. Science of The Total Environment **667**, 532–539.

Shi YZ, Zhu XF, Wan JX, Li GX, Zheng SJ. 2015. Glucose alleviates cadmium toxicity by increasing cadmium fixation in root cell wall and sequestration into vacuole in Arabidopsis. Journal of Integrative Plant Biology **57**, 830–837.

Shukla A, Suprasanna SS and P. 2017. Genomics of Metal Stress-Mediated Signalling and Plant Adaptive Responses in Reference to Phytohormones. Current Genomics **18**, 512–522.

Siedlecka A, Baszynski T. 1993. Inhibition of electron flow around photosystem I in chloroplasts of Cd-treated maize plants is due to Cd-induced iron deficiency. Physiologia Plantarum **87**, 199–202.

Silk WK. 1984. Quantitative Descriptions of Development. Annual Review of Plant Physiology and Plant Molecular Biology **35**, 479–518.

Silk WK. 1992. Steady form from changing cells. International Journal of Plant Science **153**, s49–s58.

Silk WK, Erickson RO. 1979. Kinematics of plant growth. Journal of Theoretical Biology **76**, 481–501.

Silva SAE, Techio VH, de Castro EM, de Faria MR, Palmieri MJ. 2013. Reproductive, Cellular, and Anatomical Alterations in *Pistia stratiotes* L. Plants Exposed to Cadmium. Water, Air, & Soil Pollution **224**, 1454.

Singh M, Kumar J, Singh S, Singh VP, Prasad SM. 2015. Roles of osmoprotectants in improving salinity and drought tolerance in plants: a review. Reviews in Environmental Science and Biotechnology **14**, 407–426.

Singh UM, Sareen P, Sengar RS, Kumar A. 2013. Plant ionomics: A newer approach to study mineral transport and its regulation. Acta Physiologiae Plantarum **35**, 2641–2653.

Singh S, Singh VP, Prasad SM, Sharma S, Ramawat N, Dubey NK, Tripathi DK, Chauhan DK. 2019. Interactive Effect of Silicon (Si) and Salicylic Acid (SA) in Maize Seedlings and Their Mechanisms of Cadmium (Cd) Toxicity Alleviation. Journal of Plant Growth Regulation **38**, 1587–1597.

Sinnott EW. 1939. Growth and Differentiation in Living Plant Meristems. Proceedings

of the National Academy of Sciences **25**, 55–58.

Skirycz A, Claeys H, De Bodt S, *et al.* 2011. Pause-and-stop: The effects of osmotic stress on cell proliferation during early leaf development in Arabidopsis and a role for ethylene signaling in cell cycle arrest. The Plant Cell **23**, 1876–1888.

Van Slycken S, Witters N, Meers E, *et al.* 2013. Safe use of metal-contaminated agricultural land by cultivation of energy maize (*Zea mays*). Environmental Pollution **178**, 375–380.

Smeekens S, Ma J, Hanson J, Rolland F. 2010. Sugar signals and molecular networks controlling plant growth. Current Opinion in Plant Biology **13**, 273–278.

Smolders E, Mertens J. 2013. Cadmium. Heavy metals in Soils.283–311.

Sneideris LC, Gavassi MA, Campos ML, D'Amico-Damião V, Carvalho RF. 2015. Effects of hormonal priming on seed germination of pigeon pea under cadmium stress. Anais da Academia Brasileira de Ciencias **87**, 1847–52.

Sobkowiak R, Deckert J. 2003. Cadmium-induced changes in growth and cell cycle gene expression in suspension-culture cells of soybean. Plant Physiology and Biochemistry **41**, 767–772.

Sobkowiak R, Deckert J. 2004. The effect of cadmium on cell cycle control in suspension culture cells of soybean. Acta Physiologiae Plantarum **26**, 335–344.

Sobrino-Plata J, Meyssen D, Cuypers A, Escobar C, Hernández LE. 2014. Glutathione is a key antioxidant metabolite to cope with mercury and cadmium stress. Plant and Soil **377**, 369–381.

Song G, Yuan S, Wen X, Xie Z, Lou L, Hu B, Cai Q, Xu B. 2018. Transcriptome analysis of Cd-treated switchgrass root revealed novel transcripts and the importance of HSF/HSP network in switchgrass Cd tolerance. Plant Cell Reports **37**, 1485–1497.

Spielmann J, Ahmadi H, Scheepers M, *et al.* 2020. The two copies of the zinc and cadmium ZIP6 transporter of *Arabidopsis halleri* have distinct effects on cadmium tolerance. Plant Cell and Environment **43**, 2143–2157.

Spollen WG, Lenoble ME, Samuels TD, Bernstein N, Sharp RE. 2000. Abscisic acid accumulation maintains maize primary root elongation at low water potentials by restricting ethylene production. Plant Physiology **122**, 967–976.

Sprangers K, Avramova V, Beemster GTS. 2016. Kinematic Analysis of Cell Division and Expansion: Quantifying the Cellular Basis of Growth and Sampling Developmental Zones in *Zea mays* Leaves. Journal of Visualized Experiments, 1–11.

Sprangers K, Thys S, van Dusschoten D, Beemster GTS. 2020. Gibberellin Enhances the Anisotropy of Cell Expansion in the Growth Zone of the Maize Leaf. Frontiers in Plant Science **11**, 1–13.

Staswick PE, Tiryaki I. 2004. The Oxylipin Signal Jasmonic Acid Is Activated by an Enzyme That Conjugates It to Isoleucine in Arabidopsis. The Plant Cell **16**, 2117–2127.

Stoyanova S, Geuns J, Hideg É, Van Den Ende W. 2011. The food additives inulin and stevioside counteract oxidative stress. International Journal of Food Sciences and Nutrition **62**, 207–214.

Sugimoto-Shirasu K, Roberts K. 2003. "Big it up": endoreduplication and cell-size control in plants. Current Opinion in Plant Biology **6**, 544–553.

Sun Y, Lu Q, Cao Y, Wang M, Cheng X, Yan Q. 2019. Comparative Transcriptome Analysis of the Molecular Mechanism of the Hairy Roots of *Brassica campestris* L. in Response to Cadmium Stress. International Journal of Molecular Sciences **21**, 180.

Sun X, Zhang J, Zhang H, Ni Y, Zhang Q, Chen J, Guan Y. 2010. The responses of *Arabidopsis thaliana* to cadmium exposure explored via metabolite profiling. Chemosphere **78**, 840–845.

Suttle JC, Banowetz GM. 2000. Changes in cis-zeatin and cis-zeatin riboside levels and biological activity during potato tuber dormancy. Physiologia Plantarum **109**, 68–74.

Svitashev S, Schwartz C, Lenderts B, Young JK, Mark Cigan A. 2016. Genome editing in maize directed by CRISPR-Cas9 ribonucleoprotein complexes. Nature Communications **7**, 1–7.

Sylwia W, Anna R, Ewa B, Stephan C, Danuta Maria A. 2010. The role of subcellular distribution of cadmium and phytochelatins in the generation of distinct phenotypes of AtPCS1- and CePCS3-expressing tobacco. Journal of Plant Physiology **167**, 981–988.

Sytar O, Kumari P, Yadav S, Brestic M, Rastogi A. 2019. Phytohormone Priming: Regulator for Heavy Metal Stress in Plants. Journal of Plant Growth Regulation **38**, 739–752.

Tajti J, Németh E, Glatz G, Janda T, Pál M. 2019. Pattern of changes in salicylic acid-induced protein kinase (SIPK) gene expression and salicylic acid accumulation in wheat under cadmium exposure. Plant Biology **21**, 1176–1180.

Takahashi R, Bashir K, Ishimaru Y, Nishizawa NK, Nakanishi H. 2012. The role of heavy-metal ATPases, HMAs, in zinc and cadmium transport in rice. Plant Signaling & Behavior **7**, 1605–1607.

Takatsuka H, Umeda M. 2019. ABA inhibits root cell elongation through repressing the cytokinin signaling. Plant Signaling & Behavior **14**, 1–3.

Tardieu F, Reymond M, Hamard P, Granier C, Muller B. 2000. Spatial distributions of expansion rate, cell division rate and cell size in maize leaves: a synthesis of the effects of soil water status, evaporative demand and temperature. Journal of Experimental Botany **51**, 1505–1514.

Tchounwou PB, Yedjou CG, Patlolla AK, Sutton DJ. 2012. Molecular, clinical and environmental toxicicology Volume 3: Environmental Toxicology. Molecular, Clinical and Environmental Toxicology **101**, 133–164.

Thomas PD, Campbell MJ, Kejariwal A, Mi H, Karlak B, Daverman R, Diemer K,

Muruganujan A, Narechania A. 2003. PANTHER: A library of protein families and subfamilies indexed by function. Genome Research **13**, 2129–2141.

Thomas BF, ElSohly MA. 2016. Biosynthesis and Pharmacology of Phytocannabinoids and Related Chemical Constituents. The Analytical Chemistry of Cannabis. Elsevier, 27–41.

Ueno D, Milner MJ, Yamaji N, Yokosho K, Koyama E, Clemencia Zambrano M, Kaskie M, Ebbs S, Kochian L V., Ma JF. 2011. Elevated expression of TcHMA3 plays a key role in the extreme Cd tolerance in a Cd-hyperaccumulating ecotype of Thlaspi caerulescens. Plant Journal **66**, 852–862.

Uraguchi S, Kamiya T, Sakamoto T, Kasai K, Sato Y, Nagamura Y, Yoshida A, Kyozuka J, Ishikawa S, Fujiwara T. 2011. Low-affinity cation transporter (OsLCT1) regulates cadmium transport into rice grains. Proceedings of the National Academy of Sciences of the United States of America **108**, 20959–20964.

Vanderstraeten L, Depaepe T, Bertrand S, Van Der Straeten D. 2019. The Ethylene Precursor ACC Affects Early Vegetative Development Independently of Ethylene Signaling. Frontiers in Plant Science **10**, 1–14.

Vatehová Z, Malovíková A, Kollárová K, Kučerová D, Lišková D. 2016. Impact of cadmium stress on two maize hybrids. Plant Physiology and Biochemistry **108**, 90–98.

Veach YK, Martin RC, Mok DWS, Malbeck J, Vankova R, Mok MC. 2003. O-glucosylation of cis-Zeatin in maize. Characterization of genes, enzymes, and endogenous cytokinins. Plant Physiology **131**, 1374–1380.

Verbruggen N, Hanikenne M, Clemens S. 2013. A more complete picture of met al hyperaccumulation through next-generation sequencing technologies. Frontiers in Plant Science **4**, 1–7.

Verbruggen N, Hermans C, Schat H. 2009. Mechanisms to cope with arsenic or cadmium excess in plants. Current Opinion in Plant Biology **12**, 364–372.

Vergauwen R, Van Den Ende W, Van Laere A. 2000. The role of fructan in flowering of *Campanula rapunculoides.* Journal of Experimental Botany **51**, 1261–1266.

Vishwakarma K, Upadhyay N, Kumar N, *et al.* 2017. Abscisic Acid Signaling and Abiotic Stress Tolerance in Plants: A Review on Current Knowledge and Future Prospects. Frontiers in Plant Science **08**, 1–12.

Vlaams Parlement. 1998. Bulletin van vragen en antwoorden. Vragen van de Vlaamse volksvertegenwoordigers en antwoorden van de ministers **12**.

Vögeli-Lange R, Wagner GJ. 1996. Relationship between cadmium, glutathione and cadmium-binding peptides (phytochelatins) in leaves of intact tobacco seedlings. Plant Science **114**, 11–18.

Volenec JJ, Nelson CJ. 1981. Cell Dynamics in Leaf Meristems of Contrasting Tall Fescue Genotypes. Crop Science **21**, 381–385.

Volkov RA, Panchuk II, Mullineaux PM, Schöffl F. 2006. Heat stress-induced H2O2 is required for effective expression of heat shock genes in Arabidopsis. Plant Molecular Biology **61**, 733–746.

Voorend W, Nelissen H, Vanholme R, De Vliegher A, Van Breusegem F, Boerjan W, Roldán-Ruiz I, Muylle H, Inzé D. 2016. Overexpression of GA 20- OXIDASE 1 impacts plant height, biomass allocation and saccharification efficiency in maize. Plant Biotechnology Journal **14**, 997–1007.

Walter A, Spies H, Terjung S, Küsters R, Kirchgeßner N, Schurr U. 2002. Spatio-temporal dynamics of expansion growth in roots: Automatic quantification of diurnal course and temperature response by digital image sequence processing. Journal of Experimental Botany **53**, 689–698.

Wang MQ, Bai ZY, Xiao YF, Li Y, Liu QL, Zhang L, Pan YZ, Jiang BB, Zhang F. 2019. Transcriptomic analysis of *Verbena bonariensis* roots in response to cadmium stress. BMC Genomics **20**, 1–14.

Wang L, Ruan YL. 2013. Regulation of cell division and expansion by sugar and auxin signaling. Frontiers in Plant Science **4**, 1–9.

Wang P, Yang B, Wan H, Fang X, Yang C. 2018. The differences of cell wall in roots between two contrasting soybean cultivars exposed to cadmium at young seedlings. Environmental Science and Pollution Research **25**, 29705–29714.

Weber M, Trampczynska A, Clemens S. 2006. Comparative transcriptome analysis of toxic metal responses in Arabidopsis thaliana and the Cd^{2+}-hypertolerant facultative metallophyte *Arabidopsis halleri*. Plant, Cell and Environment **29**, 950–963.

van der Weele CM, Jiang HS, Palaniappan KK, Ivanov VB, Palaniappan K, Baskin TI. 2003. A New Algorithm for Computational Image Analysis of Deformable Motion at High Spatial and Temporal Resolution Applied to Root Growth. Roughly Uniform Elongation in the Meristem and Also, after an Abrupt Acceleration, in the Elongation Zone. Plant Physiology **132**, 1138–1148.

Wei T, Lv X, Jia HL, Hua L, Xu HH, Zhou R, Zhao J, Ren XH, Guo JK. 2018. Effects of salicylic acid, Fe(II) and plant growth-promoting bacteria on Cd accumulation and toxicity alleviation of Cd tolerant and sensitive tomato genotypes. Journal of Environmental Management **214**, 164–171.

West C, Briggs GE, Kidd F. 1920. Methods and significant relations in the quantitative analysis of plant growth. New Phytologist **19**, 200–207.

West G, Inzé D, Beemster GTS. 2004. Cell cycle modulation in the response of the primary root of arabidopsis to salt stress. Plant Physiology **135**, 1050–1058.

Wickham H. 2014. Tiday Data. Journal of Statistical Software **59**, 1–23.

Willems G, Frérot H, Gennen J, Salis P, Saumitou-Laprade P, Verbruggen N. 2010. Quantitative trait loci analysis of mineral element concentrations in an *Arabidopsis*

halleri × *Arabidopsis lyrata* petraea F2 progeny grown on cadmium-contaminated soil. New Phytologist **187**, 368–379.

Williams NH. 2000. Magnesium Ion Catalyzed ATP Hydrolysis. Journal of the American Chemical Society **122**, 12023–12024.

World Health Organization. 2010. Exposure to cadmium: a major public health concern. Preventing Disease Through Healthy Environments, 1–6.

World Health Organization. 2011. Safety evaluation of certain food additives and contaminants in food. Prepared by the Seventy-third meeting of the Joint FAO/WHO Expert Committee on Food Additives (JECFA), 543.

Wu J, Mock HP, Giehl RFH, Pitann B, Mühling KH. 2019. Silicon decreases cadmium concentrations by modulating root endodermal suberin development in wheat plants. Journal of Hazardous Materials **364**, 581–590.

Xian J, Wang Y, Niu K, Ma H, Ma X. 2020. Transcriptional regulation and expression network responding to cadmium stress in a Cd-tolerant perennial grass *Poa pratensis*. Chemosphere **250**, 126158.

Xiao Y, Du Z, Qi X, Wu H, Guo W, Zhao Z. 2019. RNA-sequencing analysis reveals transcriptional changes in the roots of low-cadmium-accumulating winter wheat under cadmium stress. Acta Physiologiae Plantarum **41**, 1–10.

Xu ZR, Cai SW, Huang WX, Liu RX, Xiong ZT. 2018. Differential expression of vacuolar and defective cell wall invertase genes in roots and seeds of metalliferous and non-metalliferous populations of *Rumex dentatus* under copper stress. Ecotoxicology and Environmental Safety **147**, 17–25.

Yan H, Filardo F, Hu X, Zhao X, Fu DH. 2016. Cadmium stress alters the redox reaction and hormone balance in oilseed rape (*Brassica napus* L.) leaves. Environmental Science and Pollution Research **23**, 3758–3769.

Yang Y-J, Cheng L-M, Liu Z-H. 2007. Rapid effect of cadmium on lignin biosynthesis in soybean roots. Plant Science **172**, 632–639.

Ye W, Guo G, Wu F, Fan T, Lu H, Chen H, Li X, Ma Y. 2018. Absorption, translocation, and detoxification of Cd in two different castor bean (*Ricinus communis* L.) cultivars. Environmental Science and Pollution Research **25**, 28899–28906.

Ye W, Wu F, Zhang G, Fang Q, Lu H, Hu H. 2020. Calcium Decreases Cadmium Concentration in Root but Facilitates Cadmium Translocation from Root to Shoot in Rice. Journal of Plant Growth Regulation **39**, 422–429.

Youssef OA, Tammam AA, Bakatoushi RF, Elframawy AM, Emara MM, El-Sadek LM. 2020. Hematite nanoparticles influence ultrastructure, antioxidant defenses, gene expression, and alleviate cadmium toxicity in *Zea mays*. Journal of Plant Interactions **15**, 54–74.

Yu H, Wang J, Fang W, Yuan J, Yang Z. 2006. Cadmium accumulation in different rice

cultivars and screening for pollution-safe cultivars of rice. Science of the Total Environment **370**, 302–309.

Yuan H-M, Huang X. 2016. Inhibition of root meristem growth by cadmium involves nitric oxide-mediated repression of auxin accumulation and signalling in Arabidopsis. Plant, Cell & Environment **39**, 120–135.

Yue R, Lu C, Qi J, *et al.* 2016*a*. Transcriptome Analysis of Cadmium-Treated Roots in Maize (*Zea mays* L.). Frontiers in Plant Science **7**, 1–11.

Yue J, Zhang X, Liu N. 2016*b*. Cadmium permeates through calcium channels and activates transcriptomic complexity in wheat roots in response to cadmium stress. Genes and Genomics **39**, 1–14.

Zaid A, Mohammad F, Fariduddin Q. 2019. Plant growth regulators improve growth, photosynthesis, mineral nutrient and antioxidant system under cadmium stress in menthol mint (*Mentha arvensis* L.). Physiology and Molecular Biology of Plants.

Zeeman SC. 2015. Carbohydrate metabolism. In: Buchanan BB,, In: Gruissem W,, In: Jones RL, eds. Biochemistry and Molecular Biology of Plants. West Sussex, 567–609.

Zhan Y, Zhang C, Zheng Q, Huang Z, Yu C. 2017. Cadmium stress inhibits the growth of primary roots by interfering auxin homeostasis in Sorghum bicolor seedlings. Journal of Plant Biology **60**, 593–603.

Zhao X, Ding C, Chen L, Wang S, Wang Q, Ding Y. 2012. Comparative proteomic analysis of the effects of nitric oxide on alleviating Cd-induced toxicity in rice (*Oryza sativa* L.). Plant OMICS **5**, 604–614.

Zhao FY, Hu F, Zhang SY, Wang K, Zhang CR, Liu T. 2013*a*. MAPKs regulate root growth by influencing auxin signaling and cell cycle-related gene expression in cadmium-stressed rice. Environmental Science and Pollution Research **20**, 5449–5460.

Zhao Q, Tobimatsu Y, Zhou R, *et al.* 2013*b*. Loss of function of cinnamyl alcohol dehydrogenase 1 leads to unconventional lignin and a temperaturesensitive growth defect in *Medicago truncatula*. Proceedings of the National Academy of Sciences of the United States of America **110**, 13660–13665.

Zhao J, Xia B, Meng Y, Yang Z, Pan L, Zhou M, Zhang X. 2019. Transcriptome Analysis to Shed Light on the Molecular Mechanisms of Early Responses to Cadmium in Roots and Leaves of King Grass (*Pennisetum americanum* × *P. purpureum*). International Journal of Molecular Sciences **20**, 2532.

Zhong M, Huang F, Luo R, Lv Y, Ali U, Sheng Z, Tang S, Wei X, Hu P. 2019. The effect of cadmium on the microRNAome, degradome and transcriptome of rice seedlings. Plant Growth Regulation **90**, 15–27.

Zhou Y, Liu C, Li G, Hao L. 2019*a*. Ethylene insensitive mutation increases Arabidopsis tolerance to Cd in NPR1-dependent manner. Plant and Soil **441**, 49–69.

Zhou Z, Zhang B, Liu H, Liang X, Ma W, Shi Z, Yang S. 2019*b*. Zinc effects on cadmium

toxicity in two wheat varieties (*Triticum aestivum* L.) differing in grain cadmium accumulation. Ecotoxicology and Environmental Safety **183**, 109562.

Zhou M, Zheng S, Liu R, Lu L, Zhang C, Zhang L, Yant L, Wu Y. 2019*c*. The genome-wide impact of cadmium on microRNA and mRNA expression in contrasting Cd responsive wheat genotypes. BMC Genomics **20**, 1–19.

Zhou H, Zhu W, Yang W-T, Gu J-F, Gao Z-X, Chen L-W, Du W-Q, Zhang P, Peng P-Q, Liao B-H. 2018. Cadmium uptake, accumulation, and remobilization in iron plaque and rice tissues at different growth stages. Ecotoxicology and Environmental Safety **152**, 91–97.

Zhu H, Chen L, Xing W, *et al.* 2020. Phytohormones-induced senescence efficiently promotes the transport of cadmium from roots into shoots of plants: A novel strategy for strengthening of phytoremediation. Journal of Hazardous Materials **388**, 122080.

Zhu XF, Jiang T, Wang ZW, Lei GJ, Shi YZ, Li GX, Zheng SJ. 2012. Gibberellic acid alleviates cadmium toxicity by reducing nitric oxide accumulation and expression of IRT1 in *Arabidopsis thaliana*. Journal of Hazardous Materials **239**–**240**, 302–307.

Zia Ul Haq M, Zhang Z, Wei J, Qiang S. 2020. Ethylene Biosynthesis Inhibition Combined with Cyanide Degradation Confer Resistance to Quinclorac in *Echinochloa crus-galli* var. mitis. International Journal of Molecular Sciences **21**, 1573.

Addendum

Publications

Bertels J, Huybrechts M, Hendrix S, Bervoets L, Cuypers A, Beemster GTS. 2020. Cadmium inhibits cell cycle progression and specifically accumulates in the maize leaf meristem. Journal of Experimental Botany 71, 6418–6428.

Bertels J, Beemster GTS. 2020. leafkin — An R package for automated kinematic data analysis of monocot leaves. Quantitative Plant Biology **1**.

Huybrechts M, Hendrix S, **Bertels J**, Beemster GTS, Vandamme D, Cuypers A. 2020. Spatial analysis of the rice leaf growth zone under controlled and cadmium-exposed conditions. Environmental and Experimental Botany 177, 104120.

Slovak R, Setzer C, Roiuk M, **Bertels J**, Göschl C, Jandrasits K, Beemster GTS, Busch W. 2020. Ribosome assembly factor Adenylate Kinase 6 maintains cell proliferation and cell size homeostasis during root growth. New Phytologist **225**, 2064–2076.

Oral presentations

Biology Research Day 2017. Antwerp, Belgium. Identification of the molecular and physiological mechanisms involved in cadmium inhibited leaf growth in the maize leaf growth zone.

National PhD Symposium Plant Sciences 2018. Antwerp, Belgium. Kinematic analysis of the cadmium exposed maize leaf.

National PhD Symposium on Molecular Plant Physiology 2019. Hasselt, Belgium. Cadmium inhibited maize leaf growth: A closer look at cell cycle impact.

Biology Research Day 2019. Antwerp, Belgium. Cadmium inhibited maize leaf growth: A closer look at cell cycle impact.

Poster presentations

Biology Research Day 2018. Antwerp, Belgium. Cadmium inhibited leaf growth: A kinematic analysis sheds light on the affected processes at a cellular level.

Research visits & Collaborations

CMK - Centre for Environmental Sciences. University of Hasselt, Belgium. Prof. Dr. Ann Cuypers. Performing flow cytometry. Two week research stay, January 2019.

EMAT - Electron microscopy for materials science. University of Antwerp, Belgium. Prof. Dr. Sara Bals. Performing SEM-EDX to detect Cd and situate Cd in maize leaf segments. March 2019.

Molecular Biotechnology of Plants and Micro-organisms. KU Leuven, Belgium. Prof. Dr. Wim Van den Ende. Performing sucrose, glucose and fructose measurements. September 2019.

Teaching

Assistant in the practicum of Molecular Biology. Prof. Dr. Gerrit T.S. Beemster 2016-2017, 2017-2018, 2018-2019

Assistant in the practicum of Laboratory skills. Prof. Dr. Els Prinsen. 2018-2019, 2019-2020

Supervision of Bachelor thesis students. Geoffrey Hibbs (2019-2020), Leen Vandenberghe (2019-2020)

Organising

Chair of the Biology Research Day organising committee. One day congress of the university of Antwerp with over 200 participants. 2018.

Additional courses

2nd Antwerp Introductory course to Next-Generation Sequencing data analysis. Centrum Medische Genetica. Antwerp, Belgium. September, 2017.

RNA-seq analysis for differential expression in GenePattern. VIB. Leuven, Belgium. April, 2018.

Graphics in R. FLAMES, Flanders' training network for methodology and statistics. Ghent, Belgium. May, 2018.

Data Carpentry. Data analysis in R. Elixir Belgium. Brussels, Belgium. June, 2018

Factor Analysis. FLAMES Summer School Methodology & Statistics. Leuven, Belgium. September, 2018

Acknowledgements

First and foremost, I want to thank Prof. Gerrit Beemster for believing in my sincere interest and motivation to perform this PhD study. If it was not for his decision, I might not have been able to further develop myself like I had during the past four years. During my PhD, Gerrit taught me a new way of scientific reasoning, presenting and writing, supported me through tough times and gave me the freedom to add my personal touch, which allowed me to find and pursue my passion for data analysis. Gerrit, sincerely, thank you again for this life changing experience and for your guidance along this long journey.

I also want to thank the members of the IMPRES lab group. Thank you Prof. Han Asard, Prof. Els Prinsen and Prof. Kris Vissenberg for providing insight during our meetings, but also for your effort in creating and managing a research group which hosts a broad range of expertise. Thank you, Prof. Hamada AbdElgawad, for being a friend, helping and guiding me where possible. Thank you, Jesper, for being my office buddy, where we could share our passion for R, science and some jokes on the side. And thank you, all other members of the IMPRES research group (and beyond), which helped me, made me laugh, had nice conversations with and so much more, thank you dr. Sébastjen, dr. Bulelani, Danny, Sophie, Sevgi, Alexandra, Chris, Gosia, dr. Daria, Naomi, Brigitte, Renato, Ahmed, Lin, Romain, Cindy, Niko and Pièrre.

In addition to the IMPRES research group, I want to thank the Centre for Environmental Sciences (UHasselt), all of its members, and in particular Prof. Ann Cuypers, dr. Sophie Hendrix and Michiel Huybrechts. Thank you Ann for making this joint research project possible. Your expertise in plant heavy metal stress, clear vision and guidance, is in part responsible for the success of this project. Also thank you for your hospitality, where multiple visits and a two week research stay always resulted in a nice outcome. Thank you Sophie and Michiel for your help with the flow cytometry measurements. And

thank you Michiel for our countless talks about the topic, our results, but also about PhD life itself. Good luck in your future career, whatever it may bring!

I also want to explicitly thank Prof. Els Prinsen and Sevgi Oden, for their help and dedication in the complex analysis of several phytohormones in a large batch of samples. Thank you Prof. Lieven Bervoets, dr. Kayawe Valentine Mubian and Steven Joosen, for your help, advice and excellent measurements of Cd and mineral contents. And thank you to the lab of Prof. Wim Van den Ende (KU Leuven) for performing the measurements of sucrose, glucose and fructose in a large batch of samples.

I also want to thank all other members of my committee, not mentioned above. Thank you prof. Kris Laukens (Antwerp University, Belgium), prof. Nathalie Verbruggen (Université libre de Bruxelles, Belgium) and prof. Stephan Clemens (Universität Bayreuth, Germany) for agreeing to be in my external jury, find the time to read my thesis and providing valuable feedback to further improve my thesis.

Besides thanking all the people I have met in academia, it is of utmost importance to thank my parents, Martine and Ivo. They were there from the start, day 0, and supported me throughout my entire life as a student and person. They offered me numerous possibilities to develop myself and allowed me to become the person I am today. Without you, I would not stand here today. Besides my parents, I want to thank my sister, Sofie. Your kind and supporting words, at the right time, gave me strength during the harder times of my PhD study. Of course, besides this direct and close family, there are all the other family members and close friends, a list which is too long to mention, but I am sure that each of them can assess their impact on my life's journey and PhD study. Thank you all for your support and for offering me numerous occasions to clear mind.

To conclude the acknowledgements, there is one person in particular which deserves to be in the spotlight, and that is dr. Katrien Sprangers, *Katrientje*. My soulmate for already more than a decade. Thank you for making working besides you such a pleasant experience. Not only did you learn me everything I needed to know to get

started at IMPRES, but also your help from time to time was invaluable. At home, during COVID lockdown, I was working on my thesis for more than half a year. Especially at the end, this was a period which was quite hard to endure, yet your comforting words and sympathetic ear made me push through to the end. Thank you, so much, my lovely Katrien.